# Characterisation of novel cell models of Huntington's disease; insights into pathogenesis

**Dr. Rhia Ghosh**

***University College London***

A thesis submitted in partial fulfilment of the requirements for the degree of Doctor of Philosophy from University College London

2018

# Declaration

I, Rhia Ghosh, confirm that the work presented in this thesis is my own. Where information has been derived from other sources or the contributions of others have been involved, this has been clearly indicated in the text.

# Acknowledgments

I would firstly like to express my sincere gratitude to my primary supervisor Professor Sarah Tabrizi for providing inspiration, encouragement and the wonderful opportunity to work at the forefront of Huntington's disease research throughout these last five years. The utmost thanks must also go to Dr. Ralph Andre for his tutelage and mentorship on all scientific matters, and to Dr. Alison Wood-Kaczmar for her advice and guidance through all the highs and lows of lab-based research. I have also been fortunate to work with a number of fantastic colleagues in the Tabrizi group (Luci, Jamie, Caroline, Grace, Sahar and Davina, to name a few), all of whom have enriched my time at UCL. I remain indebted also to all the patients who have spared their time to participate in HD research, without whom progress would not be possible. I am much obliged to my parents and parents-in-law for all their help during this time, especially since the arrival of Amaya and Lila into the world. Finally, I am eternally grateful for the love, patience and practical support provided by my husband Michael, who has always been my truest of advocates. I dedicate this thesis to you all.

# Abstract

Huntington's disease (HD) is an adult-onset, autosomal dominant neurodegenerative disease characterised by progressive movement disorder, psychiatric and cognitive symptoms. The causative genetic mutation is an abnormally expanded CAG triplet repeat near the N-terminus of exon 1 of the huntingtin gene (*HTT*), and longer CAG repeat lengths are associated with earlier age of disease onset. The aim of this thesis was to create a HTT allelic series cell model of HD in which the effects of increasing CAG repeat length, against a stable genetic background, could be observed within human neurons.

Initially, recombinant adeno-associated virus (rAAV) was used to knock-in different CAG expansions into an immortalised human neural stem cell line (ReNcellVM), but due to low rates of homologous recombination, this was not successful. Instead, work was undertaken to optimise and characterise a transgenic HTT exon 1 allelic series in the ReNcellVM line; there is much evidence to suggest that HTT exon 1 is the pathogenic species in HD and generates phenotypes over a faster timescale than full-length HTT models. In ReNcellVM neurons the expression of pathogenic HTT exon 1 led to the formation of mutant HTT aggregates in a proportion of cells, in a manner that was related to CAG-repeat length and levels of HTT exon 1 expression. No overt cell-death phenotypes were seen but subtle differences between control and mutant lines were observed.

To complement the HTT exon 1 model, an induced pluripotent stem cell (iPSC) model was generated from an HD family who carried a range of CAG-repeat length mutations. These cells were differentiated into medium spiny neurons (MSNs) and both models were used to study the trafficking of huntingtin within cells; whilst differences were observed between the trafficking of control and mutant HTT exon 1, these were not apparent in the MSNs which express full-length HTT.

# Impact statement

This thesis describes the production and optimisation of two novel cell models of Huntington's disease. The first is a human neural stem cell allelic series that overexpresses HTT exon 1 with increasing CAG-repeat lengths. This model displays robust differentiation into neurons within two weeks and is amenable to high content imaging as demonstrated in chapter four of this work. The model therefore lends itself to high content screening of therapeutic compounds and has been used in industrial collaborations with Takeda (now Cerevance) to advance this purpose. The model was also used in collaboration with Proteostasis Therapeutics Inc (PTI) to assess the ability of various compounds (USP14 inhibitors) to clear pathogenic mutant HTT exon 1 from neurons, as described in chapter five. This model continues to be available for further therapeutic research within industry or academia, and to the wider academic community for basic science research in HD and general neuroscience.

An induced pluripotent stem cell (iPSC) cell model of HD has also been generated from a family of HD patients as described in chapter three. These cells differentiate into medium spiny neurons and have been used to study the trafficking of HTT protein, as discussed in chapter six. This model is unique as the genetically related background of the donors goes some way to eliminating the genetic heterogeneity that can affect comparisons between control and mutant HD iPSC cells. This model forms the basis of ongoing work in the HD research group at UCL. The fibroblasts derived from the patients' skin biopsies have been used to demonstrate the presence of pathogenic HTT exon 1 protein, as described in the publication "The pathogenic exon 1 HTT protein is produced by incomplete splicing in Huntington's disease patients" (Neueder, Landles,

Ghosh et al 2017; Sci Rep 7(1):1307). This model is also a useful tool for the wider HD research community both in academia and industry.

A manuscript entitled “Expression of mutant huntingtin exon 1 fragments in human neural stem cells and neurons causes inclusion formation and mitochondrial dysfunction”, which describes work in chapters four and five of this thesis is being prepared for publication in FASEB journal, and in addition aspects of this work have been presented at the European Huntington’s Disease Network (EHDN) meeting in Sept 2016, which is attended by scientists, clinicians and patients. In this way, the main findings of this thesis have been disseminated to a broader audience.

# Table of contents

# List of figures

# List of tables

# Abbreviations

| | |
|---|---|
| ≤ | Less than or equal to |
| µl | Microliter |
| µm | Micrometre |
| AAV | Adeno-associated virus |
| ADL | Activities of daily living |
| ALS | Amyotrophic lateral sclerosis |
| ANOVA | Analysis of variance |
| ASO | Anti-sense oligonucleotide |
| B3T | Beta-3 tubulin |
| BDNF | Brain derived neurotrophic factor |
| bp | Base pair |
| C | Celsius |
| CAG | Triplet repeat encoding glutamine |
| cAMP | Cyclic adenosine monophosphate |
| Cas9 | CRISPR associated protein 9 |
| CBT | Cognitive behavioural therapy |
| cDNA | Complementary deoxyribonucleic acid |
| cGMP | Cyclic guanosine monophosphate |
| CNS | Central nervous system |
| CRISPR | Clustered Regularly Interspaced Short Palindromic Repeats |
| CSF | Cerebrospinal fluid |
| Ct | Threshold cycle |
| DAPI | 4′,6-diamidino-2-phenylindole |
| DARPP-32 | Dopamine- and cAMP-regulated phosphoprotein, 32 kDa |

| | |
|---|---|
| dd | Day of differentiation |
| DMSO | Dimethyl sulfoxide |
| DNA | Deoxyribonucleic acid |
| DNase | Deoxyribonuclease |
| dNTP | Deoxyribonucleotide triphosphate |
| e.g. | For example |
| EAAT2 | Excitatory amino acid transporter 2 |
| ERK | Extracellular signal-regulated kinase |
| ESC | Embryonic stem cell |
| FACS | Fluorescence activated cell sorting |
| FOXP1 | Forkhead box protein P1 |
| g | Gram |
| GC | Genome copies |
| gDNA | Genomic DNA |
| GDNF | Glial cell-derived neurotrophic factor |
| GFAP | Glial fibrillary acidic protein |
| GFP | Green fluorescent protein |
| gRNA | Guide RNA |
| HD | Huntington's disease |
| HEAT | Huntingtin, elongation factor 3, protein phosphatase 2A, and the lipid kinase TOR. |
| HEK | Human embryonic kidney |
| hrs | Hours |
| HTT | Human huntingtin protein |
| Htt | Murine huntingtin gene |
| HTT | Human huntingtin gene |
| Htt | Murine huntingtin protein |

| | |
|---|---|
| i.e. | id est (that is) |
| iPSC | Induced pluripotent stem cell |
| JHD | Juvenile Huntington's disease |
| JNK | c-Jun N-terminal kinase |
| LDH | Lactate dehydrogenase |
| LV | Lentivirus |
| M | Molar |
| MAPK | Mitogen activated protein kinase |
| mHTT | Mutant HTT |
| mins | Minutes |
| miRNA | Micro-ribonucleic acid |
| MKP-1 | MAPK phosphatase 1 |
| MLK2 | Mixed lineage kinase 2 |
| mm | Millimetre |
| MMP | Matrix metalloproteases |
| MOI | Multiplicity of infection |
| mRNA | Messenger RNA |
| MSD | Meso Scale Discovery |
| MSN | Medium spiny neuron |
| MTT | 3-[4,5- dimethylthiazol-2-yl]-2,5-diphenyl tetrazolium bromide |
| NfL | Neurofilament light chain |
| NIAD4 | [[5'-(4-Hydroxyphenyl)[2,2'-bithiophen]-5-yl]methylene]-propanedinitrile |
| nM | Nanomolar |
| NSC | Neural stem cell |
| OCD | Obsessive compulsive disorder |
| P38 | P38 mitogen-activated protein kinases |
| PBS | Phosphate buffered saline |

| | |
|---|---|
| PCR | Polymerase chain reaction |
| PDE10A | Phosphodiesterase 10A |
| PI | Propidium iodide |
| PolyQ | Polyglutamine |
| polyQ | Polyglutamine |
| pre-mRNA | Precursor mRNA |
| PTI | Proteostasis Therapeutics Inc |
| Q | Amino acid glutamine |
| rAAV | Recombinant AAV |
| RNA | Ribonucleic acid |
| RNAi | RNA interference |
| sec | Seconds |
| siRNA | Small interfering RNA |
| SMA | Spinal muscular atrophy |
| SNP | Single nucleotide polymorphism |
| SOD1 | Superoxide dismutase 1 |
| SSRI | Selective seretonin reuptake inhibitor |
| TBZ | Tetrabenazine |
| TFC | Total functional capacity |
| ThioT | Thioflavin T |
| TMS | Total motor score |
| UCL | University College London |
| UHDRS | Unified Huntington's disease rating scale |
| ZFP | Zinc finger protein |

# 1 Introduction

## 1.1 Huntington's disease

Huntington's disease (HD) is an autosomal dominant neurodegenerative disease, characterised by a triad of motor, cognitive and psychiatric features. There is typically adult onset, with irreversible progression of symptoms over 10-15 years (Ross & Tabrizi, 2011). It was first described by an American doctor, George Huntington, in 1872 (Huntington, 1872). He noted that certain families were affected by a hereditary condition marked by chorea and psychiatric symptoms and that the disease was *"one of the incurables".* Almost 150 years later we now know much about the genetics and the pathogenesis of HD, and international collaborative research efforts continue with the hope of finding an effective therapy. Studies in HD basic science research remain essential in realising this goal.

### 1.1.1 Epidemiology of HD

The prevalence of HD varies across the globe. In Western and European populations, it has typically been quoted at around 4-10/100,000 people (Harper, 2002), however a more recent study from the UK suggests it may be closer to 12.3/100,000 population (Evans et al, 2013; Rawlins, 2010). This makes it among the more common of the inherited neurological diseases. There has traditionally been great stigma attached to the diagnosis of HD (Wexler, 2010); from accusations of witchcraft to the more recent

and disturbing eugenics movement of the last century, families affected by HD may feel pressured into hiding their condition – often at the expense of getting medical help. This is believed to have led to an underestimation of the true prevalence of the disease.

HD was originally thought to have migrated from North-West Europe to other parts of the world. Although migration is undoubtedly a major contributor of HD prevalence, de novo genetic mutations also make a significant contribution. In some communities, the prevalence of HD is exceptionally high. One of the best studied of these is the population living near the edge of Lake Maracaibo in Venezuela, where 700/100,000 people have HD. In 1983, genetic linkage studies in this group of people paved the way for the identification of the genetic mutation causative of Huntington's disease ten years later (1993; Gusella et al, 1983; Huntington's Disease Collaborative Research Group, 1993)

### 1.1.2 Genetics of HD

Huntington's disease is caused by an expanded CAG triplet repeat in exon 1 of the gene encoding huntingtin protein, which lies on the short arm of chromosome 4. This creates an elongated polyglutamine (polyQ) stretch at the N-terminus of the mutated protein. HD displays autosomal dominant inheritance and so the presence of the gene mutation on *either* allele leads to the disease state. The wild type gene carries 10-35 CAG repeats, with a mean value of 18 repeats across the UK population (Snell et al, 1993). The mutation is fully penetrant at 40 or more repeats. Those who inherit 36-40 repeats have a reduced penetrance form of the disease – they may develop symptoms

of HD in older age, or they may never become symptomatic (Rubinsztein et al, 1996). Individuals with 27-35 CAG repeats are said to carry an “intermediate allele”, and have long been thought to remain asymptomatic. However, a recent study suggests that there may be a behavioral phenotype in this group of people (Killoran et al, 2013). Intermediate alleles can expand during meiosis, leading to the potential acquisition of a disease gene carrying 36 or more repeats in the offspring. A recent PCR analysis of sperm cell DNA suggests that the highest risk of this is where the CAG repeat lengths are 34 or 35, with the risk of a new pathogenic mutation being 2.4% and 21% respectively (Semaka et al, 2013).

Seemingly sporadic cases of HD can arise when there has been misdiagnosis of the condition in other family members, or death has occurred by some other means before symptoms of HD have developed in prior generations. Occasionally non-paternity also leads to “sporadic” cases of HD. This highlights the importance of taking a detailed and complete family history when considering the diagnosis of HD. Approximately 6-8% of cases of newly diagnosed HD arise in families with no apparent family history (Almqvist et al, 2001; Siesling et al, 2000).

#### 1.1.2.1 Anticipation

There is inherent instability of the CAG repeat during meiosis, which can lead to expansions (and sometimes contractions) in the number of CAG repeats inherited by successive generations (Zühlke et al, 1993). Longer CAG repeat lengths correlate with an earlier age of onset of disease, and so as the condition is passed down the family symptoms can develop at progressively younger ages. This is a phenomenon known

as anticipation. Anticipation is more likely to occur when inherited down the paternal bloodline. This is hypothesized to be due to differences in spermatogenesis and oogenesis (Kremer et al, 1995). In rare instances, large increases in CAG repeat occur leading to juvenile HD (JHD) when the age of onset is <20 years old. Paternal inheritance is seen in 90% of JHD cases (Barbeau, 1970; Kremer, 2002).

#### 1.1.2.2 Effects of CAG repeat length

As stated above, longer CAG repeat lengths correlate with an earlier age of disease onset. Studies at a population level have shown that 50-70% of the variability in age of onset is determined by the CAG repeat length. Recent studies have shown that genetic variants in DNA repair proteins account for some of the remainder of the variability (Consortium, 2015). It is important to emphasize that it is not possible in a clinical setting to predict an individual's age of onset of disease from their CAG repeat length, particularly as the majority of patients with HD have CAG repeats ranging from 40-50, a range at which great unpredictability is observed.

A conditional probability model developed by Langbehn et al takes into account not only the CAG repeat length, but also the number of disease-free years already lived (Langbehn et al, 2004; Langbehn et al, 2010). It is based on data from a large cohort of 3000 patients and is more accurately able to estimate the percentage chance of disease free survival over a set number of years (usually 5 years). However, even this more sophisticated model is based on population data and so cannot be extrapolated to apply in a clinic setting. Patients often experience psychiatric and cognitive

symptoms for many years before their official disease onset (as defined by the presence of definitive motor signs), further complicating the issue.

The rate of clinical disease progression after motor onset has also shown some correlation with CAG repeat length (Rosas et al, 2011; Rosenblatt et al, 2012), and again variants in DNA repair proteins contribute (Hensman Moss et al, 2017). It is worth noting that CAG repeat length does not predict the exact disease phenotype; for example, it is much less strongly correlated to the age at onset of psychiatric symptoms than motor symptoms. The duration of disease from diagnosis to death is also independent of CAG repeat length.

### 1.1.3 Clinical aspects of HD

Huntington's disease is characterized by motor, cognitive and psychiatric symptoms. Generally the disease develops in adult life with an average age of onset of 40 years, though cases of HD have been diagnosed in patients as young as 2 years old, ranging up to 87 years. From the time of disease onset, symptoms progress over 15 to 20 years; the most common cause of death is pneumonia (Lanska et al, 1988).

#### 1.1.3.1 Natural history and disease progression

Patients are said to have onset of "manifest" disease only when there is the presence of unequivocal motor signs (e.g. chorea, dystonia, bradykinesia, rigidity) that have no explanation other than HD; however it is quite common to have psychiatric or cognitive

symptoms and subtle motor signs for many years before this (Ross & Tabrizi, 2011). This prodromal phase of HD corresponds to neurobiological changes including striatal atrophy and loss of corticostriatal connectivity (Tabrizi et al, 2012; Tabrizi et al, 2013).

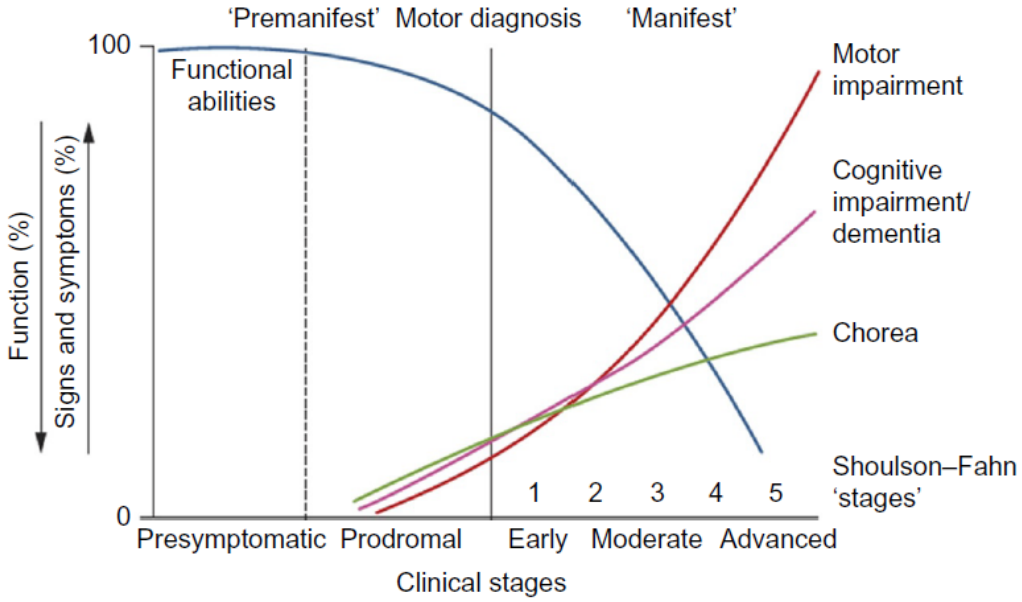


**Figure 1.1: The natural history of Huntington disease,** showing premanifest and manifest disease with corresponding clinical changes. (Reproduced from Ross CA, Aylward EH, Wild EJ, et al. (2014) Huntington disease: natural history, biomarkers and prospects for therapeutics. Nat Rev Neurol 10: 204–216, with permission from Springer Nature)

Patients who are known to carry the HD gene mutation but who have not yet developed motor onset of disease are defined as "premanifest", however it does not necessarily follow that they are completely asymptomatic (although generally up to 10-15 years prior to disease onset they are clinically indistinguishable from controls) (Ross et al, 2014). More recently, the term "perimanifest" disease has been used to describe that

group of patients with *prodromal* HD who are felt by their clinician to be developing the motor signs that will lead to a diagnosis of "manifest" HD in the near future.

#### 1.1.3.2 Clinical presentation

*Motor Features*

Motor symptoms of HD consist of involuntary movements seen predominantly in early-moderate stage typical adult onset disease, and impaired voluntary movements that are more common in advanced disease and JHD. More subtle motor changes also occur many years prior to disease onset. The TRACK-HD study found differences in speeded tapping over 36 months between control and premanifest patients who were predicted to be over 10.8 years from disease diagnosis (Tabrizi et al, 2013).

Chorea is one of most striking features of HD. Indeed, the disease was initially named Huntington's chorea before this was changed to give recognition to the wide range of non-motor features. Chorea comprises involuntary, excessive movements, which are short lived and may appear semi-purposeful. Other motor symptoms include dystonia, myoclonus and tics. Gait and postural reflexes are affected and walking aids may be needed. As the disease progresses, hyperkinetic movements decrease and instead bradykinesia, akinesia and rigidity dominate.

*Cognitive features*

Cognitive symptoms are universal in HD and may emerge years before disease onset (Paulsen et al, 2008; Stout et al, 2011). Symptoms range from subtle deficits to frank

dementia later in the course of disease. Executive functioning i.e. high-level processing that controls other more basic aspects of cognitive function is commonly affected in HD. There may also be general cognitive slowing, impaired short-term memory (with problems learning and retrieving new material) and poor emotion recognition (Peavy et al, 2010; Stout et al, 2012; Stout et al, 2011). There is some overlap with psychiatric symptoms in terms of disinhibition and impulsive behaviours, with accompanying lack of insight (Duff et al, 2010). Semantic memory remains relatively preserved (Craufurd D, 2002). Some patients with advanced disease may develop a severe frontal and subcortical dementia.

### *Psychiatric features*

Psychiatric symptoms can be the most distressing aspect of HD for both patients and their carers and are common (affecting 33-76% of patients (van Duijn et al, 2007)). Indeed suicide is the second most common cause of death in HD (Lanska et al, 1988). Symptoms occur in both prodromal and manifest HD and arise not only as a response to the diagnosis, but due to the underlying neurobiology of the disease. Depression is the most common condition, followed by anxiety (Paulsen et al, 2005). Apathy is also a common and disabling feature of HD that tends to worsen over time. Other neuropsychiatric symptoms include irritability and aggression, obsessive, compulsive thoughts and behaviours, and psychosis.

### *Other neurological symptoms*

Speech difficulties arise from a combination of dysarthria and word finding difficulties secondary to cognitive dysfunction. Swallowing problems similarly arise from a combination of incoordination of oral and pharyngeal muscles, and cognitive

impairment. This can cause choking and in more severe cases lead to aspiration and subsequent pneumonia (the leading cause of death in HD). Sleep disturbance is a common complaint of patients (Videnovic et al, 2009), resulting from low mood, anxiety or night-time chorea or intrinsic circadian rhythm dysfunction.

### *Systemic symptoms*

Though the most dramatic effects of HD are on the nervous system, a range of systemic symptoms can also be observed (van der Burg et al, 2009). Severe weight loss often occurs, greater than that seen in other hyperkinetic movement disorders, and may lead to cachexia. It is thought to be secondary to an underlying catabolic state as part of the disease pathology and not simply due to feeding or swallowing difficulties or chorea. This may begin during the prodromal phase of HD and there is an association between higher body mass index at disease onset and slower rate of disease progression (Myers et al, 1991). In addition, heart failure is seen in 30% of patients, compared to 2% of age-matched controls (Lanska et al, 1988). Both osteoporosis and skeletal muscle atrophy are observed, despite the muscle hyperactivity secondary to chorea. Endocrine problems with thyroid dysfunction and impaired glucose tolerance occur. Testicular atrophy with reduced numbers of germ cells and abnormal seminiferous tubules is noted. Despite reduced levels of testosterone in men, fertility remains unaffected.

There is evidence for widespread activation of the immune system in HD as plasma samples from patients show increased levels of IL-6 and IL-8 (Bjorkqvist et al, 2008), which may contribute to the peripheral phenotype described. The range of peripheral

effects is perhaps not surprising given that cells throughout the body, and not just in the nervous system, express huntingtin protein.

*Juvenile Huntington's disease*

Juvenile HD (JHD) generally arises in those who have inherited >55 CAG repeats (Andrew et al, 1993), and is defined by an age of onset less than 20 years old. The clinical presentation of JHD varies from the adult form in that rigidity, bradykinesia and akinesia are present from disease onset, rather than the hyperkinetic presentation commonly seen in adult onset HD. There may also be learning difficulties and behaviour disturbance whilst at school. Seizures occur in 30-50% of patients (Kremer, 2002). This rigid phenotype of HD is also known as the Westphal or akinetic-rigid variant and on rare occasions presents as adult onset disease.

### 1.1.3.3 Diagnosis of HD

Diagnosis relies on clinical findings, which must include unequivocal motor signs, in combination with a positive family history suggestive of an autosomal dominant pattern of inheritance. The role of neuroimaging and CSF testing is only for the investigation of other causes of chorea. Genetic testing to determine the CAG repeat length in the HD gene confirms the diagnosis (Craufurd et al, 2014).

Diagnostic tests are carried out on those people who are displaying motor signs consistent with HD; generally they are requested by neurologists to confirm a suspected diagnosis. Predictive tests are carried out in asymptomatic individuals with a

positive family history of HD and must be carried out in accordance with international guidelines (1994; Craufurd & Tyler, 1992; Went, 1990). Overall just under 20% of patients at risk of HD proceed with predictive genetic testing (Baig et al, 2016).

#### 1.1.3.4 Management of HD

The clinical management of HD requires a multidisciplinary approach. There are currently no disease-modifying treatments available, and so treatments aim to alleviate symptoms and optimize function (Bonelli & Hofmann, 2007; Frank, 2014; Mason & Barker, 2009). Anti-chorea medication should be considered if there is functional impairment, for example in terms of manual dexterity or falls. A Cochrane review of studies for the symptomatic treatment of HD examined 22 studies and concluded that only tetrabenazine (TBZ) showed clear efficacy for the control of chorea (Mestre et al, 2009), although in practice, atypical neuroleptics such as olanzapine, risperidone and quetiapine are also used, especially if there are psychiatric comorbidities. The benzodiazepine clonazepam may be used if there is dystonia, rigidity or myoclonus. Tizanidine and baclofen can help with spasticity and rigidity that develop in later stages and botulinum toxin injections can be effective in the treatment of muscle spasm (Novak & Tabrizi, 2010).

There is a lack of evidence base to guide specific treatment of psychiatric symptoms, however depression often responds well to non-stimulating selective serotonin reuptake inhibitors (SSRIs) such as citalopram. If insomnia is also a problem, mirtazapine, which is a sedating antidepressant, can be used. Cognitive behavioural therapy (CBT) can also be useful for appropriately selected patients. Other psychiatric

symptoms such as anxiety, irritability, aggression, obsessive-compulsive behaviours and psychosis may also respond to treatment with both typical and atypical neuroleptics (Novak & Tabrizi, 2010).

### 1.1.4 Therapeutics research in HD

#### 1.1.4.1 Disease-modifying therapies

Over 30 years have passed since the discovery of the causative gene mutation in HD, but there remains an urgent and as yet unmet need for treatments. However a number of promising avenues to disease modification have been identified recently (Wild & Tabrizi, 2014), many of which are proceeding to clinical trials in the near future (figure 1.2).

*Reducing huntingtin expression*

Huntingtin (HTT) lowering through gene silencing is an approach that has seen enormous advances in recent years. Mutant HTT is known to primarily cause disease through a dominant toxic effect, and so any reduction in its expression should reduce its downstream pathological effects. Strategies to lower HTT levels include both post-transcriptional inhibition such as RNA interference (RNAi) and anti-sense oligonucleotides (ASOs), and genome editing techniques such as zinc finger proteins (ZFPs).

Administration of complementary small interfering RNA molecules (siRNAs) results in Argonaut-2 mediated cleavage and degradation of mature, spliced HTT mRNA in the cytosol. ASOs have a more upstream site of action and recruit RNaseH1, an endogenous enzyme that recognises RNA/DNA duplexes and degrades HTT pre-mRNA (Keiser et al, 2016).

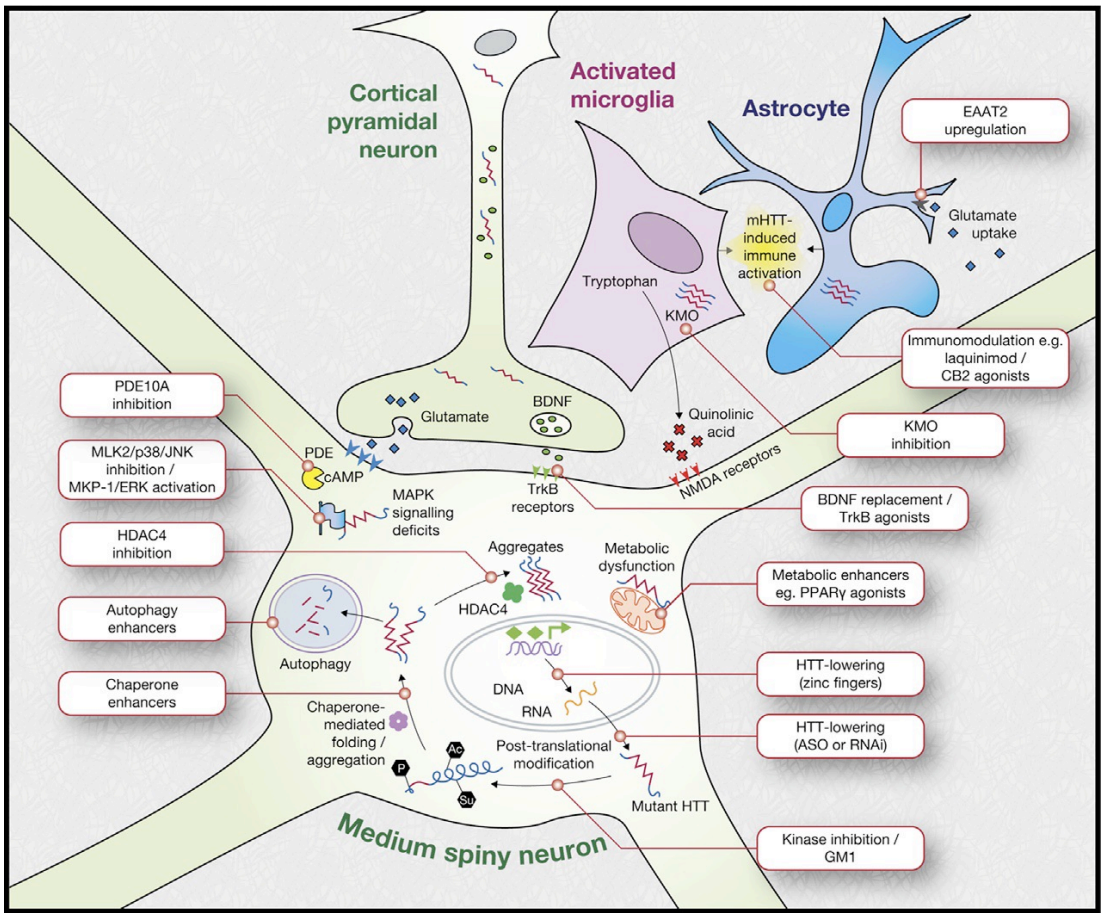


**Figure 1.2**: Schematic depicting current priority **preclinical therapeutic targets under investigation for Huntington's disease**. BDNF, brain-derived neurotrophic factor; HDAC, histone deacetylase; HTT, huntingtin; KMO, kynurenine monooxygenase; NMDA, N-methyl-D-aspartate; PDE, phosphodiesterase; Trk, tyrosine receptor kinase. (Reproduced from Wild EJ, Tabrizi SJ (2014) Targets for future clinical trials in Huntington's disease: what's in the pipeline? Mov Disord 29: 1434–1445.)

Both siRNAs (Harper et al, 2005; Stanek et al, 2014) and ASOs (Kordasiewicz et al, 2012) designed to lower total HTT levels have been shown to improve disease symptoms in rodent models. A potential concern in humans is the long-term effect of reducing wild-type HTT, although reduction in endogenous wild-type HTT has been shown to be well tolerated in non-human primates (Grondin et al, 2012; McBride et al, 2011). Allele-specific lowering of mutant HTT only (without affecting wild-type HTT) has been challenging. However ASOs complementary to the expanded CAG have recently been produced which have selectivity for mHTT over HTT, and have led to phenotypic improvement in two different mouse models of HD (Datson et al, 2017). siRNAs designed to target single nucleotide polymorphisms (SNPs) that reside only on the mutant HTT allele could also be used to achieve allele specific suppression (Miller et al, 2017; Pfister et al, 2009). ASOs targeting mutant-allele linked SNPs have also been designed that lead to even greater (up to 50-fold) selectivity of the mHTT allele over the normal allele (Carroll et al, 2011; Southwell et al, 2014). Such compounds are proceeding to clinical trials in the near future, and will involve screening potential trial subjects for the presence of specific SNPs before drug administration.

Gene suppression can also be achieved at the transcriptional level, using effectors that bind to specific DNA sequences. Zinc finger proteins (ZFPs) contain a zinc finger domain that can be synthetically manipulated to bind HTT DNA, fused to a functional domain such as a nuclease. Delivery of such agents is through the use of viral vectors, and this approach will also be proceeding into clinical trials soon. Another recently discovered genome editing technique is through manipulation of the endogenous clustered regulatory interspaced short palindromic repeat (CRISPR)/Cas9 system

which recognises and destroys foreign DNA in prokaryotic cells. Incorporation of a synthetic guide RNA (gRNA) strand that targets a particular DNA location for cutting, followed by the insertion of a desired DNA sequence (for example stop codons), is used to inactivate the mutant allele (Cox et al, 2015). The technique has been successfully demonstrated in HD patient-derived fibroblasts, leading to the dramatic reduction of mutant HTT RNA and mHTT protein (Shin et al, 2016).

A seminal Phase 1/2a clinical trial (IONIS-HTTRx) has recently been undertaken by Ionis Pharmaceuticals to test the safety and tolerability of an ASO targeting human HTT, delivered by lumbar intrathecal bolus administration to early stage HD patients. The trial included neuroimaging assessments and exploratory endpoints to assess the effect on cognitive, motor, and neuropsychiatric symptoms. Encouragingly, results from this trial have confirmed target engagement, with a reduction in mHTT seen in the CSF of trial subjects (Tabrizi et al, 2018). Intrathecal delivery of ASO treatment has shown dramatic benefit in patients with spinal muscular atrophy (SMA) (Finkel et al, 2017; Mercuri et al, 2018) with trials of ASOs in amyotrophic lateral sclerosis (ALS) also demonstrating the safety and tolerability of this general approach (Miller et al, 2013).

### *Stem cell therapy*

Over the last 15 years there have been a number of small trials of foetal striatal transplantation in patients with HD carried out in the United Kingdom (Barker et al, 2013; Reuter et al, 2008; Rosser et al, 2002), France (Bachoud-Lévi et al, 2006; Bachoud-Lévi et al, 2000), Germany (Capetian et al, 2009), Italy (Gallina et al, 2010), and the United States (Hauser et al, 2002), but the conclusions so far have been mixed. Some have reported improvement or stabilization in motor, functional, and

neuropsychological scores (Bachoud-Lévi et al, 2006), but this has not been found consistently across groups (Barker et al, 2013; Hauser et al, 2002). This may be due to the small numbers of patients treated at each centre, and also the differences in patient selection in terms of disease stage between the studies. In addition there were subtle differences in methodology with respect to the tissue type transplanted (cells from whole ganglionic eminence compared to lateral ganglionic eminence, and also different foetal gestation) as well as the preparation of the donor tissue and numbers of cells transplanted (Barker et al, 2013). Post-mortem studies, where available, have revealed poor long-term graft survival. This may be due to allograft immunoreactivity, excitotoxicty, or microglial responses directed against donor tissue (Wijeyekoon & Barker, 2011). A more recent study has shown the presence of mHTT aggregates in the genetically normal, unrelated grafted donor cells, thus raising questions regarding the spread of mutant protein between neurons (Cicchetti et al, 2014) and the long-term success of any foetal striatal transplantation therapy.

### *Small molecule approaches to disease modification*

Basic science research carried out in cellular, mouse, and mammalian models of disease has identified a role for huntingtin protein in several different cellular pathways. Thus a plethora of potential targets for disease modification exist. Approaches that have been shown to be beneficial in animal models, and in some cases are in clinical trials are summarised in Table 1.1.

**Table 1.1: Targets for small molecule approaches to disease modification in Huntington's disease.**

| Target | Mechanism |
|---|---|
| **Histone deacetylases (HDACs)** | HDAC4 reduction delayed cytoplasmic aggregate formation, restored BDNF transcript levels, rescued synaptic function and improved phenotype and lifespan in HD mouse models. (Butler & Bates, 2006; Mielcarek et al, 2013). |
| **Post-translational modifications** | Phosphorylation of mHtt by ganglioside GM1 at specific residues attenuates huntingtin toxicity, and restores normal motor function in already symptomatic HD mice (Di Pardo et al, 2012). Acetylation of mHTT promotes its clearance by autophagy, and the inhibition of the deacetylase sirtuin 1 by selisistat has been shown to have benefit in various HD models and is safe and tolerable for patients (Süssmuth et al, 2015). |
| **Phosphodiesterase (PDE) 10A** | PDE 10A is expressed in the striatum and regulates cAMP and cGMP signalling, synaptic plasticity, and the response to cortical stimulation. Inhibition has beneficial effects in animal models (Giampà et al, 2010). However, the recently completed Pfizer "Amaryllis" trial of PDE10A inhibition in patients has not found any beneficial effect on motor function, or other HD symptoms that were tested (NCT02197130). |
| **Brain-derived neurotrophic factor (BDNF)** | Administration of BDNF improved neurological dysfunction and survival in R6/2 mice (Giampà et al, 2013). Small molecule agonism of TrkB, through which BNDF acts, also improved striatal pathology and symptoms in HD mouse models (Simmons et al, 2013). However cysteamine, which is also thought to act through increasing BDNF |

| | |
|---|---|
| | levels, has not demonstrated efficacy in a recent clinical trial (CYST-HD) (Verny et al, 2017). |
| **Immune modulation** | Peripheral modulation through inhibition of kynurenine 3 monooxygenase extends life span, prevents synaptic loss, and decreases microglial activation in R6/2 mice (Zwilling et al, 2011). Central modulation with laquinimod (an immunomodulatory drug with unknown mechanism of action), has been shown to reduce NF-kB activation in astrocytes (Brück et al, 2012) and has demonstrated potential in the treatment of multiple sclerosis (Comi et al, 2012). The effect of laquinimod on motor function and brain imaging in early HD is currently being assessed in LEGATO-HD (NCT02215616). |
| **Chaperone proteins** | Upregulation of chaperone proteins reduces potential misfolding of mHTT and subsequent aggregate formation (Labbadia et al, 2012; Sontag et al, 2013). |
| **Autophagy** | Induction of autophagy with rapamycin (an mTOR inhibitor) aids the clearance of mHTT and its cleavage products, and reduces toxicity in fly and mouse models of HD (Ravikumar et al, 2004). |
| **Mitogen-activated protein kinases (MAPKs)** | MAPK signalling regulates a variety of cellular functions, and has been found to be abnormal in HD. Over-activation or upregulation of ERK and MKP-1 has been found to be neuroprotective (Apostol et al, 2006; Taylor et al, 2013), whereas inhibition of MLK2, JNK, and p38 has beneficial effects (Apostol et al, 2008; Taylor et al, 2013). The role of MAPKs in HD is not completely understood. |

| | |
|---|---|
| **Cellular metabolism** | Cellular metabolism is known to be affected in HD. The administration of rosiglitazone, an agonist of transcription factor peroxisome proliferator-activated receptor γ (which has a key role in regulating genes involved in energy metabolism) has been shown to attenuate mHTT-induced toxicity in striatal cells and improve motor function in HD mice (Jin et al, 2013).. |
| **Excitotoxicty** | Excitotoxicity is a known pathogenic mechanism in HD. Administration of ceftriaxone, which upregulates expression of the EAAT2 glutamate transporter, has been shown to be beneficial in HD mouse models (Miller et al, 2008). |

#### 1.1.4.2 Biomarkers

Assessing the impact of any potential treatment can be difficult due to the heterogeneity of motor/psychiatric and cognitive problems in HD and the natural variation in rates of progression. Therefore biomarkers are needed to objectively and accurately reflect disease status. Furthermore, genetic testing allows us to identify premanifest HD patients, in whom the goal would be to introduce medication to delay onset of or even prevent neurodegeneration from occurring; biomarkers are essential in helping to decide on the timing of such interventions when they become available.

Thanks to large-scale longitudinal studies such as TRACK-HD (Tabrizi et al, 2009; Tabrizi et al, 2012; Tabrizi et al, 2011; Tabrizi et al, 2013) and PREDICT-HD (Biglan et al, 2013; Harrington et al, 2012; Paulsen et al, 2008), we now have a much clearer idea

of the natural progression of HD from premanifest through to manifest disease. Structural magnetic resonance imaging has demonstrated significantly faster rates of decline in striatal volume in premanifest and manifest individuals compared with age-matched controls, even in those estimated to be >15 years from estimated disease onset (Aylward et al, 2011). Other imaging modalities that may serve as potential biomarkers of disease include diffusion tensor imaging, which has shown abnormalities in neuronal fibre orientation and integrity in white matter and subcortical grey-matter structures in both premanifest and manifest HD, functional magnetic resonance imaging techniques, and 18F-fluorodeoxyglucose positron emission tomography (Ross et al, 2014). Clinical measures that have been found to track decline in premanifest individuals include performance on the speeded tapping task and deterioration in emotion recognition; in those with early HD, performance on the Stroop test and indirect circle tracing also tracked clinical decline (Tabrizi et al, 2013).

An ultrasensitive single-molecule counting mHTT immunoassay has been developed that can quantify very low levels (in the femtomolar range) of mHTT in the cerebrospinal fluid. The level of mHTT detected was associated with proximity to disease onset and diminished cognitive and motor function, and is a promising biomarker being taken forward into clinical trials (Wild et al, 2015). Levels of tau in the cerebrospinal fluid also show promise as a biomarker in HD (Rodrigues et al, 2016). Recently the level of neurofilament light protein (NfL) in plasma, which can be obtained through a simple blood test, has demonstrated potential as a prognostic blood biomarker of disease onset and progression in Huntington's disease (Byrne et al, 2017).

## 1.2 Pathogenesis of HD

### 1.2.1 Wild type HTT structure and function

Huntingtin is a very large protein with an estimated molecular weight of 348kDa (Hoogeveen et al, 1993). The first exon consists of an N-terminal alpha helix, followed by a polyQ stretch, and then a polyproline helix. X-ray crystallography has shown the PolyQ stretch to be flexible, adopting alpha helix, random coil and extended loop structures (Kim et al, 2009). This flexibility of the PolyQ region is thought to allow the flanking N17 domain (the first 17 amino acids of exon 1) and downstream polyproline region to come into close spatial proximity, and is impaired with expanded PolyQ tracts (Caron et al, 2013). A recent cryo-electron microscopy study has found that full length HTT is largely alpha-helical and consists of 3 major domains; the N- and C-terminal domains contain HEAT (huntingtin, elongation factor 3, protein phosphatase 2A and lipid kinase TOR) repeats arranged in a solenoid fashion, connected by a smaller bridge domain containing different types of tandem repeats (Guo et al, 2018). It has many interaction sites suggesting that it is a scaffolding protein that helps to co-ordinate other proteins and cellular functions (Zuccato et al, 2010).

The protein undergoes extensive post-translational modifications, including phosphorylation, SUMOlyation, ubiquitination, palmitoylation and acetylation. HTT is also subject to cleavage by a variety of caspases, calpains and cathespins and MMPs (matrix metalloproteases). These modifications are all thought to play a role in the regulation of HTT activity (Zuccato & Cataneo, 2014).

HTT is ubiquitously expressed throughout the body, but the highest concentrations are found in the CNS and testes (Li et al, 1993). Knocking out Htt prior to neural development is embryonic lethal in mice (Nasir et al, 1995; Zeitlin et al, 1995). A developmental role for HTT has also been recently suggested by the finding that HTT knockout in human ESCs undergoing neuronal differentiation results in chromosomal instability that impairs neurogenesis (Ruzo et al, 2018). A broader systemic role for HTT is suggested by the peripheral phenotype seen in patients with HD, and by a study that shows conditional knockout of Htt in young mice leads to death from acute pancreatitis (Wang et al, 2016). HTT has also been shown to have a neuroprotective function through its anti-apoptotic activity (Rigamonti et al, 2001; Zhang et al, 2006).

HTT enhances BDNF production at the level of gene transcription through stimulatory action on *Bdnf* promoter II (Zuccato et al, 2001), and also promotes BDNF vesicular trafficking in neurons (Gauthier et al, 2004). BDNF is important for the survival of striatal and cortical neurons. Subsequently it has been shown that through its interaction with a complex of proteins, wild-type Htt causes retention of the REST/NRSF transcriptional regulator in the cytoplasm, thus reducing the activity of RE1/NRSE within the *Bdnf* promoter II. The RE1/NRSE site is present on over 1300 genes, thus implicating wild type HTT more broadly in transcriptional regulation (Zuccato & Cataneo, 2014). HTT also plays a role in vesicular (Velier et al, 1998) and axonal transport (Gunawardena et al, 2003), trafficking of organelles such as mitochondria (Trushina et al, 2004), and control of synaptic activity in neurons (Smith et al, 2005). Thus wild type HTT seems to have a variety of functions; a recent study has shown that the reduction of mHTT in cortical or striatal neurons in mice improves different aspects of the disease phenotype, suggesting distinct roles for the protein in these neuronal populations (Wang et al, 2014).

### 1.2.2 Overview of HD pathology

Compared to the wild-type protein, the mutant protein contains an expanded CAG (polyglutamine) repeat in exon 1, immediately following the N17 domain. PolyQ expansion increases the α-helical properties of huntingtin, and alters the intramolecular interactions between the remaining HTT protein domains (Vijayvargia et al, 2016). Ultimately aggregates of abnormal HTT form in neuronal nuclei (intra-nuclear inclusion bodies are considered the pathognomic signature of HD), and also to a lesser extent in the cytoplasm, dendrites and axon terminals. The definitive role of these aggregates (whether toxic or protective) has not yet been established (Arrasate & Finkbeiner, 2012; Ross & Tabrizi, 2011) (see section 1.4.1 for further detail). At a macroscopic level, post-mortem studies have revealed massive neuronal degeneration in the striatum of brains from patients with advanced HD. Up to 95% of the GABAergic medium spiny neurons (MSNs) that project to the globus pallidus and substantia nigra are lost, and there is atrophy (though less so) of the cerebral cortex, subcortical white matter, thalamus and hypothalamic nuclei (Halliday et al, 1998).

HD is thought to arise predominantly from a gain of toxic function, as suggested by dominant genetic transmission, and data from HD models (Dragatsis et al, 1998; Hodgson et al, 1996). A myriad of different mechanisms, both cell autonomous and non-cell autonomous, have been shown to play a role but the relative contribution of most of these pathways to HD pathogenesis is not fully understood.

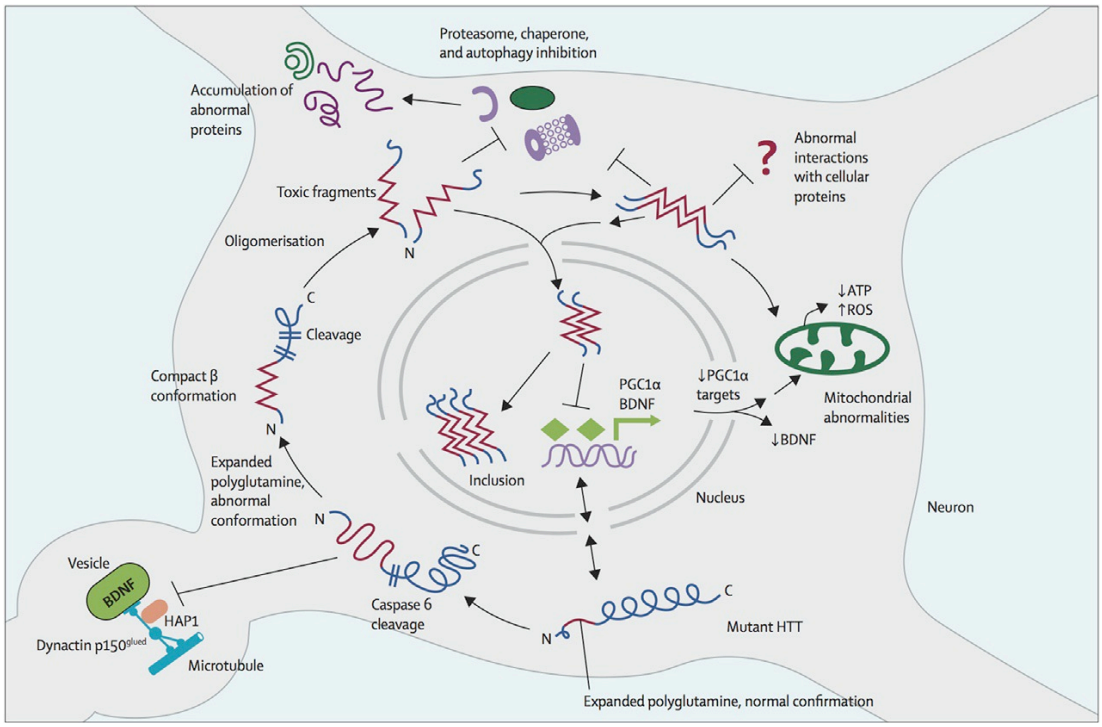


**Figure 1.3: Postulated intracellular pathogenesis of Huntington disease.** ATP, adenosine triphosphate; BDNF, brain-derived neurotrophic factor; HTT, huntingtin; PGC1a, the transcription factor peroxisome proliferator-activated receptor g, coactivator 1a; ROS, reactive oxygen species. (Reproduced from Ross CA, Tabrizi SJ (2011) Huntington's disease: from molecular pathogenesis to clinical treatment. Lancet Neurol 10: 83–98, with permission from Elsevier.)

### 1.2.3 Cell autonomous mechanisms of HD pathogenesis

#### 1.2.3.1 Generation of mutant HTT fragments

Multiple lines of evidence support the "toxic fragment hypothesis" that proteolytic cleavage of mutant HTT liberates toxic N-terminal fragments containing the expanded polyQ tract, which contribute to cell death through accumulation and the additional

activation of further proteolytic caspases (Zuccato et al, 2010). Recent evidence also shows that these short N-terminal fragments arise from alternative splicing of exon 1 of HTT (Sathasivam et al, 2013). Mutant *HTT* transcripts allow read through into intron 1 which has a stop codon at its start, and so on translation an exon 1 fragment is produced (Sathasivam et al, 2013). The smallest N-terminal HTT fragment detected in a mouse model of HD was exactly equivalent to an exon 1 product and exon 1 proteins are known to be highly neurotoxic (Landles et al, 2010).

#### 1.2.3.2 Clearance of mHTT

Two major cellular pathways for degradation of misfolded proteins are the ubiquitin-proteasome system (UPS) and autophagy. Impairment of the UPS has been noted in HD mouse models and human post-mortem brain tissue (Bennett et al, 2007a). In addition, mHTT can interfere with target recognition and impair autophagic clearance (Martinez-Vicente et al, 2010; Qi et al, 2012) (see section 1.4.2.1 for further detail).

#### 1.2.3.3 Post-translational modification of mutant HTT

The expanded PolyQ tract affects the post-translational modification events that are known to occur in wild-type HTT, and these in turn affect mHTT toxicity. Their full significance, interdependence and exact role in any pathogenic mechanism remains largely unknown (Hughes & Jones, 2014).

#### 1.2.3.4 Transcriptional dysregulation

Transcriptional dysregulation occurs before symptom onset in HD, and affects a large number of different transcription factors and regulatory DNA target sequences (e.g. the CREB-binding protein (CBP) (Steffan et al, 2000) and repressor element 1 transcription factor (REST) (Zuccato et al, 2003)). This has been confirmed by DNA microarray studies (Hodges et al, 2006). Mutant HTT has also been shown to inhibit histone acetyltransferase activity, thus leading to the condensation of chromatin and a downregulation of gene transcription. This paves the way for histone deacetylase (HDAC) inhibitors as a potential therapy (Butler & Bates, 2006).

#### 1.2.3.5 Somatic instability and impaired DNA repair

Somatic expansion of the CAG repeat has been shown to occur in the human striatum (Kennedy et al, 2003) and is associated with younger onset, thus may contribute to disease pathogenesis (Swami et al, 2009). Impairment of DNA repair pathways has been implicated in this (Dragileva et al, 2009), and large cohort genetic studies in HD patients have shown that variants in DNA repair proteins affect age of onset (Consortium, 2015) and rate of HD progression (Hensman Moss et al, 2017).

#### 1.2.3.6 RAN translation

A phenomenon known as repeat-associated non-ATG (RAN) translation leads to the expression of expansion proteins from all three reading frames, without an AUG start

codon. Four novel, homopolymeric expansion proteins (polyAla, polySer, polyLeu and polyCys) have been shown to accumulate in HD human brains, particularly in the striatum and white matter. These proteins have been shown to be toxic to neural cells (Bañez-Coronel et al, 2015).

#### 1.2.3.7 Mitochondrial dysfunction

Mutant HTT affects the axonal transport of mitochondria and also has a direct effect on mitochondrial function. Mitochondrial calcium handling is impaired, and transcription of nuclear genes responsible for the proper functioning of this organelle is affected, leading to impaired respiration (Jin & Johnson, 2010). An increase in mitochondrial DNA mutations has also been found in neurons from the cortex of HD patients (Siddiqui et al, 2012; Wang et al, 2013).

#### 1.2.3.8 Excitotoxicity

Injection of quinolinic acid (an NMDA receptor agonist) into the striatum of mouse models recapitulates many aspects of the HD phenotype (Beal et al, 1986). In addition it has now been shown that alterations in glutamatergic signalling occur through changes in glutamate release (Joshi et al, 2009), over activity of glutamate receptors (Benn et al, 2007), decreased levels of glutamate transporters and reduced glutamate uptake (Huang et al, 2010). Increased MSN excitability has also been shown to result from decreased potassium channel expression in mHTT expressing astrocytes (Tong et al, 2014).

#### 1.2.3.9 Cytoskeleton signalling and vesicular trafficking

Through its interactions with huntingtin-associated protein 1 (HAP1), huntingtin-associated protein of 40 kDa (HAP40) and dynein, HTT regulates vesicle transport and recycling (Pardo et al, 2010). Expression of mHTT disrupts this transport, including vesicular trafficking of BDNF (Gauthier et al, 2004; Roux et al, 2012). mHTT aggregates can also physically obstruct subcellular transport due to their large size (Li et al, 2003).

### 1.2.4 Non-cell autonomous mechanisms of HD pathogenesis

#### 1.2.4.1 Loss of neurotrophic (BDNF) support

Loss of BDNF support from cortico-striatal projections may be responsible for the selective MSN degeneration seen in HD, as mHTT is known to interfere with both the expression and trafficking of BDNF (Zuccato et al, 2008).

#### 1.2.4.2 Loss of glial support

Specific astrocytic expression of mHTT leads to a neurological phenotype in mice (Bradford et al, 2009). Furthermore, co-culture experiments have shown that glial

expression of mHTT causes the death of neurons which do not express mHTT (Shin et al, 2005).

#### 1.2.4.3 Trans-neuronal spread

Recently evidence for the non-cell autonomous, trans-neuronal spread of mHTT has come to light. Mutant HTT was shown to spread to wild-type human neurons within an HD mouse model. This was blocked by botulinum neurotoxins, suggesting the involvement of synaptic machinery (Pecho-Vrieseling et al, 2014). Furthermore, post-mortem studies of HD patients who have received experimental treatment with neural stem cell transplantation have revealed the presence of huntingtin inclusions in the grafted donor tissue (Cicchetti et al, 2014).

#### 1.2.4.4 Inflammation

Microglial activation has been demonstrated in HD patients, both in manifest (Pavese et al, 2006) and premanifest disease (Tai et al, 2007). Recent evidence suggests that this is at least in part a cell-autonomous effect, as microglia that express mHTT have been shown to have enhanced transcription of pro-inflammatory factors (Crotti et al, 2014). A peripheral inflammatory response has also been shown with raised levels of pro-inflammatory cytokines found in blood samples of manifest and premanifest HD patients (Bjorkqvist et al, 2008).

## 1.3 Models of Huntington's disease

Research on animal and cell models have given us enormous insights into the pathogenesis of HD. Models also provide an invaluable platform on which to develop and test potential therapeutics. The wide ranges of models available for HD research are detailed below, with particular emphasis on *in vitro* systems.

### 1.3.1 Animal models of HD

Mouse models are among the most common animal models in HD, with the R6/2 mouse the most widely used (Mangiarini et al, 1996). This is a transgenic model which expresses human *HTT* exon 1 carrying around 150 CAG repeats. Its early phenotype onset and rapid disease progression are advantageous. Other N-terminal mouse models include the short-stop line (Slow et al, 2005), the N171-82Q line (Schilling et al, 1999) and the HD line (Laforet et al, 2001). Full length human *HTT* expressing mouse models include the transgenic YAC128 (Slow et al, 2003) and BACHD (Gray et al, 2008) mice. Knock-in mouse models have been generated by inserting expanded CAG repeats into the endogenous mouse *Htt* gene (such as the "Detloff" lines (Heng et al, 2010; Lin et al, 2001)), or by replacing the mouse exon 1 *Htt* with mutated human exon 1 *HTT*, creating a chimera (the "Zeitlin" lines (Menalled et al, 2012; Menalled et al, 2003)). Other mammalian models of HD include transgenic rats expressing truncated (von Hörsten et al, 2003) and full-length (Yu-Taeger et al, 2012) HTT, pigs (Yang et al, 2010), sheep (Jacobsen et al, 2010) and rhesus macaques (Gray et al, 2008). Numerous invertebrate HD models in *Caenorhabditis elegans* and *Drosophila*

*melanogaster* have been designed, which are useful for high-throughput analyses with genetic screens or the testing of compound libraries (Bates & Landles, 2014).

### 1.3.2 Cell models of HD

In vitro models have also helped to decipher new pathways of pathogenesis in HD, and have been useful in validating findings in animal models. Advantages of cell- based experimental systems are the ready supply of cells, the ability to work on human tissue, and suitability for high-throughput and high content analysis. There are a wide range of HD cell models available to the HD community, derived from both animal and human tissue, expressing both full length and exon 1 of the huntingtin gene. A few examples of these are listed in table 1.2. Arguably, the most useful cell models should recapitulate the main features of HD as closely as possible. Although mHTT is expressed throughout the body and causes systemic effects, the main site of pathology is in neuronal cells. Human neural cell models of HD are therefore of particular value, both in terms of elucidating disease mechanisms and testing therapeutics.

**Table 1.2: Cell models used in Huntington's disease.**

| Cell line | Construct | Pathogenic insights |
|---|---|---|
| **Animal cells** | | |
| **PC12:** Rat phaeochromocytoma | Full length 16Q, 48Q, 89Q | mHtt expression leads to cell morphology changes and disruption of cell signalling, mediated by NGF and EGF (Song et al, 2002). |
| **ST14A:** Rat striatal progenitors | *Htt* exon 1 25Q, 47Q and 72Q, with GFP tag | Probability of a cell remaining aggregate free drops exponentially with time (Colby et al, 2006). |
| **HC2S2:** Immortalised rat neural progenitors | *Htt* exon 1-28Q or 74Q, with eGFP tag | mHtt-expressing cells show time-dependent nuclear fragmentation and neuritic degeneration (Dong et al, 2011). |
| **COS-7:** Monkey kidney | eGFP-tagged *Htt* exon 1 with 25Q, 46Q and 97Q | Aggregate/inclusion formation is dynamic, four phase process (Ossato et al, 2010). |
| **Human cells** | | |
| **HEK293T:** Human embryonic kidney | 548 and 151 amino acid fragments of *HTT* with 15Q and 128Q | Toxicity is more affected by the rate of aggregation than the localization (Hackam et al, 1999). |

| | | |
|---|---|---|
| **SK-N-SK:** Human neuroblastoma | pFlag-GFP exon 1 21Q and 72Q with full length *HTT* co-transfection. | Full length HTT reduces cell death in mHTT expressing cells but has no effect on inclusion formation (Ho et al, 2001). |
| **SH-SY5Y**: Human neuroblastoma | Full length 60Q and 150Q-eGFP | ATP synthase alpha suppresses the formation of insoluble inclusions and reduces toxicity (Wang et al, 2009). |
| **hESC:** human embryonic stem cell | HTT exon 1 with 23Q, 73Q and 145Q | Demonstrates quantitative relationship between neurodegeneration and soluble monomeric mHTT levels (Lu & Palacino, 2013). |
| | Full length (knock-in) with 45, 50, 58, 67 and 74Q | Disrupted neurogenesis during development occurs in a CAG-length dependent fashion (Ruzo et al, 2018). |
| **iPSC:** induced pluripotent stem cell | 14 lines generated from controls and HD patients (ranging up to 180Q). | Changes in electrophysiology, metabolism, cell adhesion and cell death occur in HD iPSC derived neural cells (The Hd Ipsc Consortium, 2012). |

#### 1.3.2.1 Fragment and full length mHTT cell models

Both full-length and N-terminal HTT expressing models are useful. Full-length mHTT expressing models more closely reflect the actual cellular physiology of HD. However, N-terminal or exon 1 models give rise to disease phenotypes, for example aggregate formation, on a time-scale more compatible with *in vitro* experiments. There is also good evidence to suggest that mutant HTT exon 1 is the pathogenic species in HD. Post-mortem studies of human brain tissue demonstrate that nuclear and cytosolic inclusions are composed primarily of N-terminal fragments (DiFiglia et al, 1997). The R6/2 mouse over-expressing human HTT exon 1 has the fastest and most aggressive HD phenotype, and has been used extensively in HD research (Mangiarini et al, 1996), and the transgenic expression of mHtt exon 1 has also been shown to produce an HD-like phenotype in non-human primates (Yang et al, 2008). The smallest N-terminal fragment detected by western blotting using a panel of HTT antibodies in a full length mouse model of HD was exactly equivalent to an exon 1 product (Landles et al, 2010). A study in transgenic *Drosophila* engineered to express one of seven naturally occurring N-terminal HTT fragments against a constant genetic background, revealed that the exon 1 peptide is particularly toxic in terms of survival and degeneration of photoreceptor neurons (Barbaro et al, 2015).

A mechanism for generation of mutant HTT exon 1 has been demonstrated in mouse models expressing full length mutant Htt (mouse) and HTT (human) (Sathasivam et al, 2013), and also in patient derived fibroblasts and post-mortem human brain tissue (Neueder et al, 2017); abnormal splicing in the presence of an expanded CAG repeat allows read through into intron 1 which contains a stop codon at its start, producing a

mutant exon 1 fragment on translation. Furthermore, multiple cell models have demonstrated rapid onset of cell toxicity and cell death on expression of mHTT exon 1 (Ho et al, 2001; Miller et al, 2010; Sahoo et al, 2016).

#### 1.3.2.2 HD-iPSC derived models

The discovery that human fibroblasts could be reprogrammed into pluripotent stem cells through the expression of four specific transcription factors (Oct3/4, Sox2, c-Myc, and Klf4) has led to a revolution in cell biology (Takahashi & Yamanaka, 2006). Induced pluripotent stem cells (iPSCs) have been generated from HD patient fibroblasts (Park et al, 2008), and subsequently differentiated into neurons, including MSNs (Arber et al, 2015; Delli Carri et al, 2013). Such models perhaps most closely reflect the disease state. Stem cells and iPSC-derived neurons have been shown to demonstrate enhanced lysosomal activity (Camnasio et al, 2012). Aggregate formation also occurs, but only on the addition of a stressor (Jeon et al, 2012). More recently HD iPSCs have been shown to have impaired neurogenesis compared to control cells (Conforti et al, 2018).

One issue with iPSC research is the genetic heterogeneity that occurs between patient derived cell lines, making it difficult to draw comparisons between them (although very recently, a genetic allelic series of isogenic human embryonic stem cell (hESC) lines with graded increases in CAG repeat length has been engineered (Ruzo et al, 2018)). Neuronal differentiation protocols for iPSCs are also currently rather long and complex (Delli Carri et al, 2013), making this cell type less suited to high throughput studies;

although with improvements in iPSC culture techniques, and better high content screening platforms, this is likely to change in the near future.

## 1.4 HTT protein aggregation, trafficking and clearance

### 1.4.1 Mutant HTT aggregation and its role in disease pathogenesis

Many neurodegenerative diseases have protein aggregates as a cardinal feature, for example amyloid inclusions derived from amyloid precursor protein (APP) in Alzheimer's disease, and alpha synuclein in Parkinson's disease. In HD, mHTT positive inclusions are found in the nuclei and neurites of patient derived brain tissue (DiFiglia et al, 1997). Inclusion frequency and rate of formation are polyglutamine length dependent, and inclusion size increases with disease duration (Hughes & Jones, 2014). At the structural level, pathological polyQ expansion in exon 1 triggers the formation of antiparallel-β-rich and detergent resistant filamentous aggregates, similar to amyloid fibrils (Hoffner & Djian, 2014). Mutant HTT fragments are able to fold into different conformations under different conditions such as their phosphorylation state (Caron et al, 2014) or surrounding temperature (Nekooki-Machida et al, 2009).

The definitive role of these inclusions (whether toxic or protective) has not yet been established. Toxicity is suggested by experiments showing that the reduction of aggregate formation in mice correlated with improvements in phenotype (Labbadia et al, 2011; Labbadia et al, 2012). Inclusions are thought to sequester and decrease

levels of essential cellular proteins such as transcription factors (Schaffar et al, 2004), chaperones (Park et al, 2013) and nuclear-cytoplasmic transport machinery (Woerner et al, 2016), and mHTT aggregates can also physically obstruct subcellular transport due to their large size (Li et al, 2003). However, in human HD brains, the distribution of aggregates does not correspond to sites of known pathology (Gutekunst et al, 1999), and MSNs which are the most vulnerable cell type in HD have no or few aggregates (Kuemmerle et al, 1999). A transgenic mouse model expressing an N-terminal mHTT fragment with exon 1 and 2 develops many inclusions but does not display any neuronal dysfunction (Slow et al, 2005). Longitudinal survival studies of primary neurons expressing fluorescently tagged mHTT exon 1 showed that the formation of inclusions in particular neurons correlated with neuronal survival (Arrasate et al, 2004).

The location of aggregates may be important; R6 mouse lines with >200 CAG repeats show mHTT localised to the cytoplasm and have a much milder phenotype with later disease onset than R6 lines with <200 CAG repeats (Dragatsis et al, 2009; Morton et al, 2009). This contrasts with the findings of Woerner et al who showed that cytoplasmic rather than nuclear accumulation of fibrillar amyloid aggregates in HEK293T cells led to increased toxicity (Woerner et al, 2016). It may be possible that distinct structural forms of HTT aggregates may be of differing importance in terms of their relative contribution to cell toxicity (Caron et al, 2014; Nekooki-Machida et al, 2009). Another recent study that reconciles these differing views of IB toxicity shows that the formation of HTT IBs triggers a state of cellular quiescence and redirects cells from fast apoptosis to a slower cell death by necrosis, as a result of co-aggregation with other proteins (Ramdzan et al, 2017).

### 1.4.2 Cellular mechanisms for protein clearance: the UPS and autophagy

There are two major pathways for the degradation of proteins in eukaryotic cells. The ubiquitin-proteasome system (UPS) clears the majority (80-90%), mostly comprising soluble and short-lived or damaged proteins. Autophagy primarily removes long-lived or aggregated proteins, and damaged organelles. Both pathways are critical for the maintenance of cellular homeostasis, and their activities are tightly regulated (Lilienbaum, 2013).

Degradation of a protein via the UPS involves two successive steps; firstly conjugation of a minimum of four K48-linked ubiquitin (Ub) monomers to the substrate followed by degradation of the tagged protein by the downstream 26S proteasome complex (Glickman & Ciechanover, 2002). This consists of a 20S proteolytic particle and one or two 19S regulatory particles. The cylindrical 20S proteasome is a hollow four-ring structure that contains in each of its central β-rings three types of active sites, which are chymotrypsin-like, trypsin-like, and caspase-like in specificity. Its outer α-rings contain a gated channel for substrate entry. The 19S regulatory particle performs many functions, including binding and disassembly of the Ub chain, ATP hydrolysis, and the unfolding and translocation of the substrate into the 20S core (Kim & Goldberg, 2017).

Autophagy is a conserved pathway that delivers cytoplasmic contents to the lysosome for degradation, by means of double-membraned vesicles called autophagosomes. The first step is the formation of a double-membraned, cup-shaped autophagosome precursor (the phagophore), that engulfs substrates as its edges extend. After the phagophore edges close to form a vesicle, the completed autophagosomes traffic

along microtubules to enable autophagosome-lysosome fusion, which leads to the degradation of its contents by lysosomal hydrolases (Menzies et al, 2017).

#### 1.4.2.1 The UPS and autophagy in HD

Impairment of the UPS has long been considered an attractive hypothesis for neuronal dysfunction in HD. Inclusion bodies in HD mouse models and patient brains are rich in ubiquitin and proteasome components, suggesting that the UPS may be affected. However, studies into UPS function in HD have yielded conflicting results. Accumulation of polyubiquitin chains and increased levels of monoubiquitinylated histone H2A have been reported in HD mouse tissues (Bett et al, 2009a). Assays of proteasome activity showed normal or increased activity in brain extracts of an HD mouse model (Díaz-Hernández et al, 2003), however, human post-mortem HD brains have shown diminished core proteasome activity (Seo et al, 2004). In support of a general blockade of UPS-dependent protein degradation, it has been shown that the presence of a mutant polyQ tract can hinder a protein's proteasomal degradation (Holmberg et al, 2004), and it has also been reported that eukaryotic proteasomes are unable to degrade polyglutamine tracts (Venkatraman et al, 2004). However, Pratt et al have demonstrated that polyglutamine tracts *are* degraded efficiently by eukaryotic proteasomes (Pratt & Rechsteiner, 2008), and this was supported by the finding that mHtt exon 1 was completely digested by mammalian proteasomes (Juenemann et al, 2013).

These conflicting results raise the possibility that mutant polyQ tracts may exert different effects on the UPS depending on expression levels, subcellular localisation

and cell-type. Since the UPS is a highly ATP-dependent system (Schrader et al, 2009), defective mitochondria transport that is known to occur in HD neurons (Reddy & Shirendeb, 2012) may lead to ATP deficiency in neurites and nerve terminals, thus impeding the local degradation of mHtt by the proteasome in these subcellular regions (Zhao et al, 2016). Upregulation of the UPS is an attractive therapeutic avenue in HD, and the overexpression of ube3a, an ubiquitin E3 ligase, can activate the UPS and decrease mHtt aggregates in the brains of HD knock-in mice (Bhat et al, 2014).

A role for autophagy in the clearance of mHTT aggregates is indicated by studies showing that upregulation of autophagy leads to a reduction of mHTT aggregates (Qin et al, 2003; Sasazawa et al, 2015). On the other hand, mHtt compromises autophagy by perturbing cargo recognition and autophagosome motility (Martinez-Vicente et al, 2010; Wong & Holzbaur, 2014). Using an optical pulse-chase method, Tsvetkov et al have shown that abnormally expanded polyQ peptides are specifically recognised and targeted for degradation, in a process particularly dependent on autophagy. Faster clearance of mutant polypeptides correlated with longer neuronal survival, and speed of clearance varied between neuronal subtypes which may help explain the selective MSN vulnerability observed in HD (Tsvetkov et al, 2013).

### 1.4.3 Trafficking of HTT and mHTT

Much can be inferred about the trafficking of HTT from its myriad functions; its role in neuronal vesicle trafficking and axonal transport, mitochondrial trafficking, control of synaptic activity, and transcriptional regulation. It is likely that HTT shuttles between different cellular compartments to facilitate these processes. An understanding of how

the trafficking of mutant HTT differs from that of the wild type protein may lend insights into which mechanisms are most important in triggering the neurodegeneration seen in HD.

Initial studies into the subcellular location of HTT found differences between mutant and wild type forms (Gourfinkel-An et al, 1997), though results were often conflicting. Various cell culture models found huntingtin in the cytoplasm but not in the nucleus (Persichetti et al, 1995; Trottier et al, 1995). N-terminal fragments of mutant huntingtin formed aggregates in the cytoplasm and the nucleus, but full-length huntingtin with either normal or expanded repeats was localised to the cytoplasm (Cooper et al, 1998). Further immunofluorescence studies found that full-length wild type Htt could be detected in the nucleus of multiple mammalian cell lines (De Rooij et al, 1996; Dorsman et al, 1999), but that in HD autopsy brain, neuronal intra-nuclear inclusions could only be detected by N-terminal antibodies (Dorsman et al, 1999). Subcellular fractionation studies confirmed the presence of huntingtin in the nucleus of human skin fibroblasts (De Rooij et al, 1996). These early studies may have been hampered by the lack of well characterised antibodies and by working in non-human and/or non-neuronal cells.

More recent studies have shown that the trafficking of HTT is dependent on the cell context. Under normal conditions, the huntingtin N-terminal is thought to be a membrane binding domain that can reversibly target to the endoplasmic reticulum (ER) and vesicles. On ER stress, huntingtin dissociates and enters the nucleus(Atwal et al, 2007). Nuclear huntingtin also increases at certain points during the cell cycle (Martín-Aparicio et al, 2002), and localises to the mitotic spindle during cell division (Godin et

al, 2010). Within the nucleus, huntingtin has been localised to chromatin (Benn et al, 2008). Stress dependent phosphorylation at Ser13 and Ser16 targets full-length HTT to chromatin-dependent sub-regions of the nucleus, the mitotic spindle and cleavage furrow during cell division (Atwal et al, 2011). Huntingtin has also been shown to transport to the nuclear compartment during the meiotic stage of spermatogenesis (Im et al, 2014).

In response to reactive oxygen species (ROS) stress the N17 domain undergoes structural change, resulting in HTT dissociation from the ER membrane, increased N17 phosphorylation, and nuclear targeting (DiGiovanni et al, 2016). Using novel chromobodies, HTT was shown to localise to sites of DNA damage, where it acts as a scaffold for proteins of the DNA damage response pathway, and this process is deficient in HD patient fibroblasts (Maiuri et al, 2017). HTT also localises to early endosomes and forms cytosolic puncta, termed huntingtin stress bodies (HSBs) as part of a rapid cell stress response, and this is associated with the arrest of endosomal trafficking which conserves ATP use. Mutant HTT displays defective recovery from this stress response (Nath et al, 2015).

As HD progresses, shuttling of HTT in and out of the nucleus may become disrupted, leading to its accumulation in the nucleus. HTT is known to contain a nuclear localisation signal (NLS) near its N-terminus, between aa 174-207 (Desmond et al, 2012). This may explain the rapid pathology in the R6/2 mouse, which expresses amino acids 1-81 of Htt and does not contain the NLS. This small fragment may be able to pass unrestricted into the nucleus by diffusion through the nuclear pore complex (NPC), whereas larger proteins require an NLS to enter using a facilitated

diffusion mechanism. With CAG repeat lengths >200 in the R6/2 mouse, nuclear localisation is inhibited due to the larger fragment size, and lack of the NLS. This may account for the amelioration in toxicity that is seen. Huntingtin also contains two nuclear export signals (NES), one at its C-terminus (Xia et al, 2003) and one within the N17 domain (Maiuri et al, 2013).

## 1.5 Aims of this project

The first goal of my PhD work was to create a HTT allelic series human neuronal cell model of Huntington's disease, in which the effects of increasing CAG-repeat length could be assessed against a fixed genetic background. Three different approaches were used:

1. Knock-in of different CAG repeat lengths (50Q, 80Q and 125Q) into the endogenous *HTT* gene locus of a human NSC line using recombinant adeno-associated virus (AAV). This would create a truly isogenic cell series in which the mHTT is expressed at physiological levels; however ultimately this approach was not successful.

2. Optimisation and validation of a transgenic human NSC allelic series that overexpresses HTT exon 1 with 29, 71 and 129 CAG repeats. NSCs were differentiated into immature neurons for further experiments.

3. Generation of an iPSC panel from siblings who have JHD and carry mutations with 56, 67 and 73 CAG repeats respectively, and their unaffected mother. iPSCs were differentiated into MSNs using established protocols.

The second part of my PhD work aimed to use the models generated to:

1. Investigate the effect of HTT exon 1 with increasing CAG repeat lengths on cell differentiation and morphology, cell viability and response to cell stress.

2. Study the effect of increasing CAG repeat length on HTT aggregation, and response to UPS and autophagy inhibitors.

3. Assess the ability of a novel proteasomal activator to clear mHTT from exon 1 overexpressing NSCs.

4. Study the differences in the trafficking of huntingtin protein in MSNs derived from related control and JHD iPSCs.

# 2 Materials and Methods

Sigma-Aldrich laboratory chemicals, Gibco cell culture reagents, Nunc cell culture plasticware and Invitrogen molecular biology reagents were used throughout unless stated otherwise.

## 2.1 Cell culture

### 2.1.1 Neural stem cell culture

The ReNcellVM neural stem cell (NSC) line was obtained from ReNeuron. The line was originally derived from ten-week gestation foetal midbrain, in accordance with national ethical and legal guidelines, and immortalised by transduction with the v-myc oncogene (Donato et al, 2007; Pollock et al, 2006). The STROC05 human NSC line was also provided by ReNeuron. The cells were originally isolated from twelve-week gestation whole ganglionic eminence and transfected with a retroviral vector encoding the conditional immortalization gene cmyc-ER$^{TAM}$ (El-Akabawy et al, 2011).

Both NSC lines were grown as a monolayer on laminin coated plasticware in NSC medium (appendix A.1.1). To maintain STROC05 proliferation in the stem cell state, 4-hydroxy-tamoxifen (4-OHT) at 0.1 nM was added to the NSC medium. For routine culture, cells were seeded at a density of $1.2x10^4$ cells/cm$^2$. Flasks were pre-coated with 10 µg/ml mouse laminin-1 [Culturex PathClear; Trevigen] in cold Dulbecco's

Modified Eagle's Medium (DMEM): Nutrient Mixture F-12 (F12), incubated at 37°C for a minimum of 2 hrs, and washed with warm DMEM:F12 just prior to use.

NSCs required media change every 3-4 days and were passaged at 80-90% confluence. To passage, cells were washed with Hank's Balanced Salt Solution (HBSS), and trypsinised using Trypzean-EDTA [Lonza] that was added in sufficient volume to coat the surface of the flask and incubated at 37°C, 5% $CO_2$ for 5 min. The equivalent volume of defined trypsin inhibitor (DTI) was added to the flask, and the cells were triturated and transferred to a Falcon tube for centrifugation at 300 x*g* for 5 mins at room temperature. The resulting cell pellet was re-suspended in warm NSC media, and the cells counted with a haemocytometer prior to re-seeding into laminin coated plasticware.

### 2.1.2 Freezing and storage of neural stem cells

Both ReNcellVM and STROC05 cells were frozen in cryovials of at least 1 million cells, in 1 ml of NSC media containing 10% dimethyl sulfoxide (DMSO). The vials were placed into a Mr. Frosty™ Freezing Container [Nalgene] and into the freezer at -80°C for at least 2 hrs, and then transferred to liquid nitrogen for long-term storage.

### 2.1.3 Differentiation of neural stem cell lines

On reaching 90% confluence, ReNcellVM NSCs were media changed into differentiation medium (appendix A.1.2) supplemented with 2 ng/ml glial cell-derived

neurotrophic factor (GDNF) [Peprotech] and 0.5 mM dibutyryl cyclic adenosine monophosphate (cAMP) [Calbiochem]. Differentiating cell cultures were media changed every 3-4 days. After two weeks, the differentiation medium was no longer supplemented with GDNF or cAMP, and a lower L-glutamine concentration of 0.5 mM was used. ReNcellVM neurons have been maintained in this long-term differentiation media for over six weeks, with media changes every 3-4 days.

STROC05 NSCs were differentiated on reaching 80-90% confluence; the differentiation medium was supplemented with 1 μM purmorphamine [Calbiochem]. Cells were media changed every 3-4 days until seven days post-differentiation, the media was switched to Neurobasal medium supplemented with 1 x B27 supplement [Invitrogen], 2mM L-glutamine, 10ng/ml bFGF and 1 μM purmorphamine. At fourteen days post start of differentiation Neurobasal medium supplemented with 1x B27 supplement, 2 mM L-glutamine and 1μM purmorphamine was used to media change the cells. Cells were analysed at 21 days post-differentiation. This protocol is adapted from El-Akabawy et al 2011 (El-Akabawy et al, 2011).

### 2.1.4 Antibiotic kill curves

NSCs were seeded at the usual cell density into laminin coated 6-well plates. Puromycin was added to the culture medium after 24 hrs to achieve a range of final concentrations between 0-150 ng/ml. The cells were observed and percentage confluence of the wells recorded at the same time every day for one week. The minimum concentration of antibiotic needed to kill wild-type cells over 3-4 days was determined.

### 2.1.5 Human embryonic kidney cells (HEK-293T) culture

Human embryonic kidney (HEK) cells were obtained from ReNeuron. Cells were seeded at 8 x $10^4$ cells/$cm^2$ and grown as a monolayer on untreated plasticware in HEK culture medium (appendix A.1.3). Cells were passaged at 80-90% confluency. Spent culture medium was aspirated and discarded. An appropriate volume of warmed TrypZean-EDTA [Lonza] sufficient to cover the surface area of the flask was added, and the flask incubated for 5 mins at 37°C; 5%$CO_2$. An equal volume of warmed HEK293 medium was added, followed by gentle trituration. The cell suspension was transferred to a Falcon tube and centrifuged at 300 x*g* for 5 mins at room temperature. The cell pellet was resuspended in media, cells counted using a haemocytometer (or a 1:10 split ratio), and reseeded.

### 2.1.6 HCT116 human colon adenocarcinoma cell line culture

HCT116 cells were obtained from ReNeuron. Cells were seeded at a density of 5 x $10^4$ cells/$cm^2$ and grown as a monolayer on untreated plasticware in HCT116 medium (appendix A.1.4). Post seeding, flasks were placed in the incubator at 37°C; 5%$CO_2$ and media changed every 2-3 days. Cells were passaged at 80-90 % confluency, as described above for HEK cells, but using HCT116 medium in lieu of HEK medium. Following resuspension of the cell pellet, cells were counted using a haemocytometer (or a split ratio of 1:10-1:20), and reseeded.

### 2.1.7 Mycoplasma testing

All cell lines were tested for the presence of mycoplasma immediately post thawing, and also routinely during passage to ensure no contamination. Spent media was tested using the LookOut Mycoplasma PCR Detection Kit [Sigma].

## 2.2 Induced pluripotent stem cells (iPSCs)

Fibroblasts were derived from skin biopsies taken from three siblings who have juvenile HD and carry *HTT* mutations with 56, 67 and 73 CAG repeats respectively, and their mother who is an unaffected control.

### 2.2.1 Consent and ethics

All skin biopsies were performed in accordance with the Declaration of Helsinki and approved by the University College London (UCL)/UCL Hospitals Joint Research Ethics Committee (LREC 03/N008, amendment 16). The subjects were recruited through the Huntington's disease clinic at the National Hospital for Neurology and Neurosurgery, London. All subjects provided informed written consent.

### 2.2.2 Skin biopsy procedure

Two adjacent 3 mm punch biopsies were taken from each subject's forearm using a sterile 3 mm biopsy punch blade [Medline]. 0.5 ml 1% lignocaine with 1/10000 adrenaline was used as local anaesthetic and injected subcutaneously using a 25G needle 5 mins prior to the procedure. The full thickness skin specimen was placed directly into a sterile container with fibroblast medium. Pressure was applied using gauze to the biopsy site for 10 mins and the wound closed using steristrips. A sterile dressing was then applied; no sutures were required. A follow up telephone call was made to the subject 24 hrs later to ensure that no complications had developed. In all cases the skin sample arrived in the laboratory within 2 hrs, and was kept at room temperature during transport.

### 2.2.3 Fibroblast culture

Each skin sample was cut into squares of 0.5-1 $mm^2$ and placed epidermis side up into one well of a 6-well plate containing two drops of warm fibroblast medium (appendix A.1.5) with 2.5 ml/L amphotericin B [Sigma], which was added for the first two weeks of culture. A sterile coverslip was placed over the pieces of tissue to help them adhere to the plate, and then a further 2 ml warmed medium was added to the well, making sure not to dislodge the coverslip. The plate was placed undisturbed in the incubator at 37°C; 5%$CO_2$ for two days, taking care not to jolt the incubator at all. After this time the plate was checked for infection.

One week after plating the biopsy, the media was changed; at this point epithelial cells were seen surrounding the skin piece and fibroblasts emerging beyond them. Henceforth, cells were media changed every 3-4 days. After two weeks the cells were passaged. The spent media was removed and the cells washed with 2 ml PBS, ensuring that it reached under the coverslip. One millilitre of 0.05% Trypsin-EDTA [Gibco] was added for 5 mins at 37°C and, after checking that the fibroblasts had dissociated (epithelial cells do not transfer), an equal volume of fibroblast medium was added. The cells were triturated and transferred to a 15 ml Falcon tube, taking care not to transfer any pieces of skin. The cells were centrifuged at 300 x*g* for 5 min. The cell pellet was resuspended in 1ml of medium, and cells counted using a haemocytometer. The cells were then reseeded into uncoated flasks at a density of $1x10^4$ cells/$cm^2$ with an appropriate volume of medium (without amphotericin B).

Fibroblasts were expanded and frozen down at passage 3, 4 and 5. Half a million cells were frozen per cryovial [Corning] in 1ml of fibroblast medium containing 30% additional FBS and 10% DMSO. Vials were stored in liquid nitrogen.

### 2.2.4 Induced pluripotent stem cell (iPSC) generation

Vials of frozen fibroblasts were sent to Professor Ali Brivanlou at the Laboratory of Stem Cell Biology at Rockefeller University. The cells were used to generate iPSCs by Sendai virus reprogramming using the CytoTune-iPS 2.0 Sendai reprogramming kit. These were verified by the expression of pluripotency markers, differentiation into all germ layers using a self-organisation assay, karyotyping, Sanger sequencing to

confirm the CAG repeat length and confirmation of the absence of exogenous Sendai virus. Three different clones of iPSCs were generated from each subject.

### 2.2.5 Induced pluripotent stem cell (iPSC) culture

This protocol was adapted from Shi et al 2012 (Shi et al, 2012). iPSCs were cultured on Geltrex coated 6-well plates in Essential 8 medium containing Essential 8 supplement (10ml 50X supplement was added to 500ml Essential 8 medium to make Essential 8 medium+ (E8+)). To coat the plates, 1 ml 1:100 Geltrex:cold sterile DMEM:F12 was used per well of a 6-well plate, and plates were incubated at 37°C for a minimum of 1 hr prior to use. One vial of frozen iPSCs was thawed into one well of a 6-well plate. The vial was removed from liquid nitrogen and immersed in a water bath at 37°C (without submerging the cap). Once thawed, cells were immediately transferred into a sterile 15ml falcon tube and 10mls of E8+ at room temperature was added drop-wise. The cells were centrifuged at 200 x*g* for 5 mins. The supernatant was discarded and the cell pellet resuspended in 2 ml of E8+ by gentle pipetting. Following removal of the Geltrex solution from the pre-coated Geltrex well, this iPSC cell suspension was added drop-wise to the well, and cells dispersed across the well surface with gentle side to side motion. The plate was then placed in the incubator at 37°C; 5% $CO_2$ and full media changes carried out daily with E8+ until cells reached 85% confluency.

iPSCs were passaged when reaching 80-85% confluency, or when individual colony size became too large or too dense, or on the appearance of morphologically different cells that were starting to differentiate. Generally a split ratio of 1:6 was used. For cells

undergoing passage, spent medium was aspirated and cells rinsed in 2 ml D-PBS. One millilitre of 0.5 mM EDTA in D-PBS was added and cells incubated at 37°C for 3-4 mins. When iPSCs appeared to separate and become phase bright, the EDTA was aspirated. Two millilitres of E8+ was added to the cells and titurated gently, and the cell suspension was then made up to the appropriate volume with further E8+. The suspension was then added drop-wise to a pre-coated Geltrex plate (removing the Geltrex solution just prior to plating), with a final volume of 1.5 ml per well. The plate was returned to the incubator with daily media changes thereafter. Generally iPSCs needed to be passaged every 4-5 days.

For freezing and storage of iPSCs, the procedure was carried out as for iPSC passage described but following aspiration of EDTA, 1 ml of ice cold E8+ with 10% DMSO was added per well to titurate the cells. The suspension was transferred to a cryovial and placed in a Mr Frosty™ Freezing Container [Nalgene] at -80°C, with transfer to liquid nitrogen the next day for long term storage.

### 2.2.6 Medium spiny neuron (MSN) differentiation

On reaching 80% confluence with appropriate colony sizes and cell morphology, iPSCs were passaged from one well of a 6-well plate into six wells of a 12-well plate. iPSCs were maintained in this format until reaching 80-90% confluency, after which MSN differentiation was commenced. Spent media was removed and iPSCs washed with D-PBS. Two millilitres per well of room temperature N2B27 differentiation medium (appendix A.1.6) supplemented with SMAD inhibitors: 100 nM LDN (1:5000), 10 μM SB431542 (1:1000) and 200 nM dorsomorphin (1:5000) was added. Cultures were

maintained in this medium until passage 1, with half volume media changes on alternate days.

An initial passage was carried out at dd9 (though this could be delayed to dd12 for less developed cultures), at a ratio of 2:3 onto fibronectin coated 12-well plates. Fresh plates were coated with 0.5 ml per well of 25 µg/ml fibronectin solution in D-PBS (1:40), incubated at 37°C for at least 1 hr and washed with D-PBS prior to use. One hr prior to passaging, spent media was removed from the cells and replaced with 1.5 ml N2B27 differentiation medium (appendix A.1.6) supplemented with 25 ng/ml (1:4000) activin A and 10 µM ROCK inhibitor (1:1000) and incubated at 37°C. After 1 hr, this "conditioned" media was removed into a falcon tube and the cells were washed with D-PBS. 0.5 ml 0.02% EDTA was added for 1 minute at 37°C. The EDTA was aspirated and the conditioned media was added to the cells at a volume of 1 ml per well. The well surface was then scratched with the tip of a 10 ml serological pipette held upright to generate large clusters of cells, as shown in scratch pattern 1 (figure 2.1). The cells were collected into a sample tube and made up to an appropriate volume to achieve a 2:3 split ratio, using the remainder of the conditioned media plus fresh N2B27 with activin A and ROCK inhibitor as above. After removing PBS from the fibronectin coated plates, the cell suspension was distributed drop-wise into the new 12-well plate at a volume of 1.5 ml per well. The day following this passage, 1 ml medium was replaced with 1.5 ml fresh N2B27 medium containing activin A but no ROCK inhibitor. Half volume media changes were carried out on alternate days, thereby gradually diluting out the ROCK inhibitor.

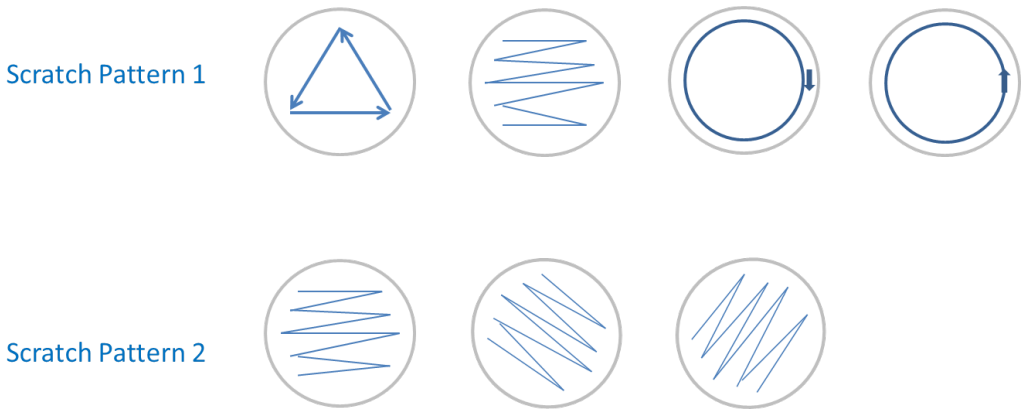


**Figure 2.1**: **Scratch patterns used in passage 1 and passage 2 respectively during MSN differentiation.**

A second passage was carried out between dd19-dd22, at the neural progenitor cell stage. Cultures were observed to be multi-layered with occasional rosette formation. Cells were passaged at a ratio of between 1:1 and 1:4 onto poly-D- lysine/laminin coated plates; commonly cells were plated into 6-well plates or 10 cm dishes at this stage. To coat, 1 ml per well of a 6-well plate of 0.01% poly-D-lysine in $dH_2O$ was added and the plate incubated at 37°C for at least 2 hrs. Plates were then washed with sterile $dH_2O$ and 1 ml of 20 µg/ml laminin diluted in cold DMEM-F12 was added and further incubated at 37°C for at least 1 hr. Spent media was aspirated from the cells undergoing passage, and the cells washed in D-PBS. 0.5 ml 0.02% EDTA was added directly to the cells and incubated for 1-2 mins at 37°C. EDTA was aspirated and 1ml of N2B27 medium with activin A was added to each well. The well surface was scratched with the tip of a P1000 pipette, to generate small clusters of cells, as shown in scratch pattern 2 (figure 2.1). The cell clusters were collected into a falcon tube and resuspended by tituration with a 5 ml stripette. The cell suspension was made up to an appropriate volume with further N2B27 medium with activin A, and reseeded at a

volume of 2 ml per well of a 6-well plate, or 10 ml in a 10 cm dish. Half volume media changes were carried out with N2B27 medium with activin A on alternate days.

At dd26 a half volume media change with N2B27 media with vitamin A (see appendix A.1.6) supplemented with activin A (25 ng/ml), 20 ng/ml BDNF and 20 ng/ml GDNF was carried out. Thereafter cultures were maintained in N2B27 media with vitamin A with added activin A, 10 ng/ml BDNF and 10 ng/ml GDNF, changing half the volume of media on alternate days. This was continued up to and including at least dd35. As reported by Arber et al (Arber et al, 2015), by dd35 80% of cells are neuronal (NeuN+), of which 80% display CTIP2 staining and 40-60% are DARPP32 positive. Neurons have been cultured up to 150 days (*personal communication)*.

## 2.3 Molecular biology

### 2.3.1 RNA extraction

Spent media was removed from a confluent T25 flask and the cells washed with HBSS. TRIzol 2.5 ml was added (1 ml per $cm^2$) and the cells lysed directly in the flask by trituration. One ml of the suspension was transferred to an Eppendorf tube and incubated for 5 mins at room temperature. 0.2 ml chloroform was added, and the tube shaken for 15 sec, followed by further incubation for 2-3 mins at room temperature. The sample was centrifuged at 12,000 x*g* for 15 mins at 4°C. The colourless, upper aqueous phase of this sample containing the RNA was removed and placed into a new tube. 0.5 ml of 100% isopropanol was added and incubated for 10 mins at room

temperature. The sample was centrifuged at 12,000 x*g* for 10 mins at 4°C. The supernatant was removed and the RNA pellet was washed: 1ml of 75% ethanol was added, the sample vortexed and centrifuged at 7500 x*g* for 5 mins at 4°C. The wash was discarded and the pellet air dried for 5-10 min. The pellet was resuspended in 50 µl of RNase-free water, incubated at 55°C for 15 mins and then stored at -70°C. Prior to storage, the concentration of RNA was determined using a NanoDrop microspectrophotometer.

### 2.3.2 cDNA synthesis

cDNA was generated from RNA using SuperScript II Reverse Transcriptase. One µl random primers (50-250 ng), 1 µl 10 mM dNTP mix and 1 ng – 5 µg of extracted RNA were added to a nuclease free microcentrifuge tube and made up to 12 µl with RNase/DNase-free water. The mixture was heated to 65°C for 5 min, quick-chilled on ice and briefly centrifuged. Four microlitres 5X First Strand Buffer and 2 µl 0.1M dithiothreitol (DTT) was added, the contents mixed gently and incubated for 2 mins at room temperature. One microlitre of SuperScript II RT was added and mixed by pipetting. The reaction mixture was incubated as follows: 10 mins at 25°C, 50 mins at 42°C, and 15 mins at 70°C.

### 2.3.3 PCR for huntingtin gene

Using primers against the *HTT* sequence, (to amplify bp 153-449 and bp 9171-9361) polymerase chain reaction (PCR) was undertaken on cDNA using REDTaq DNA Polymerase kit [Sigma]. 25 µl of REDTaq ReadyMix, 2.5 µl of forward primer (0.5 µM),

2.5 µl of reverse primer (0.5 µM), 1 µl of template cDNA was added to a reaction tube and made up to 50 µl using water. PCR cycling conditions were: 94°C for 1 min, 55°C for 1 min, 72°C for 2 mins for 35 cycles. The reaction was visualised on a 1% agarose gel (1 g agarose, 100 ml 1x Tris/Borate/EDTA (TBE) buffer and 10 µl ethidium bromide).

### 2.3.4 DNA purification

DNA was purified using Gene Elute Blood Genomic DNA Kit [Sigma]. This was undertaken prior to mycoplasma testing of spent media, and on PCR reactions on DNA bands extracted from agarose gel.

## 2.4 Western blotting

### 2.4.1 Protein extraction

Cell pellets for western blotting and HTT quantification were prepared: a confluent cell culture flask was washed with HBSS, trypsinised and an equal volume of DTI added after 5 min. The resulting cell suspension was transferred to a 15ml Falcon tube and centrifuged at 300 x*g* for 5 min. The cell pellet was resuspended in 1 ml of phosphate-buffered saline (PBS) with 1x protease inhibitor (PI) cocktail [Roche], centrifuged again, the supernatant discarded and the pellet snap frozen and stored at -80°C.

Cell pellets were thawed on ice and resuspended in 100 µl lysis buffer (appendix A.3) with 1/1000 benzonase 250 U\µl [Novartis]. The protein concentration of each sample was measured using the Bradford assay [Bio-Rad]. In a 96-well plate reader, 200 µl of x1 Bio-Rad reagent was added to 10 µl of a 20-fold dilution (in PBS) sample, and also to a series of protein standards of known concentration between 0-500 µg/ml, and the plate read using Tecan, X-Fluor 4. A standard curve was plotted and the concentrations of samples calculated against this.

### 2.4.2 Western blotting procedure

Lysates were diluted to 1 mg/ml using lysis buffer. When blotting for HTT protein a methanol precipitation step was included. One hundred microlitres of each sample (containing 100 µg of protein) was added to 900 µl of ice cold methanol in a 1.5ml Eppendorf tube and incubated at -20°C for at least 30 mins (the methanol precipitation step is used to remove lipids, unfolded proteins and Triton X). The samples were then centrifuged for 10 mins at 4°C at 18,000 x*g*. The methanol was then poured off and the resulting pellet air-dried for 20 min.

100 µl of 1x sample buffer (appendix A.3) was added to each dried sample pellet, incubated on a shaking heater at 95°C, 800 rpm for 10 min, and checked to ensure the pellet had dissolved. Twenty microlitres per sample and 10 µl LI-COR Chameleon molecular weight marker was loaded onto a Novex 12% Tris-Glycine gel (or when blotting for HTT a gradient 12-20% Tris-Glycine gel) which was first clamped into the Invitrogen Novex Mini-Cell Gel tank and filled with running buffer (appendix A.3). The tank was connected to a power pack and the gel was run at 90 V until the samples

lined up at the edge of the gel stack (after approximately 10 min) and then increased to 150 V to run for at least 1 hr or longer.

The gel was then carefully removed from the gel running apparatus and covered with nitrocellulose membrane for protein transfer, then layered into the transfer apparatus with sponges and Whatmann filter paper soaked in 1x transfer buffer (appendix A.3). The transfer apparatus was then clamped into the tank and filled up with transfer buffer. The transfer stack was connected to the power pack and run at 35 V for 2 hrs, or at 15 V overnight. The membrane was then removed from the transfer apparatus and washed in 1x PBS on a gentle shake to remove any buffer.

The membrane was blocked in 8 ml Odyssey Blocking Buffer (LI-COR Biosciences) for 1 hr at room temperature in a staining tray placed on a shaking platform. Primary antibody was added directly to the blocking buffer and incubated at 4°C overnight (with continual shaking). Primary antibody was washed off with 0.1% PBS Tween-20 (PBST), using five 10 ml washes over 30 min, with shaking throughout. Secondary antibodies were added to the membrane in 8 ml blocking buffer, and incubated for 1 hr at room temperature in the dark with gentle shaking. Unbound secondary antibody was removed with three washes in 0.1% PBST over 20 min, with shaking throughout. The primary and secondary antibodies used are listed in appendix table A.1.

The membrane was visualised directly using the LI-COR Odyssey image system. Image resolution was set at 169 μM, and images obtained in the 700 nM and 800 nM channels, both set at intensity 5.0 as a starting point.

## 2.5 Immunoassays for HTT quantification

Cell pellets of each available ReNcellVM line were sent to Evotec for quantification of total and mutant HTT levels using the ELISA-based Meso Scale Discovery electrochemiluminescence platform (Macdonald et al, 2014). The 2B7/4C9 antibody pair was used to detect total HTT and 2B7/MW1 antibody pair was used to detect mutant HTT. For studies of HTT trafficking described in chapter 6, whole cell pellets and cell fractions of 129Q and 29Q HTT exon 1 ReNcellVM lines and three clones of control and 73Q MSN were again sent to Evotec, but on this occasion total and mHTT levels were measured using the ultra-sensitive Erenna Singulex human HTT protein detection assay (Wild et al, 2015).

## 2.6 Transduction with recombinant adeno-associated virus (rAAV) vectors

### 2.6.1 Generating recombinant adeno-associated virus (rAAV)

rAAV vectors were created in conjunction with Horizon Discovery. Three vectors carrying exon 1 of the *HTT* gene with 50, 80 and 125 CAG repeats respectively were made. The vectors also contained a puromycin resistance gene, flanked by LoxP sites, and right and left homology arms containing *HTT* intronic sequence. The overall vector size was around 7 kb.

Plasmid vectors (pVector), as well as plasmids encoding viral replication and coat proteins (pDJ) and helper proteins (pHelper) [Agilent technologies] were used to carry out lipofectamine transfection of HEK-293T cells, thus generating adeno-associated virus containing our *HTT* exon 1 cassette.

On reaching 70-80% confluency, the spent media was removed from a T75 flask of HEK-293 cells and replaced with 9 ml fresh media. The transfection mix was prepared; per T75 flask 18.75 µg of pVector, 18.75 µg of pDJ and pHelper (combination supplied by Horizon), and 37.5 µl of PLUS reagent [Invitrogen] were added to 1ml of HEK cell medium without serum and incubated at room temperature for 5 min. Fifty six microlitres of lipofectamine [Invitrogen] was then added to this, and further incubated for 30 mins at room temperature. The transfection mixture was then added to the T75 flask (already containing 9 ml medium), and rocked gently to distribute evenly. The flask was then incubated at 37°C; 5% $CO_2$ for 18-24 hrs, inspected for toxicity/cytopathic effects and then returned to the incubator for a further 48 hrs. Overall, ten T75 flasks of HEK-293T cells were transfected per vector.

72 hrs post transfection, the culture medium was collected into 50 ml Falcon tubes and centrifuged at 1000 x*g* for 5 min. The clarified supernatant was stored in a fresh 50 ml tube, and the remaining cell pellet kept. Three millilitres of PBS was added to wash each T75 flask, and transferred to a 50 ml falcon tube and centrifuged at 1000 x*g* for 5 min. The PBS was then discarded, and the remaining small cell pellet kept. Two millilitres of 1x trypsin-EDTA was added to each flask, incubated for 5 mins at 37°C, 5% $CO_2$. Dissociated cells were resuspended in 2 ml HEK-293T cell medium, and the cell suspension transferred to a 50 ml Falcon tube and centrifuged at 1000 x*g* for 5

mins. The supernatant was discarded and the cell pellet kept. The three cell pellets were resuspended in 10 ml of HEK cell medium, and the suspension centrifuged at 1000 x*g* for 5 mins. The supernatant was discarded. The resulting cell pellet and the clarified supernatant were stored at -80°C.

### 2.6.2 AAV purification

The clarified supernatant (crude lysate) and cell pellet were removed from the -80°C freezer and warmed for 30 mins in the water bath at 37°C. The cell pellet was resuspended in 3 ml lysis buffer (0.15M NaCl, 50 mM Tris-HCl pH 8.5), and the tube placed into a dry ice ethanol bath for 10 mins to snap freeze the contents. The cell suspension was then thawed again in a 37°C waterbath and vortexed to aid disruption of the cells. This freeze-thaw cycle was repeated a further two times. The treated cell suspension and thawed crude lysate were then combined and distributed between 50 ml Falcon tubes and centrifuged at 2900 rpm for 30 min.

The supernatant was collected into a T75 flask, 1 µl benzonase nuclease (384 U/µl) [Sigma] added for every 10 ml, and incubated at 37°C for 30 min. The addition of benzonase nuclease removes any contaminating DNA in the supernatant. The benzonase treated virus supernatant was then purified using the AAV purification VIRAKIT$^{TM}$ [Virapur] which uses a membrane based filtration method and a series of filtration, washing and elution steps. The eluted virus was distributed into sterile 1.5 ml tubes in 0.5 ml aliquots, and stored at -80°C.

### 2.6.3 AAV copy number quantification

Purified rAAV2 was quantified by quantitative real-time PCR (qPCR). Ten units amplification grade DNase1 and 5 µl of 10x DNase1 buffer was added to 5 µl of purified virus and the volume made up to 50 µl with molecular grade water. This was incubated at 37°C for 30 mins and then at 95°C for 2 min. Treatment with DNase1 is to eliminate and residual contaminating DNA. To each 50 µl sample, 1 µl proteinase K (20mg/ml) [Roche], 75 µl proteinase K buffer 2 x (1% SDS, 200 µM NaCl) and 24 µl of molecular grade water was added and the sample incubated at 56°C for 1 hr and then at 95°C for 5 mins at 95°C. Treatment with proteinase K was used to release the encapsidated viral genome.

The sample was diluted to 10% in $dH_20$. A series of five-fold dilutions of a pAAV plasmid containing the puromycin resistance gene of known concentration was prepared as shown in Table 2.1. The calculation of the number of copies of puromycin$^R$/ml in 1 µg of double stranded pAAV is based on the following formula:

$(2 \times 6.02 \times 10^{23}) / (610 \times 7000 \times 10^6) = 2.821 \times 10^{11}$ where:

2 = number of copies of puromycin$^R$ gene per double stranded pAAV

$6.02 \times 10^{23}$ = number of molecules (copies) per mole of substance

610 = average molecular weight (MW) in (g/mole) of 1 nucleotide base pair

7000 = average number of base pairs in one pAAV

| Standard | µg/ml | Copies puromycin$^{R}$/ml |
|---|---|---|
| 1 | 1.000 $e^{0}$ | 2.821 $e^{11}$ |
| 2 | 2.000 $e^{-1}$ | 5.642 $e^{10}$ |
| 3 | 4.000 $e^{-2}$ | 1.128 $e^{10}$ |
| 4 | 8.000 $e^{-3}$ | 2.257 $e^{9}$ |
| 5 | 1.600 $e^{-3}$ | 4.514 $e^{8}$ |
| 6 | 3.200 $e^{-4}$ | 9.027 $e^{7}$ |
| 7 | 6.400 $e^{-5}$ | 1.805 $e^{7}$ |
| 8 | 1.2800 $e^{-5}$ | 3.611 $e^{6}$ |
| 9 | 2.560 $e^{-6}$ | 7.222 $e^{5}$ |
| 10 | 5.120 $e^{-7}$ | 1.444 $e^{5}$ |
| 11 | 1.024 $e^{-7}$ | 2.889 $e^{4}$ |
| 12 | 2.048 $e^{-8}$ | 5.777 $e^{3}$ |

**Table 2.1: Standards used in calculation of AAV quantification**. For derivation see text.

To quantify the concentration of rAAV2 qPCR reactions were set up in triplicate, with each of the standards, the virus and a negative control. For each reaction a master mix was assembled with 0.225 µl of 100 µM forward primer (CACGCGCCACACCGTCGACCC). 0.225 µl of 100 µM reverse primer (GGGAACCGCTGAACTCGGCCA), 11.05 µl PCR grade water and 12.5 µl of SYBR Green master mix [Applied Biosystems]. 24 µl of master mix and 1 µl of sample were added to each well.

Reactions were set up in a MicroAmp fast optical 96-well reaction plate, and sealed with MicroAmp optical adhesive film [Applied Biosystems]. The plates were centrifuged

for 10 sec and 300 x*g* and were run on a 7500 Fast real-time PCR machine [Appied Biosystems] using 7500 software. The PCR cycling conditions were as follows: 95°C for 3 mins followed by 40 cycles of 95°C for 15 sec and 60°C for 1 min.

The amplification plots were analysed to determine the Ct (threshold cycle value) for each standard and a standard curve was plotted of initial copies of puromycin$^R$/ml vs Ct. This was used to determine the rAAV2 titre in genome copies (GC)/ml; the Ct of the sample was used to determine corresponding value of copies of puromycin$^R$/ml, and this was multiplied by the overall dilution factor of the sample, including during sample preparation (i.e. a factor of 300).

### 2.6.4 Transduction of cells

ReNcellVM NSCs were seeded in NSC media at the usual density into a T25 flask, and placed in the incubator at 37°C; 5% $CO_2$. After 24 hrs cells were media changed and AAV virus added to achieve a multiplicity of infection (MOI) of 100 000. On adding virus, the cells were returned to the incubator for 72 hrs. Confluent cells were then passaged into a T75 flask, with fresh NSC media (without virus) and grown for 24 hrs, before adding puromycin at a concentration of 75 ng/ml. Simultaneously, 75 ng/ml puromycin in NSC media was added to a control flask of ReNcell VM NSCs, to ensure lethality at this dose. The infected cells were expanded and grown under antibiotic selection for two weeks, following which stocks of each line were frozen down.

### 2.6.5 Screening cells for integration

ReNcellVM NSCs were screened for positive integration of the vector into the native *HTT* exon 1 locus. After antibiotic selection, as described, cells were seeded into 96-well plates at a density of 10 cells per well and grown in the incubator at 37°C; 5% $CO_2$ for 10-14 days. Generally 2-4 plates were seeded per vector, per round of screening. Once the wells had reached confluence, the plates were passaged into new 96-well plates, whilst taking samples for lysis and subsequent screening PCR.

In order to harvest gDNA from pools of cells (each cell "pool" derives from one well of the 96-well plate), 20 µl lysis buffer comprising DirectPCR lysis buffer [Viagen] with 1% proteinase K of >800U/ml [Roche] was added to each well of a 96-well PCR plate [Thermo]. Lysis plates were prepared just prior to passaging the cells.

Confluent 96-well screening plates were prepared as follows: spent media was removed and cells washed with 100 µl HBSS per well. Trypzean 25 µl was added per well and incubated for 5 mins at 37°C. The wells were triturated and 5 µl of cell suspension was transferred into the pre-prepared lysis plate. The same volume of DTI was then added to the remaining cells in Trypzean, and 25 µl of this suspension was transferred into a new laminin coated 96-well plate containing 100 µl NSC media per well. It was imperative that the orientation of the 96-well plates remained the same between the cell culture plates and the lysis plates, so that any positive pools could be identified and expanded. The lysis plates were sealed with optical adhesive cover and placed on the PCR Tetrad machine with conditions as follows: 55°C for 15 mins and then 85°C for 45 mins. The lysis plates were stored at 4°C until PCR.

### *2.6.5.1* PCR screening strategy

All primers were designed using Primer 3 software, and the position relative to the vector and specificity to intended binding sites checked with BLAST nucleotide. RH For 2 (ccctggaaaagctgatgaag) and RH Rev 2 (gcaaatgcaggttctgtcaa) were selected for screening as an internal positive control band is generated from the wild type allele, thus confirming that the PCR reaction has worked. In theory, a correctly targeted vector gives rise to three different products, as shown in figure 3.9. Using RH2 primers, the size in base pairs of the expected products following positive homologous recombination is shown in table 3.2 (chapter 3).

PCR reaction master mix was assembled using the GoTaq DNA Polymerase kit from Promega. For 100 reactions master mix was made up as follows:

400 µl x5 Green GoTaq Reaction Buffer (supplied)

50 µl dNTPs [Promega]

120 µl $MgCl_2$ (supplied)

120 µl DMSO

20 µl GoTaq enzyme (supplied)

1060 µl PCR grade $H_20$

15 µl forward primer (100 µM) [Sigma, custom]

15 µl reverse primer (100 µM) [Sigma, custom]

18 µl of master mix and 2 µl of sample (lysed cell pools) were added per reaction into a 96-well PCR plate, again ensuring that orientation of the lysis plate and PCR plate matched. A touchdown PCR protocol was used with the parameters shown in table 2.2.

PCR products were visualised using gel electrophoresis on a 1% agarose gel (Tris/Borate/EDTA (TBE) buffer with 1% agarose, heated to boiling point, cooled and 1/10,000 SYBR Safe [Thermo] added) in an extra-large gel tank to allow simultaneous processing of 96 samples. End wells were loaded with Hyperladder 1kb [Bioline].

| Step | Number of cycles | Temperature °C | Incubation time (sec) |
|---|---|---|---|
| 1 | 1 | 94 | 180 |
| 2 | 3 | 94<br>64<br>70 | 15<br>30<br>240 |
| 3 | 3 | 94<br>61<br>70 | 15<br>30<br>240 |
| 4 | 3 | 94<br>58<br>70 | 15<br>30<br>240 |
| 5 | 35 | 94<br>57<br>70 | 15<br>30<br>240 |
| 6 | 1 | 70 | 300 |
| 7 | | 4 | Hold |

**Table 2.2: Touchdown PCR protocol for use with screening primers**

#### 2.6.5.2 Other screening primers

As described in the results, we also used other screening primers to isolate positively integrated pools (table 2.3).

| Primer Set | Forward (For) | Reverse (Rev) |
|---|---|---|
| RH2 Nest | gggtcttcccttgtcctctc | aaatctcggctcctccaagt |
| RH2 Sp* Nest | aagctgatgaaggtcgacataa | tcccaacacacataggcaaa |
| A | atagcagctttgctccttcg | aaatgccatctgggacacat |
| B | atagcagctttgctccttcg | gcaaatgcaggttctgtcaa |
| C | gtcaccgagctgcaagaact | aaatgccatctgggacacat |
| LH2 | gggtgcactcccataaagaa | ccctggtttctc gcaaataa |
| PGK/Puromycin | atagcagctttgctccttcg | agttcttgcagctcggtgac |

**Table 2.3: Alternative screening primers used.**

## 2.7 Immunofluorescence imaging

### 2.7.1 Immunofluorescence studies

Cells were seeded onto laminin coated baked glass coverslips contained in a 4-well dish, at an appropriate density for optimal cell growth, and differentiation was commenced. At various time-points cells were fixed using 100 µl of 4% paraformaldehyde (PFA) per well for 20 mins at room temperature, and stored in 100 µl

PBS with 0.2 % sodium azide at 4°C. To permeabilise the cells, the PBS with 0.2 % sodium azide was removed and 100 µl of 0.2 % Triton X-100 added for 15 mins at room temperature. This was then removed and the cells blocked with 100 µl per well of 10% goat serum and 1 % BSA in PBS for 1 hr at room temperature. (When using the sheep anti-S830 antibody, donkey serum was used to block instead of goat serum).

Primary antibodies were added in 100 µl PBS at concentrations shown in appendix table A.2, and incubated overnight at 4°C. The wells were then washed gently five times in 100 µl PBS and secondary antibodies (appendix table A.2) added at a dilution of 1/1000. The coverslips were incubated for 1 hr in the dark at room temperature. Following this, two further PBS washes were carried out and Hoescht [Sigma] 1/10,000 in PBS was added for 5 mins at room temperature. The coverslips were washed 3 more times in PBS and then left in 100 µl PBS, at 4°C in the dark, until imaging. Coverslips were mounted onto slides [Superfrost Thermo] with Dako fluorescent mounting medium with DAPI [Agilent] and visualised using a Zeiss 710 confocal microscope.

### 2.7.2 High content imaging

96-well ClearView plates [Perkin Elmer] were seeded with HTT exon 1 overexpressing ReNcellVM cells as well as GFP only and wild-type cells, at a density of 25,000 cells/well. The cells were differentiated from the next day using the protocols previously described. Plates were fixed at various time-points, permeabilised and stained with antibodies as described in section 2.7.1.

Image capture for high content screening was initially carried out using the Perkin Elmer Opera LX automated confocal microscope, which has a UV channel plus three laser lines exciting at 488, 560 and 640 nm. Cell nuclei stained with Hoescht were detected by the UV channel, and the 488 channel detected the GFP expressed by the ReNcellVM HTT exon 1 cell model, thus allowing visualization of cell boundaries. The remaining two channels were used to detect antibodies as shown in appendix table A.2. Following the installation of the newer Opera Phenix machine, training was undertaken to operate this system and subsequent image capture for analysis of neuronal phenotypes in ReNcellVM HTT exon 1 lines.

#### 2.7.2.1 Image analysis

Images captured on the Opera LX microscope, namely those of the time course of inclusion body formation in the ReNcellVM HTT exon 1 lines, were analysed in conjunction with Dr. Janos Kriston-Vizi at the UCL Laboratory of Cell and Molecular Biology, using Image J and R. Subsequent image analysis of images from the Opera Phenix were analysed by Dr. Rhia Ghosh using Columbus software; this software allows the construction of a modular pipeline to analyse multiple cell parameters such as nuclear morphology, staining patterns and intensity across thousands of images in an objective manner. Results were exported to Microsoft Excel and reformatted for analysis using GraphPad Prism.

### 2.7.3 Super-resolution imaging

This was undertaken in conjunction with Dr. Ed Smith from the laboratory of Professor Gillian Bates (UCL). Super resolution fluorescent images were captured using a Nikon Eclipse Ni-E N-SIM Super Resolution system and Andor Ixon camera. Images were saved as ND2 files and processed using NIS Elements AR software with n-SIM module. Final images were exported as TIFF files images. Acquisition was performed in a 3D SIM mode using the 100× 1.49 NA total internal reflection fluorescence objective lens with 28 z steps per stack at a step interval of 0.1 µm.

## 2.8 Cytotoxicity assays

### 2.8.1 Lactate dehydrogenase (LDH) assay

The LDH assay was carried out using the Promega 96® non-radioactive cytotoxicity assay. ReNcellVM cells were cultured in standard 96-well plates, in 200 µl of media per well. A row of "positive control" wells were treated with 22 µl of 10% Triton-X to achieve a final concentration of 1% Triton-X in media for total cell lysis (to give the maximal LDH concentration equivalent to 100% cell death) over 1 hr at 37°C. Fifty microlitres of media was then removed per well and placed into a 96-well microplate [Greiner], to be used for the LDH assay. A row of wells containing media only was also included to calculate the background absorbance. Fifty microlitres of CytoTox 96® Reagent was then added to each test well; the plates were covered with foil to protect them from

light, and incubated for 30 mins at room temperature. Fifty microlitres of Stop Solution was then added to each well. Any large bubbles were popped using a syringe needle, and absorbance was recorded at 490 nm using the Tecan Sunrise plate reader. After subtracting the background absorbance of the media only wells from all the wells, percentage cell death was calculated in the test wells as a proportion of the total cell death in the positive control wells.

Variability between cell numbers was seen to occur in some cases due to delamination from the laminin coated culture plates, and was thought to have an effect on the results of the LDH assay. To account for this, the above protocol was modified to carry out whole plate lysis and calculate a percentage cell death in each well tested. Fifty microlitres of media was removed per well of the cell culture plate and placed into a 96-well microplate. Ten percent Triton-X was then added to all the wells at a volume of 16.7 µl (creating a final volume of 166.7 µl per well) to trigger 100% cell lysis over 1 hr at 37°C. Fifty microlitres of this "lysed" media was then transferred into a separate 96-well assay plate, and a row of media-only wells was also included. Fifty microlitres of CytoTox 96® Reagent was then added to each test well of both the assay plates (both pre- and post-lysis test wells), and the protocol carried out as described above. To calculate the percentage cell death in each well, following subtraction of background the absorbance of the pre-lysis test wells was multiplied by the dilution factor due to addition of 10% Triton-X (in this case 150/167) and divided by the value of the absorbance in the post-lysis test wells.

### 2.8.2 MTT assay

The MTT (3-[4,5- dimethylthiazol-2-yl]-2,5-diphenyl tetrazolium bromide) assay was carried out using the MTT based In Vitro Toxicology Assay Kit [Sigma]. Cell cultures in 96-well plate format were removed from the incubator and placed in the laminar flow hood. MTT was reconstituted in media to a concentration of 5 mg/ml. This was added to the cells in an amount equal to 10% of the culture medium volume. The cells were returned to the incubator for 4 hrs. Following this time, cultures were removed from the incubator and a volume of DMSO equal to the original culture medium volume was added to each well to dissolve the resulting formazan crystals. The culture plate was then placed in the Tecan Sunrise absorbance microplate reader and background absorbance measured at 690 nm, and subtracted from absorbance at 570 nm.

### 2.8.3 Alamar Blue assay

The alamar blue assay was carried out using the alamarBlue® Cell Viability Assay Protocol from ThermoFisher. Cell cultures in 96-well plate format were removed from the incubator and placed in the laminar flow hood. AlamarBlue® cell viability reagent (10X) was added directly to the cell culture medium at $1/10^{th}$ of the total volume. Cells were then returned to the incubator for 4 hrs. The absorbance of the plate was measured using the Tecan Sunrise absorbance microplate reader at 570 nm using 600 nm as a reference wavelength, using a blank of media only. The percentage difference in reduction of resazurin between control (wild-type ReNcellVM cells) and test wells (HTT exon 1 ReNcellVM cells) was calculated as follows:

$$\text{Percentage difference} = \frac{(O2 \times A1) - (O1 \times A2)}{(O2 \times P1) - (O1 \times P2)} \times 100$$

Where:

**O1** = molar extinction coefficient (E) of oxidised alamarBlue at 570 nm (in this case E=80586)
**O2**= E of oxidised alamarBlue at 600 nm (in this case E=117216)
**A1** = absorbance of test well at 570 nm
**A2** = absorbance of test well at 600 nm
**P1** = absorbance of control well at 570 nm
**P2** = absorbance of positive growth control well at 600 nm

### 2.8.4 Imaging markers of cytotoxicity

Imaging methods to ascertain cytotoxicity in the HTT exon 1 ReNcellVM lines were complicated by the expression of GFP in these cells, which therefore precluded the use of any green fluorescent cytotoxicity markers designed for the detection in the 488 channel.

#### 2.8.4.1 Propidium iodide (P.I.) staining

1 mg/ml of P.I. [Invitrogen] was diluted 1:3000 in 2x SSC (0.3 M NaCl, 0.03 M sodium citrate, pH 7.0) to make a final working concentration of 500 nM. Cells on coverslips were fixed and permeabilised as described in section 2.8.1. Three hundred microlitres of 500 nM P.I. per coverslip was added for 5 mins, and then washed off in SSC.

Hoescht staining was then carried out, followed by mounting of the slides and visualisation using confocal microscopy, as described in section 2.7.1.

#### 2.8.4.2 Mitotracker Red labelling

MitoTracker® Red CMXRos was purchased from Invitrogen. The product was dissolved in DMSO to make a stock solution of 1 mM. This was further diluted in media to achieve final working concentrations of 100 nM and 500 nM that were added to the ReNcellVM cells being tested. The cells were then incubated for 30 mins, after which the media containing MitoTracker Red was removed, and cells washed in warm PBS. The cells were imaged after fixation, permeabilisation and further staining (Hoescht) was carried out, as described in section 2.7.1. A concentration of 100 nM was found to be the optimal concentration of MitoTracker Red for labelling the ReNcellVM lines.

#### 2.8.4.3 Activated Caspase 3 antibody staining

Antibody to activated caspase 3 (rabbit polyclonal) was purchased from Abcam (ab13847). This was tested for immunocytochemistry on GFP only ReNcellVM cells treated with 1 μM staurosporin (STS) at various dilutions, as described in section 2.7.1. An optimal dilution of 1/100 was ascertained, and this was used to stain a 96-well plate of the differentiated HTT exon 1 ReNcellVM panel which was then imaged on the Opera Phenix, with image analysis carried out using Columbus (section 2.7.2).

## 2.9 Subcellular fractionation

This was carried out using the Subcellular Protein Fractionation Kit for Cultured Cells (Thermo; cat no 78840), making minor adaptations to the standard protocol for optimisation in the ReNcellVM and iPSC lines. Stepwise separation of cytoplasmic, membrane, nuclear soluble, chromatin-bound and cytoskeletal protein extracts from differentiated cells was carried out using a series of sequential buffers. Following differentiation, neuronal cell pellets of ReNcellVM cells were prepared as described in section 2.5.1. iPSC-derived MSNs pellets were formed by removal of spent media followed by the addition of an appropriate volume of Accutase for 5 mins; the cells were gently removed using a 10 ml stripette and centrifuged in a falcon tube at 500 x*g* for 5 mins followed by a PBS wash. Each cell pellet was divided into two, with one being snap frozen as a whole cell pellet, and the other for subcellular fractionation.

The subcellular fractionation protocol was carried out on ice. Starting with a packed cell volume of 50 µl for each cell pellet, 200 µl of ice-cold Cytoplasmic Extraction Buffer (CEB) with 1:100 protease inhibitors (Thermo Scientific Halt Protease Inhibitor Cocktail) was added to the dry cell pellet and incubated at 4°C for 10 mins with gentle mixing. This reagent causes selective cell membrane permeablisation, releasing soluble cytoplasmic contents. The tube was centrifuged at 500 ×*g* for 5 mins and the supernatant (cytoplasmic extract) was immediately transferred to a clean pre-chilled tube on ice. Two hundred microlitres of ice-cold Membrane Extraction Buffer (MEB) containing protease inhibitors was added to the pellet and the tube vortexed for 5 s on the highest setting, followed by incubation at 4°C for 10 mins with gentle mixing. This reagent dissolves plasma, mitochondria and ER/Golgi membranes but does not solubilise nuclear membranes. The tube was then centrifuged at 3000 ×*g* for 5 mins

and the supernatant (membrane extract) transferred to a clean pre-chilled tube on ice. Two hundred microlitres of ice-cold Nuclear Extraction Buffer (NEB) containing protease inhibitors was added to the pellet and vortexed for 15 s. The solution was incubated at 4°C for 30 mins with gentle mixing, followed by centrifugation at 5000 ×*g* for 5 mins. This reagent yields the soluble nuclear extract from previously intact nuclei. The supernatant (soluble nuclear extract) was transferred to a clean pre-chilled tube on ice.

A second nuclear extraction was performed to release chromatin-bound nuclear proteins. Chromatin-bound extraction buffer (CEB) was prepared by adding protease inhibitors, 10 µL of 100 mM $CaCl_2$ and 6 µL of micrococcal nuclease (600 units) to 200 µL of room temperature NEB. This was added to the pellet and vortexed 15 s. Benzonase 1 µL was added and the solution incubated in a 37°C water bath for 30 mins. After incubation, the sample was again vortexed on the highest setting for 15 s and centrifuged at 18,000 ×*g* for 5 mins. The supernatant (chromatin-bound nuclear extract) was transferred to a clean pre-chilled tube on ice. One hundred microlitres of room temperature Pellet Extraction Buffer (PEB) containing protease inhibitors was added to the pellet and the tube vortexed for 15 s followed by incubation at room temperature for 10 mins. This final reagent isolates cytoskeletal proteins. The sample was centrifuged at 16,000 ×*g* for 5 mins. The supernatant (the cytoskeletal extract) was transferred to a new tube. All fractions were transferred from ice to storage at -80°C for HTT quantification at a later date.

## 2.10 Statistical analysis

All graphs were created and statistical analysis carried out using GraphPad Prism 6 (GraphPad). To analyse the effect of HTT exon 1 overexpression on neuronal differentiation in ReNcellVM cells, images were analysed on Columbus and data on multiple parameters was exported to Microsoft Excel. This was reformatted into tables suitable for GraphPad. One-way ANOVA with Bonferroni's correction was used to analyse the effect of increasing CAG repeat length on β3-tubulin, GFAP and nestin expression, as well as nuclear metrics. For cytotoxicity experiments in these lines, two-way ANOVA with Bonferroni's correction was used to analyse the time course of LDH release, with one-way ANOVA to determine the effect of HTT exon 1 overexpression on the reduction of alamar blue and on activated caspase-3 staining in these cells. The dose-response curves for $H_2O_2$, MG132 and lactacystin in the HTT exon 1 ReNcellVM lines were analysed using two-way ANOVA with Bonferroni's correction. The impact of chronic application of toxins over time was also analysed using this method.

The time course of nuclear inclusion formation in the HTT exon 1 ReNcellVM cells was analysed using two-way ANOVA with Bonferroni's correction to determine the effect of increasing CAG repeat length and increasing time on the percentage of cells containing nuclear IBs. The total nuclear count across all lines at dd7 and dd14 was also analysed in this way. Two-way ANOVA with Bonferroni's correction was also used to analyse the effect of increasing CAG repeat length and increasing time on the number of IBs formed per IB-containing cell. The number of peri-nuclear inclusions and the intensity of cytoplasmic HTT exon 1 staining over time were also assessed using two-way ANOVA with Bonferroni's correction. The effect of IB formation on nuclear size was

assessed using one-way ANOVA with Bonferroni's correction within each line. Two-tailed unpaired t-test was used to assess the impact of IB formation on the expression of B3-tubulin. The effect of MG132 and bafilomycin on HTT staining levels across the HTT exon 1 ReNcellVM panel was analysed using two-way ANOVA with Bonferroni's correction, and this was also used to analyse the effect of PTI compounds on HTT exon 1 clearance in these cells.

For the study of HTT trafficking described in chapter 6, the distribution of total HTT levels in control and 73Q MSNs and MSN cell fractions were compared using two-way ANOVA. Two-tailed unpaired t-test was used to analyse differences between total HTT levels in 29Q and 129Q HTT exon 1 ReNcellVM whole cell pellets, and to compare the percentage of nuclear HTT (as a proportion of total cell HTT) between these two lines.

# 3 Generating a HTT allelic series neuronal cell model of Huntington's disease

## 3.1 Background

The importance of the length of the CAG repeat expansion mutation in the *HTT* gene is clinically evident. It determines whether patients will get adult onset HD (40+ CAG repeats), juvenile onset HD (>55 CAG repeats), or a reduced penetrance form of HD (36-40 CAG repeats). Patients who inherit 35 or less CAG repeats will remain free of the disease, though CAG repeat lengths from 27-35 may expand in future generations to cause HD. In addition CAG repeat length is the most important factor that determines age of onset of HD on a population level (Langbehn et al, 2010). The effect of increasing CAG repeat length in an otherwise constant model system in order to create an "allelic series" may lend insight into how this factor drives HD pathogenesis, and may also provide a useful tool for the testing of pre-clinical compounds in the search for disease modifying treatments.

The ideal cell model must reflect the disease state as closely as possible. In the case of HD, this means using cells which are human derived (HD is an exclusively human disease) and neuronal (to reflect the primary site of HD pathology). In addition cell models should be renewable, and thus easily shared by the research community, and have robust differentiation protocols. The ReNcellVM neural stem cell (NSC) line, derived from ten-week gestation foetal midbrain, and the STROC05 human NSC line,

originally isolated from twelve-week gestation whole ganglionic eminence, were thought to fulfil these requirements, and it was decided to use these as a basis for a novel cell model of HD. Inserting increasing CAG repeat lengths into the endogenous *HTT* locus of these lines would form an isogenic allelic series, in which full length HTT and mHTT would be expressed at physiological levels. The only difference between the lines in the series would be the length of the polyglutamine tract in the HTT protein, thus eliminating any genetic heterogeneity that could affect results.

Prior to the development of CRISPR/Cas9 technology that has recently revolutionised genome editing, viral transduction with adeno-associated virus (AAV) was considered to be one of the most efficient methods of gene targeting in mammalian cells (Vasileva & Jessberger, 2005). Homologous recombination rates varying from 1 in 10,000 up to 1 in 100 have been achieved in human cells using this method, compared to less than 1 in 1,000,000 with other transfection methods. AAV has been proven to infect a wide range of human cells and to introduce many types of genetic modifications including insertions as well as deletions and point mutations. Other advantages of AAV include its single stranded genome, which allows efficient delivery to the nucleus, relatively easy construction using PCR-based methods and non-pathogenicity (Khan et al, 2011). Indeed recombinant AAV (rAAV) remains a key tool in the delivery of potential genetic therapies, including for HD (Miniarikova et al, 2018). It was therefore decided to utilise this technology to develop an isogenic allelic series human neuronal model of HD.

One potential concern over the use of full length HTT cellular models is the timescale taken for disease associated phenotypes to develop. HD is generally an adult onset disease and even in juvenile HD cases it is extremely rare to have onset of symptoms

in early childhood. One method of simulating the effect of aging in neuronal cultures is to subject the cells to various cellular stressors. Alternatively, transgenic cell models expressing N-terminal fragments are known to give rise to disease phenotypes in a matter of days, or sometimes hours, depending on the cell line transduced and levels of overexpression. This is particularly useful for high-throughput therapeutics screening. A HTT exon 1 overexpression human neuronal model of HD was therefore optimised and characterised, to study the impact of increasing HTT exon 1 CAG repeat-length on neuronal phenotypes.

Recent developments in iPSC technology, both in terms of their generation and differentiation into specific neuronal subtypes of interest, have made them increasingly attractive for modelling HD due to their close physiological representation of the disease state. MSNs, which are the earliest neurons to degenerate in HD, can be generated following a 36 day differentiation protocol that yields 20-50% of DARPP32 positive cells. This protocol mirrors the developmental changes seen in neurogenesis, and uses activin A to induce lateral ganglionic eminence (LGE) characteristics in neural progenitors derived from pluripotent stem cells (Arber et al, 2015). The genetic backgrounds of iPSCs donors are known to have an effect on transcription and differentiation of the resulting cell lines (Kyttälä et al, 2016). Therefore direct comparisons between different HD-iPSC lines can be difficult. Consequently, a panel of iPSCs was generated from a family of HD-affected siblings (who have a relatively similar genetic background) and their mother as a control, with three clones from each line.

## 3.2 Aims

1. To characterise and assess suitability of a human neural stem (NSC) cell line to be used for the generation of a new cell model of HD.

2. To create an isogenic HTT allelic series in this NSC line using rAAV to knock in increasing CAG repeat lengths into the endogenous *HTT* locus.

3. To optimise and characterise a transgenic HTT exon 1 overexpressing allelic series cell model in this same NSC line.

4. To generate a panel of HD iPSCs with increasing CAG repeat lengths from HD affected siblings, and their unaffected mother as a genetically related control.

## 3.3 Methods

For characterisation of the ReNcellVM and STROC05 lines, NSCs were cultured and differentiated as described (section 2.1.1 and 2.1.3). In order to confirm endogenous *HTT* transcription in these lines, RNA extraction, cDNA generation, and PCR (section 2.3) was carried out. HTT protein expression was confirmed by Western blotting (section 2.4). Antibiotic kill curves were generated for each line (section 2.1.4).

Immunofluorescence studies of the STROC05 line were carried out as described (section 2.7.1).

In order to create the Horizon knock-in allelic series, recombinant AAV (rAAV) carrying the HTT 50, 80 and 125 CAG repeat vectors was first generated (section 2.6.1). After purification (section 2.6.2) and quantification using qPCR (section 2.6.3), the virus was used to transduce the ReNcellVM line (section 2.6.4), and cells were then screened for positive homologous recombination as described (section 2.6.5). The HTT exon 1 overexpression lines were thawed (section 2.1) and expanded. HTT exon 1 expression was confirmed on Western blotting (section 2.4) and further quantification carried out by Evotec using the MSD assay (section 2.5). For generation of the iPSC panel, ethics and consent were obtained (section 2.2.1) and then punch biopsies of the skin carried out (section 2.2.2). Fibroblast cultures were developed from these (section 2.2.3) and frozen vials sent to Professor Ali Brivanlou at the Rockefeller centre for iPSC generation (section 2.2.4). iPSCs were differentiated into MSNs as detailed in section 2.2.6.

## 3.4 Contributions

The work described in this chapter was carried out with collaborators in the following areas:

Horizon Discovery Ltd., who provided the vectors and plasmids used in the generation of rAAV.

Professor Gill Bates who gifted the ReNcellVM lines with GFP and HTT exon 1 inserted.

Evotec Ltd who carried out the HTT MSD assay.

Professor Ali Brivanlou who generated iPSC lines from our patient-derived fibroblasts.

All other work was carried out by Dr. Rhia Ghosh.

## 3.5 Results

### 3.5.1 Characterisation of the ReNcellVM and STROC05 neural stem cell lines

In order to ensure that the neural stem cell lines were suitable for generation of HD cell models, it was necessary to ensure that they were expressing native HTT. Previous sequencing of *HTT* in both lines had confirmed that they carry two wild-type alleles with 19/21 CAG repeats in the ReNcellVM line and 20/22 repeats in the STROC05 line.

#### 3.5.1.1 Characterisation of ReNcellVM neural stem cell line

RNA was extracted from ReNcellVM NSCs and cDNA synthesis using reverse transcriptase was carried out as described. PCR was performed out using two sets of primers against *HTT*, with results as shown in figure 3.1. This confirmed that the ReNcell line was transcribing the wild type *HTT* gene.


**Figure 3.1: PCR on ReNcellVM cDNA template.** Samples are shown in lanes 1, 3 and 5 with negative control water in lanes 2, 4, and 6. Lanes 1 and 2 show results using *HTT* 9171/9361 primers, lanes 3 and 4 show results using *HTT* 153/449 primers, and lanes 5 and 6 show results using *GAPDH* primers as a positive control for the PCR reaction.

Western blotting of protein extracted from a cell pellet of ReNcellVM NSCs was carried out using the MAB2166 antibody against HTT directed against (amino acids 181-810). This revealed that the ReNcellVM line was expressing HTT protein (figure 3.3).

ReNcellVM NSCs were differentiated on coverslips for two weeks and tested by our collaborator Dr. Stephanie Schorge for electrophysiological activity. Despite previous work that had demonstrated electrical activity (Donato et al, 2007), the neurons were not found to generate action potentials, suggesting that these cells are still relatively immature in terms of neuronal development.

Finally, antibiotic kill curves calculated by Dr. Andre demonstrated that a concentration of **75 ng/ml** of puromycin was sufficient to kill wild-type ReNcellVM NSCs – therefore this concentration was used when infecting the cells with the AAV vectors (see below).

### 3.5.1.2 Characterisation of STROC05 neural stem cell line

RNA extraction and cDNA synthesis was also carried out in STROC05 NSCs, and PCR performed using 2 sets of primers against *HTT*, with results as shown in figure 3.2. This confirmed that the STROC05 line was transcribing the wild type *HTT* gene.

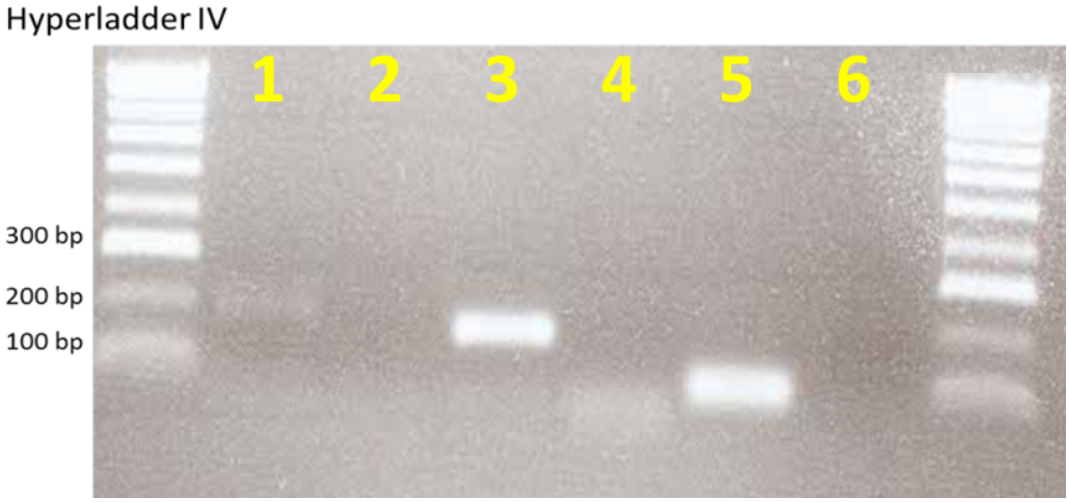


**Figure 3.2: PCR on STROC05 cDNA template.** Samples are shown in lanes 1, 3 and 5 with negative control water in lanes 2, 4, and 6. Lanes 1 and 2 show results using *HTT* 9171/9361 primers, lanes 3 and 4 show results using *HTT* 153/449 primers, and lanes 5 and 6 show results using *GAPDH* primers as a positive control for the PCR reaction.

Western blotting of protein extracted from a cell pellet of STROCO5 NSCs with MAB2166 antibody revealed that the STROC05 line was also expressing HTT protein (figure 3.3).

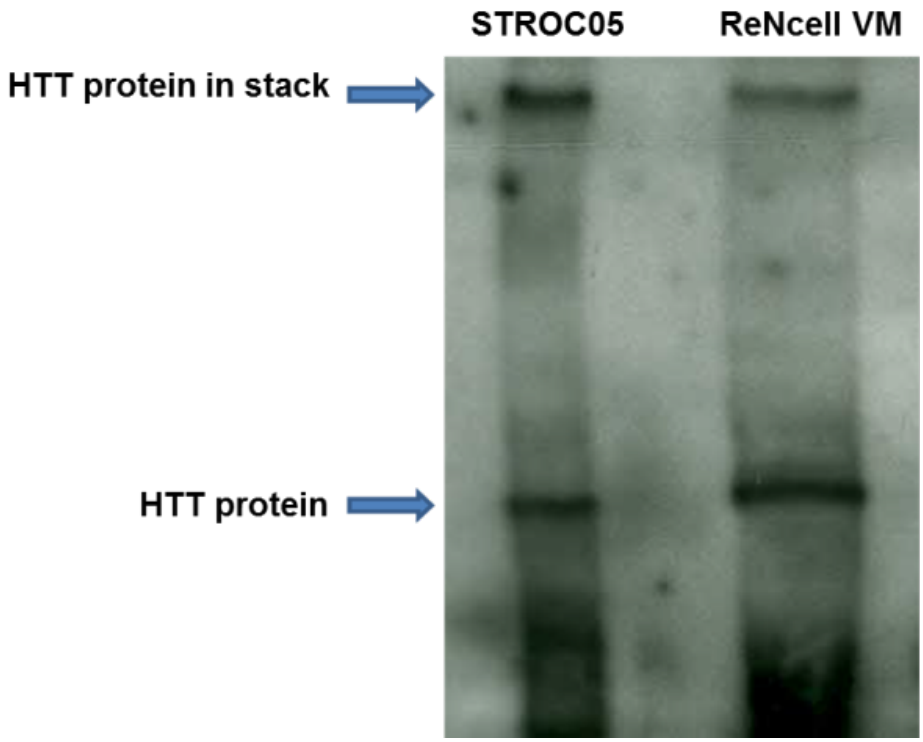


**Figure 3.3: Western blot of protein extracted from STROC05 and ReNcellVM NSCs.** Probing with the anti-HTT MAB2166 antibody confirms the expression of HTT protein in both STROCO5 and ReNcellVM NSC lines.

STROC05 cells were differentiated on coverslips for 3 weeks as per our standard protocol, and tested for electrophysiological activity. The differentiated neurons did not generate action potentials.

Antibiotic kill curves for puromycin were determined and the data is shown in figure 3.4. From this a concentration of **50 ng/ml** was determined to be the minimum required to kill wild-type STROC05 cells over 3-4 days.

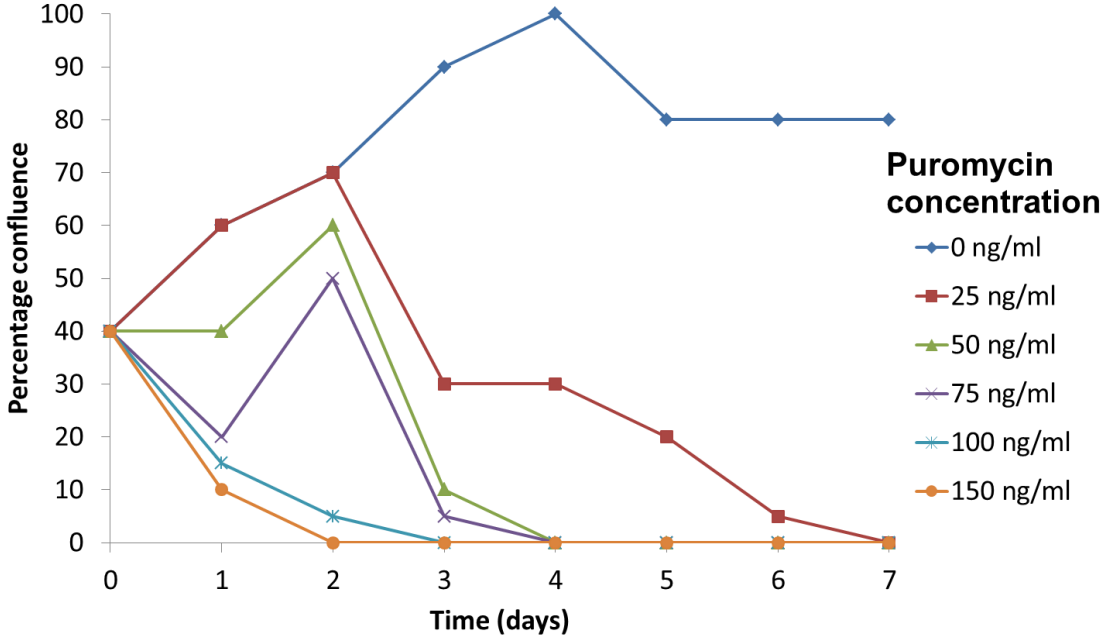


**Figure 3.4**: **Puromycin kill curve in STROC05 NSCs.** Cells were exposed to a range of puromycin concentrations from 0-150 ng/ml, and percentage confluence of the culture was recorded daily. 50 ng/ml is shown to be the lowest concentration of puromycin that kills STROCO5 NSCs over 4 days.

*Effect of activin A on STROC05 cell differentiation*

GABAergic MSNs are the principal projection neurons of the striatum and are defined by their expression of the dopamine- and cAMP-regulated phosphoprotein (DARPP-32). These cells specifically degenerate in early HD. Previous studies have shown that

STROC05 cells differentiate into neurons of which a small proportion are DARPP-32 positive, and this proportion increases on the addition of the Hedgehog agonist purmorphamine (El-Akabawy et al, 2011). Therefore, this was used as the standard differentiation protocol in this study.

The effect of adding activin A at 25 ng/ml throughout the standard 3-week differentiation protocol, both instead of and as well as purmorphamine, was tested. Activin A is a multifunctional TGFβ family protein that has been shown to induce forebrain neurogenesis in a neuronal subtype-restricted manner, and increases striatal neuron differentiation in human pluripotent stem cells (Arber et al, 2015). Primary antibodies against DARPP-32 and FOXP1 (a marker of striatal neuron precursors, normally expressed in the lateral ganglionic eminence) were used to detect MSNs. As can be seen from figure 3.5, STROC05 NSCs yield very few medium spiny neurons on differentiation (as reflected by DARPP-32 and FOXP1 staining), and the addition of activin A made little difference. This may be because the STROC05 cells are derived at too late a gestational stage for activin A to influence striatal development.

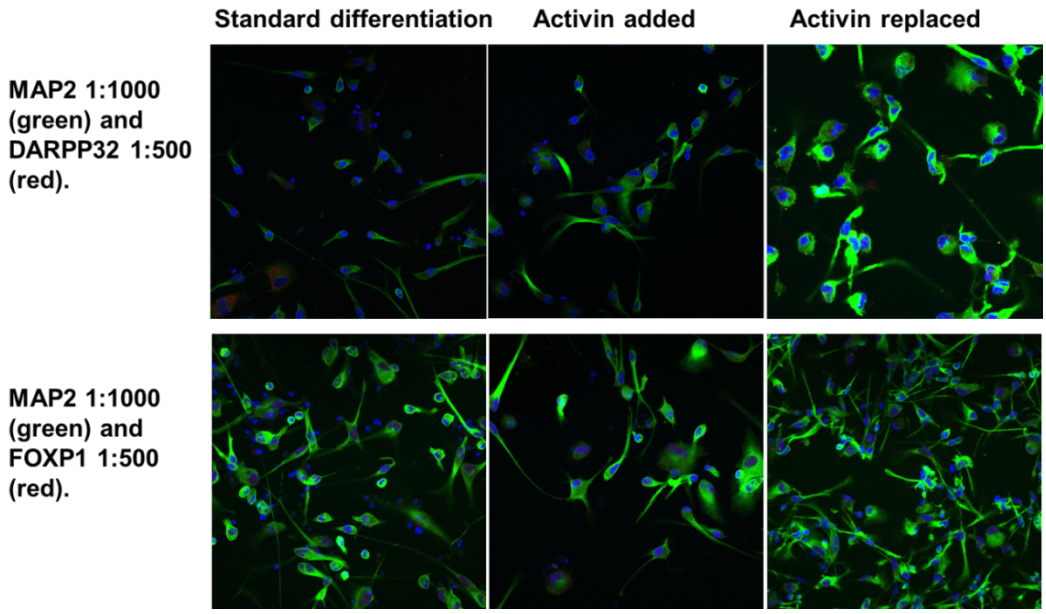


**Figure 3.5**: **Immunofluorescence of dd21 STROC05 cells reveals very few striatal neurons** following the standard differentiation protocol (left images), the addition of activin to the standard protocol (middle images) and the replacement of purmorphamine with activin in the protocol (right images). The addition of activin A to the STROC05 differentiation protocol does not increase the MSN yield in this line. Neuronal marker MAP2 – green; striatal markers DARPP-32 (top panel) and FOXP1 (bottom panel) – red; nuclei (Hoescht) - blue.

Generally, the STROC05 cells were found to be more slow-growing than the ReNcellVM. They did not tolerate repeated passaging as well, and later work found them to be very sensitive to the effects of AAV infection – critical for creation of the knock-in allelic series. For these reasons, in combination with the very low MSN yield on differentiation, future neural stem cell work and cell modelling efforts were concentrated on the ReNcellVM line.

### 3.5.2 Generation of an AAV-mediated knock-in HTT exon 1 allelic series in the ReNcellVM neural stem cell line

The overall aim was to create an isogenic HTT allelic series in the ReNcellVM line, by using AAV to knock-in different CAG repeat lengths (50Q, 80Q and 125Q) at the endogenous *HTT* exon 1 locus. Full length HTT and mHTT would be expressed at physiological levels and direct comparisons between cell lines could be made. An overview of the processes used to generate this line is shown in figure 3.6.

#### 3.5.2.1 Recombinant AAV production and ReNcellVM infection with rAAV

HTT exon 1 vectors with 50, 80 and 125 CAG repeats were created by Horizon Discovery, as per figure 3.7. Vectors contained the puromycin resistance gene to allow for selection of cells that had taken up the vector successfully. LoxP sites flanked the resistance gene, for its later removal by the addition of Cre recombinase in successfully integrated cells. Right and left homology arms containing *HTT* intronic sequence were included to target the vector for homologous recombination. The overall vector size was 7 kb.

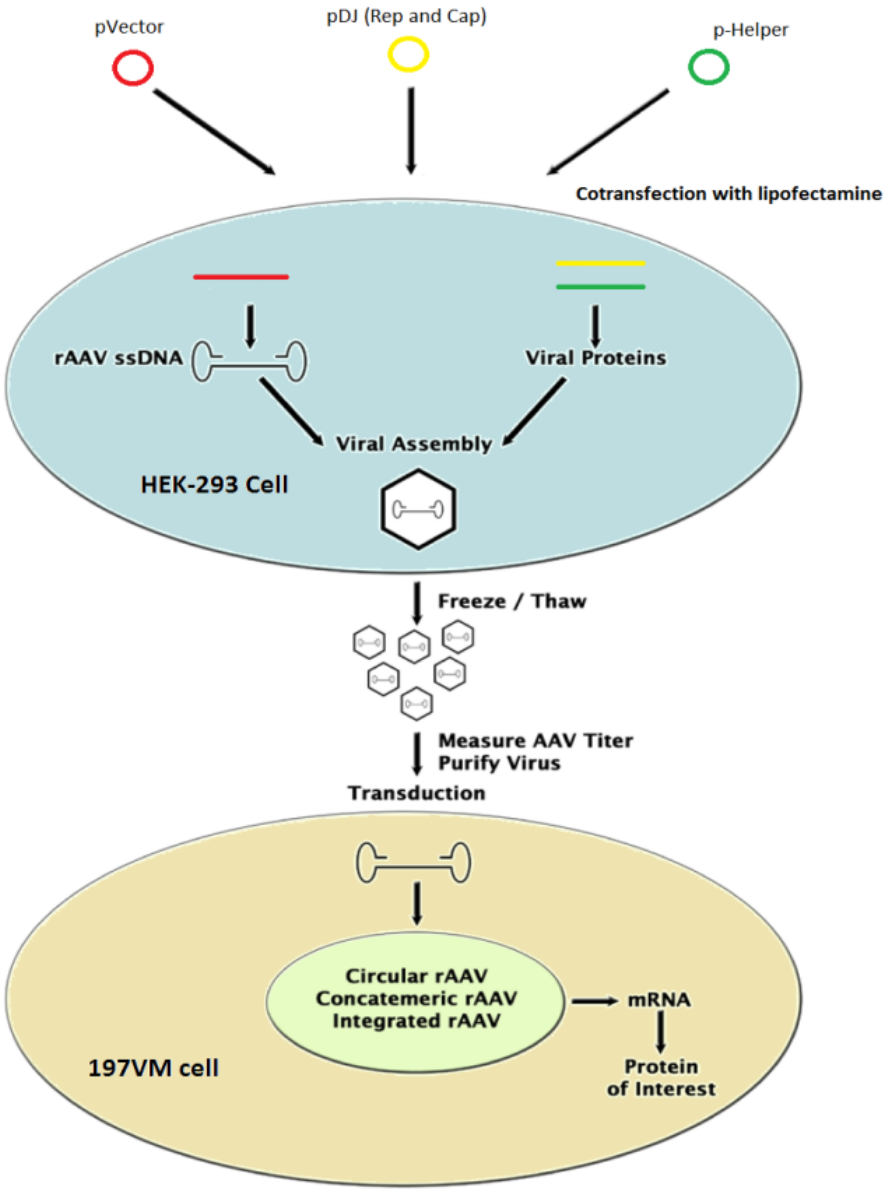


**Figure 3.6**: Overview of recombinant adeno-associated virus generation and subsequent transduction of the ReNcellVM line.

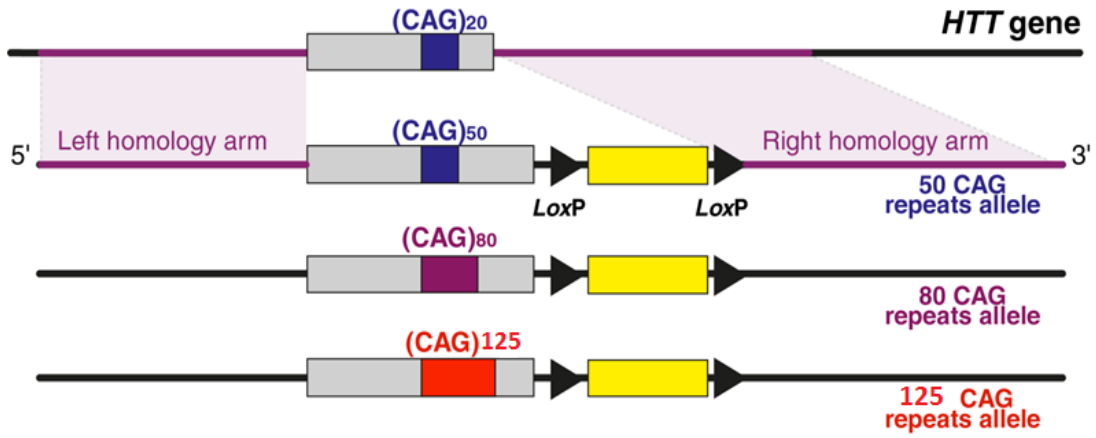


**Figure 3.7**: **Panel of rAAV vectors with three different CAG repeat lengths.** Vectors containing 50, 80 or 125 CAG repeats were generated, each containing a puromycin resistance gene (yellow box) flanked by LoxP sites (black triangle). This was flanked on each side by maximal length left and right homology arms to target the vector correctly for homologous recombination.

Plasmid vectors were packaged into HEK 293T cells using lipofectamine transfection, along with plasmids encoding viral replication and coat proteins, and helper proteins. The resulting rAAV generated was purified, quantified and used to infect ReNcellVM NSCs. An example amplification plot for qPCR for the quantification of rAAV80Q is shown in figure 3.8. Viral titres were calculated for each construct, as shown in table 3.1.

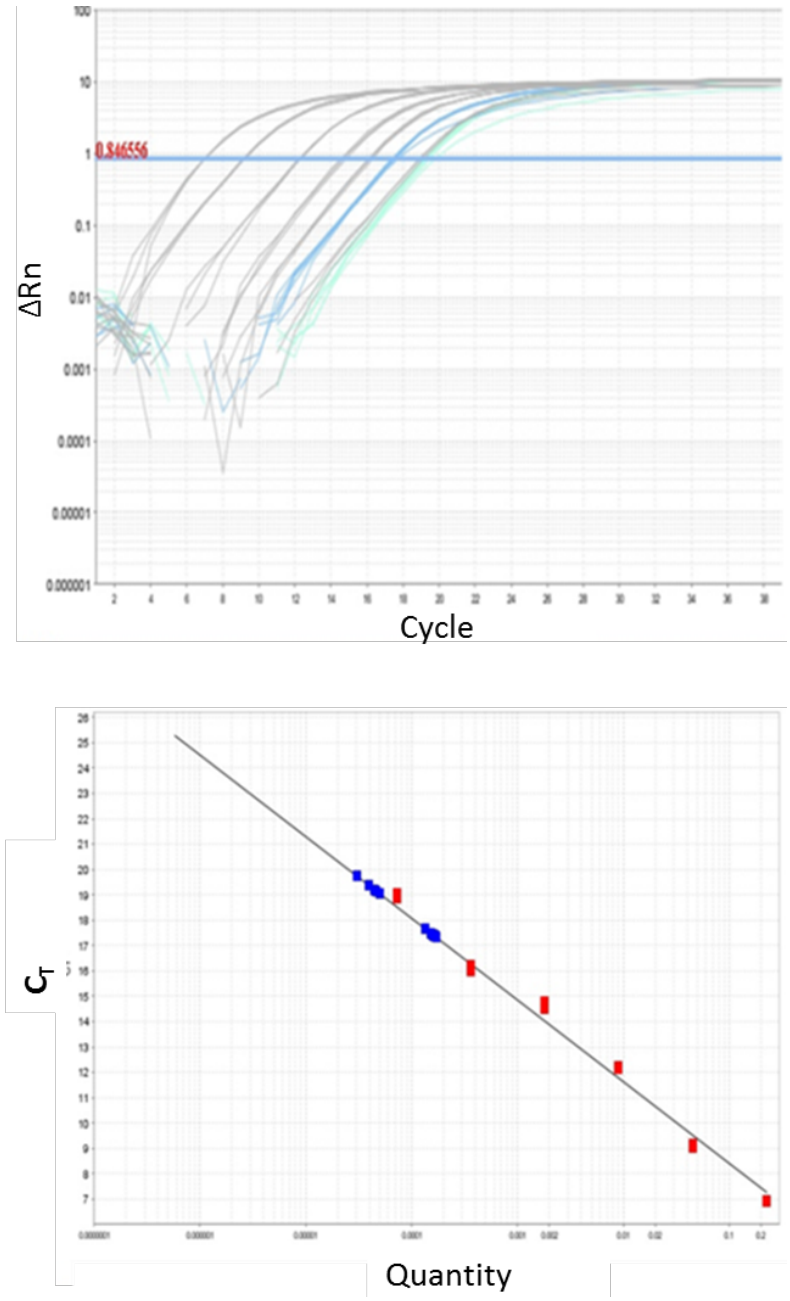


**Figure 3.8**: **Top: Amplification plot for qPCR of AAV80.** Curves in grey correspond to the standards (loaded in triplicate). The blue curve is a 1:15 dilution of the sample, the green curve is 1:30 dilution. $C_T$ values were determined at the threshold shown. **Bottom: Standard curve generated from $C_T$ values** of the standards (plotted in red). The dark blue points correspond to the samples, at the respective dilutions. On calculating the final viral titre, this dilution factor and the dilution used throughout the RT-PCR setup was multiplied by the quantity generated from the standard curve.

| Virus construct | Genome Copies /ml (also equivalent to MOI) |
|---|---|
| rAAV50 | $7.85 \times 10^{11}$ |
| rAAV80 | $9.7 \times 10^{11}$ |
| rAAV125 | $5.56 \times 10^{11}$ |

**Table 3.1**: Viral titres of all three constructs.

Following infection and two weeks of antibiotic selection with puromycin, vials of selected ReNcellVM NSCs of at least $1x10^6$cells were frozen down and stored in liquid nitrogen.

### 3.5.2.2 Screening ReNcellVM NSCs for homologous recombination of rAAV HTT exon 1 vectors

A PCR-based screening strategy was employed. Primers were designed that would distinguish a positively integrated vector, and also generate an internal positive control band from the wild type allele, thus confirming that the PCR reaction had worked. The DNA sequence of the forward primer site in the left homology arm was also included in the vector just after the puromycin resistance gene, forming a second “nested” forward primer site. In theory, a cell with a correctly targeted vector gives rise to three different products, as shown in figure 3.9. The screening primer was referred to “RH2”.

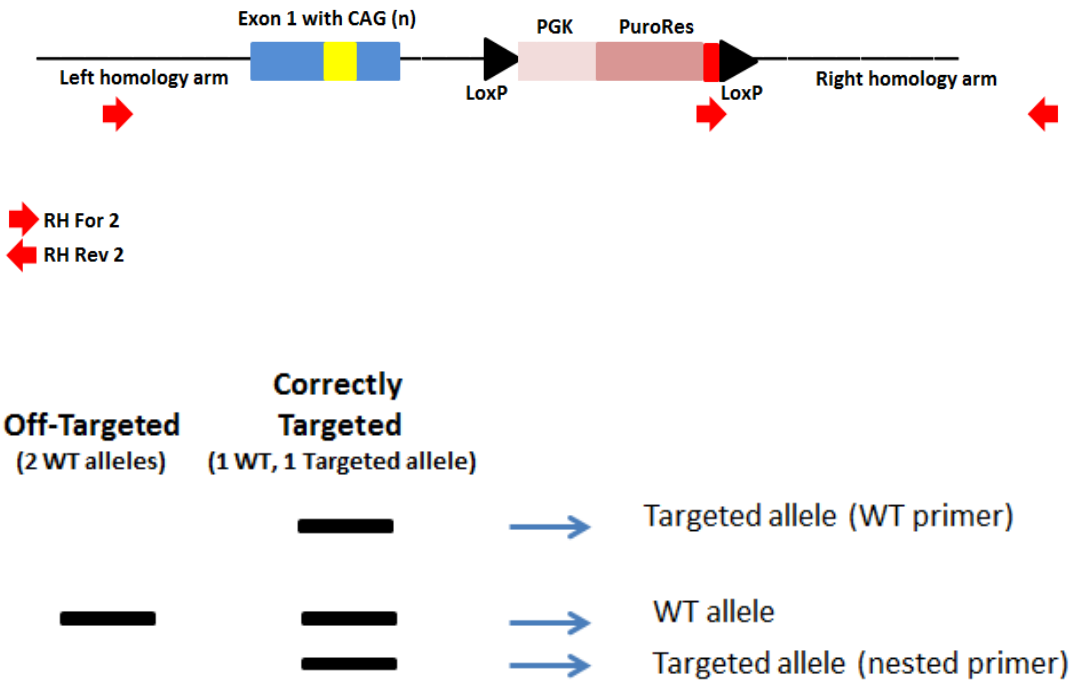


**Figure 3.9: Top panel - design of screening primers "RH2".** The DNA sequence of the forward primer site in the left homology arm is also present immediately following the puromycin resistance gene, forming a second "nested" forward primer site. The RH2 forward primer would therefore amplify from both these sites, paired with the RH2 reverse primer, giving rise to two PCR products of different lengths from a correctly targeted allele. **Bottom panel - PCR bands generated from off target and correctly targeted integration of vector.** In the case of a correctly targeted cell, two PCR bands are generated from the positively integrated allele and one further PCR band from the wild type allele, as shown.

Using RH2 primers, the size in base pairs of the expected products following positive homologous recombination is shown in table 3.2.

| | Targeted allele | Wild-type allele | Nested allele |
|---|---|---|---|
| **AAV 50** | 3351 | 1960 | 1652 |
| **AAV 80** | 3441 | 1960 | 1652 |
| **AAV 125** | 3576 | 1960 | 1652 |

**Table 3.2**: Expected size of DNA bands generated from PCR with RH2 primers.

Due to the large size of the full-length targeted allele and the need for PCR amplification over a long CAG repeat in order to form this product, it was not necessarily expected to see this product following PCR reactions. The presence of the nested allele in addition to a wild-type allele would indicate successful “on-target” recombination.

Cells were seeded at a density of ten cells per well into 96-well plates and grown until confluent. Our screening strategy was to identify a well containing a positively integrated cell (or colony), and to then carry out single cell dilution from this “positive pool” in order to isolate a positively integrated clone. A density of 100 cells per well was also attempted for screening of pools, however no positive pools were identified using this approach. This was thought to be due to the PCR screen not being able to amplify any potential “nested allele” in the presence of a much higher ratio of wild type alleles (around 1:200 assuming one positive integration per well), due to competition for the same primers. Single cell dilution into 96 well plates and PCR screening of subsequent colonies was also attempted. However, due to the low homologous recombination rate, this approach did not yield any positive hits and so a seeding density of ten cells per

well was employed. It was however confirmed that the ReNcellVM lines were able to tolerate single cell dilution.

Cells from each well of a 96-well plate seeded at 10 cells per well were lysed and screened using PCR as described. Overall, the following numbers of corresponding pools that were screened in this way are shown in table 3.3. This suggests a very low rate of homologous recombination of the rAAV vector in our ReNcellVM line.

| Cell line | Number of pools screened | Putative positive pools identified |
|---|---|---|
| ReNcellVM 50Q | 780 | 0 |
| ReNcellVM 80Q | 734 | 3 |
| ReNcellVM 125Q | 679 | 0 |

**Table 3.3:** Total screened number of pools derived from seeding density of 10 cells per well.

*Identification and verification of a ReNcellVM pool containing a correctly integrated rAAV vector*

An example of a PCR reaction identifying our first positive pool (P1) following a screen of ReNcellVM 80Q is shown in figure 3.10.

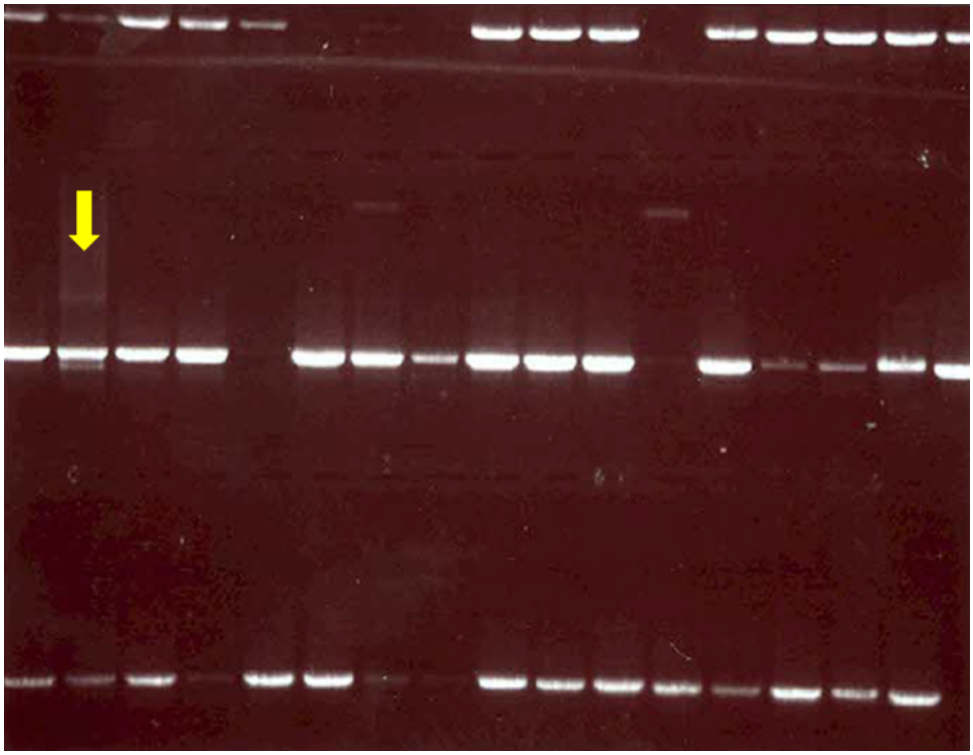

**Figure 3.10**: **Identification of ReNcellVM NSC pool containing a correctly integrated rAAV 80Q vector.** PCR reaction with RH2 primers showing amplification of a wild-type band and “nested” allele underneath it.

The PCR product was also run out further on the gel in order to more accurately size the lower product (figure 3.11).

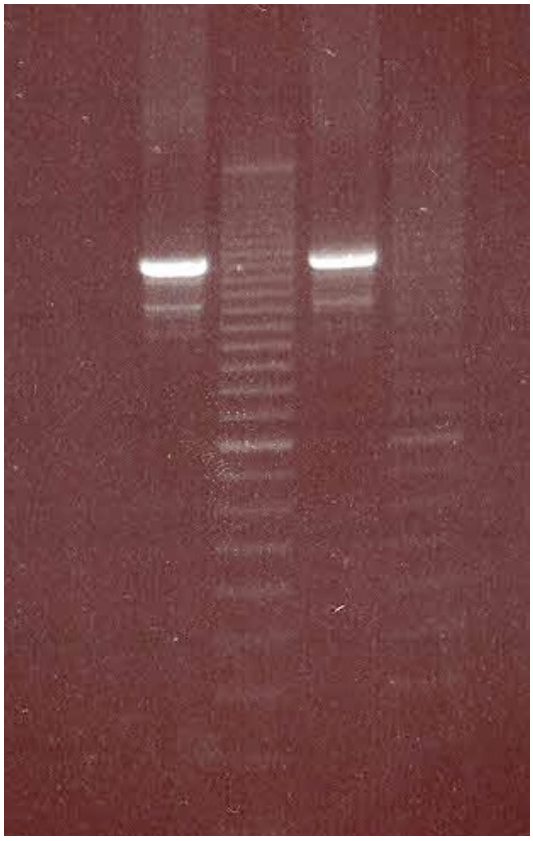

**Figure 3.11: Further testing of ReNcellVM NSC pool containing a potentially correctly integrated rAAV 80Q vector.** Duplicate PCR reactions with RH2 primers on lysed gDNA from P1 cells was carried out and the PCR products were run out further on the agarose gel in order to more accurately size the lower band. The nested allele is confirmed to be between 1600-1700bp in size (Expected size=1652).

Due to the small size difference between the wild type and nested allele, the PCR product was run for 3 hrs to achieve sufficient separation for sizing. This led to leaching of SYBRSafe from the agarose gel, causing difficulties in visualisation, but the problem was overcome by placing the gel in a 1/10,000 SYBR-bath for 30 min with agitation before imaging. The lower band was of the expected size corresponding to the nested allele.

The positive pool of cells was expanded, and vials were frozen down and stored in liquid nitrogen. Further experiments were undertaken to verify this potential positive pool. It was not possible to directly sequence the pool as it contained mixed clones. Therefore the lower band was extracted from the agarose gel and purified. Sixty µl of purified DNA was obtained, at a concentration of 2.7 ng/ml, but ultimately this was not sufficient for successful sequencing.

A “nested PCR” strategy was therefore employed to confirm the identity of the lower band of PCR product. Primers were designed as shown in figure 3.12, and used to test the extracted, purified DNA from the lower gel band.

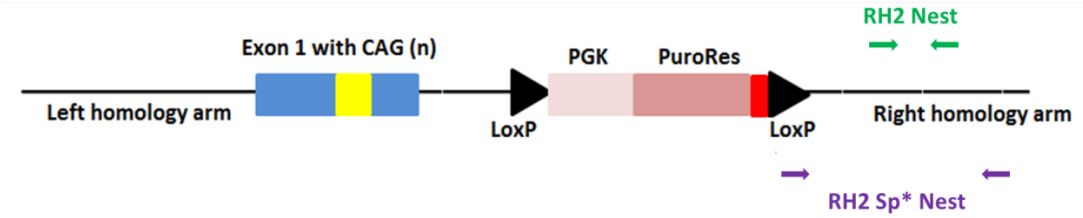


**Figure 3.12: Design of “nested PCR” primers.** Primers RH2 Nest and RH2 Sp* Nest designed to confirm identity of the extracted lower band from PCR of the potential ReNcellVM 80Q NSC pool.

The RH2 Nest primers would amplify from both the integrated vector and also the wild type band (which may be contaminating the purified sample due to its proximity to the lower band on the gel). The RH2 Sp* Nest primer set would only amplify from an integrated vector and not the wild type band due to the forward primer being sited in the LoxP site. Results of PCR using these primer sets are shown in figure 3.13.


**Figure 3.13: "Nested PCR" confirms that the ReNcellVM pool P1 does contain the correctly integrated 80Q rAAV vector.** PCR on DNA from extracted lower band on agarose gel (lanes 1 + 4), wild type ReNcell whole genomic DNA (lanes 2 + 5) and water (lanes 3+6). Lanes 1-3 were amplified using RH2 Nest primers and lanes 4-6 using RH2 Sp* Nest primers. The amplification of PCR product in lanes 1 and 4 confirms that the DNA from the extracted band contained the 80Q rAAV vector. The band in lane 2 is to be expected as RH2 Nest primers can amplify from the wild-type *HTT* allele.

**This suggests that this particular cell pool (P1) did contain a positively integrated clone.**

*Identification of further ReNcellVM pools containing a correctly integrated rAAV vector*

Two further potentially positive ReNcellVM 80Q pools (P2 and P3) were identified as shown in figure 3.14. On running these products out further on the gel (figure 3.15), P2 was sized correctly for the nested allele but P3 was not. However, on performing gel extraction and DNA purification of the P2 lower band, followed by nested PCR reactions as described above (figure 3.16), this was also proven to be a false positive.

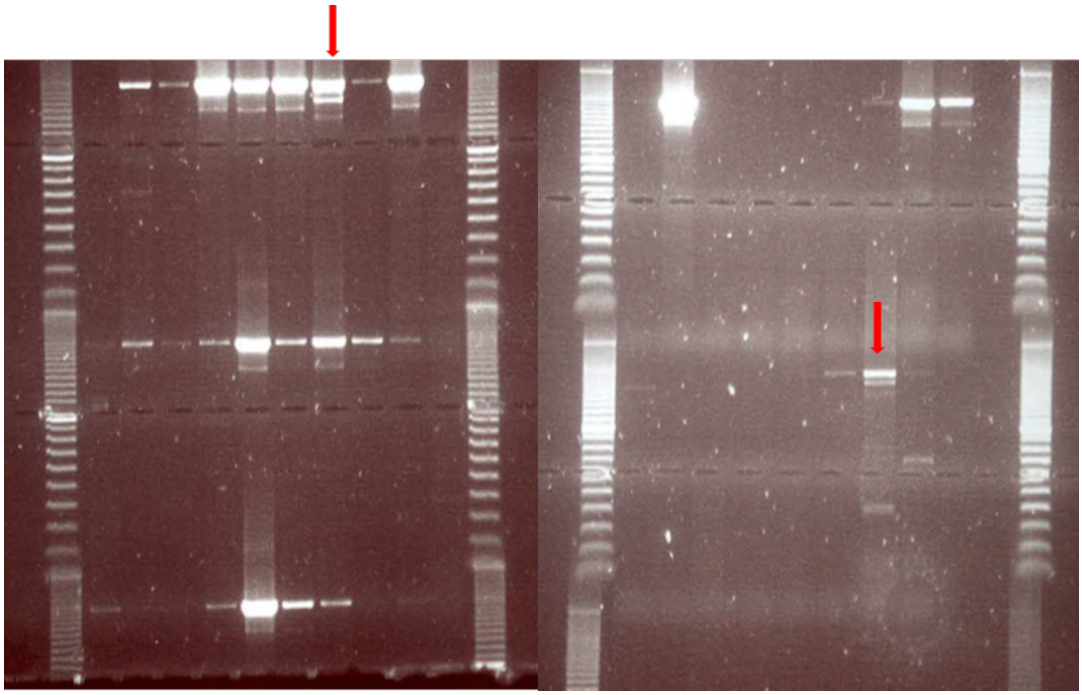

**Figure 3.14**: **Identification of further potential ReNcellVM NSC pools containing a correctly integrated rAAV 80Q vector.** Two further ReNcellVM 80Q pools, designated P2 and P3, gave a possible “nested” band on PCR (red arrows).

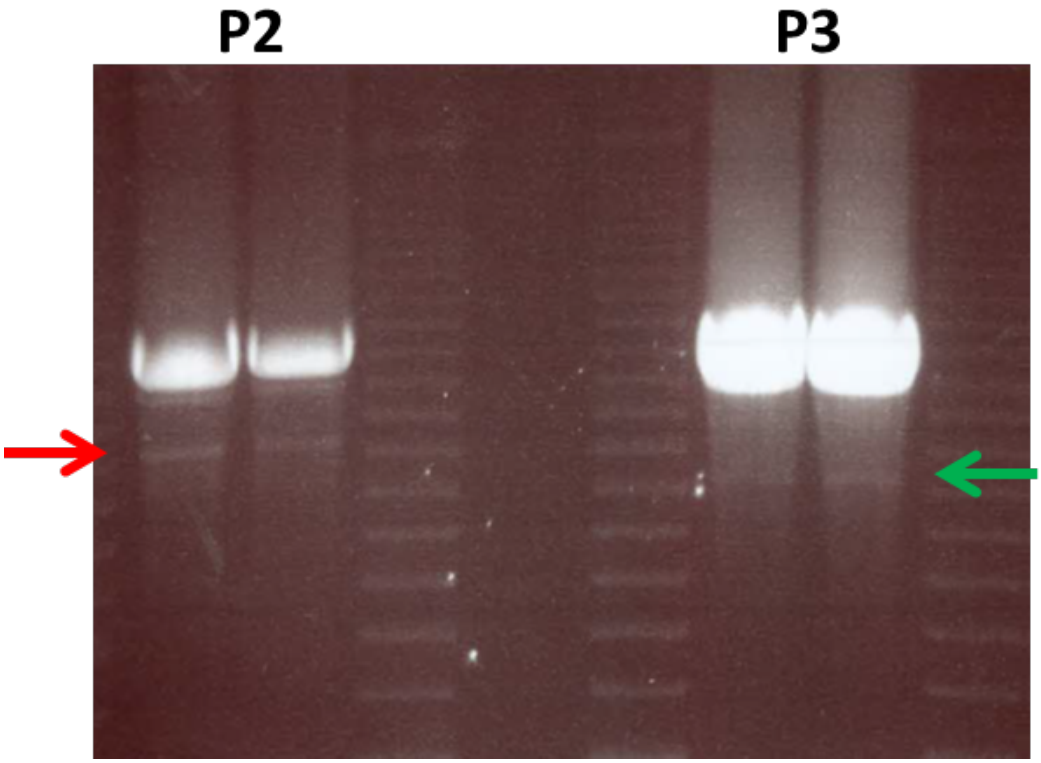


**Figure 3.15: Further testing of P2 and P3 ReNcellVM NSC pools.** Duplicate PCR reactions with RH2 primers on lysed gDNA from P2 and P3 cells was carried out and the PCR products were run out further on the agarose gel in order to more accurately size the lower band. P2 is on left, and is sized correctly (between 1600 and 1700bp) for the expected product (red arrow). However, P3 on the right is too small (green arrow).

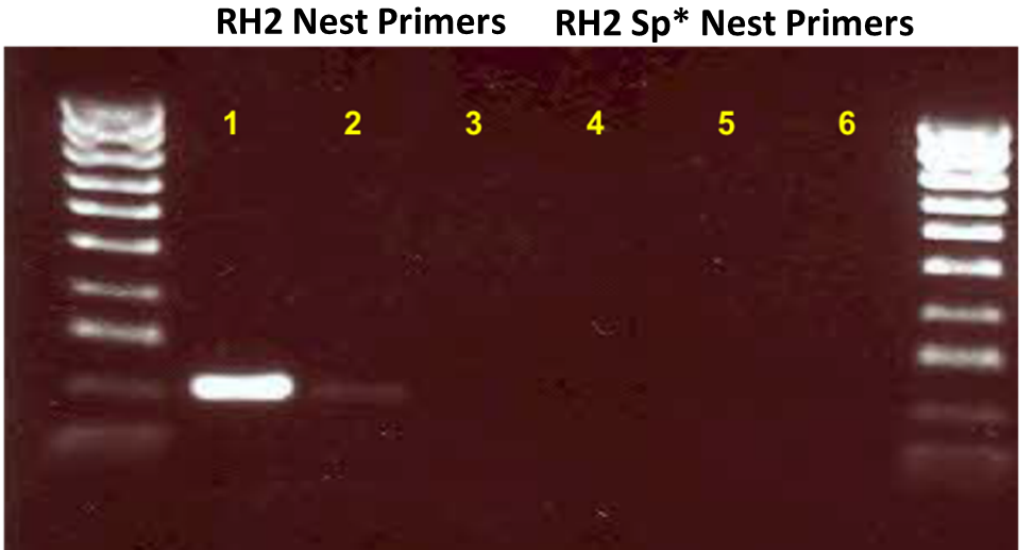


**Figure 3.16: "Nested PCR" shows that the ReNcellVM pool P2 does not contain the correctly integrated 80Q rAAV vector.** PCR on P2 DNA from extracted lower band on agarose gel (lanes 1 + 4), wild type ReNcell whole genomic DNA (lanes 2 + 5) and water (lanes 3+6). Lanes 1-3 were amplified using RH2 Nest primers and lanes 4-6 using RH2 Sp* Nest primers. The amplification of PCR product in lanes 1 and 2 is likely to be amplification from a wild-type HTT allele, given the lack of any PCR product in lane 4.

### 3.5.2.3 Isolating a single positively integrated clone within a positive ReNcellVM pool

Having isolated one positive pool (P1) of ReNcellVM 80Q cells, the plan was to isolate at least one clone with the positively integrated AAV-80Q construct. The clonal line would then be treated with Cre recombinase in order to remove the PGK/Puromycin cassette which is flanked by LoxP sites within the vector. This would leave only the expanded HTT exon 1 in its native gene locus.

Initially the screening PCR with RH2 primers was repeated on DNA from lysed P1 cells. On confirming that this pool still contained the integrated AAV-80Q vector, 5 x 96-well plates were seeded at 1 cell per well (single cell dilution) to make clonal populations. The positive pool was expanded and vials were frozen down. Overall, over a 2 week period 52 clones were identified, genomic DNA was isolated and PCR screened with RH2 primers. Unfortunately, none of these clones contained the positively integrated vector.

On thawing frozen vials of P1 cells for further single cell cloning, the pools were retested to ensure that they still contained the positively integrated vector. Unfortunately, it was found that this was not always the case. Most of the thawed vials of banked P1 cells were negative for the positively integrated vector; the few that displayed a nested allele when tested immediately post thaw, then tested negative by the subsequent passage. This would suggest that any positively integrated cells within the pool have a survival disadvantage on freeze-thawing and/or repeated passaging.

#### 3.5.2.4 Alternative screening strategies to identify and isolate ReNcellVM NSCs containing correctly integrated rAAV vectors

Bulk pools of ReNcellVM 80Q NSCs that had been frozen down post antibiotic selection were tested using PCR with primers designed to amplify only in the presence of a homologous recombined construct. These were designed such that the forward primer was sited in sequence specific to the vector (i.e. the LOXP site, PGK promoter

or puromycin resistance gene) and the reverse primer was outside the right homology arm. These primers are designed to be used directly on lysed gDNA from the ReNcells. Unfortunately there is no internal positive control band generated, as there is with our RH2 screening primers – for this reason these primer sets were not used in our initial screening approach. However, as there are no competing DNA products (nothing is amplified from the wild type allele), the PCR reaction would have sufficient power to detect even a very small proportion of homologous recombined cells.


**Figure 3.17: PCR of DNA from bulk pool ReNcell 80Q lysate with 10 different screening primer sets.** In lanes 1-9 primers were designed as described above. Lane 10 primers were entirely within the PGK/Puromycin segment, which would detect the presence of the 80Q vector anywhere in the genome. PCR bands of the expected size are seen in lane 1, 2 and 7, suggesting this pool did contain the correctly integrated rAAV 80Q vector.

Three of the nine primer sets that were designed to detect homologous recombination directly from lysed cells amplified products of the expected size (figure 3.17),

confirming that the original bulk pool did contain the positively integrated product. These three primer sets were designated A, B and C.

Using the same primer sets (A, B and C) bulk pools of ReNcellVM 125Q were thawed and tested, and also showed that the positively recombined vector was present (figure 3.18).

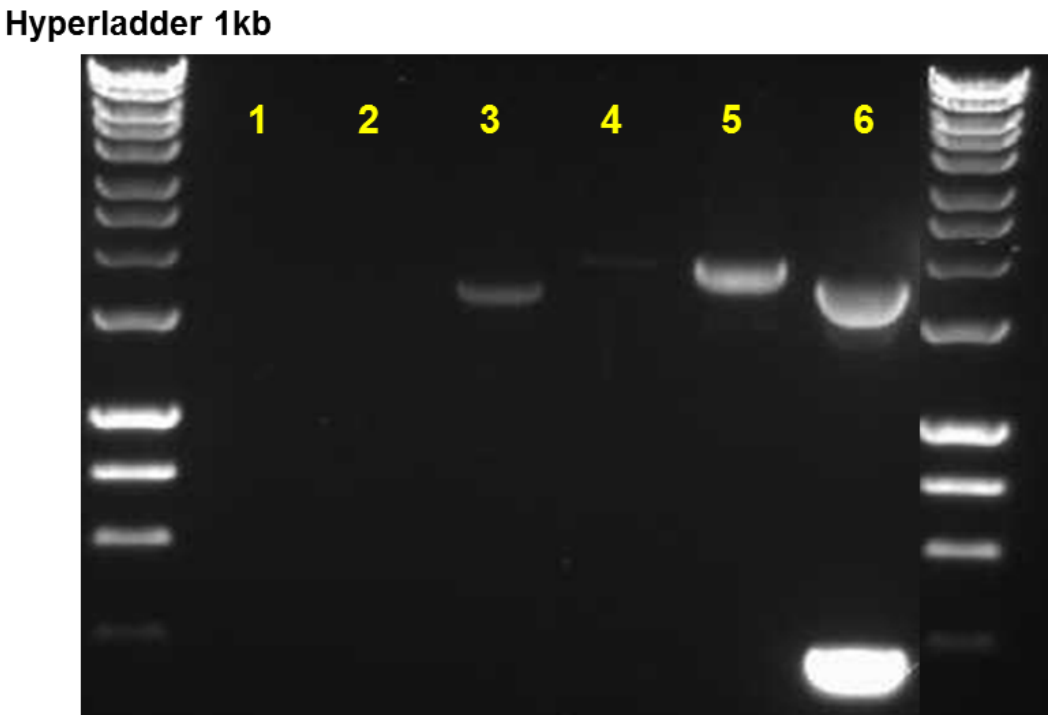


**Figure 3.18: PCR of DNA from bulk pool ReNcell 125Q lysate.** DNA was tested with primer set A, B and C (lanes 1-3 respectively), LH2 primers (lane 4) RH2 primers (lane 5) and PGK/Puromycin primers (lane 6). The amplified band in lane 3 suggests correctly integrated rAAV 125Q vector in this pool of ReNcellVM NSCs.

However, other vials of cells that were frozen down at the same time and from the same batch did not amplify anything using these primers, just as was observed for P1

cells. On seeding the positive bulk pool ReNcellVM 125Q at 1000 cells per well into a 96 well plate, and screening the subsequent lysates, no positive pools were identified. These two findings again raise the possibility of a selective disadvantage for positively integrated cells on thawing, or a slower rate of proliferation compared to non-integrated cells such that the percentage of positively integrated cells decreases exponentially with each passage.

#### 3.5.2.5 HCT116 cell line infection with rAAV and subsequent screening for homologous recombination of rAAV HTT exon 1 vectors

It was also considered that the homologous recombination rate in the ReNcellVM line may be very low due to intrinsic properties of the neural stem cells. HCT116 cells are a robust and commonly used human colonic cancer cell line that has previously been to be generally amenable to AAV infection and site directed genetic manipulation (Khan et al, 2011). HCT116 cells were therefore infected with rAAV 125Q at 100,000 viral particles/cell for 72 hrs, and the infected cells were expanded. After 24 hrs puromycin (0.35 µg/ml) was added to the NSC medium, and the cells remained under antibiotic selection for two weeks. Post selection, vials of cells were frozen down.

Lysate from bulk pools of infected, selected HCT116 125Q cells was tested using PCR with various screening primers as shown in figure 3.19.

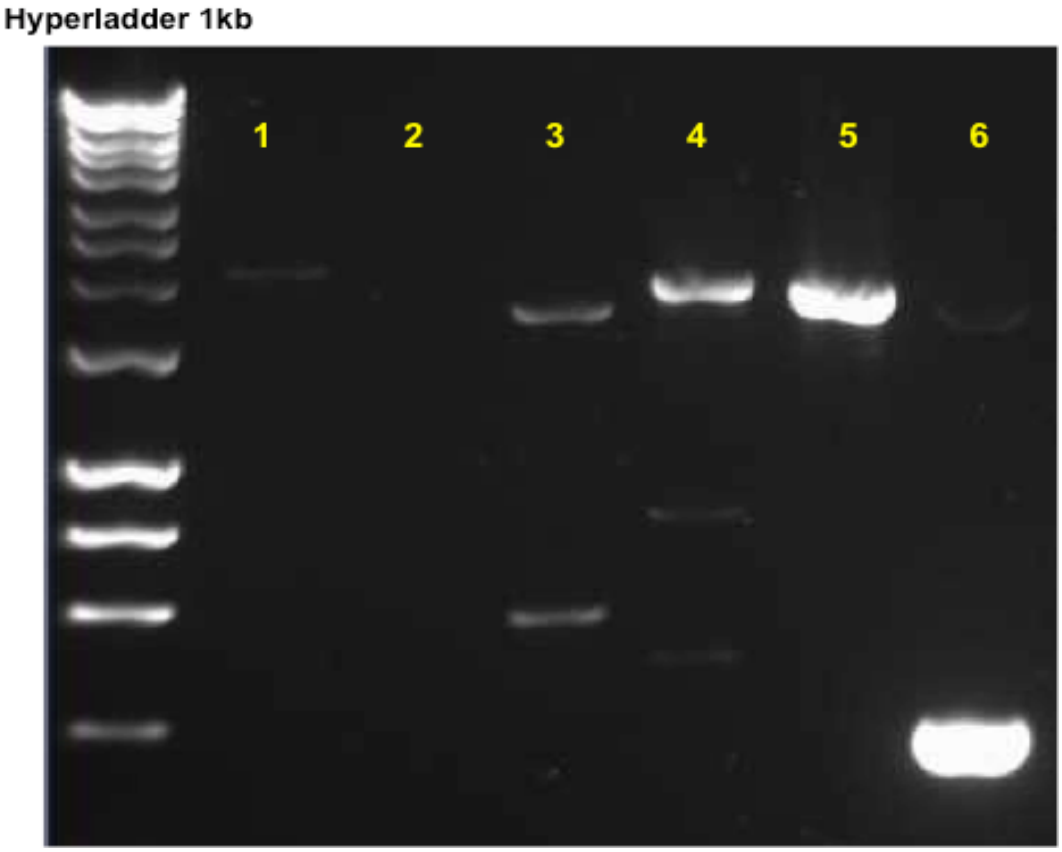


**Figure 3.19: PCR of DNA from bulk pool HCT116-125Q lysate.** DNA was tested with primer set A, B and C (lanes 1-3), LH2 primers (lane 4) RH2 primers (lane 5) and PGK/Puromycin primers (lane 6). Amplification of bands in lanes 1 and 3 suggest correct integration of the rAAV 125Q vector in these cells.

This confirmed positive integration of AAV125 in the HCT116 cells, and the infected, selected cells were therefore seeded at 1000 cells per well into 20 wells of a 96-well plate and once confluent, gDNA lysate was tested using primer set A, B and C. The results using primer set C showed the clearest amplification and the results are shown in figure 3.20.

**Figure 3.20: PCR of DNA from 1000 cell per well pools of HCT116-125Q cells.** Of the 20 wells tested with primer set C, 3 were found to be positive i.e. to contain cells with the homologous recombined vector.

Cell pools from these three wells were then expanded, frozen down and stored, and at the same time, one cell pool was reseeded at 100 cells per well into 20 wells of a 96 well plate, and re-screened with primer set A and C when confluent. A PGK/Puromycin primer set was also used as a positive control for the PCR reaction and to confirm the presence of the rAAV vector anywhere in the cells. From this, one positive pool was identified and designated HCT-P1 (figure 3.21).

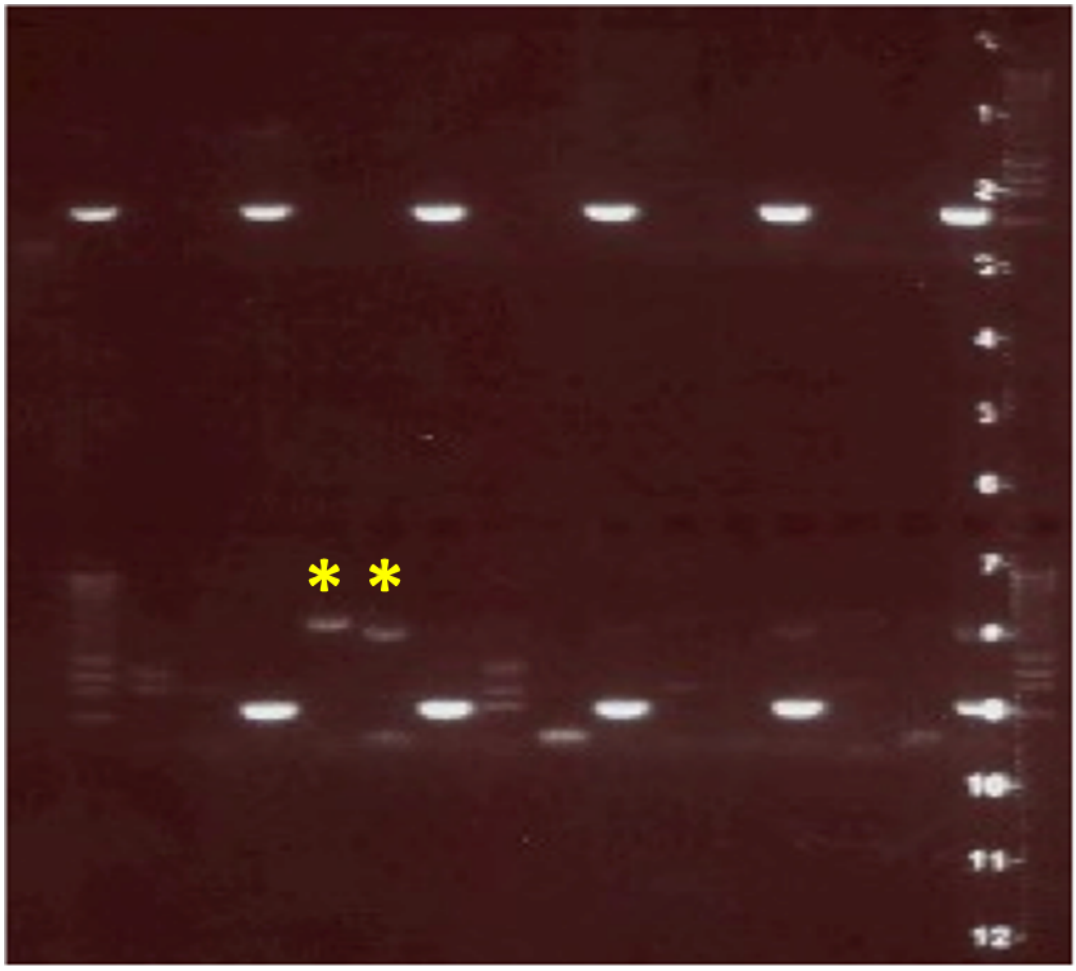


**Figure 3.21: PCR of DNA from 100 cell per well pools of HCT116-125Q cells.** 10 separate pools were tested. For each pool, primer sets A, C and PGK/Puromycin were used (loaded left to right for each sample). 1 positive pool (marked by yellow stars) was identified.

HCT-P1 cells were plated out directly at 10 cells per well into 48 wells of a new 96W plate (i.e. with no further passages between), but on PCR testing the subsequent lysates from these wells using primer set A, B and C, no positive pools were identified. Therefore although with the HCT116 line three positive pools were identified from twenty wells seeded at 1000 cells per well, suggesting a higher recombination rate than the ReNcellVM line, ultimately the problem of loss of positive signal over subsequent passages, freeze/thawing and expanding from low cell seeding density (which places

extra stress on the cells) precluded the successful isolation of a single homologously recombined HCT116 clone.

### 3.5.3 Generation and characterisation of an allelic series HTT exon 1 overexpression model in the ReNcellVM neural stem cell line

#### 3.5.3.1 Generation of HTT exon 1 overexpressing ReNcellVM cells

This line was gifted to us by Professor Gillian Bates (King's College London). Briefly, ReNcellVM NSCs underwent lentivirus transduction with vectors containing *HTT* exon 1 with 29, 71 and 129 CAG repeats respectively, each linked with an internal ribosome entry site (IRES) to the gene encoding green fluorescent protein (GFP) (figure 3.22).

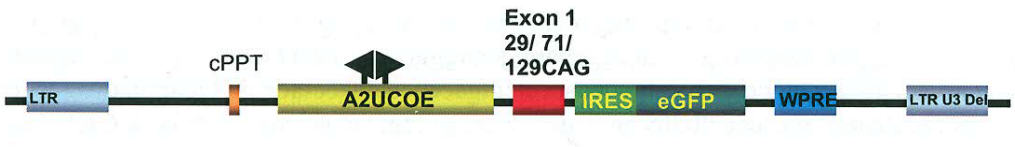


**Figure 3.22**: **Plasmid vector used to create the HTT exon 1 overexpression line.** Reproduced from Sirinathsingh: "Generation of human stem cell models of Huntington's disease".

The vectors were created by Dr. Sirinathsingh using molecular cloning methods. The A2UCOE promoter reduces the chance of post-integration transgene silencing by

conferring a dominant chromatin opening function that is a more transcriptionally active structure. The internal ribosome entry site (IRES) sequence allows translation initiation in the middle of an mRNA, allowing for the independent translation of *HTT* exon 1 and *GFP*. The woodchuck post-transcriptional regulatory element (WPRE) is commonly inserted into lentiviral contructs to increase mRNA transport out of the nucleus, hence increasing viral titre (Sirinathsingh, 2009). To create a negative control line, ReNcellVM NSCs were transduced with a *GFP*-only expressing vector.

It is worth noting that each *HTT* exon 1 vector terminates the polyglutamine CAG tract with a further CAA-CAG. Therefore on translation a protein with 31, 73 and 131Q is formed from 29, 71 and 129 CAG respectively. However for the sake of clarity, throughout the rest of this thesis, they will be referred to as 29, 71 and 129Q or CAG interchangeably depending on whether the protein (Q) or gene (CAG) is being discussed.

For each line, the cells were sorted by fluorescence activated cell sorting (FACS) on the basis of GFP expression. Four populations of low to high expressing cells were pooled for each line, and these were labelled POP7 (lowest expression level), POP4 (low middle expression level), POP5 (high middle expression level), and POP6 (highest expression level). Vials of cells were received that had been transduced with GFP-only and *HTT* exon 1 29Q, 71Q and 129Q constructs, of different POP numbers.

These vials were thawed, mycoplasma tested, expanded over 2-3 passages and pellets prepared for Western blotting and HTT quantification using the ELISA-based MSD electrochemiluminescence assay. The aim was to find a panel of cell lines with

similar expression levels of HTT exon 1 in order to ascertain the effect of increasing CAG repeat length on cellular phenotypes and the behaviour of the HTT exon 1 protein itself.

### 3.5.3.2 Quantification of HTT exon 1 expression in ReNcellVM lines

Western blotting with 4C9 and S830 antibody identified at least one ReNcellVM line expressing each of the constructs. Both these antibodies are HTT specific. 4C9 is a monoclonal antibody raised against the human specific proline-rich region (amino acid 65–84). S830 also binds to the N-terminal of HTT (amino acids 1-90) but has a higher affinity for expanded polyglutamine lengths. As can be seen from figure 3.23, of the cells that were tested only one HTT exon 1 129Q expressing line was identified. HTT exon 1 29Q and 71Q lines with a matched or similar level of expression were therefore sought.

The membrane was stripped and re-probed with GFP and β-actin antibody, and the results were analysed using densitometry to calculate the intensity of the bands, as shown in figure 3.24. The GFP:β-actin ratio was determined to give an indication of the levels of GFP expression in the cell, and the percentage of GFP expression relative to the 129Q POP 7 line was calculated. Due to the design of the transgene construct, with the GFP gene linked via an IRES construct to HTT exon 1, the levels of GFP expression are assumed to be proportional to the level of HTT exon 1 expression.

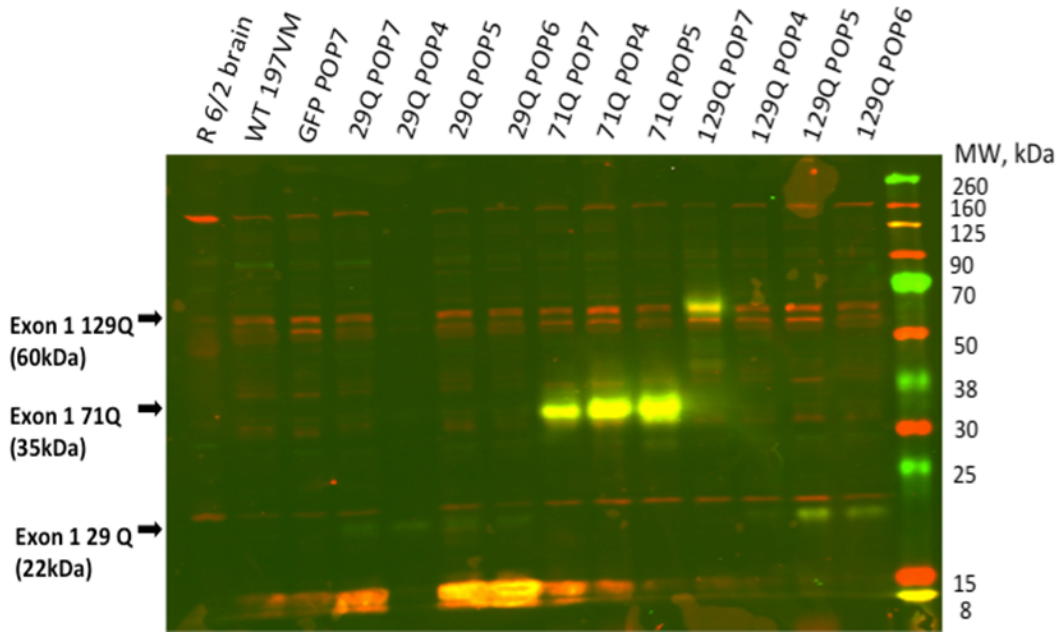


**Figure 3.23**: **Western blot of HTT exon 1 overexpressing and GFP only ReNcellVM NSCs.** Of the 129Q lines, only 129Q POP7 is expressing the mutant 129Q exon 1 – the remaining 4 129Q lines are not (indeed, they seem to be expressing a 29Q exon 1 product). Green – S830 antibody, Red – 4C9 antibody.

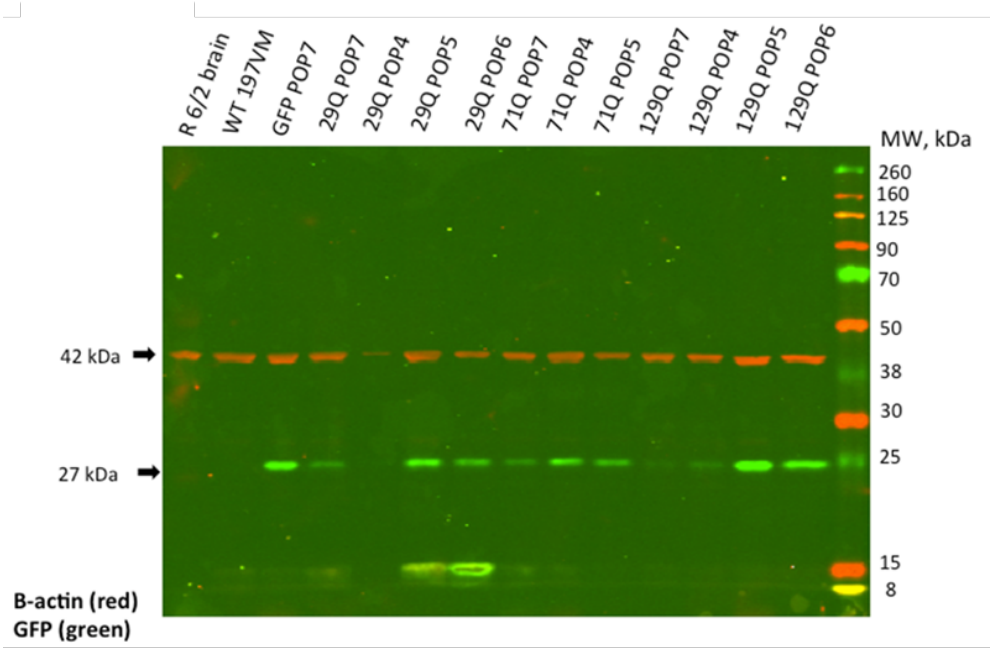


| Band intensity as determined using densitometry | | | | Relative % expression |
|---|---|---|---|---|
| Sample | GFP | b-actin | GFP:b-actin | |
| R6/2 | 0.0 | 3566.6 | 0.00 | **0** |
| 197VM WT | 0.0 | 5880.0 | 0.00 | **0** |
| 29Q POP 4 | | 695.0 | 0.00 | **0** |
| 129Q POP 7 | 913.1 | 4669.3 | 0.20 | **100** |
| 129Q POP 4 | 1431.9 | 4583.0 | 0.31 | **160** |
| 29Q POP 7 | 2194.2 | 5123.3 | 0.43 | **219** |
| 71Q POP 7 | 1795.4 | 3840.4 | 0.47 | **239** |
| 71Q POP 4 | 5431.5 | 5471.4 | 0.99 | **508** |
| 71Q POP 5 | 3900.5 | 3184.2 | 1.22 | **612** |
| 29Q POP 6 | 4267.7 | 3237.8 | 1.32 | **674** |
| 29Q POP 5 | 7630.6 | 5496.0 | 1.39 | **710** |
| 129Q POP 6 | 10385.6 | 7409.0 | 1.40 | **717** |
| GFP POP 7 | 8456.9 | 5142.0 | 1.64 | **841** |
| 129Q POP 5 | 11631.5 | 6839.4 | 1.70 | **870** |

**Figure 3.24: Top panel: Western blot of GFP and β-actin in HTT exon 1 overexpressing ReNcellVM lines.** Green – GFP, Red - β-actin. **Bottom panel: Quantification of blot using densitometry** of bands to determine GFP expression relative to the 129Q POP 7 line (the only 129Q expressing line). A matched expressing HTT exon 1 29Q/71Q/129Q panel is highlighted in green, and a matched highly expressing HTT exon 1 29Q/71Q pair of lines are highlighted in blue.

Using this method some variability of GFP expression level was found, even between lines of the same POP. However, a pair of HTT exon 1 29Q and 71Q highly-expressing lines were identified. An allelic series of ReNcellVM HTT exon 1 29Q, 71Q and 129Q POP 7 cells with lower, and relatively well matched expression levels of HTT exon 1 was also identified.

To ensure that the stripping process did not have an effect on the GFP analysis, the same gel samples were run again, and the membrane probed directly with GFP and β-actin antibody. On this occasion the band intensity was calculated directly using the Licor Odyssey software. Direct probing of the membrane revealed even greater variability of relative GFP expression levels across constructs of the same POP level, and across the whole range of lines generally, however this analysis also confirmed the well matched high-expressing ReNcellVM HTT exon 1 29Q/71Q pair of cell lines and the lower expressing, matched panel of HTT exon 1 29Q/71Q/129Q POP7 cells to be taken forward for further experiments.

Western blotting using 4C9 and S830 antibodies was also performed on the same panel of cells following two weeks of differentiation, to ensure that this did not affect expression of the transgene (figure 3.25). This confirmed that transduced ReNcellVM neurons were still expressing the construct.

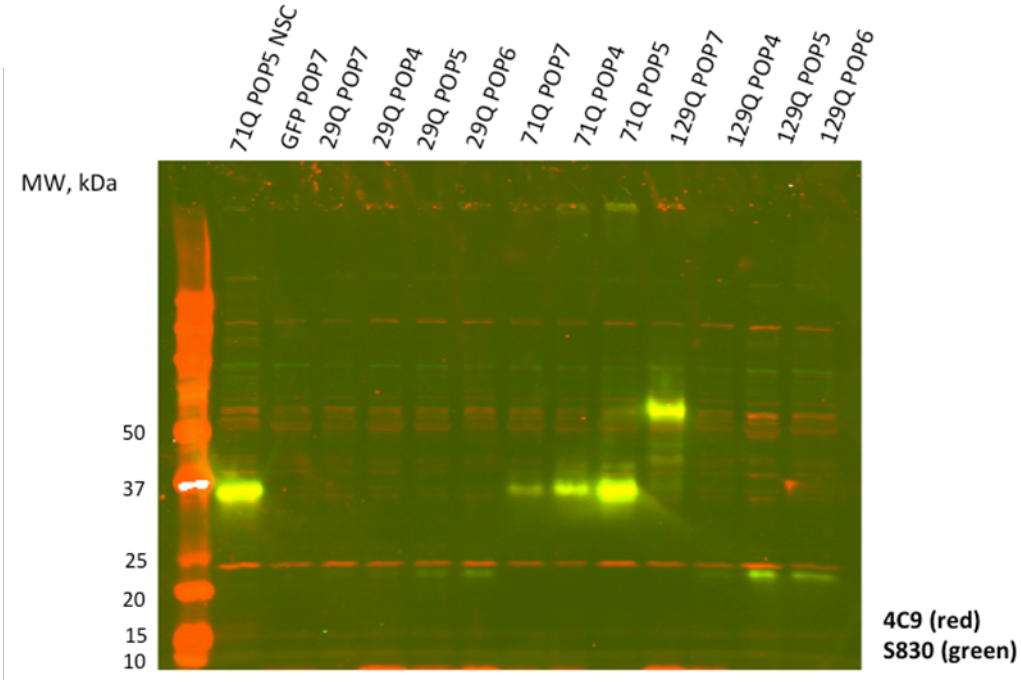


**Figure 3.25: Western blot confirms expression of HTT exon 1 in ReNcellVM neurons after differentiation.** Red – 4C9, Green – S830.

In order to confirm and further quantify the expression of HTT exon 1 in these cells, whole cell pellets from thirteen cell lines (including wild-type ReNcellVM) were analysed by Evotec using the ELISA-based MSD assay. For each cell line, pellets of neural stem cells and differentiated cells (day 14) were sent. Total HTT levels were measured using the 2B7/4C9 antibody pair, and mutant HTT using the 2B7/MW1 antibody pair. Overall, the MSD assays confirmed that all the ReNcellVM HTT exon 1 lines were definitively expressing the HTT exon 1 construct. The expression levels of HTT exon 1 in the 29Q and 71Q lines were ranked POP7<POP4<POP5<POP6 as expected. Both the 29Q and 71Q lines displayed higher total/expanded HTT expression levels in differentiated neurons than in NSC state, however in the 129Q line there was no difference. As expected, there was no expression of expanded HTT in the

wild-type and GFP only control lines. It is worth noting that the MW1 mutant HTT antibody displays polyQ length dependency, and therefore the results of the mutant HTT assay cannot be used to make comparisons between cell lines. The 4C9 antibody binds to the polyproline region of HTT and is not affected by polyQ length. Levels of total HTT were therefore compared across all the cell lines, and with endogenous HTT expression in wild-type and GFP only lines. This data is shown in figure 3.26.

**A panel of cell lines with relatively low, well-matched HTT exon 1 expression levels and a highly expressing 71Q line (71Q-H) was then taken forward for further experiments (table 3.4).**

| Day 14 differentiation | |
|---|---|
| Exon 1 line | Level of HTT exon 1 relative to endogenous wild type HTT (mean +/- SEM) |
| *29Q* | x3.4 +/- 1.2 |
| *71Q* | x6.2 +/- 2.0 |
| *129Q* | x3.2 +/- 1.3 |
| *71Q H* | x56.4 +/- 25.5 |

**Table 3.4:** The level of HTT relative to endogenous HTT (which is the only HTT present in the GFP only line).

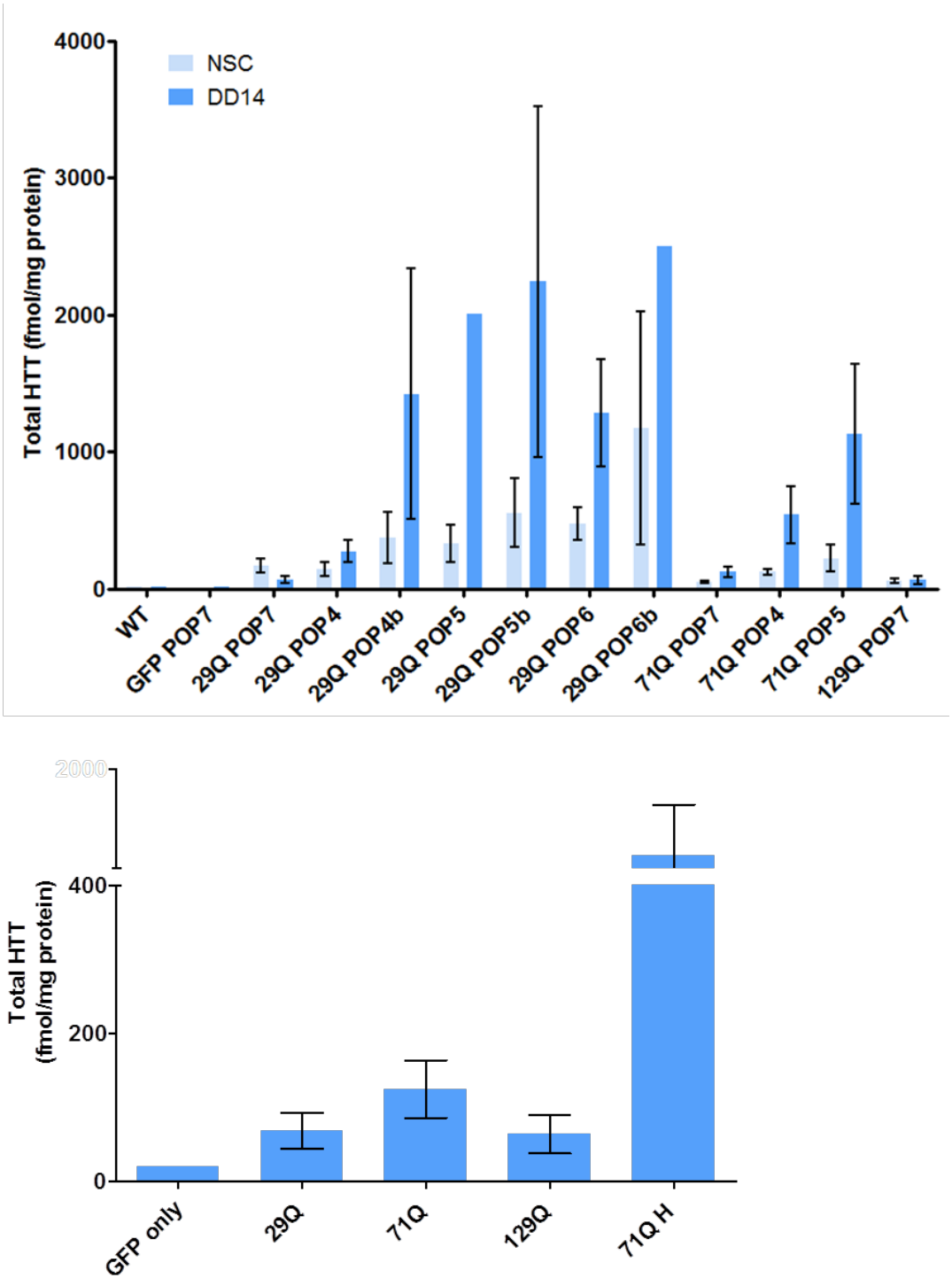


**Figure 3.26: Quantification of total HTT levels in ReNcellVM HTT exon 1 lines. Top graph:** Total HTT levels measured by 2B7/4C9 MSD assay in NSC and dd14 cells. **Bottom graph:** Total HTT levels in panel of HTT exon 1 lines with closest matching expression levels, and the high expressing 71Q comparator (71Q-H). (n=3, technical replicates)

### 3.5.3.3 Characterisation of HTT exon 1 ReNcellVM lines

The full panel of HTT exon 1 cells was differentiated for two weeks and culture composition was analysed. Immunofluorescence of 14-day differentiated cells demonstrated the expression of B3-tubulin, GFAP and nestin (see figure 3.27). The formation of inclusion bodies (IBs) that bound to S830 anti-HTT antibody was noted. There was no evidence of expression of other cell type markers - MAP2, Olig1, HuD, or neurofilament (NF200), nor did the cells express glutamate receptors (Western blotting for GluR2 and VGlut1 was negative).

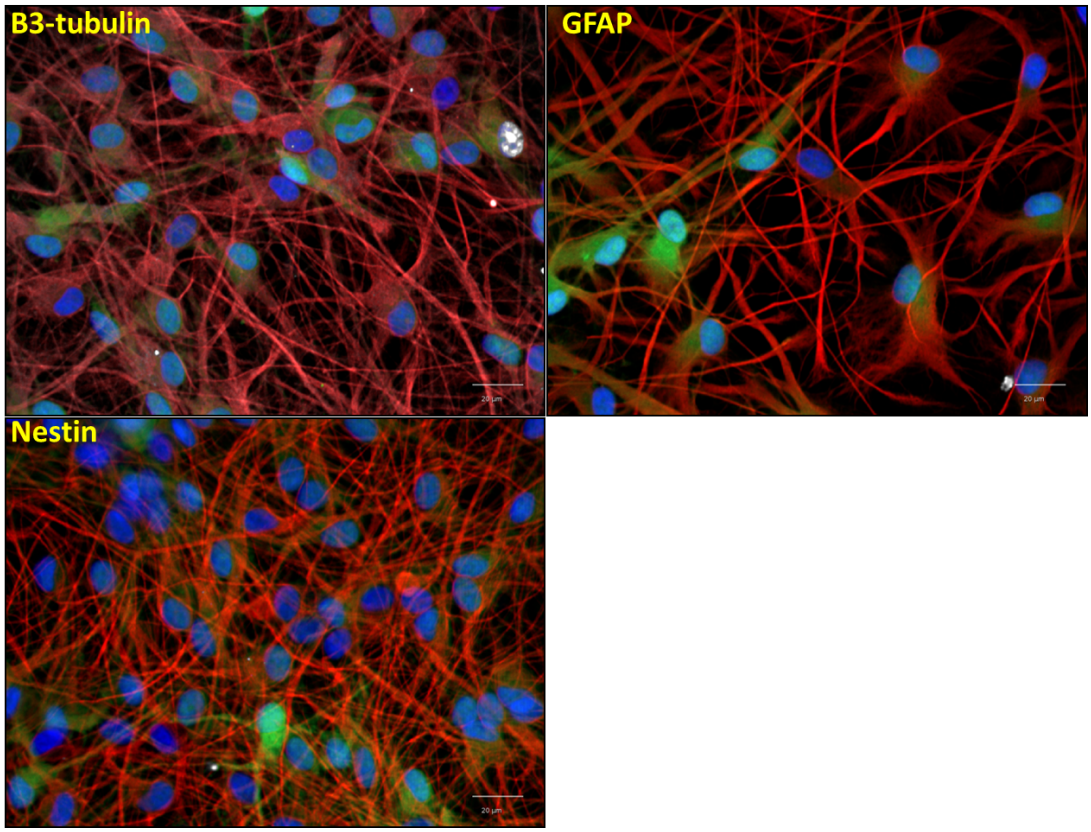


**Figure 3.27: Immunocytochemistry of 71Q-H line at day 14 of differentiation.** Cells are shown to have expression of B3-tubulin, GFAP and nestin. Blue – Hoescht (nuclei), Green – GFP, White – S830 HTT antibody, Red – cell marker as shown.

These findings were confirmed on Western blotting (figure 3.28).

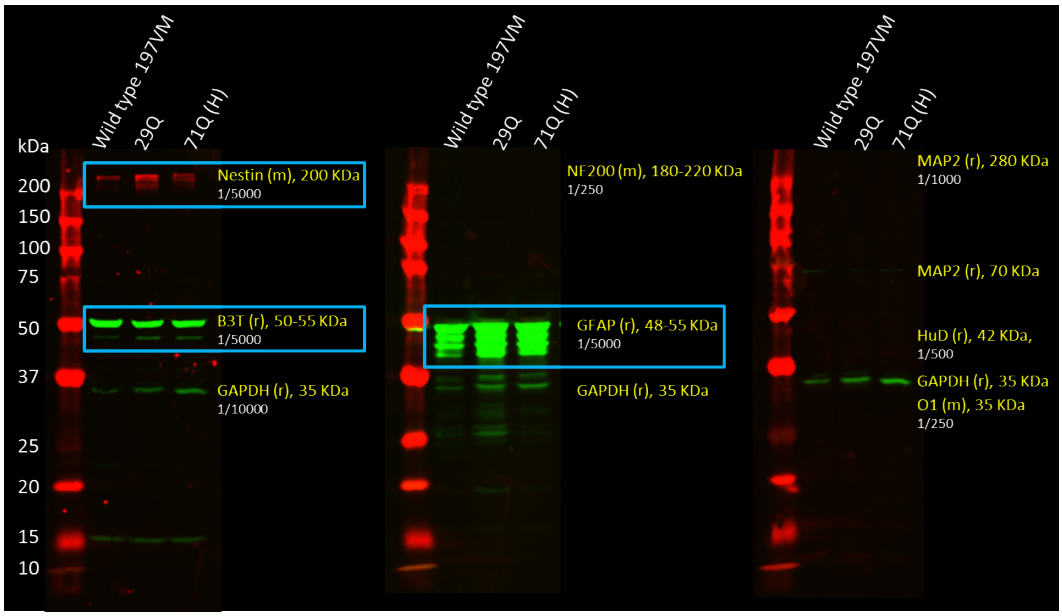


**Figure 3.28: Western blotting at day 14 of wild-type, 29Q and 71Q-H lines confirms that B3-tubulin, GFAP and nestin are expressed in these cells.** There is no expression of MAP2, HuD, Olig1 or neurofilament (NF200).

The lack of glutamate receptor expression likely contributed to the lack of electrophysiological activity in this cell line, and indicates that they are not true mature neurons. In addition, there appears to be an overlap in staining pattern of B3-tubulin, GFAP and nestin (each of which was imaged in separate experiments). B3-tubulin is a microtubule protein predominantly expressed in neurons, and is a standard neuronal marker used in immunohistochemistry. The pattern of B3-tubulin staining in the HTT exon 1 ReNcellVM cells displays a neuronal morphology, however the persistence of abundant nestin (an intermediate filament protein and neuroectodermal stem cell marker) indicates that the neuronal culture is still very immature.

More surprising is the pattern of GFAP staining observed, which appears to be axonal and overlapping with B3-tubulin staining. GFAP is an intermediate filament protein expressed predominantly in glial cells, including astrocytes, and would not be expected to overlap with the distribution of B3-tubulin. A small amount of GFAP staining is known to occur in immature neurons, however in this case the extent of overlap raises the possibility that the HTT exon 1 ReNcellVM cells are not differentiating into true neuronal cells but rather forming neuron/astrocyte hybrid cells or "asterons", as have been previously described (Laywell et al, 2005). These findings must be kept in mind, though for this thesis the ReNcellVM cells are referred to as "neurons" due to the strong presence of B3-tubulin and their characteristic neuronal morphology.

The effect of increasing CAG length on differentiation and culture composition was further assessed at a later date (see chapter 4), and an in-depth analysis of HTT inclusion formation was also carried out (see chapter 5).

### 3.5.4 HTT allelic series iPSC model of Huntington's disease

Neurons derived from HD-iPSCs are likely the most genetically precise model of Huntington's disease. Through utilisation of established differentiation protocols, HD-iPSC derived MSNs (the most vulnerable neuronal subtype in HD) can be studied. In creating a panel of iPSCs from an HD family who carry different CAG repeat length mutations, and their unaffected biological mother, it was hoped that some of the issues raised by genetic heterogeneity, when comparing different HD-iPSC lines, would be

ameliorated. The relatively similar genetic background of the lines will allow us to better assess the effect of increasing CAG repeat length on cellular phenotypes.

#### 3.5.4.1 Generation of iPSC lines

This family was known to the Tabrizi group through the Huntington's Disease clinic at the National Hospital for Neurology and Neurosurgery. Three siblings aged 26, 22 and 20 years old at the time of biopsy had inherited the HD gene mutation from their father (since deceased). All three transmitted mutations underwent expansion (anticipation) such that the siblings were all diagnosed with Juvenile HD at the ages of 14, 17 and 12 respectively, although in all cases symptoms had preceded the diagnosis by many years. Genetic testing has confirmed that their HD gene mutations contain 67, 56 and 73 CAG repeats respectively. Their mother was aged 46 at the time of biopsy, and is the genetically related control.

Punch biopsies of the skin were carried out as described. There were no immediate or late complications. Explant cultures were set up as described, with all four samples. Fibroblasts were successfully isolated, expanded and frozen down in vials from passage 3-5 as summarized in table 3.5.

| Line | CAG-repeat length | Passage | Date frozen | No of vials | No of cells per vial |
|---|---|---|---|---|---|
| **QS-01-FB** | 56 | P3<br>P4 | 20.7.14<br>25.7.14 | 13<br>10 | 513 500<br>560 000 |
| **QS-02-FB** | Control | P3<br>P4<br>P5 | 20.7.14<br>25.7.14<br>28.7.14 | 3<br>7<br>2 | 516 000<br>506 000<br>500 000 |
| **QS-03-FB** | 73 | P3<br>P4<br>P3* | 20.7.14<br>25.7.14<br>31.7.14 | 7<br>15<br>2 | 546 000<br>559 000<br>500 000 |
| **QS-04-FB** | 67 | P3<br>P4 | 25.7.14<br>28.7.14 | 7<br>3 | 500 000<br>500 000 |

**Table 3.5: Summary fibroblast lines frozen and stored in liquid nitrogen.**

Vials of frozen cells were sent to Professor Ali Brivanlou and his team at the Rockefeller Centre, and the fibroblasts were reprogrammed into iPSCs via Sendai reprogramming. Vials of iPSCs (at least three clones per subject) were sent back to us. Verification of the iPSCs included confirmation of expression of pluripotency markers, karyotyping, Sanger sequencing to confirm the *HTT* polyQ repeat-length, confirmation

of the absence of exogenous Sendai virus and mycoplasma testing. The ability to differentiate into all germ layers was also confirmed by longer-running teratoma assays.

#### 3.5.4.2 Differentiation of iPSCs into MSNs

Following a differentiation protocol of at least 36 days, adapted from the laboratory of Meng Li (Arber et al, 2015), MSNs were obtained for all three clones of the 73Q line (designated 73Q clone 1, 73Q clone 2 and 73Q clone 3) and the control lines (designated 20Q clone 1, 20Q clone 2 and 20Q clone 3). This protocol is known to generate up to 50% MSNs in culture (defined by positive DARPP32 staining). Figure 3.29 shows bright field images of all these lines following the MSN differentiation protocol, and figures 6.5 and 6.6 (chapter 6) show immunocytochemistry confirming the presence of DARPP-32 positive cells with characteristic MSN morphology. Experiments were carried out using the control 20Q and the longest CAG repeat 73Q lines to increase chances of demonstrating a pathogenic effect. Three clones were used in parallel in order to mitigate the effects of clonal variability that is known to occur in iPSCs and provide biological replicates.

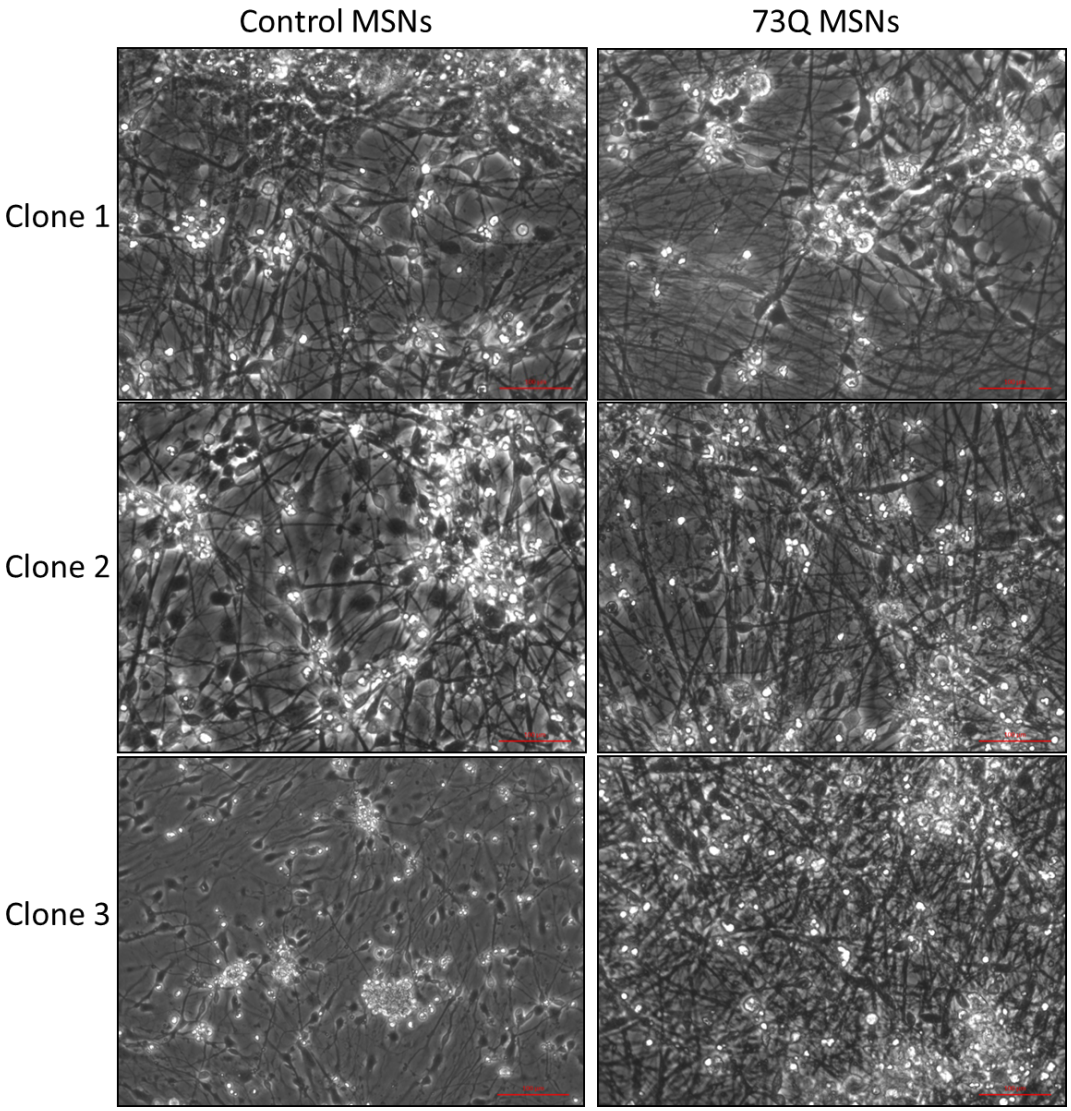


**Figure 3.29: Differentiation of three control (20Q) and three mutant (73Q) iPSC lines.** Bright field images of three clones of control and 73Q MSNs, from top to bottom. Images taken between days 38-49 of differentiation.

## 3.6 Discussion

The ReNcellVM line is a well validated NSC line that has been shown to differentiate into neurons, astrocytes and oligodendrocytes (Donato et al, 2007). The line has previously been used to study aspects of disease pathogenesis in Parkinson's disease (Gandhi et al, 2009); its robust growth, straightforward differentiation protocol and amenability to viral transduction also make it a useful line for the development of an HD model. The STROC05 NSC line has previously been shown to produce 7% DARPP-32 positive cells on differentiation (El-Akabawy et al, 2011) and therefore was an appealing choice of cell line as MSNs are the most affected cells in HD. However, its slow growth and poor tolerance of viral transduction led to a shift in focus of cell modelling efforts onto the ReNcellVM line.

The attempt to create an isogenic HTT allelic series in the ReNcellVM line using rAAV vectors to knock in increasing CAG repeat lengths into the endogenous *HTT* locus was not successful. There are a number of potential reasons to account for this. Firstly, the rate of homologous recombination (HR) in the ReNcellVM line was much lower than expected, based on observations in other cell types (Khan et al, 2011; Khan et al, 2010). It was considered that this may be due to neural stem cell specific factors, and attempts were made to create the allelic series in the HCT116 colorectal cancer line, which has previously been successfully engineered using AAV transfection (Khan et al, 2011); however low rates of recombination were again encountered. AAV is limited by the size of vector it can incorporate; the vector size of 7kb is at the upper limit. It is possible that the length of the desired insertion sequence was too long relative to the length of the homology arms to successfully guide HR of the full construct.

A different issue was that in both ReNcellVM and HCT116 lines, pools of cells that were identified on screening as containing the positively integrated vector lost their positive signal over subsequent passages and freeze/thaw. This may be due to selective advantage of wild-type cells (without mHTT knock-in), both in the speed of cell division/doubling time, and in the tolerance of cell stress (in this case the freeze/thaw process). Indeed there is evidence that mHTT affects mitotic spindle formation (Godin et al, 2010) and cells expressing mHTT are known to be more sensitive to stress (Zhang et al, 2010).

Genome editing may also be achieved using engineered nucleases composed of sequence-specific DNA-binding domains fused to a non-specific DNA cleavage module. These include zinc finger nucleases (ZFNs) and transcription activator-like effector nucleases (TALENs). More recently this field has been revolutionised by the discovery of CRISPR (clustered regularly interspaced short palindromic repeats)/Cas9 (CRISPR-associated system 9) nuclease, which is a prokaryotic immune system conferring acquired immunity to phages (Horvath & Barrangou, 2010). The system has been manipulated to perform targeted genome editing in mammalian cells; using a specific 20 bp single-guide RNA (gRNA), complexed mutant Cas9 is guided to the target region, which is followed by a 5'-NGG protospacer adjacent motif (PAM). Mutant Cas9 produces a single strand DNA break upstream of the PAM, which lends itself to repair via homologous recombination (Yang et al, 2014). This method has since been used to introduce CAG repeats into HEK-293 cells and HD-iPSCs (An et al, 2014), and more recently CRISPR/Cas9 has also been used to create an isogenic HTT allelic series in human ESCs (Ruzo et al, 2018).

The aim of optimisation and characterisation of a neural stem cell HTT exon 1 overexpression model of HD was achieved. An allelic series containing HTT exon 1 with 29Q, 71Q and 129Q repeats with relatively matched expression levels has been generated in ReNcellVM NSCs. The panel can be differentiated into B3-tubulin positive cells, and the pathogenic lines develop HTT inclusion bodies, a pathognomic hallmark of HD. HD is a disease of adult onset, and so one consideration when designing cell models is the timescale over which mutant phenotypes would develop. HTT exon 1 animal models such as the R6/2 mouse rapidly develop an aggressive phenotype which is amenable to study (Mangiarini et al, 1996). Similarly, HTT exon 1 cell models of rat striatal progenitors (Colby et al, 2006) and human neuroblastoma (Ho et al, 2001) show early aggregate formation. Human HD-iPSC derived neuronal models do not show spontaneous aggregate formation (Consortium, 2012), however neurons derived from human embryonic stem cells (hESCs) expressing the mHTT exon 1 transgene (Q73 and Q145) display EM48 positive aggregates after several months (Lu & Palacino, 2013).

Multiple lines of evidence highlight the importance of HTT exon 1 in the pathogenesis of HD. Post-mortem studies of human brain tissue demonstrate that nuclear and cytosolic inclusions are composed primarily of N-terminal fragments (DiFiglia et al, 1997). The smallest N-terminal fragment detected by western blotting using a panel of HTT antibodies in a full length mouse model of HD was exactly equivalent to an exon 1 product (Landles et al, 2010). A mechanism for generation of mutant HTT exon 1 has been demonstrated in mouse models expressing full length mutant Htt (mouse) and HTT (human), and also in patient derived fibroblasts and post-mortem human brain

tissue (Neueder et al, 2017); abnormal splicing in the presence of an expanded CAG repeat allows read through into intron 1 which contains a stop codon at its start, producing a mutant exon 1 fragment on translation (Sathasivam et al, 2013). A study in transgenic Drosophila engineered to express one of seven naturally occurring N-terminal HTT fragments against a constant genetic background, revealed that the exon 1 peptide is particularly toxic in terms of survival and degeneration of photoreceptor neurons (Barbaro et al, 2015). This HTT exon 1 overexpressing ReNcellVM model is therefore a useful tool to study pathogenic mechanisms in HD, particularly in a high-throughput format.

The generation of disease relevant cell models has been revolutionised since the discovery by Yamanaka and colleagues (Takahashi et al, 2007) that human fibroblasts can be re-programmed into self-renewing pluripotent stem cells through the expression of 4 key factors (Oct3/4, Sox2, Klf4, and c-Myc). iPSCs derived from patients are the most genetically precise disease model, and as such, provide an exciting platform from which to discover or validate disease mechanisms and test therapeutics. There are now many methods to generate iPSCs. Retroviral vectors encoding reprogramming genes require integration into the host genome for expression; DNA based vectors such as plasmid vectors, adenovirus and AAV remain as episomes and do not require integration, however they do sometimes still incorporate into host chromosomes and can potentially disrupt other important genes. iPSCs from this HD family were generated using a modified, non-transmissable form of Sendai virus (SeV), which are always non-integrating and remain in the cytoplasm (Fusaki et al, 2009).

HD-iPSCs have been generated (Park et al, 2008) that show no apparent differences from wild-type cells, but on neuronal differentiation, differences in protein expression, differentiation efficiency and neurite length (Chae et al, 2012), as well as in lysosomal function (Camnasio et al, 2012) can be observed. Even at early stages of differentiation, increased caspase 3/7 activity is seen, suggesting that mHTT containing cells are more susceptible to stress (Zhang et al, 2010). Restoration of the CAG repeat to wild type length was shown by the Ellerby group to prevent cell death, increase BDNF transcription, recue mitochondrial dysfunction and normalise elevated caspase 3/7 activity in HD-iPSC lines (An et al, 2012). Recently, HD-iPSC lines have been shown to display neurodevelopmental abnormalities on differentiation, from the acquisition of neuroectodermal fate (early) to striatal and cortical identity (late) (Conforti et al, 2018).

In general terms research using iPSC cells has, been limited by the genetic heterogeneity between patient derived cell lines, which makes direct comparisons between lines of different CAG repeat lengths difficult. The impact of donor cell type, age of donor and method of iPSC reprogramming can also all have an effect on iPSC behaviour (Cahan & Daley, 2013). It is hoped that by generating iPSC lines using fibroblasts from the same genetically related family by means of the same reprogramming method will, this background noise will be diminished. Another limitation has been the development of robust neuronal differentiation protocols (Hu et al, 2010). However, recently Professor Meng Li's group has shown yields of around 20-50% MSNs on differentiation of ESCs and iPSCs and the neurons have been shown to have electrophysiological activity (Arber et al, 2015). One remaining issue is the degree to which iPSC clones (derived from the same donor) vary from each other, and the number of clones required for experimental validity. Subtle inter-clone variations have

been observed in the HD-family iPSC lines in terms of speed of cell proliferation and ease of neuronal differentiation. This may be due to differences that arise during the reprogramming process and may relate to persistence of epigenetic modifications on iPSC derivation.

## 3.7 Summary

Two HD cell models have been generated and validated and form the basis for the work described in this thesis. The first is a neural stem cell (ReNcellVM) HTT exon 1 allelic series with relatively matched expression levels of 29Q, 71Q and 129Q (and a GFP only control). This will be used to study the impact of HTT exon 1 on neuronal phenotypes and the effect of increasing polyglutamine length on the HTT protein itself. The second is a panel of iPSCs derived from a genetically related HD family who have Juvenile HD, and their mother (as control). These will be differentiated into MSNs in order to study differences between the trafficking of wild-type and mutant HTT.

# 4 Effect of increasing HTT exon 1 CAG repeat length on neuronal phenotypes

## 4.1 Background

Following the successful generation of a HTT exon 1 allelic series in the ReNcellVM human neural stem cell line as described in chapter 3, this model was taken forwards for further experiments to determine the effect of increasing HTT exon 1 CAG repeat length on neuronal viability and response to cell stress. HTT CAG repeat length determines HD disease status, age of onset and the rate of disease progression; therefore determining CAG repeat length dependent neuronal phenotypes is key to understanding how this factor impacts on HD pathogenesis.

HTT exon 1 and other N-terminal fragments have been shown to exert toxicity in a variety of cellular model systems, as shown in table 4.1. Pathological effects of mHTT exon 1 expression can sometimes be observed within 24 hours and in most cases by a few days. Increased cell death has been recorded both at baseline and in response to toxin exposure. Many such models are however in non-human and/or non-neuronal cells, and therefore may not reflect the disease state. The effect of an allelic series HTT exon 1 (29Q, 71Q and 129Q) overexpression on neuronal differentiation and cell viability in the human ReNcellVM NSC line was therefore studied.

| Model | Construct | Toxicity |
|---|---|---|
| HEK-293<br><br>N2a mouse neuroblastoma | N63 and N171 each with 18Q or 82Q | 48 hrs post transfection, increased vulnerability to treatment with STS 500 nM for 4hrs in both 82Q lines, as determined by PI staining. More prominent in shorter fragment (Cooper et al, 1998). |
| HEK-293 | Transient transfection with N-terminal fragments of various lengths, each with 15Q or 128Q | Increased cell death (MTT assay) in 128Q lines, particularly in shorter fragments, following treatment with Tamoxifen 35 μM (Hackam et al, 1998). |
| SK-N-SH human neuroblastoma<br><br>COS-7 monkey kidney | HTT exon 1 with 21Q and 71Q | Higher cell death as determined by nuclear fragmentation in 71Q than 21Q (Ho et al, 2001). |
| PC12 rat phaeochromocytoma | Inducible N63 with 23Q or 148Q | On differentiation 148Q line had 50% cell death at 6 days compared to no rise above baseline cell death with 23Q (trypan blue exclusion assay) (Igarashi et al, 2003). |
| Rat embryo derived striatal neurons | Inducible N548 26Q and 165Q | Decreased viability (MTS assay) in 165Q line compared to 26Q on 24 hours exposure to MG132 (0-200UM), 3NP and QA (Seo et al, 2007). |
| N2a mouse neuroblastoma | N-terminal with 20Q and 150Q. | Increased PI staining, decreased neurite outgrowth.<br>Increased activated caspase 3 on WB at baseline and in response to Camptothecin (Ye et al, 2008). |
| Rat striatal neurons | Htt exon 1 with 17Q, 47Q, 72Q, 97Q and GFP. | PolyQ dependent nuclear fragmentation, neurite dystrophy and cell death (assessed by loss of reporter fluorescent protein) (Miller et al, 2010). |

| Model | Construct | Toxicity |
|---|---|---|
| HC2S2 rat neuroprogenitor line (4 day differentiation protocol) | eGFP tagged htt exon 1 with 28Q or 74Q | Increased nuclear fragmentation/shrinking in 74Q line after 6 days, increasing up to 10 days.<br>Increased neuritic degeneration in 74Q line after 4 days.<br>Increased neuronal sensitivity to $H_2O_2$ at all doses 50-200 μM (nuclear morphology assay) (Dong et al, 2011). |
| hESC-derived neurons (2 month differentiation protocol) | HTT exon 1 23Q, 73Q and 145Q (15-20 fold overexpression) | CAG-dependent cell death under "basal" medium conditions seen within 24 hrs, increased over 5 days. Live/dead imaging assays (Lu & Palacino, 2013). |
| PC12 rat phaeochromocytoma line | eGFP tagged HTT exon 1 with 25Q or 97Q | For 97Q line only:<br>Inclusion formation within 24 hrs<br>Increased cell death (LDH assay) after 24 hrs<br>Nuclear DNA damage within 6 hrs<br>Caspase 3 activation by 24 hrs<br>Decreased oxygen consumption rate by 24 hrs<br>(Sahoo et al, 2016) |

**Table 4.1: HTT exon 1 and N-terminal fragment models of Huntington's disease** with summary of the resultant cytotoxicity findings.

The presence of mHTT is known to cause increased sensitivity to a variety of cell stressors. Redox homeostasis is required for normal neuronal functioning, and oxidative stress is said to occur when oxidants overwhelm the antioxidant capacity of the cell. Oxidative stress in known to cause DNA damage and transcriptional dysregulation, and has been implicated as a primary event in HD pathogenesis (Kumar & Ratan, 2016). Striatum and cortex from HD brains at post-mortem have shown

increased levels of oxidative damage (Browne et al, 1999). Higher levels of oxidative biomarkers in the blood of HD patients compared to healthy controls have also been found (Chen et al, 2007). However it is not clear if these findings are caused by mHTT directly or are a manifestation of dying neurons or decreased turnover of oxidative biomarkers. Hydrogen peroxide ($H_2O_2$) can be used to generate oxidative stress when applied to cells in culture, and has been shown to induce increased levels of DNA damage in HD compared to control-iPSC-derived neurons (Chiu et al, 2015). The ability of $H_2O_2$ to induce cell death in the HTT exon 1 allelic series was therefore investigated.

Excitotoxicity is caused by excessive excitatory glutamatergic signalling and leads to disruption of intracellular calcium levels, mitochondrial energy failure and cell death. In HD, alterations in glutamatergic signalling occur through changes in glutamate release (Joshi et al, 2009), over activity of glutamate receptors (Benn et al, 2007), decreased levels of glutamate transporters and therefore reduced glutamate uptake (Huang et al, 2010). The resulting rise in extracellular glutamate then leads to increased signalling through glutamate receptors including AMPA and NMDA-R. The injection of the NMDA-R agonist quinolinic acid (QA) into rodent striatum has long been known to result in an HD-like phenotype (Beal et al, 1986). Hence the response of the HTT exon 1 lines to the application of glutamic acid was studied, expecting that the pathogenic lines would be more vulnerable to excitotoxic cell death.

Protein homeostasis is important for neuronal survival and involves the timely clearance of damaged or misfolded proteins from the cytoplasm. Disruption of this process occurs in HD, as evidenced by the accumulation of mHTT aggregates and

ubiquitinylated proteins in HD mouse models and patient brains. Mammalian proteasomes have been shown to completely digest mHTT exon 1 (Juenemann et al, 2013), and autophagy is also involved in the degradation of expanded polyQ peptides (Tsvetkov et al, 2013). Conversely, both the UPS and autophagy are thought to be adversely affected by the presence of mHTT (Seo et al, 2004; Wong & Holzbaur, 2014). The effect of both proteasomal and autophagy inhibitors might therefore be expected to enhance toxicity in the HTT exon 1 cell lines, and this was tested as described below.

## 4.2 Aims

To establish the effect of HTT exon 1 with increasing CAG repeat lengths on:

1. Neuronal differentiation and culture composition.

2. Neuronal viability.

3. The response of neurons to pathological stressors (oxidative stress, excitotoxic stress and disruption of protein homeostasis using UPS and autophagy inhibitors).

## 4.3 Methods

HTT exon 1 ReNcellVM NSCs were cultured and differentiated as described in section 2.1.1 and 2.1.3. To determine the effect of HTT exon 1 on neuronal differentiation cells were grown in a 96 well plate format for 2 weeks, and then fixed and stained using

antibodies to cell markers (section 2.7.1). High content imaging on the Opera Phenix was then carried out (section 2.7.2) with image analysis using the Columbus software (section 2.7.2.1). Subsequently graphs were produced and statistical analysis carried out using Prism software (section 2.10).

For the assessment of cell viability, biochemical assays (LDH, MTT and Alamar Blue) were performed as described in sections 2.8.1, 2.8.2 and 2.8.3 respectively. Imaging markers of cytotoxicity were also investigated; propidium iodide, mitotracker red and anti-activated caspase 3 antibody were all tested as described in section 2.8.4. The response of HTT exon 1 cells to various pathological stressors ($H_2O_2$, glutamate, MG132, lactacystin, epoxomicin and bafilomycin) was then tested; all toxins were purchased from Sigma and reconstituted when needed as per instructions. Viability was then assessed using the LDH assay as previously described.

## 4.4 Contributions

The work described in this chapter was carried out by Dr. Rhia Ghosh.

## 4.5 Results

### 4.5.1 Effect of HTT exon 1 overexpression on neuronal differentiation in the ReNcellVM line

High content imaging using the Opera Phenix followed by image analysis using Columbus software was carried out at day 14 of differentiation to assess the effect of CAG repeat length on neuronal differentiation and nuclear metrics. For each stain, eight wells were imaged per line, each with eighteen fields of view. The image analysis software comprises a modular "building-block" system, and an appropriate analysis pipeline can be constructed by the user depending on the pattern of staining to be analysed. In the case of cell markers for B3-tubulin, GFAP and nestin, a "mask" was generated based on cell segmentation of neurons, and cells were deemed to be positive for a marker if intensity of staining reached a certain threshold. The software then applied this threshold across all images to generate the number of positive cells per well. Total cell number per well was generated using a simple automated nuclear count, and a percentage of positive cells was calculated. Therefore results of eighteen fields of view were averaged to give the overall result per well, and each well is a technical replicate.

96-97% of cells expressed the neuronal marker B3-tubulin, with the exception of the 129Q line which had a slightly lower proportion at 94% (figure 4.1). This may indicate that the most highly pathogenic HTT exon 1 fragment is having an adverse effect on neuronal differentiation.

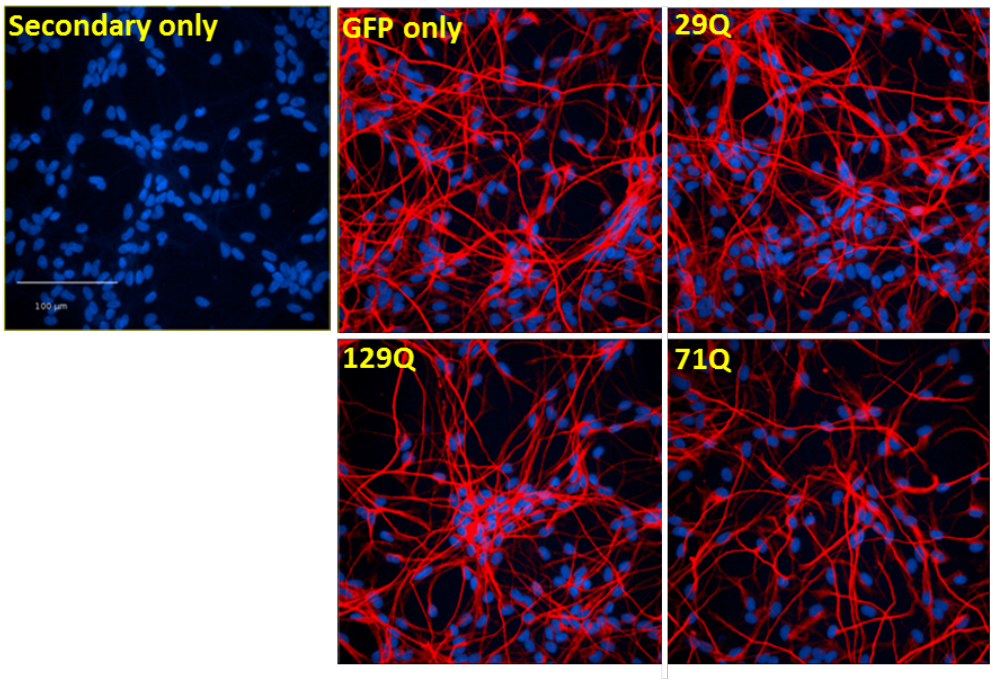


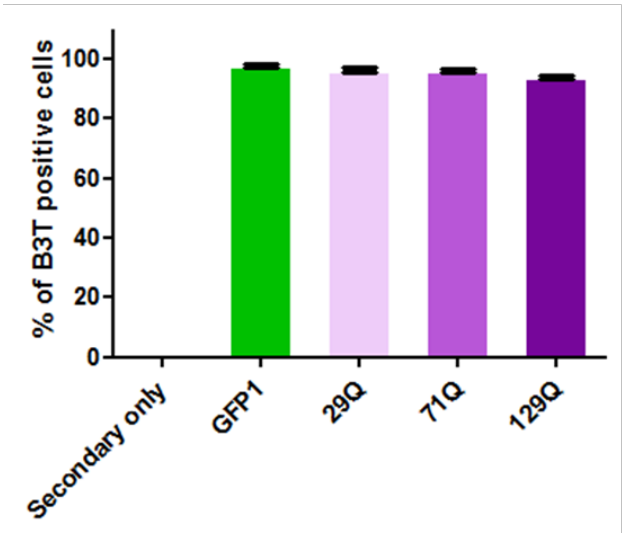


| One-way ANOVA (Bonferroni) | |
|---|---|
| GFP vs 29Q | ns |
| GFP vs 71Q | ns |
| GFP vs 129Q | P≤0.001 |
| 29Q vs 71Q | ns |
| 29Q vs 129Q | P≤0.05 |
| 71Q vs 129Q | ns |

**Figure 4.1**: **B3-tubulin staining is slightly lower in the ReNcellVM HTT exon 1 129Q line.** Full ReNcellVM HTT exon 1 panel at dd14 stained with B3-tubulin antibody shows all lines differentiate into a high proportion of B3-tubulin cells with neuronal morphology. However the 129Q line has slightly lower percentage of cells that express B3-tubulin – 94%, whereas this is 96-97% across the other lines. (One-way ANOVA with Bonferroni's correction, n=8 (technical replicates)).
Images: Red – B3-tubulin, Blue – Hoescht (nuclei).

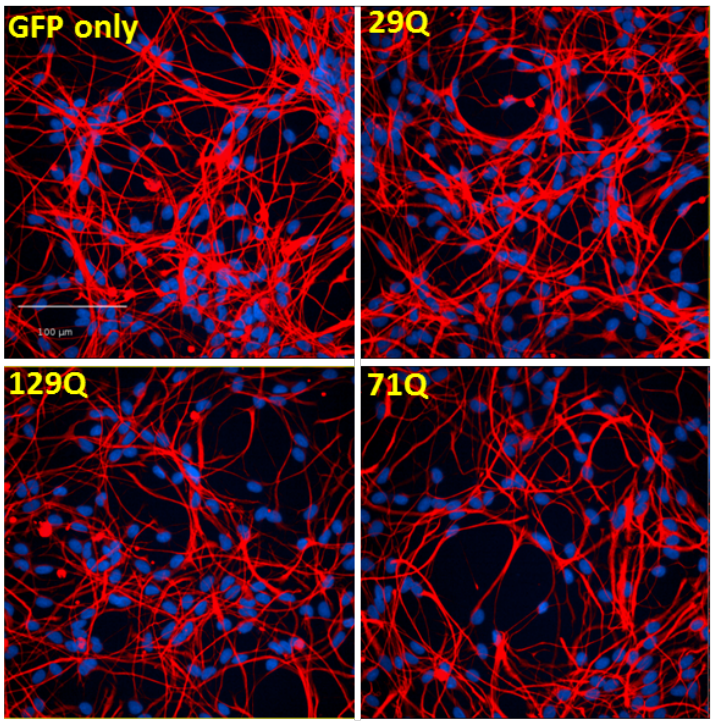


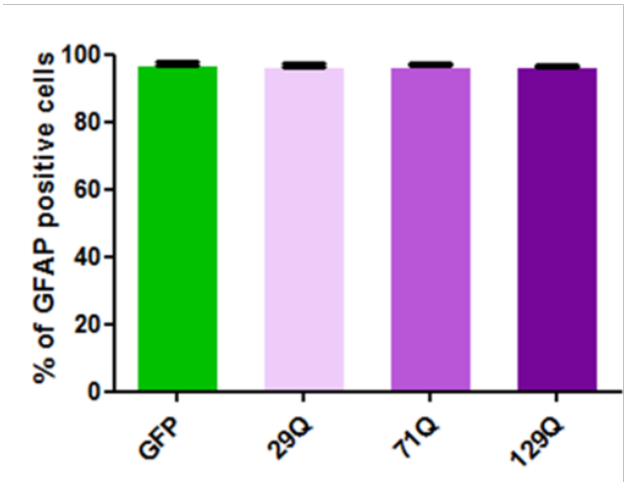


| One-way ANOVA (Bonferroni) | |
|---|---|
| GFP vs 29Q | ns |
| GFP vs 71Q | ns |
| GFP vs 129Q | ns |
| 29Q vs 71Q | ns |
| 29Q vs 129Q | ns |
| 71Q vs 129Q | ns |

**Figure 4.2**: **GFAP staining uniform across the ReNcellVM HTT exon 1 panel.** Full ReNcellVM HTT exon 1 panel at dd14 stained with GFAP (red) shows all lines express GFAP (97% of cells are GFAP positive), and there are no differences between the lines. (One-way ANOVA with Bonferroni's correction, n=8 (technical replicates)). Images: Red – GFAP, Blue – Hoescht (nuclei).

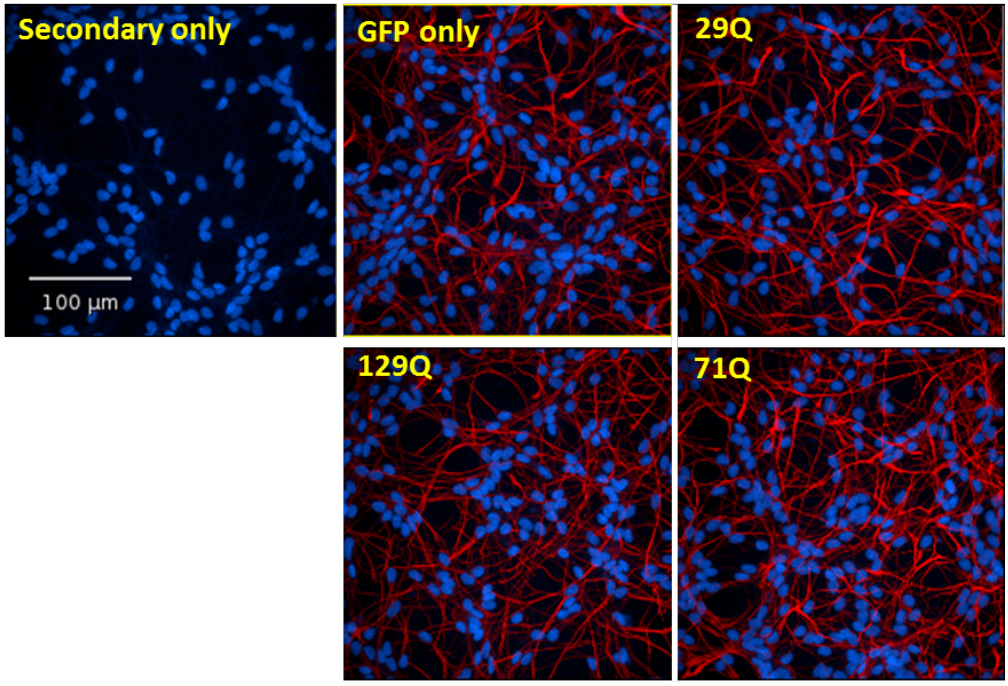


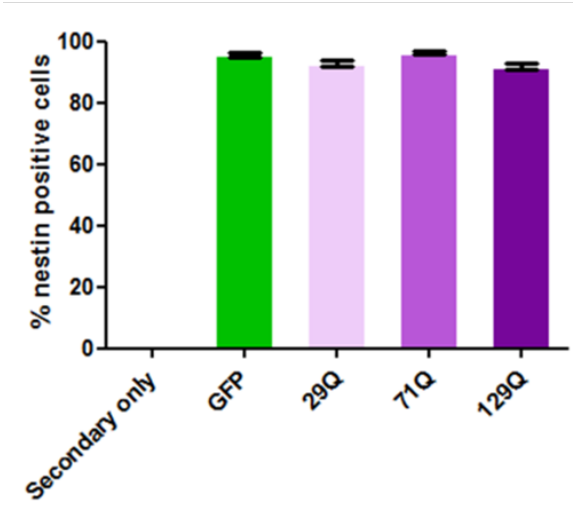


| One-way ANOVA (Bonferroni) | |
|---|---|
| GFP vs 29Q | ns |
| GFP vs 71Q | ns |
| GFP vs 129Q | P≤0.05 |
| 29Q vs 71Q | P≤0.05 |
| 29Q vs 129Q | ns |
| 71Q vs 129Q | P≤0.01 |

**Figure 4.3**: **Nestin staining across the ReNcellVM HTT exon 1 panel** at dd14 shows that 92-96% of cells express nestin. Differences between lines are not thought to be biologically significant. (One-way ANOVA with Bonferroni's correction, n=8 (technical replicates).

Images: Red – Nestin, Blue – Hoescht (nuclei).

GFAP expression was similar at 97% across all lines (figure 4.2), and persistent nestin staining was seen in 92-96% of all cells (variation between lines was not thought to be biologically significant) (figure 4.3).

As discussed in detail in section 3.5.3.3, the staining pattern of B3-tubulin, GFAP and nestin share a high degree of overlap, indicating that these neurons are highly immature, or that neuron/astrocyte hybrid cells have been formed. An alternative possibility is that the pattern of GFAP staining observed is artefact; to assess this further a negative control cell line known to have no GFAP expression would have been useful, to stain alongside the HTT exon 1 ReNellVM cells (the secondary only control was the same as for B3-tubulin (figure 4.1), with the same solution of secondary antibodies being used).

Nuclear metrics including nuclear size (area), intensity and roundness were also analysed from all three previous experiments, based on the Hoescht staining of the nuclei (figure 4.4). There were no significant differences between the lines, although the 129Q line did show a trend towards increased size. This may be due to intranuclear inclusion body formation occurring in a greater number of cells in this line (see chapter 5), leading to a small increase in mean average nuclear size.

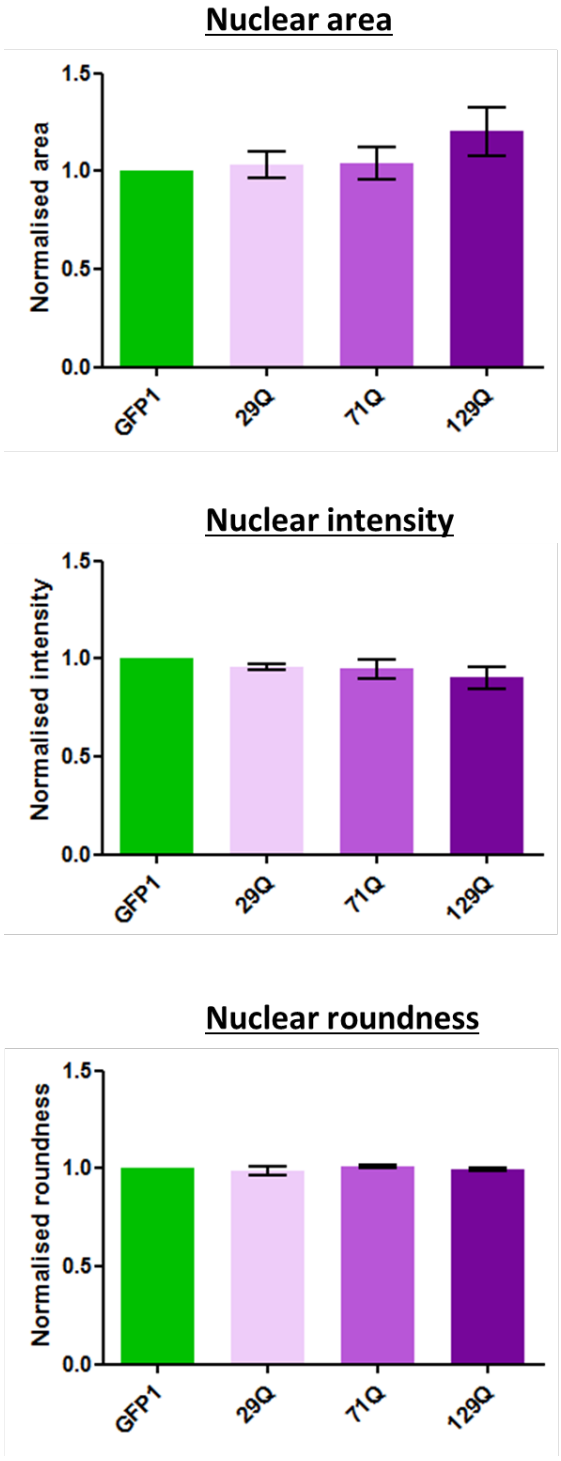


| One-way ANOVA (Bonferroni) | |
|---|---|
| GFP vs 29Q | ns |
| GFP vs 71Q | ns |
| GFP vs 129Q | ns |
| 29Q vs 71Q | ns |
| 29Q vs 129Q | ns |
| 71Q vs 129Q | ns |

| One-way ANOVA (Bonferroni) | |
|---|---|
| GFP vs 29Q | ns |
| GFP vs 71Q | ns |
| GFP vs 129Q | ns |
| 29Q vs 71Q | ns |
| 29Q vs 129Q | ns |
| 71Q vs 129Q | ns |

| One-way ANOVA (Bonferroni) | |
|---|---|
| GFP vs 29Q | ns |
| GFP vs 71Q | ns |
| GFP vs 129Q | ns |
| 29Q vs 71Q | ns |
| 29Q vs 129Q | ns |
| 71Q vs 129Q | ns |

**Figure 4.4: Analysis of nuclear metrics across the ReNcellVM HTT exon 1 panel** at dd14 shows no significant differences between the lines in terms of nuclear area, intensity or roundness. A trend towards increased nuclear size in the 129Q line is observed, but this falls short of statistical significance. (One-way ANOVA with Bonferroni's correction, n=24 (technical replicates)

#### 4.5.1.1 Problems with long term cell culture of the ReNcellVM HTT exon 1 lines

One issue that was noted on differentiation of the HTT exon 1 cell lines (including control and pathogenic lines) was the appearance of gaps in the cell monolayer that increased over time. This led to a “honeycombed” appearance of the cell cultures, which would render them unsuitable for high content imaging. It was hypothesised that this may be due to cells no longer adhering to the laminin coating after a certain period of time. Therefore, the cells were reseeded after seven days of growth onto freshly coated plates. However many cells did not continue differentiating normally once reseeded. Matrigel and Geltrex were used in lieu of laminin to coat the plasticware, but this also did not make any difference.

The density at which the cells were seeded was also considered to be playing a role. Therefore, cells were seeded at a density of 1000, 5000, 10,000 and 25,000 per well of a 96-well plate, and appearance compared after two weeks. From this it was determined that a seeding density of 10,000 cells per well reduced the frequency with which “honeycombing” occurred, compared to higher seeding densities. Seeding densities of less than 10,000 per well produced overly sparse cultures that were unsuitable for imaging. Gentle media changes exchanging half the media volume also helped.

### 4.5.2 Effect of HTT exon 1 overexpression on cell viability in the ReNcellVM line

From routine observations on cell culture, there was no overt cell death visible in these lines, including in the 129Q line and the highly expressing 71Q line. Cells were confirmed to be expressing exon 1 by checking for GFP expression using the microscope green light filter. A variety of biochemical methods were then used to ascertain any subtle differences in cell viability between the lines.

#### 4.5.2.1 Lactate dehydrogenase (LDH) assay in HTT exon 1 overexpressing ReNcellVM lines

Lactate dehydrogenase (LDH) is a stable cytosolic enzyme that is released upon cell lysis into the surrounding medium, and has a half-life of 9 hours. Released LDH in culture supernatants is measured with a 30-minute coupled enzymatic assay, which results in the conversion of a tetrazolium salt (iodonitrotetrazolium violet (INT)) into a red formazan product. The amount of colour formed is proportional to the number of lysed cells, and wavelength absorbance data collected using a standard 96-well plate reader. 6x96 well plates were seeded with the HTT exon 1 cell panel (GFP only, 29Q, 71Q, 129Q and 71Q high expressor (71Q-H)) as well as wild type ReNcellVM NSCs, at a density of 25,000 cells per well, with differentiation commenced after 24 hours. One plate was used for LDH assay at day 0, 7, 14, 28 and 42 of differentiation and the remaining plate was tested following a delayed media change at day 42. 8 wells were tested per condition, which are technical replicates.

Due to the random and variable “honeycombing” effect mentioned in section 4.5.1.1, there was potentially a variation in cell numbers between wells (despite initially seeding NSCs at the same density). Variable cell numbers would affect the results of the LDH assay, as wells containing greater numbers of cells would release more LDH for the same percentage cell death. To account for this variability, following the removal of 50 µl of media/supernatant for LDH assay, 16.7 µl of 10% TritonX was added to the remaining media in each well for 1hour at 37 degrees, in order to cause complete lysis of the remaining cells. LDH assay was then also carried out on these wells. Percentage cell death could then be calculated for each well, by comparing LDH assay results pre- and post- lysis. Results of the LDH time course are shown in figure 4.5. There were no significant differences between the lines.

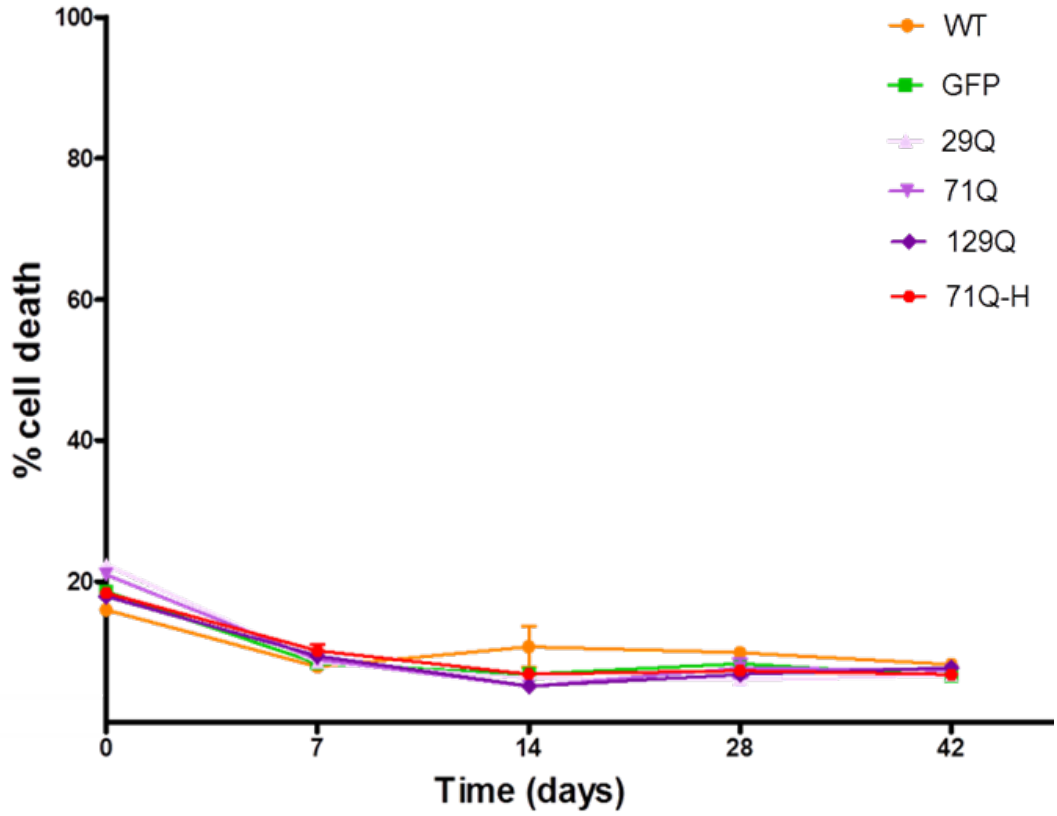


**Figure 4.5: Time course of LDH assay in HTT exon 1 and wild-type ReNcellVM cells up to 6 weeks of differentiation.** Plates were analysed at dd0, 7, 14, 21, 28 and 42 with removal of supernatant for measurement of LDH. This was followed by lysing all remaining cells in each well and recording the levels of LDH at 100% cell death. The percentage cell death per well was then calculated for each well. There are no significant differences in cell death between lines (Two-way ANOVA with Bonferroni's correction, n=8 per timepoint).

LDH assay was consistently carried out 24 hours after media changing the cells with 200 µl of fresh ReNcellVM media. At day 42 of differentiation, a delayed LDH assay was also carried out 120 hours after a media change to ensure sufficient accumulation of LDH in the supernatant. However this made no difference to the results.

#### 4.5.2.2 MTT assay in HTT exon 1 overexpressing ReNcellVM lines

MTT (3-[4,5- dimethylthiazol-2-yl]-2,5-diphenyl tetrazolium bromide) assays were carried out on 96 well plates of the HTT exon 1 panel, seeded as described for the LDH assay. Mitochondrial dehydrogenases of viable cells cleave the tetrazolium ring, yielding purple formazan crystals which are insoluble in aqueous solutions. The crystals were dissolved in DMSO and the absorbance of the resulting purple solution was spectrophotometrically measured at a wavelength of 570 nm, with background absorbance at 690 nm subtracted. Results of MTT assay carried out at day 0, 7, 14 and 28 of differentiation are shown in figure 4.6, with 8 wells or technical replicates per condition; they confirm that there are no consistent differences in cell viability, as reflected by mitochondrial activity, between the HTT exon 1 lines. In this assay it was not possible to account for variation in cell number caused by the “honeycomb” effect described previously – this may account for the greater variability seen in the results.

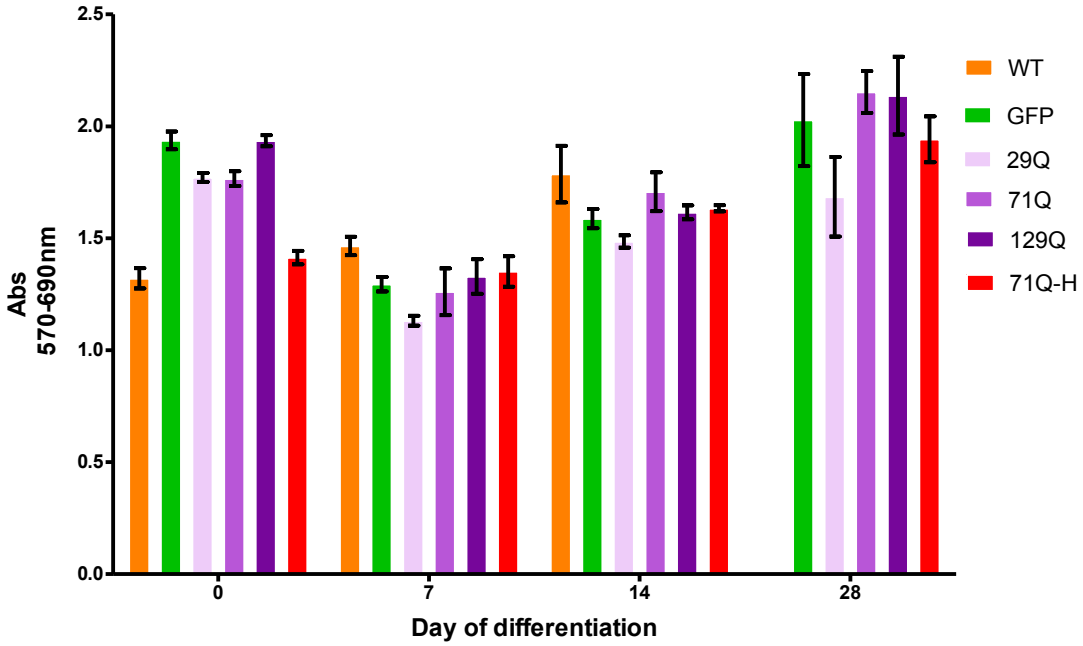


**Figure 4.6: MTT assay in HTT exon 1 and wild-type ReNcellVM up to 4 weeks of differentiation.** Cells were tested at dd0, 7, 14 and 28, but no consistent pattern of differences between cell lines was found. (n=8 per timepoint).

### 4.5.2.3 Alamar Blue assay in HTT exon 1 overexpressing ReNcellVM lines

The Alamar blue assay measures the reducing conditions within cells, as an indicator of cell viability. The active ingredient is resazurin, a non-toxic, cell permeable compound that is blue in color and virtually non-fluorescent. Upon entering cells, resazurin is reduced to resorufin, a compound that is red in color and highly fluorescent. Viable cells continuously convert resazurin to resorufin, increasing the overall fluorescence and color of the surrounding media. Absorbance was measured on a spectrophotometer at 570 nm, using 600 nm as a reference wavelength.

The assay was carried out on wild-type ReNcellVM, 29Q and the high expressing 71Q lines at day 14 of differentiation. The percentage of reduction in the HTT exon 1 lines were calculated relative to the wild-type cells as described. No significant differences were found in either the 29Q or the 71Q-H line, as compared to control (figure 4.7).

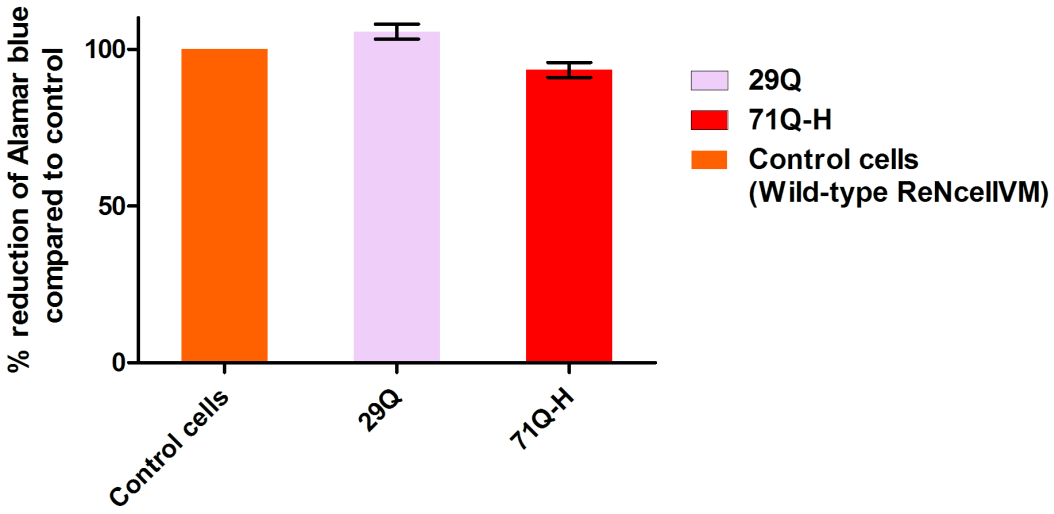


**Figure 4.7: Alamar blue assay in HTT exon 1 and wild-type ReNcellVM cells at 2 weeks of differentiation.** Percentage reduction of Alamar blue by dd14 29Q and 71Q-H HTT exon 1 ReNcellVM cells compared to wild-type dd14 ReNcellVM cells is shown. One-way ANOVA confirms no significant differences between control and either 29Q or 71Q-H lines (n=16 per condition, technical replicates).

#### 4.5.2.4 Imaging markers of cytotoxicity in HTT exon 1 overexpressing ReNcellVM lines

In order to complement the above biochemical methods, an imaging method to ascertain cytotoxicity was sought. This was complicated by the expression of GFP in the HTT exon 1 lines, which therefore precluded the use of any green fluorescent cytotoxicity markers designed for the detection in the 488 channel.

Propidium iodide (PI) is a commonly used dye used to visualise dead cells. In late apoptotic and necrotic cells, the integrity of the plasma and nuclear membranes decreases, allowing PI to pass through the membranes, intercalate into nucleic acids and display red fluorescence. However when applied to GFP only cells that had been treated with 1 μM staurosporine (STS) to induce apoptosis, it did not stain the cells (figure 4.8). As can be seen, Hoescht staining did confirm the presence of pyknotic nuclei and apoptotic bodies, therefore P.I. staining was unsuccessful.

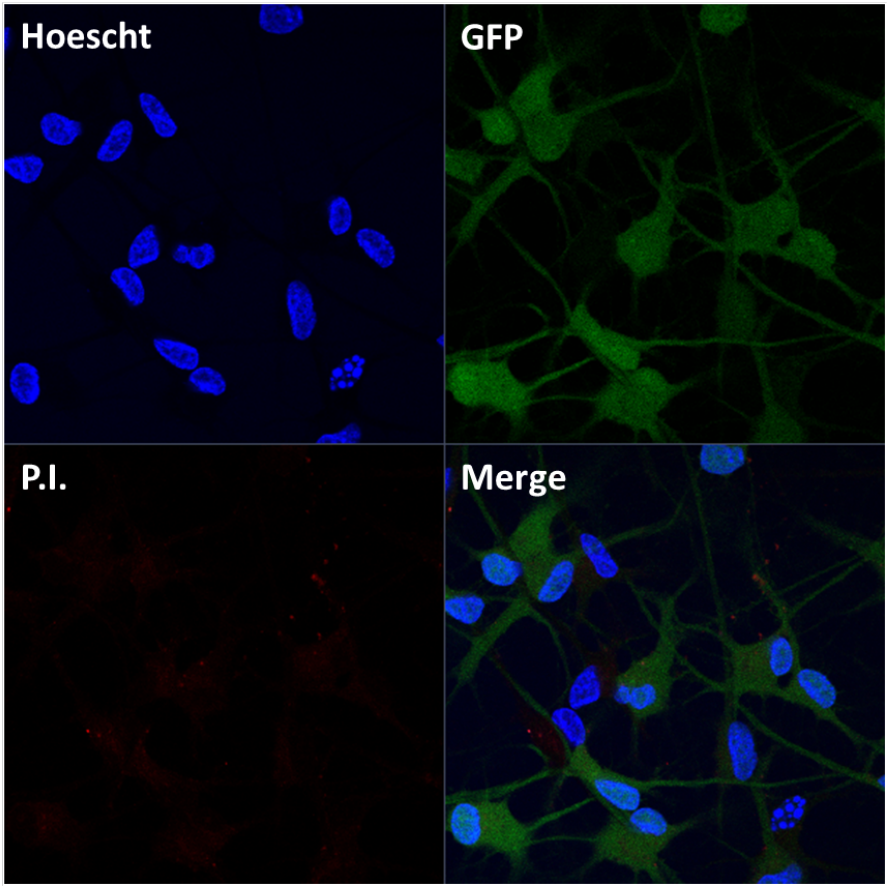


**Figure 4.8: Propidium iodide (P.I.) staining** in dd14 GFP only ReNcellVM cells treated with 1 µM STS was not successful.
Blue- Hoescht, Red – P.I., Green - GFP.

Mitotracker Red dye was also tested. This dye successfully stained mitochondria in the cells. Addition of 100 nM staurosporine changed the pattern of staining observed, with mitochondria adopting a more rounded and less tubular appearance, but there were no overt differences between control and pathogenic lines (figure 4.9). The pattern of staining observed did not to lend itself to automated image processing on Columbus and so alternative imaging markers of cytotoxicity were sought.

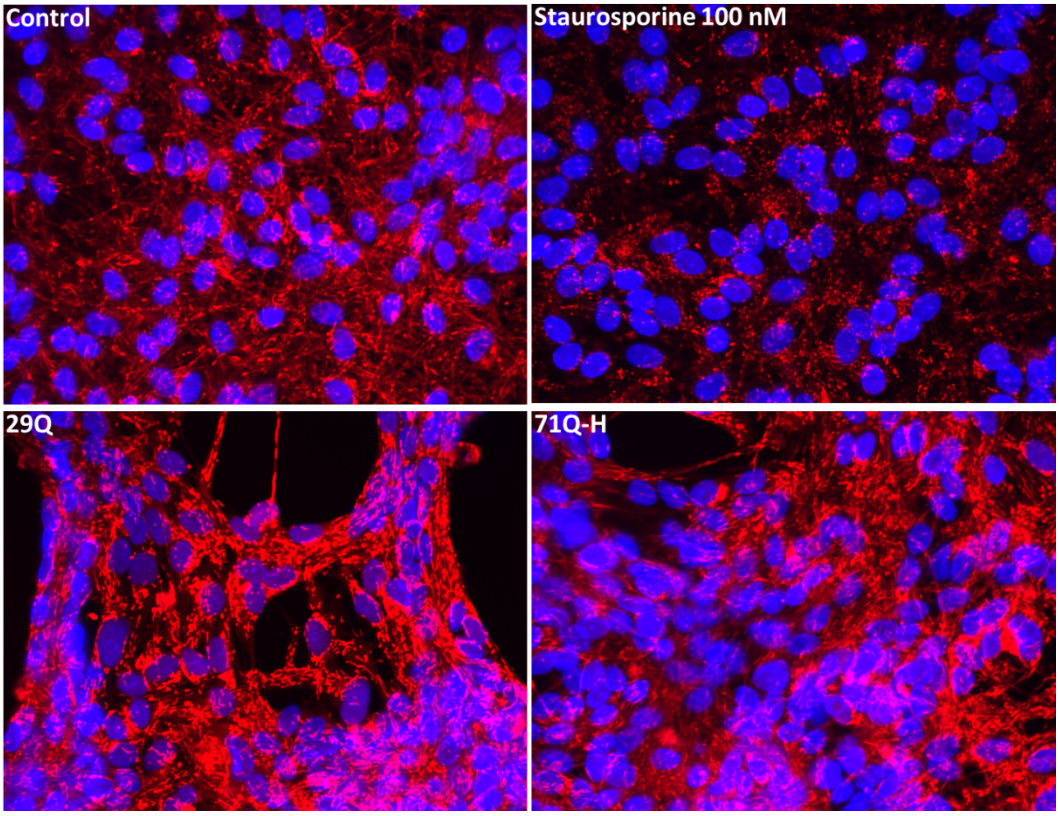


**Figure 4.9: Example of staining with Mitotracker Red dye** in dd14 control (wild-type) ReNcellVM cells +/- staurosporine (STS), and HTT exon 1 29Q and 71Q-H ReNcellVM lines. Mitochondria adopt a more rounded and less tubular appearance in response to STS treatment, but there are no overt differences seen between wild-type, 29Q and 71Q-H lines.
Red – mitotracker Red dye, Blue – Hoescht (nuclei).

The antibody to activated caspase-3 was also tested (using a secondary antibody that fluoresced at 568 nm), as a marker of early apoptosis, with results as shown in figure 4.10. It can be seen that a bright signal is obtained for apoptotic cells (which have apoptotic bodies clearly visible with Hoescht staining).

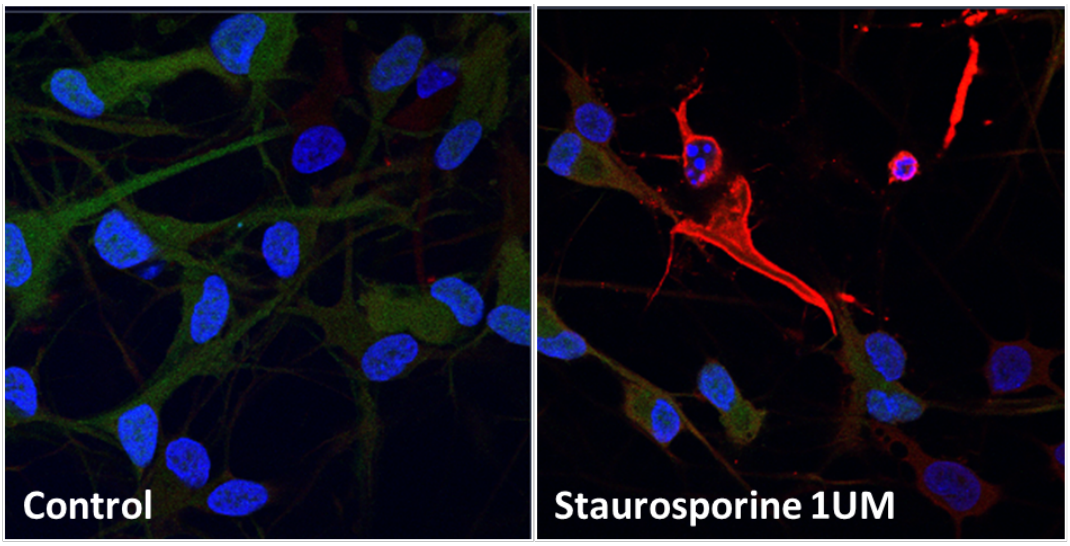


**Figure 4.10: Anti-activated caspase 3 staining in dd14 GFP only ReNcellVM cells with STS treatment and control.** On treatment with STS, some nuclei undergo apoptosis, as can be seen by the formation of apoptotic bodies visible with Hoescht staining. Apoptotic cells also are brightly staining with the anti-activated caspase 3 antibody, confirming the utility of this antibody as an imaging marker for early toxicity in high content imaging studies.
Red: anti-activated caspase 3, Green- GFP, Blue – Hoescht (nuclei).

This antibody was therefore used as an imaging marker for early toxicity in high content imaging studies, to look for differences across the HTT exon 1 lines at baseline after 14 days of differentiation. The overall intensity of anti-activated caspase 3 staining per well was divided by the total nuclear count (to account for the variability in cell number between wells). This showed small but significantly higher levels of anti-activated caspase 3 staining in the 71Q-H line compared to the control GFP line, however there was no difference between this and the other lines in the matched panel (figure 4.11).

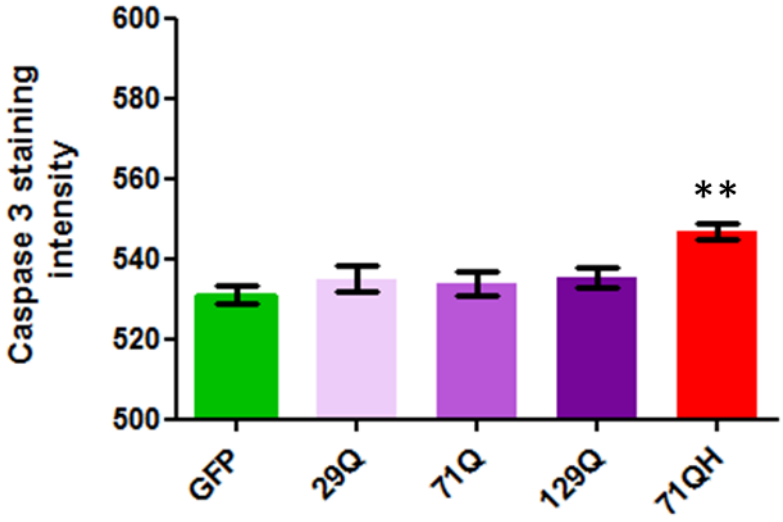


**Figure 4.11: Intensity of anti-activated caspase 3 staining in ReNcellVM HTT exon 1 lines analysed by high content imaging** at dd14 shows significantly higher activated caspase 3 staining in the 71Q-H line compared to the control GFP line (One-way ANOVA with Bonferroni's correction, **=P≤0.01, n=8 per condition, technical replicates).

#### 4.5.2.5 Effect of HTT exon 1 overexpression on the response of ReNcellVM neurons to acute cell stress

The impact of HTT exon 1 expression on vulnerability to acute cell stress for 24 hours was then investigated, using a variety of cell stressors. 29Q and 71Q-H cells were seeded at 20,000 cells/well and differentiated for two weeks in 96 well plates and then treated with various cell stressors at a range of doses. LDH assay was then carried out after 24 hours, with percentage cell death calculated compared to a positive control of 10% Triton-X which lysed all cells. For each cell line, six wells (technical replicates) were tested per dose.

#### 4.5.2.6 Hydrogen peroxide ($H_2O_2$) application in HTT exon 1 overexpressing ReNcellVM cells

Oxidative stress has previously been implicated in HD pathogenesis. Previous studies have shown that a dose of 300 μM is sufficient to cause toxicity in HD-iPSCs (Consortium, 2012), and 100 μM in SH-SY5Y cells (Nirmaladevi et al, 2014). Therefore the following doses were tested 0, 10, 50, 100, 200, 500 and 1000 μM, with results as shown in figure 4.12. The cells displayed sensitivity to $H_2O_2$ in a dose range as expected, but there were no differences between the 71Q-H and 29Q control line over the dynamic range.

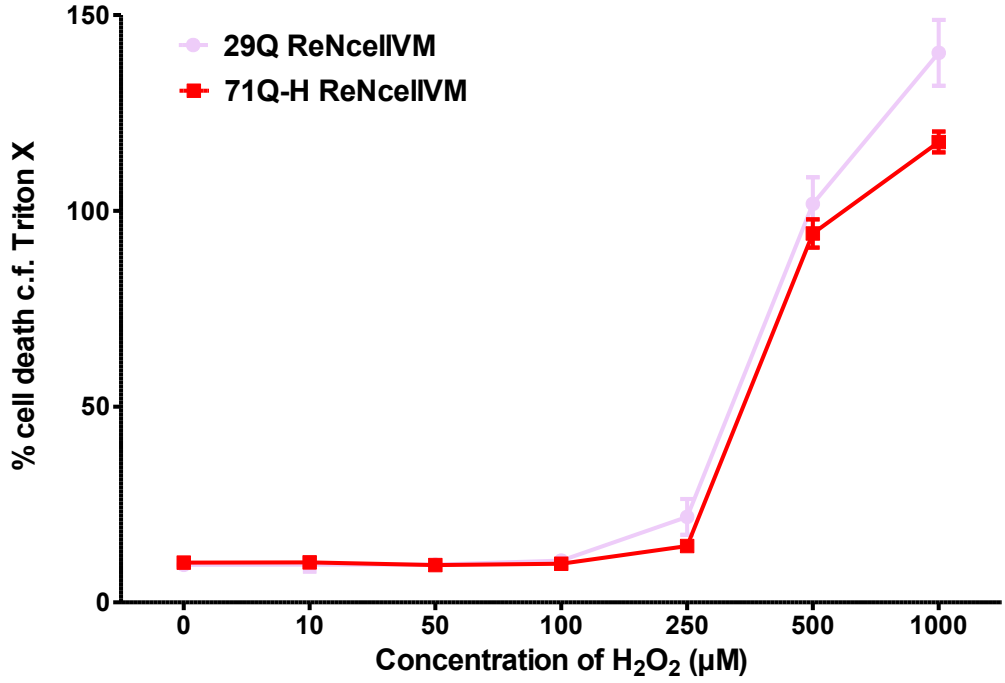


**Figure 4.12: Hydrogen peroxide dose response curve in dd14 HTT exon 1 29Q and 71Q-H ReNcellVM cells.** LDH assay was used to calculate cell death as a percentage of total cell lysis induced in positive control wells by 10% Triton-X. No significant differences are seen between the two lines in response to hydrogen

peroxide from 0-500 μM – cell death at 1000 μM is above 100% and therefore spurious (Two way ANOVA with Bonferroni's correction, n=6 per dose).

#### 4.5.2.7 Glutamate application in HTT exon 1 overexpressing ReNcellVM cells

Excitotoxicity has been implicated as a pathogenic mechanism in HD. Therefore the effect of glutamate on the HTT exon 1 cells was tested. A literature search revealed that doses of 30 μM or 125 μM had an effect on neuronal cells and so a range from 0-1000 μM was tested. Initial attempts were not successful as the hydrochloric acid used to reconstitute the L-glutamic acid inactivated the LDH assay. Therefore after 24 hours of exposure to glutamate, full media change was carried out and the LDH assay performed after a further 24 hours. It was expected that this would still exert a measureable effect on the cells, as previous published protocols have replaced neurons in regular media after glutamate exposure for 24 hours prior to performing the cytotoxicity assay. The results are shown in figure 4.13.

This flat response to very high doses of glutamate was not expected. Subsequent Western blotting for VGlut1 transporter and GluR2 (an AMPA subunit) receptors revealed that the HTT exon 1 lines were not expressing these glutamate receptors by day 14 of differentiation. Therefore these particular cells are not vulnerable to the effects of glutamate induced excitotoxicity; this may be due to the immaturity of the neuronal culture at day 14.

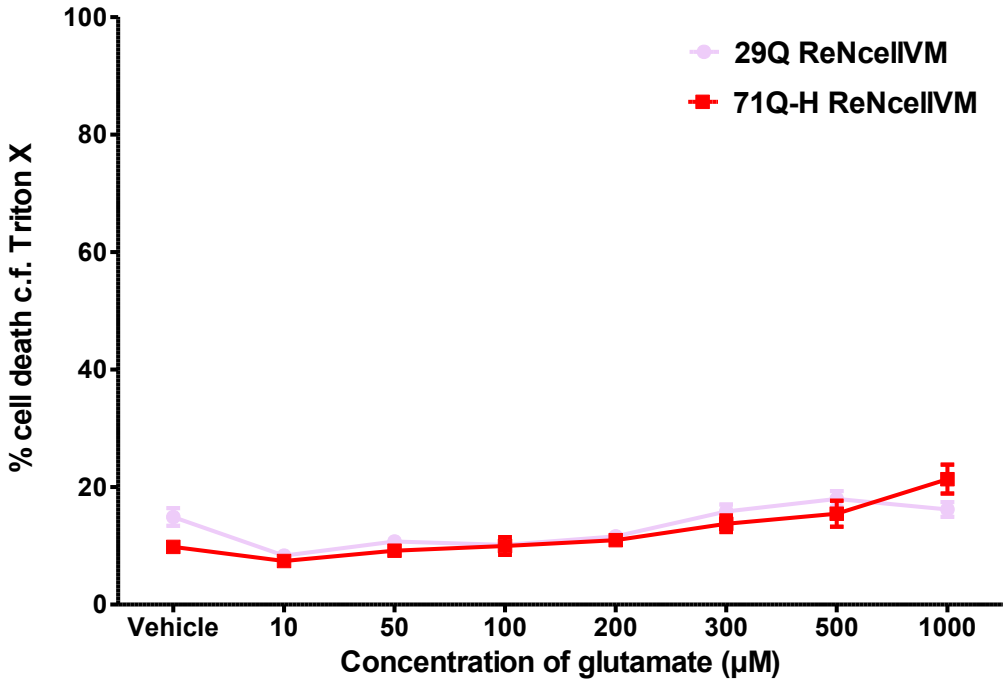


**Figure 4.13: Glutamate dose response curve in dd14 HTT exon 1 29Q and 71Q-H ReNcellVM cells** shows no response in either cell line to the application of even high doses of glutamate. LDH assay was used to calculate cell death as a percentage of total cell lysis induced in positive control wells by 10% Triton-X. (n=6 per dose).

#### 4.5.2.8 MG132 application in HTT exon 1 overexpressing ReNcellVM cells

MG132 is a commonly used, reversible proteasomal inhibitor. The UPS is known to be affected in HD and so by applying MG132 as a pathological stressor it would be expected to find increased cell toxicity in the pathogenic HTT exon 1 lines. Previous studies have shown that 24 hours of MG132 exposure at doses ranging from 0-200 µM induces cell death in mHTT expressing rat striatal neurons (Seo et al, 2007), and doses of 5 µM induce aggregate formation in HD-iPSCs (Jeon et al, 2012). Therefore a dose

range of 0-500 μM was tested in the 71Q-H and 29Q lines, with results shown in figure 4.14.

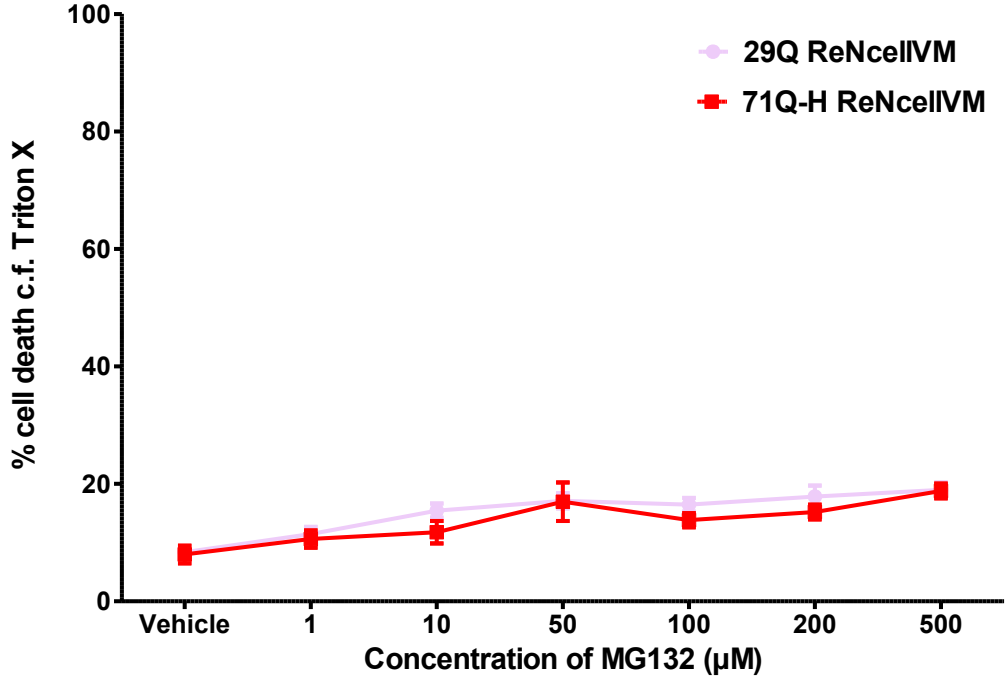


**Figure 4.14: MG132 dose response curve in dd14 HTT exon 1 29Q and 71Q-H ReNcellVM cells.** LDH assay was used to calculate cell death as a percentage of total cell lysis induced in positive control wells by 10% Triton-X. No significant differences are seen between the two lines in response to MG132 (Two-way ANOVA with Bonferroni's correction). The level of cell death in both lines is much lower than expected, even at high doses of MG132 (n=6 per dose).

There was no difference in response to MG132 between the control and pathogenic lines. The relatively small effect of MG132 on cell death was also surprising. Therefore the experiment was repeated using whole plate lysis using 10% Triton X to calculate the percentage cell death per well (figure 4.15).

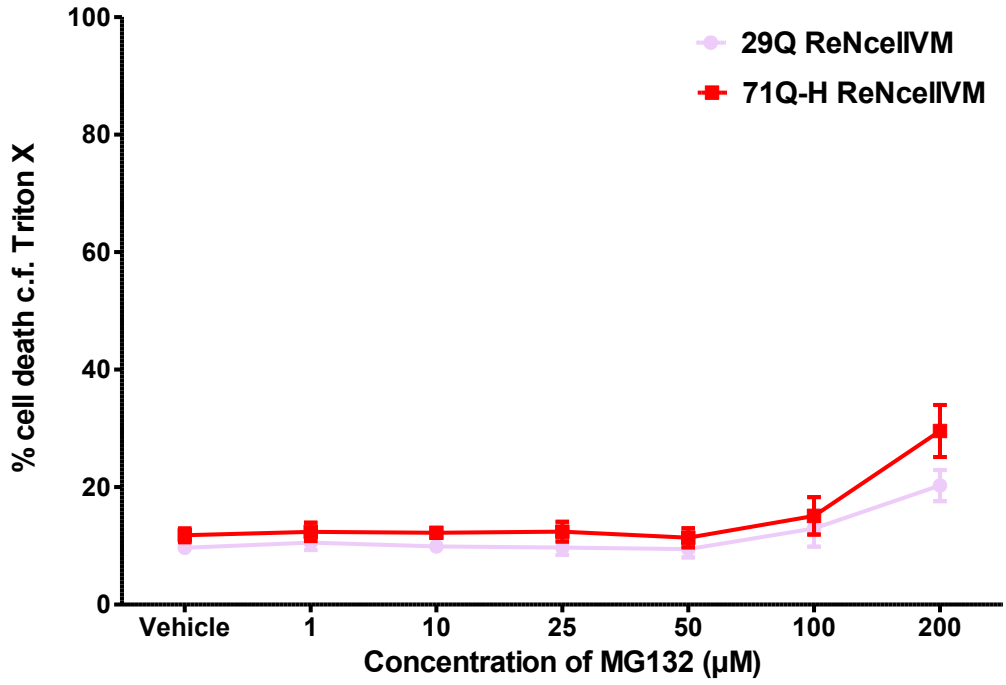


**Figure 4.15: MG132 dose response curve in dd14 HTT exon 1 29Q and 71Q-H ReNcellVM cells calculated using alternative method;** LDH assay was carried out followed by whole plate lysis with 10% Triton-X and repeat LDH assay, to calculate percentage cell death in each well. Significantly higher cell death in the pathogenic 71Q-H line compared to the control 29Q line is seen at 200 µM MG132 (Two-way ANOVA with Bonferroni correction, $p<0.05$). However this effect is small and overall the percentage of cell death is still lower than expected (n=6 per dose).

Using this method, there was significantly higher cell death in the pathogenic 71Q-H lines compared to the 29Q control at the highest dose of MG132 tested. It should be noted however that this effect was slight, and overall the percentage of cell death was still lower than expected. In order to ensure that the batch of MG132 used was not at fault, the experiment was repeated using pre-reconstituted MG132 that was from another company and on cells that had been differentiated for 4 weeks. However as

can be seen from figure 4.16, this again showed no difference between control and pathogenic lines and confirmed low levels of cell death even at high doses.

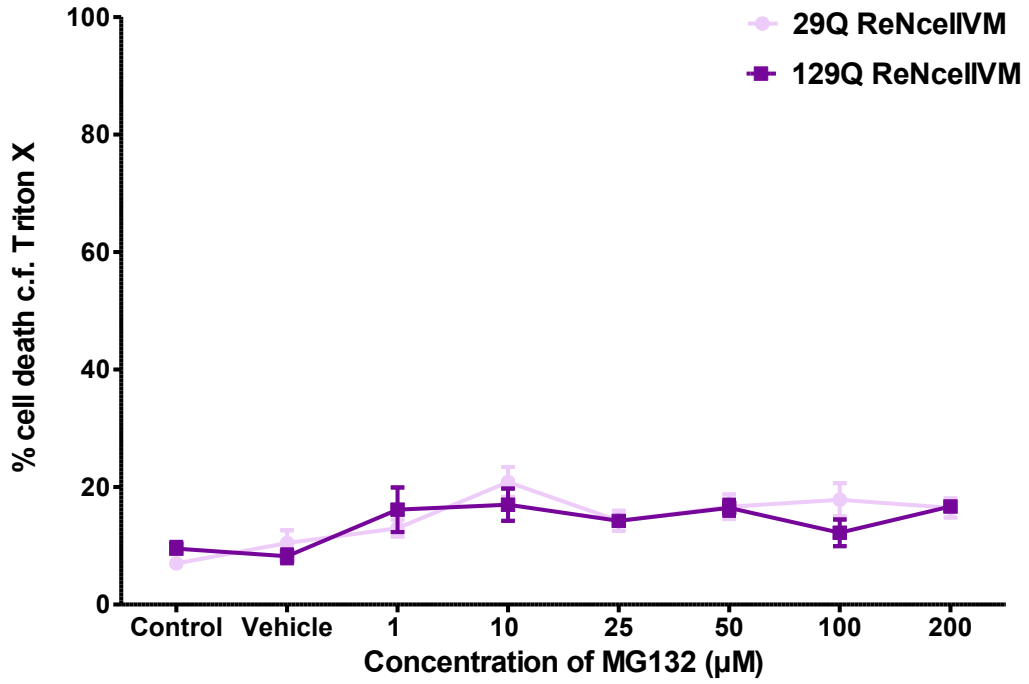


**Figure 4.16: MG132 dose response curve in dd14 HTT exon 1 29Q and 129Q ReNcellVM cells.** A new batch of pre-reconstituted MG132 was applied at appropriate concentrations. LDH assay was used to calculate cell death as a percentage of total cell lysis induced in positive control wells by 10% Triton-X. Again, no significant differences in cell death are seen between the two lines (Two-way ANOVA with Bonferroni's correction, n=6 per dose) and the level of cell death in both lines remains low.

### 4.5.2.9 Lactacystin application in HTT exon 1 overexpressing ReNcellVM cells

Lactacystin is an irreversible proteasomal inhibitor. Previous studies have shown doses between 10-50 µM induce cell death in PC12 cells (Fornai et al, 2003). A dose

response curve ranging from 0-200 μM was tested in the 71Q-H and 29Q lines, with results shown in figure 4.17. Lactacystin did not induce cell death in the cell lines tested, even at high doses.

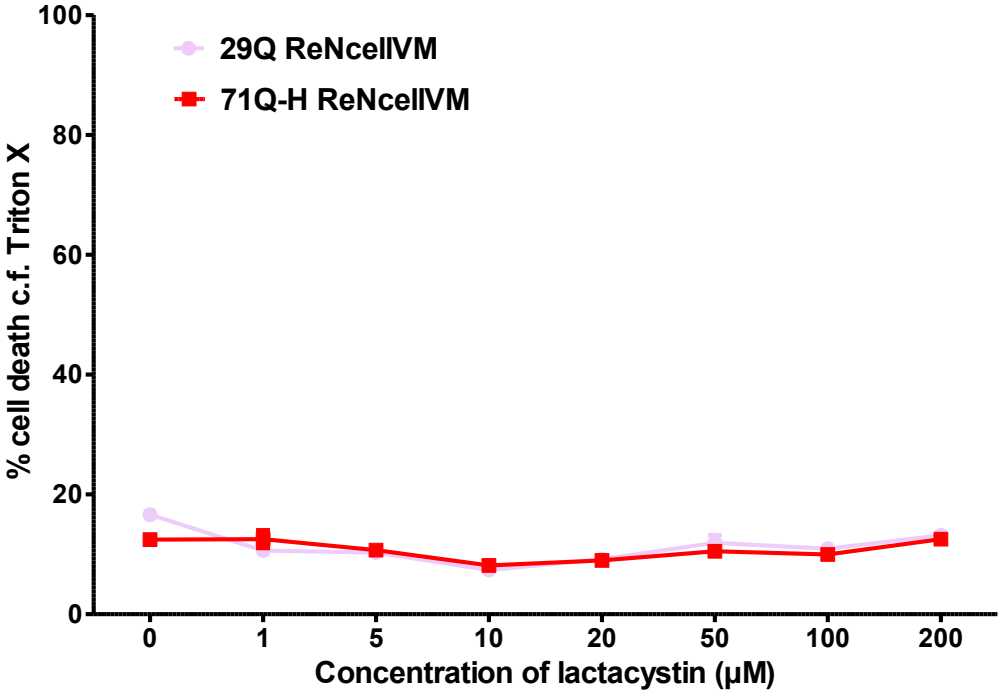


**Figure 4.17: Lactacystin dose response curve in dd14 HTT exon 1 29Q and 71Q-H ReNcellVM cells.** LDH assay was used to calculate cell death as a percentage of total cell lysis induced in positive control wells by 10% Triton-X. No significant differences are seen between the two lines in response to lactacystin (Two-way ANOVA with Bonferroni's correction, n=6 per dose). Cell death is not induced by lactacystin in either the control or mutant lines.

Repeat testing of MG132 and lactacystin was carried out on HTT exon 1 29Q, 71Q and 71Q-H ReNcellVM cells at very high doses, and compared to high dose hydrogen

peroxide, and no treatment. This confirmed lower than expected cell death in these lines in response to proteasomal inhibition, as seen in figure 4.18.

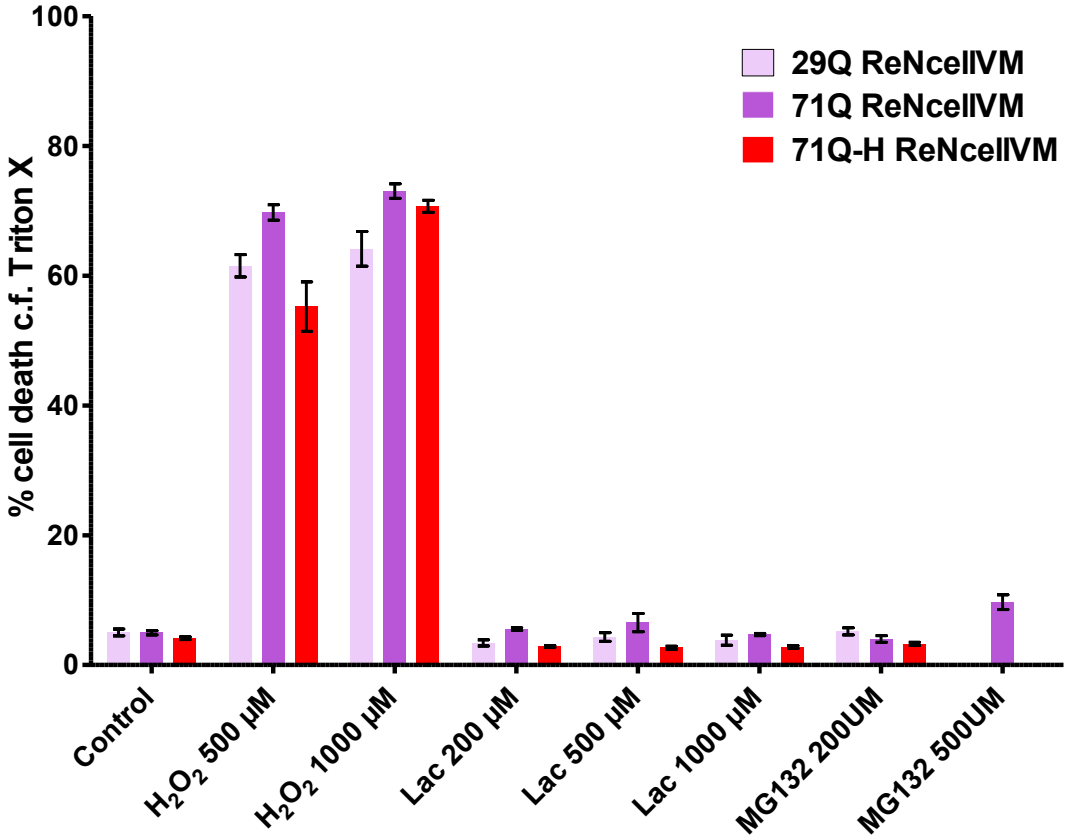


**Figure 4.18: Cell death induced by high doses of $H_2O_2$, lactacystin and MG132 in dd14 HTT exon 1 29Q, 71Q and 71Q-H ReNcellVM cells.** LDH assay again confirms minimal cell death in response to treatment with high doses of proteasomal inhibitors lactacystin (Lac) and MG132. However high doses of $H_2O_2$ do induce cell death as expected. (n=4 per dose).

#### 4.5.2.10 Epoxomicin application in HTT exon 1 overexpressing ReNcellVM cells

Epoxomicin is another irreversible proteasomal inhibitor that was tested in the 29Q and 129Q lines, but with similar lack of effect (figure 4.19).

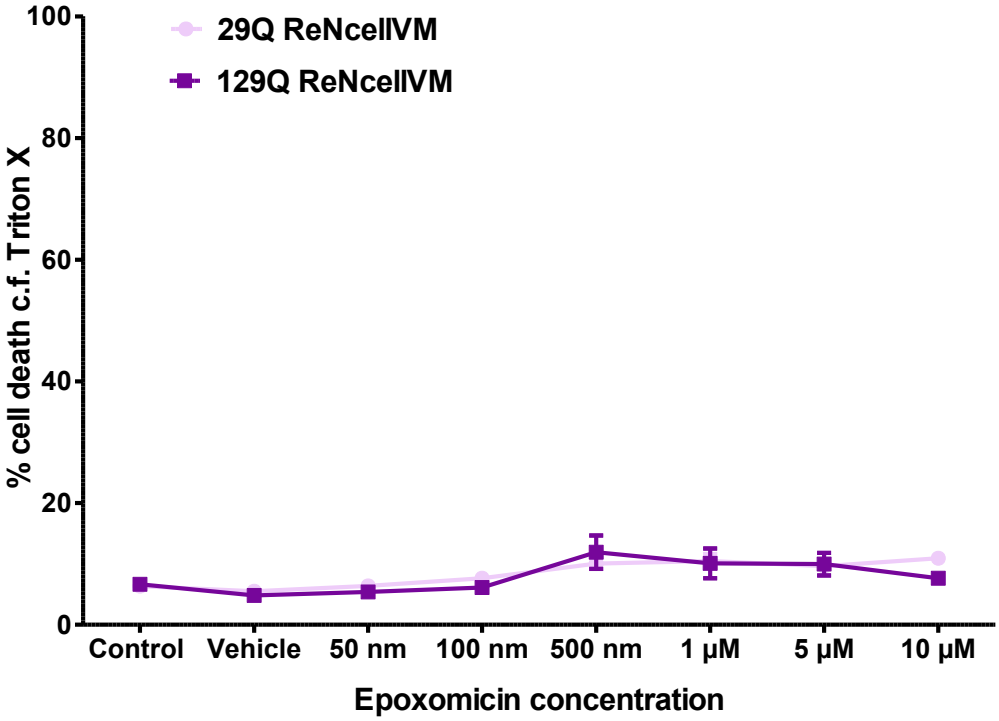


**Figure 4.19: Epoxomicin dose response curve in dd14 HTT exon 1 29Q and 129Q ReNcellVM cells.** LDH assay was used to calculate cell death as a percentage of total cell lysis induced in positive control wells by 10% Triton-X. Cell death is not induced by epoxomicin either the control or mutant line. (n=6 per dose).

#### 4.5.2.11 MVB003 confirms UPS system inhibition in HTT exon 1 overexpressing ReNcellVM cells

In order to ascertain that proteasomal inhibitors MG132, lactacystin and epoxomicin were entering the cells and inhibiting the UPS, the fluorescent probe MVB003 was used. This probe binds covalently and irreversibly with the N-terminal active site of the catalytic subunits of the proteasome, and emits red fluorescence. HTT exon 1 71Q-H ReNcellVM cells were grown on laminin coated glass coverslips for two weeks. 1% DMSO, 200 μM MG132, 200 μM lactacystin and 10 μM epoxomicin were added to the media for 24 hours. Following treatment, 1 μM of MVB003 was added to each coverslip for one hour at 37 degrees. Cells were also stained with Hoescht for 10 minutes, and then fixed and imaged. Results are shown in figure 4.20.

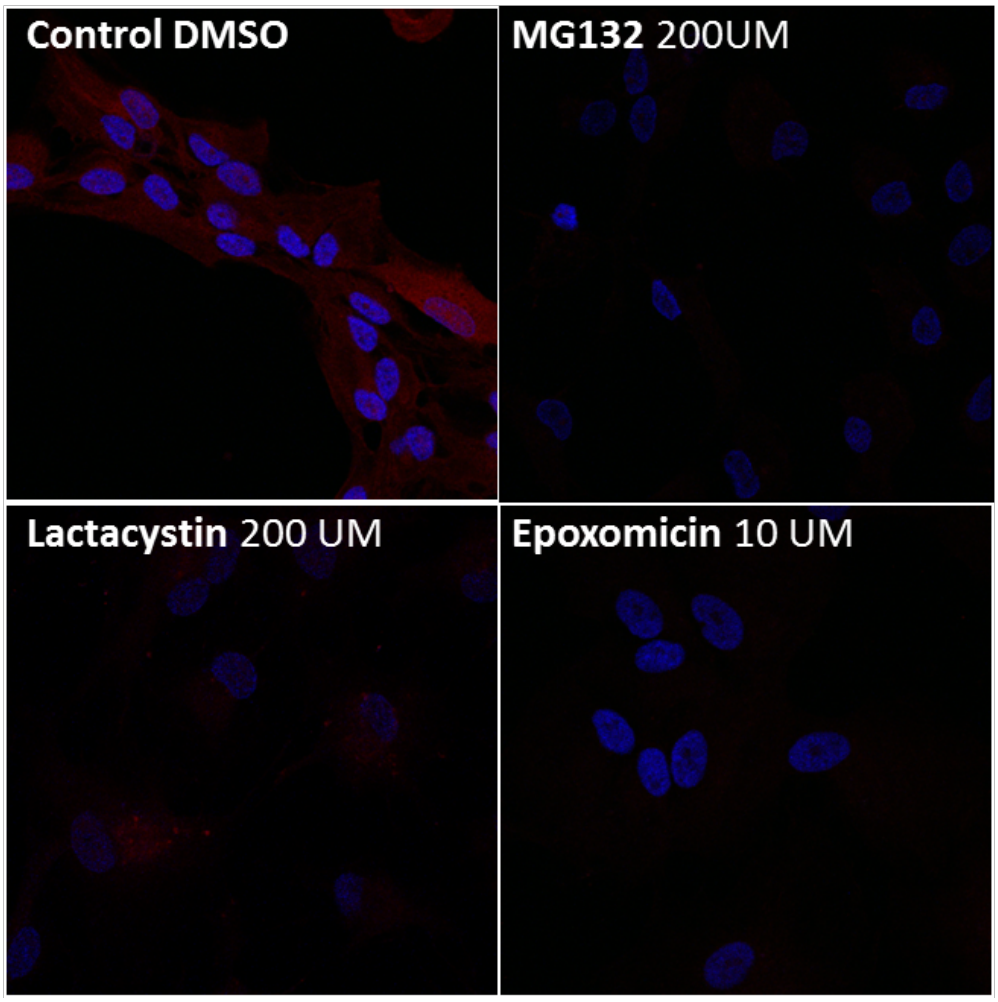


**Figure 4.20: The UPS in dd14 HTT exon 1 71Q-H ReNcellVM cells is inhibited by MG132, lactacystin and epoxomicin.** Probe MVB003 enters cells treated with only DMSO control and emits red fluorescence, confirming activation of the UPS. This red signal is absent in cells treated with MG132, lactacystin and epoxomicin, confirming that proteasomal inhibition has occurred.

This confirms that the UPS is active in the 71Q-H cells, and is inhibited by MG132, lactacystin and epoxomicin; however, as seen from the results of the LDH assays, this inhibition does not lead to high levels of cell death.

#### 4.5.2.12 Bafilomycin application in HTT exon 1 overexpressing ReNcellVM cells

Bafilomycin is a widely used as an inhibitor of autophagy. Bafilomycin A1 inhibits lysosomal hydrolase activity required for lysosomal acidification, which is important for the final autophagosome-lysosome fusion event. This is known to occur at concentrations of 400 nM (Sarkar et al, 2009), and therefore a range of doses were tested to include this (figure 4.21).

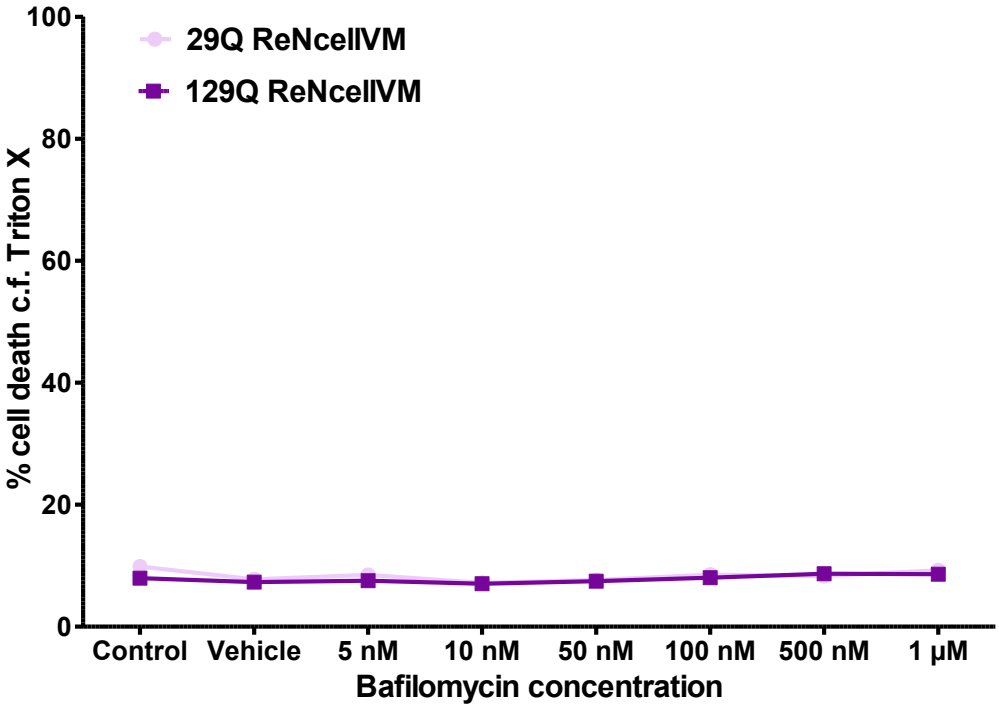


**Figure 4.21: Bafilomycin dose response curve in dd14 HTT exon 1 29Q and 129Q ReNcellVM cells** shows no cell death in response to treatment with high doses of bafilomycin, as assessed by LDH assay. (n=6 per dose).

Again, no increase in cell death is seen in response to bafilomycin, even at very high doses. This experiment was repeated with the addition of 200 μM of MG132 to the media in addition to increasing doses of bafilomycin, with results as shown in figure 4.22.

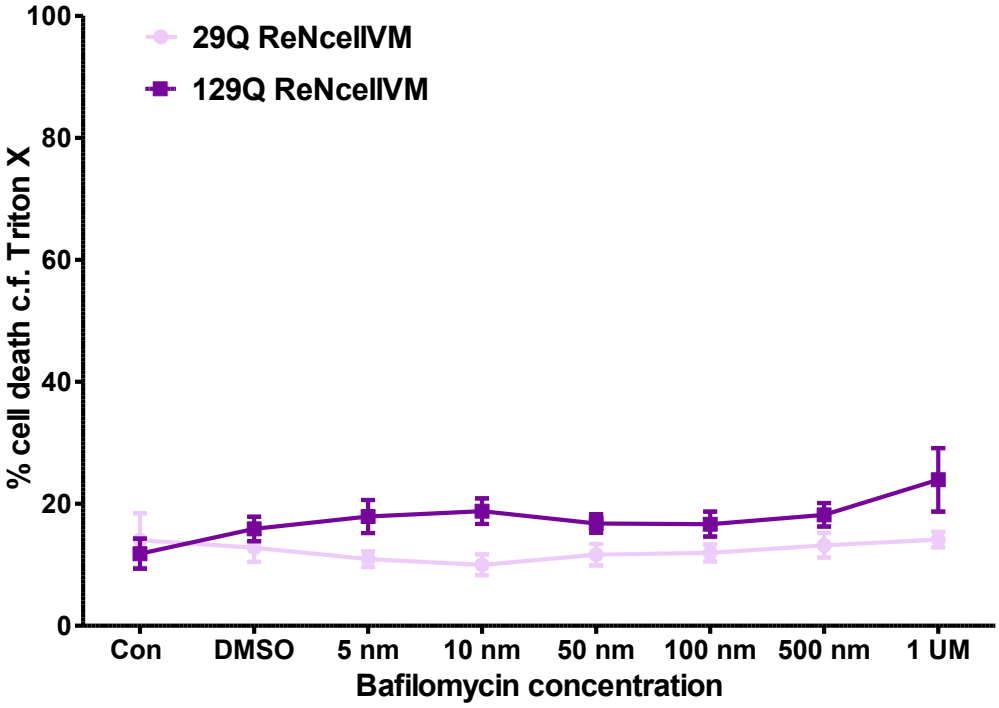


**Figure 4.22**: **Treatment of dd14 HTT exon 1 29Q and 129Q ReNcellVM cells with 200 μM MG132 and increasing doses of bafilomycin.** Cell death was determined by LDH assay. There was no significant effect of increasing bafilomycin dose in either cell line. There was a small but significant increase in cell death overall in the pathogenic 129Q line compared to the control 29Q line (two-way ANOVA with Bonferroni correction, $p<0.0001$). (n=6 per dose).

The effect of increasing bafilomycin dose was not significant in this experiment; however there was a significant difference between control (29Q) and pathogenic (129Q) lines, with slightly greater cell death observed in the pathogenic line. This may

indicate that cells expressing mHTT are more affected by high dose proteasomal inhibition. However in general terms, blocking both UPS and autophagy simultaneously for 24 hours still had minimal effect on cell viability; this would imply that our cells are able to tolerate severe disruption of protein homeostasis for up to 24 hours.

Immunocytochemistry on the 29Q and 129Q line confirms that both bafilomycin and MG132 are entering the cells and affecting the distribution of proteins, including GFP (figure 4.23), and HTT as detected by the N-terminal anti-HTT antibody aa1-82 (figure 4.24). This effect is particularly prominent in the 129Q line, and is discussed in more detail in chapter 5 (section 5.5.4).

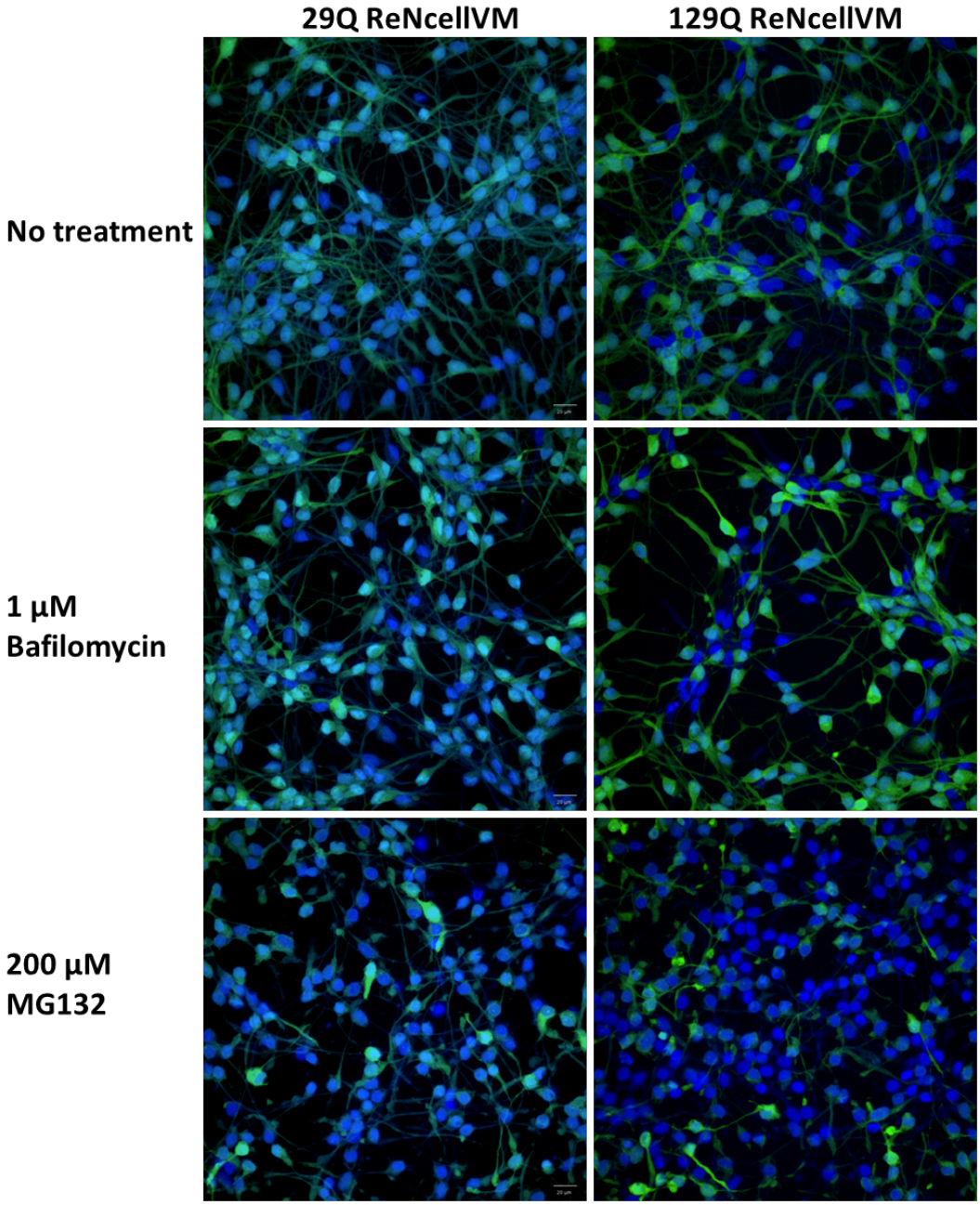


**Figure 4.23: GFP distribution in dd14 HTT exon 1 29Q and 129Q ReNcellVM cells following 24 hours of treatment with Bafilomycin and MG132.** Inhibition of both autophagy and MG132 changes the distribution of GFP in both cell lines, and this is particularly prominent in the 129Q cells.
Blue – Hoescht, Green – GFP

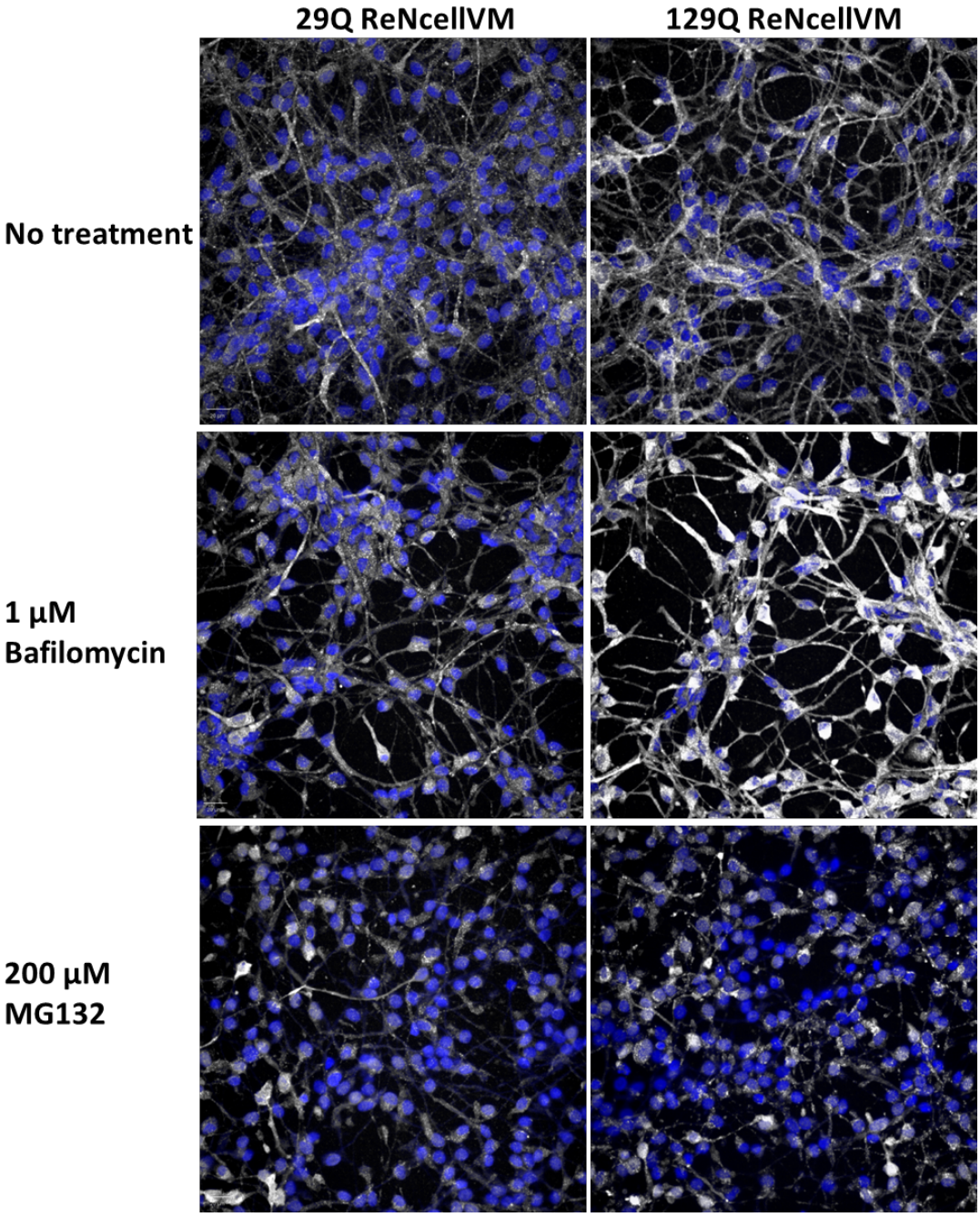


**Figure 4.24**: **HTT distribution in dd14 HTT exon 1 29Q and 129Q ReNcellVM cells following 24 hours of treatment with Bafilomycin and MG132.** Inhibition of both autophagy and MG132 changes the distribution of HTT in both cell lines and again, this is particularly prominent in the 129Q cells.
Blue – Hoescht, White – HTT.

### 4.5.3 Effect of HTT exon 1 overexpression on the response of ReNcellVM neurons to chronic cell stress

In order to allow more time for cytotoxicity to develop and for any potential compensatory mechanisms to fail, the response of 29Q and 129Q cells to five days of pathological stress was tested. Moderate and high doses of hydrogen peroxide ($H_2O_2$), MG132, epoxomicin and bafilomycin were used (epoxomicin has a favourable cost compared to lactacystin, and both are irreversible proteasomal inhibitors). Results are shown in figure 4.25.

As expected, hydrogen peroxide continues to cause cell death in both lines at the high dose of 300 μM, but not at the lower dose of 30 μM. MG132 and epoxomicin both cause total or near total cell death at higher and lower doses, indicating that the cells are not able to tolerate UPS inhibition for longer periods of time. There was still minimal response to autophagy inhibition with bafilomycin.

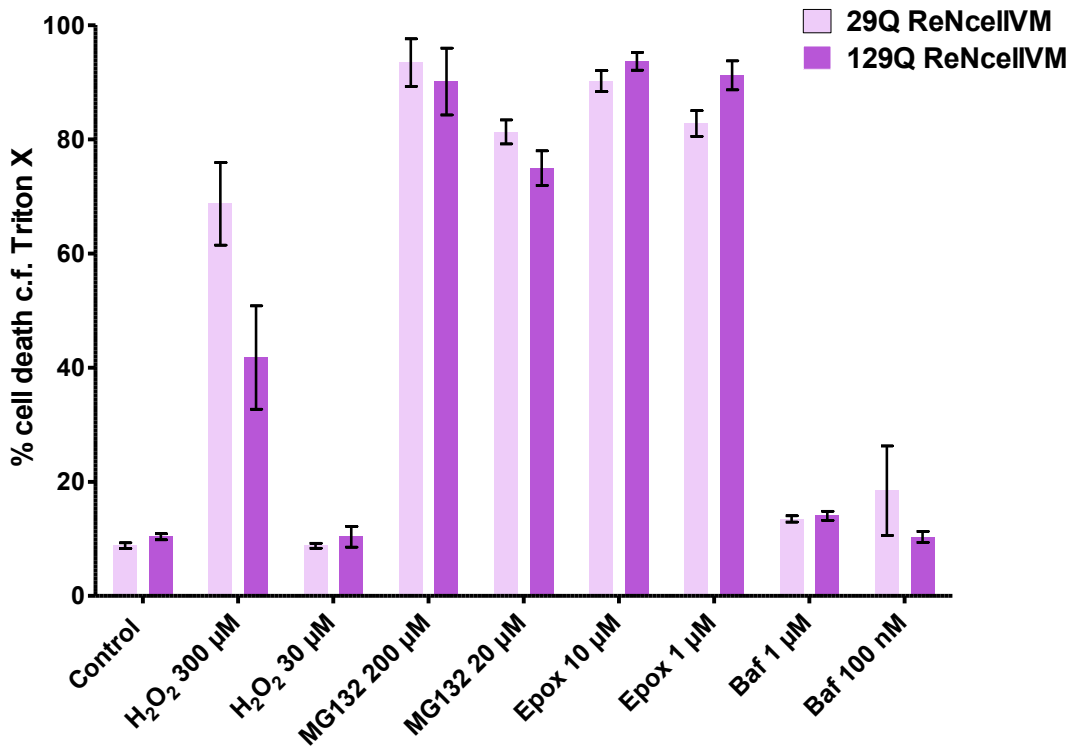


**Figure 4.25: Effect of chronic cell stress on dd14 HTT exon 1 29Q and 129Q ReNcellVM cells.** Percentage cell death was determined by LDH assay after five days of treatment with toxins as shown. Chronic application of $H_2O_2$ causes cell death in both lines at the high dose of 300 µM, but not at the lower dose of 30 µM. Proteasomal inhibition with MG132 and epoxomicin did cause high levels of cell death after five days, but there remains minimal response to bafilomycin. Two-way ANOVA shows no significant differences between 29Q and 129Q lines under any of the conditions tested, with the exception of $H_2O_2$ at 300 µM, however this was felt to be a spurious result as previous experiments had not found any differences in the response to $H_2O_2$ between control and mutant lines. (n=6 wells per condition tested) (Epox=epoxomicin, Baf=bafilomycin).

To determine whether there was any evolution of CAG length-dependent differences in response to the proteasomal inhibitors between day 1 and day 5, a time-course of cell death was carried out. The above experiment was repeated with LDH assay performed at day 1, day 3 and day 5. Results are shown in figure 4.26 and 4.27. In the case of MG132 there are no significant differences between 29Q and 129Q lines at either dose, at any time point. At day 3 epoxomicin seemed to affect the 29Q control line more than the 129Q line at both doses, however on repeating the LDH assay at this time point, the finding was not replicated.

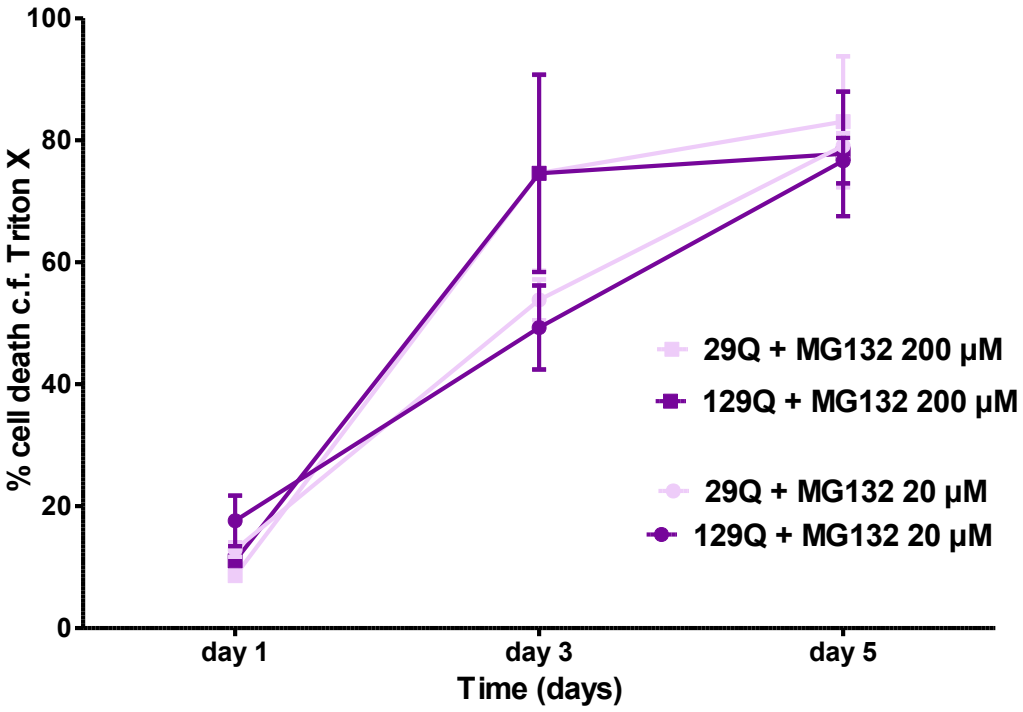


**Figure 4.26: Cell death in HTT exon 1 29Q and 129Q cells treated with low and high dose MG132 over five days.** Percentage cell death was determined by LDH assay after 1, 3 and 5 days of treatment with either 20 µM or 200 µM MG132. There are no significant differences between 29Q and 129Q lines at any time-point, at either dose (Two-way ANOVA with Bonferroni's correction, n=6 per dose).

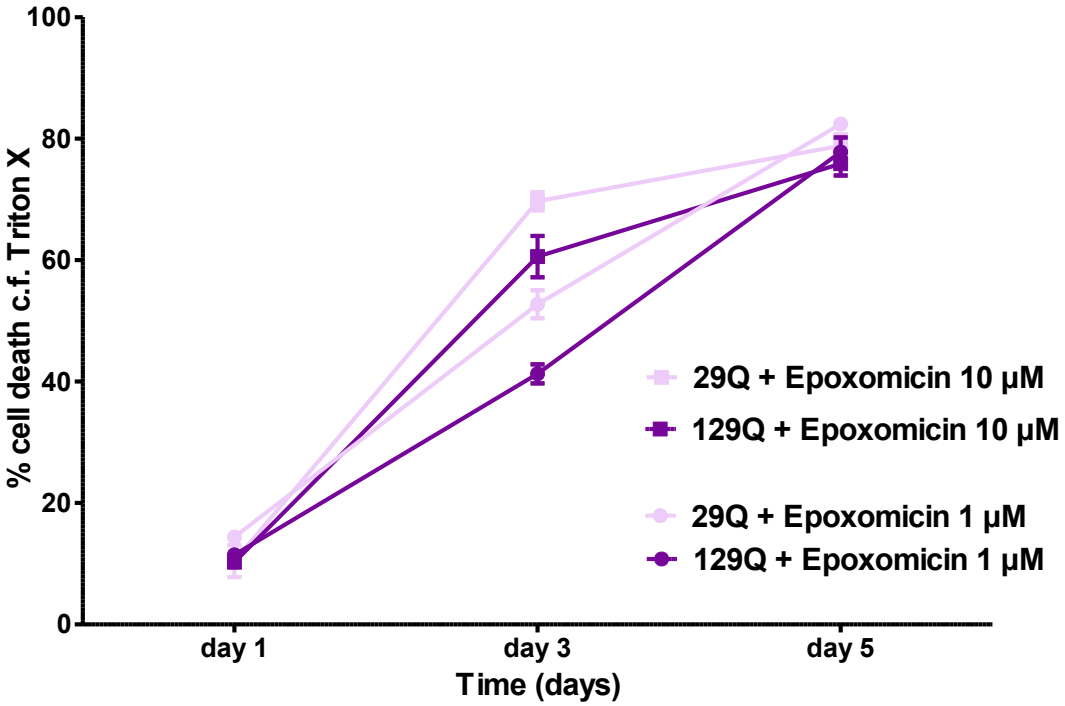


**Figure 4.27: Cell death in HTT exon 1 29Q and 129Q cells treated with low and high dose epoxomicin over five days.** Percentage cell death was determined by LDH assay after 1, 3 and 5 days of treatment with either 1 µM or 10 µM epoxomicin. Unexpectedly, there was significantly higher cell death observed in the control 29Q cells compared to the pathogenic 129Q lines at day three, both at low ($p<0.001$) and high doses of treatment ($p<0.01$) (Two-way ANOVA with Bonferroni's correction, n=6 per dose). However on repeating the LDH assay at this time point, the finding was not replicated.

Therefore, although the cells did display expected levels of cell death in response to longer application of proteasomal inhibitors, there were no CAG length-dependent effects observed.

## 4.6 Discussion

Overall the expression of mutant HTT exon 1 in the ReNcellVM cells had relatively minimal effect on both NSCs and neurons. There was a small but significant decrease in B3-tubulin expression in the ReNcellVM 129Q line, along with a trend towards larger nuclear size (though this did not reach significance). At baseline there was no increased cell death in the pathogenic cell lines, as measured by LDH, MTT, Alamar blue assays. Anti-activated caspase 3 imaging was marginally increased in the highly expressing ReNcellVM 71Q-H line. Surprisingly, there was a lack of CAG-dependent vulnerability to a range of toxins, tested both acutely and chronically.

The general lack of overt cell death or toxicity of mHTT exon 1 in this cell line would seem to contrast with the findings of the studies mentioned in table 4.1. However, it may be that in human NSCs and neurons (rather than rodent derived cells or non-neuronal cells), toxic effects take much longer to develop. HD is an exclusively human disease and even in severe cases of juvenile HD, it takes many years for symptoms to appear and neurodegeneration to occur. Another possible explanation for these results relates to the level of mHTT exon 1 overexpression in the lines; this is of particular relevance because wild-type huntingtin is known to have a neuroprotective effect in cells (Rigamonti et al, 2001). As determined by MSD assay (chapter 3) the matched panel of ReNcellVM 29Q, 71Q and 129Q lines have overexpression of HTT exon 1 at 3-6 fold over endogenous HTT levels (with the 71Q-H line expressing at over 50 times endogenous levels). Generally, published papers that use transgenic cell models do not mention the level of overexpression in their system, but extremely high levels of mHTT exon 1 could be responsible for driving the observed toxicity reported in those studies. This is supported by the finding that the only line that displayed even marginal

compromise at baseline (as determined by anti-activated caspase 3 staining) was the highest expressing ReNcellVM 71Q-H line.

The use of biochemical assays such as LDH, MTT and Alamar blue may lack the sensitivity required to pick up subtle differences in viability between the lines. The LDH assay detects gross impairments in cell viability, as it requires the plasma membrane to be “leaky” before LDH is released into the surrounding medium – this only occurs once the cells are dying/dead. The MTT and Alamar blue assays may similarly miss early pathogenic changes affecting neuronal viability. It may be that more sensitive measures, such as RNAseq or quantitative proteomics, are needed to detect CAG-repeat length phenotypes in these cells. A recent paper by Kim et al found that differentiated Neuro-2a cells expressing Htt exon 1 with 18Q, 64Q or 150+Q had aberrant protein interactions (mediated through soluble oligomers) in the pathogenic lines despite there being no overt effect on cell viability (as assessed by LDH and MTT assays carried out after 48 hours) (Kim et al, 2016).

Generally it was found that these transgenic cell lines lost their adhesion to laminin over time – on many occasions this lead to cells detaching as a sheet from the laminin coated well, at some point after ten days of differentiation. This would then render the plate unsuitable for imaging or biochemical assays, and necessitated repeating the experiment. Unfortunately the use of other coating agents (Matrigel, Geltrex) did not make any difference. Another experimental issue that caused difficulty was the “honeycombing” effect seen in these cells, as described above (section 4.5.1.1). This led to well to well variability in cell number across the 96 well-plate, despite the same seeding density – this may have led to less accurate readings on biochemical assays

of viability. In terms of imaging markers of cytotoxicity, nuclear cell count can be rapidly obtained across the plate using Columbus software, so any variability in cell number could be objectively measured and accounted for. Indeed the only finding of any mHTT exon 1 induced phenotype in unstressed cells was the increased activated-caspase 3 staining in the 71Q-H line, detected on high content imaging.

Caspase 3 is an effector of apoptosis that is activated by extrinsic (death ligand) and intrinsic (mitochondrial) pathways. On activation, it goes on to cleave and activate caspase 6 and 7, and also to cleave specific peptide bonds leading to protein degradation and cell death. In support of the findings in the ReNcellVM 71Q-H line, caspase 3 activation detected on Western blotting of cell lysates has been found to occur after 24 hours of mutant but not control length HTT exon 1 expression in PC12 cells (Sahoo et al, 2016). The activation of caspase 3 is known to be inhibited by wild type Htt, and lowering wild-type Htt leads to an increase in caspase 3 activation. The interaction of mutant Htt with caspase 3 is however much weaker (Zhang et al, 2006), and this may explain the observation in the 71Q-H line. This study also found that lowering endogenous huntingtin (with ensuing caspase 3 activation) led to increased cell death in N2a cells, but not in ST14 rat striatal cells (or ESCs and HeLa cells); this mirrors the selective cell vulnerability seen in HD. The lowering of wild-type Htt led to cell death in ST14 cells only when the cells were subjected to additional stress caused by the expression of N-terminal human mHTT. It also interesting that the authors did not find any increase in cell death following the expression of N-terminal human mHTT in ST14 cells under baseline conditions, as was also found in the pathogenic length HTT exon 1 ReNcellVM lines.

The absence of CAG-length dependent vulnerability to oxidative stress, proteasomal and autophagy inhibition was not expected. As mentioned previously, the lack of sensitivity of the LDH assay may have played a role in this, and would certainly miss any early DNA damage caused by $H_2O_2$ prior to cell death. There was minimal cell death in both pathogenic and control lines in response to proteasomal inhibitors (MG132, lactacystin, epoxomicin) applied for 24 hours, even at high doses – potentially the ReNcellVM line may be able to compensate for UPS inhibition in the short term. Chronic inhibition of the UPS over five days did produce high levels of cell death, indicating that any compensatory mechanisms may have been overwhelmed on prolonged exposure. On two occasions, statistical analysis did reveal slightly higher cell death in the pathogenic ReNcellVM line compared to control on treatment with acute high dose MG132 (figure 4.15 and 4.22). However this was not consistently found to be the case, and certainly on chronic proteasomal inhibition, no difference between pathogenic and control lines was found. Autophagy inhibition with bafilomycin did not cause cell death in either control or pathogenic line, even when applied for 5 days. However it could be seen on immunocytochemistry (figure 4.23 ad 4.24) that bafilomycin was entering the cells and affecting protein distribution even after 24 hours. There was increased HTT staining, particularly in the pathogenic line, suggesting the accumulation of HTT exon 1. This suggests that these cells are able to tolerate severe disruption of protein homeostasis, including the build-up of mutant HTT exon 1.

Recent papers have described an effect of mutant HTT on early neurodevelopment. Neural differentiation in human ESCs engineered to have graded increases in CAG repeat length was affected in pathogenic lines by chromosomal instability and failed cytokinesis (Ruzo et al, 2018). HD iPSCs with large CAG expansions showed failure of neuro-ectodermal acquisition whilst shorter expansions showed abnormalities in neural

rosette formation and disrupted cytoarchitecture in cortical organoids (Conforti et al, 2018). The finding that B3-tubulin expression (as quantified on high content imaging) is slightly reduced in the ReNcellVM 129Q line may be indicative of an adverse effect on neuronal differentiation in this line, and supports these recent findings.

However, this last finding must be interpreted with caution as the entire HTT exon 1 ReNcellVM panel, including the control GFP only line, did not differentiate into mature neurons, as evidenced by the lack of action potentials in these cells, and the co-expression of B3-tubulin, GFAP and nestin. The relative immaturity of these cells may also have contributed to the general resistance to cellular stressors that was observed, as true neurons would likely be more sensitive to the effects of oxidative and excitotoxic stress, and disruption of protein homeostasis. The lack of CAG-length dependent effects on cell death might also be partly explained by this, as neurons are known to be the cell type most vulnerable to the effects of mutant HTT.

## 4.7 Summary

The HTT exon 1 ReNcellVM allelic series did not display overt neuronal toxicity or increased vulnerability to toxins in the pathogenic lines. However a small decrease in B3-tubulin positive cells was seen in the ReNcellVM 129Q line on differentiation, and there was a marginal increase in anti-activated caspase 3 staining detected by high content imaging in the ReNcellVM 71Q-H line. There were no CAG-length dependent effects in cell death in response to modulation of protein homeostasis using UPS and autophagy inhibitors.

# 5 Effect of increasing CAG repeat length in HTT exon 1 protein in human neuronal cells

## 5.1 Background

Protein deposition is a feature of many neurodegenerative diseases, for example beta-amyloid derived from amyloid precursor protein (APP) in Alzheimer's disease (AD), tau in frontotemporal dementia (FTD) and alpha-synuclein in Parkinson's disease (PD). The role of protein deposition in disease pathogenesis is often not clear, and such is the case in HD. Inclusions of HTT protein have long been observed in post-mortem brain tissue, where they are present in neurons (DiFiglia et al, 1997) and glia (Shin et al, 2005), and are recapitulated by animal and cell models of HD. Inclusion frequency and rate of formation are polyQ repeat length dependent, and inclusion size increases with disease duration (Hughes & Jones, 2014).

Mutant HTT exon 1 is known to misfold and self-assemble via a series of aggregated species, progressing from monomeric forms into spherical oligomers, protofibrils, mature amyloid fibrils, and large fibril clusters or inclusions. The structures of these species are not fully resolved, nor the pathway of inclusion formation (Wetzel & Mishra, 2014). Mature fibrils are thought to contain antiparallel β-sheets and a recent structural study has found that the amyloid core of mHTT exon 1 fibrils are made up of two kinds of β-hairpin strands which interact via interdigitation of side chains, and this may seed aggregation (Hoop et al, 2016). Using a combination of correlative light and electron microscopy (CLEM) and time-lapse fluorescence microscopy, Peskett et al have shown

that aggregates of huntingtin exon 1 exist in distinct liquid-like and solid-like forms. Liquid-like assembly formation is driven by polyQ and proline-rich regions of exon 1. These convert into solid-like assemblies in cells, which are highly structured at the nanoscale level and resemble aggregates that have been found in the brain tissue of HD patients (Peskett et al, 2018).

The precise toxic species in HD is not known, and the contribution of HTT inclusion formation to neurodegeneration remains unclear. Marcellin et al have shown that levels of soluble monomeric full length mHtt remain constant with age in the $Hdh^{Q150}$ mouse, but the size of the oligomeric pool decreases and the level of insoluble inclusions increase (Marcellin et al, 2012). Inclusions have been shown to sequester essential cellular proteins such as transcription factors (CREB-binding protein), chaperones and proteasome components. The overexpression of a neuronal chaperone HSJ1a in R6/2 mice significantly reduced mutant huntingtin aggregation and enhanced solubility, and led to improved neurological performance (Labbadia et al, 2012). Methylene blue has also been shown to reduce aggregation and improve phenotype in R6/2 mice (Sontag et al, 2012), although in this study oligomer formation was also reduced.

In contrast a number of studies have found that promotion of HTT aggregation, for example by the chaperonin TRiC (Kitamura et al, 2006) and the small acidic protein prothymosin-α (Dong et al, 2012), have led to decreased toxicity in cell models of HD. A study by Tashiro et al showed that the prevention of correct folding of nascent GFP-HTT exon 1 72Q protein by disrupting formation of the chaperone prefoldin, inhibited the formation of insoluble inclusions but led to an increase in oligomeric forms that were more toxic to cells (Tashiro et al, 2013). Tracking inclusion formation in individual

cells over time also found correlation with improved cell survival (Arrasate et al, 2004). Inclusions are found to appear very early in R6/2 mice, before any behavioural phenotype occurs (Gong et al, 2012). Inclusion formation has also been found to precede symptom onset in the $Hdh^{Q150}$ knock-in mouse model (Landles et al, 2010). Data from human brains post-mortem shows that the anatomic pattern of inclusion formation does not spatially correlate with the main sites of pathogenesis (Gutekunst et al, 1999).

The subcellular location of inclusions may be of importance. In all mouse models, extra-nuclear inclusions have been found to vary in shape and size far more than nuclear inclusions. Extra-nuclear inclusions are composed of longer N-terminal fragments than their intra-nuclear counterparts (Hughes & Jones, 2014). R6/2 mice with super-long CAG repeats (>/= 335) have mHTT aggregation localised to the cytoplasm (as the transgenic protein is too large to past through the nuclear pore) and have delayed onset and less severe disease (Dragatsis et al, 2009). In transgenic mice, the progression of perinuclear (rather than nuclear) inclusions was shown to be accompanied by cell-cycle activation, disruption of the nuclear envelope and culminate in cell death (Liu et al, 2015).

HTT inclusions may themselves be a heterogeneous population, with different forms having differing contributions to disease. Caron et al described the formation of two types of inclusions depending on phosphorylation state: fibrillar, which are tightly packed and do not exchange protein with the soluble phase, and globular, which are loosely packed, can readily exchange with the soluble phase. Tightly packed fibrillary inclusions that do not exit the insoluble phase are thought to exert less toxicity (Caron

et al, 2014). Different polyQ amyloid conformations form under different temperatures, and loop/turn structures with exposed polyglutamines were found to exert higher toxicity than structures with extended and buried β-sheets (Nekooki-Machida et al, 2009).

A detailed examination of inclusion formation using high content imaging in the ReNcellVM HTT exon 1 lines was undertaken, in order to establish the effect of increasing CAG repeat length in human neuronal cells with matched expression levels of HTT exon 1. The impact of inclusion formation on these cells was also investigated. Subsequently the effect of proteostasis modulation on HTT accumulation and clearance in HTT exon 1 overexpressing ReNcellVM was studied.

*The effect of increasing CAG repeat length on the processing of HTT exon 1 by autophagy and the UPS*

Autophagy and the ubiquitin proteasome system (UPS) are the two main mechanisms for protein clearance in cells, and there is cross-talk between the two systems. Autophagy is used for the bulk degradation of protein complexes and damaged organelles, whereas the UPS generally clears short-lived nuclear and cytoplasmic proteins.

The term autophagy is used here to mean “macroautophagy”, in which the target cargoes are engulfed by double-membraned autophagosome precursors to form

completed autophagosomes. These are delivered to lysosomes along microtubules, and on fusion of the two structures, lysosomal hydrolases degrade its contents. Mutant HTT has been found to accumulate in vesicular structures in HD brains (Sapp et al, 1997) indicating that it is a substrate for autophagy and subsequent studies have shown that both full-length (Shibata et al, 2006) and aggregated HTT (La Spada, 2012) are cleared by this process. mTOR is a negative regulator of autophagy and has been shown to be incorporated into mHTT aggregates, with subsequent enhancement of autophagy in cells (Ravikumar et al, 2004). The autophagy enhancer rapamycin increased mHTT clearance and improved phenotype in fly and mouse models of HD (Ravikumar et al, 2004). Conversely, impaired autophagy may contribute to HD pathogenesis. A failure of cargo loading into autophagosomes has been demonstrated in HD (Martinez-Vicente et al, 2010), and impaired uptake and degradation of mHTT fragments by lysosomes has been found (Qi et al, 2012). The enhancement of autophagy is a potential therapeutic avenue in HD which is currently being explored (Sasazawa et al, 2015). The effect of bafilomycin A1 was tested in the ReNcellVM HTT exon 1 lines, to determine the impact of increasing CAG repeat length in response to autophagy inhibiton.

The UPS is responsible for the majority (80-90%) of protein clearance in eukaryotic cells, clearing both healthy and damaged or misfolded proteins. Elimination of proteins involves ubiquitination of the target protein, followed by degradation of the tagged protein by the 26S proteasome complex (Glickman & Ciechanover, 2002) (see section 1.4.2. for more detail). Mutant HTT is thought to be broken down and cleared by the UPS, and inclusion bodies are rich in ubiquitin and proteasome components (DiFiglia et al, 1997). There is conflicting evidence with regards to how UPS function is affected in HD. Seo et al found inhibition of the UPS in early and late stage HD brain regions, and

also in HD fibroblasts even on increased expression of proteasomal subunits (Seo et al, 2004). An increase in polyubiquitin chains, as a marker of UPS impairment, has been found in mouse models and HD patients (Bennett et al, 2007b). Using fluorescent reporters for the UPS, Wang et al have shown that mHTT compromised synaptic UPS activity in cultured neurons and mouse brains (Wang et al, 2008).

However, others have found no relationship between the accumulation of protein aggregates and global UPS impairment in mouse models of HD (Bett et al, 2009b). Maynard et al also showed that although mHTT caused a general inhibition of the UPS in PC12 cells, this was not the case in mouse models of HD which had a largely operative UPS. Increased ubiquitin was observed but could be attributed to an accumulation of large ubiquitin conjugates, different from the conjugates observed upon UPS inhibition (Maynard et al, 2009). The cellular environment may also play a role as polyglutamine proteins have been shown to have no effect on the UPS in SH-SY5Y cells under basal conditions, but the response of the UPS to cell stress was impaired (in the absence of cell death) (Ding et al, 2002). Thus the effect of mHTT on UPS function may be dependent on the expression levels, cellular context, model system, subcellular localisation and cell-type. Since the UPS is a highly ATP-dependent system (Schrader et al, 2009), defective mitochondria transport that is known to occur in HD neurons (Reddy & Shirendeb, 2012) may lead to ATP deficiency in neurites and nerve terminals, thus impeding the local degradation of mHTT by the proteasome in these subcellular regions (Zhao et al, 2016).

Whether a cause or a consequence of neurotoxicity in HD, impaired neuronal proteostasis may lead to the accumulation of any misfolded or old/damaged proteins

usually cleared through the UPS; this in turn may have far-reaching consequences on global cell health. The effect of the proteasomal inhibitor MG132 was tested in the ReNcellVM HTT exon 1 lines, to determine the impact of increasing CAG repeat length in response to UPS inhibition in neurons.

Upregulation of the UPS is an attractive treatment pathway in HD, and the overexpression of ube3a, an ubiquitin E3 ligase, can activate the UPS and decrease mHtt aggregates in the brains of HD knock-in mice (Bhat et al, 2014). However, overexpression of proteasomal activator PA28 increased UPS function in control but not HD fibroblasts (Seo et al, 2004). In collaboration with Proteostasis Therapeutics Inc (PTI), a number of proteasomal enhancers (specifically USP14 inhibitors) were tested for their ability to clear pathogenic length HTT exon 1 from ReNcellVM neurons. Ubiquitin-specific protease 14 (USP14) is a deubiquitinating enzyme (DUB), that cleaves ubiquitin from ubiquitinated proteins. USP14 inhibitors antagonise this, thus leading to an increase in ubiquitinated proteins which are then targeted for proteasomal degradation. As mHTT exon 1 is generally thought to exert toxicity through a multitude of pathways, any reduction in its concentration would be of potential therapeutic value.

## 5.2 Aims

1. To establish the effect of increasing CAG repeat length on HTT protein in HTT exon 1 overexpressing ReNcellVM cells.

2. To study the effect of proteostasis modulation on mHTT in HTT exon 1 overexpressing ReNcellVM cells.

## 5.3 Methods

HTT exon 1 ReNcellVM NSCs were cultured and differentiated as described in section 2.1.1 and 2.1.3. Samples were prepared for Western blotting as described in section 2.4, and a range of HTT antibodies were tested to determine the optimum method for the detection of HTT exon 1. A table of all antibodies tested and the concentrations is included in appendix table A.1. Similarly, a range of HTT antibodies for immunofluorescence detection was tested (appendix table A.2); cells were grown on laminin coated glass coverslips, fixed, permeabilised and stained using a standard immunocytochemistry protocol as described in section 2.7.1. To test the effects of amyloid dyes thioflavin T (ThioT) and NIAD-4, cells were differentiated on coverslips, fixed, permeabilised and stained with S830 as standard. However, after the wash/removal of the secondary antibody, the dyes were then added to the coverslips. ThioT compound was dissolved in methanol to form a 0.1% solution. 500Ul of this was

added directly to the coverslip for 8 minutes as per protocol. A 0.05% solution was also tested. NIAD-4 was dissolved in DMSO to form a 1 mM solution, which was then diluted in PBS to form 10 μM and 100 nM solutions that were added to the coverslips for 30 minutes as per protocol. After removal of the respective amyloid dyes, Hoescht staining for nuclei was carried out as standard.

To study the formation of HTT inclusion bodies in greater detail, a time-course analysis was carried out using high content imaging as described in section 2.7.2. Cells were seeded in a 96 well plate format onto laminin coated Perkin Elmer Cell Carrier plates for imaging. Cells were fixed at dd0, dd7 and dd14 respectively, followed by staining using the S830 anti-HTT antibody, and B3-tubulin or GFAP antibody (appendix table A.2). There were at least eight wells per condition tested (cell line and antibody combination). The plates were imaged on the Opera LX high content screening platform by Dr. Christin Luft at the UCL MRC Laboratory for Molecular Cell Biology (LMCB) with eighteen fields of view (fov) per well, and image analysis was carried out by Dr. Janos Kriston-Vizi (LMCB) using Image J and R. Data in the form of raw counts was then analysed on Prism by Dr. Rhia Ghosh and statistical analysis was carried out; two-way ANOVA with Bonferroni's correction for multiple comparisons was applied to confirm differences between cell lines across different time points (section 2.10). To study the effect of inclusions on neurons, a combination of standard confocal microscopy on the Zeiss 710 confocal microscope (section 2.7.1) and high content image analysis of the full HTT exon 1 panel stained with anti-HTT aa 1-82 antibody and imaged on the new Opera Phenix (section 2.7.2) was carried out, followed by image analysis on Columbus (section 2.7.2.1) and statistical analysis using Prism software (section 2.10).

Super-resolution imaging of the HTT exon 1 ReNcellVM lines was carried out as follows: cells were differentiated on specific Ibidi glass plates (0.17 mm thickness) for imaging, fixed and stained using S830 (section 2.7.3). Imaging was carried out with Dr. Ed Smith at the King's Nikon Centre, using the N-SIM Super Resolution System with corresponding N-SIM software.

To test the effect of proteostasis modulation on the distribution of HTT exon 1 in the ReNcellVM HTT exon 1 cells, the full panel was again plated onto 96 well Perkin Elmer Cell Carrier plates and after 14 days of differentiation, either 1 μM bafilomycin A1 or 200 μM MG132 was added to the media for 24 hours. Cells were then fixed and stained with aa1-82 as per standard protocol. Plates were imaged on the Opera Phenix, with image analysis on Columbus and statistical analysis on Prism. The effect of proteasomal activation using USP14 inhibitors supplied by PTI on the clearance of HTT exon 1 was tested using Western blotting. The pathogenic exon 1 lines were grown in 6-well format, and treated with the provided compounds and control at DD14 for 48 hours. Western blotting was optimised as described in the results section, and densitometry was carried out using Total Lab 100 (TL100) software. The density of HTT exon 1 bands was compared between control and active compounds, with statistical analysis (two-way ANOVA) carried out using GraphPad Prism. Following discussion with PTI, the experiment was repeated using the 71Q line only, this time using one-way ANOVA to assess for differences between control and active compounds.

## 5.4 Contributions

The work described in this chapter was carried out by Dr. Rhia Ghosh with collaborators in the following areas:

1. For the time-course of HTT inclusion formation, high content image acquisition using the Opera LX microscope and image analysis was carried out with the assistance of Dr. Robin Ketteler, Dr. Christin Luft and Dr. Janos Kriston-Vizi. Subsequently, with the arrival of the newer Opera Phenix microscope, both image acquisition and image analysis were carried out by Dr. Rhia Ghosh for all other high content imaging experiments described.

2. Super-resolution imaging was carried out with the assistance of Dr. Ed Smith (HD Research Group) at the King's Nikon Centre.

3. Proteasomal enhancers (USP14 inhibitors) to test on HTT exon 1 ReNcellVM neurons were supplied by industrial collaborator Proteostasis Therapeutics Inc. (PTI).

## 5.5 Results

### 5.5.1 Establishing a panel of HTT antibodies for protein detection in HTT exon 1 ReNcellVM cells

In order to assess the impact of increasing CAG-repeat length on the behaviour of the HTT exon 1 protein in ReNcellVM cells, it is essential to have reliable methods for protein detection. A number of anti-HTT antibodies are now available, with variable target sites (table 5.1). Many of these are not commercially available and have restricted supply (including S830 and 4C9). The majority are directed towards the N-terminal, and also have been raised in mouse (causing difficulty in co-staining experiments). Some of these antibodies detect mHTT only, in certain instances with some affinity to other polyQ-containing proteins. Others, that do not include the polyQ region in their epitope, do not distinguish between the normal and mutant forms of the protein. As expected, the binding of these antibodies is affected by the specific species or structure of the HTT protein; this must be taken into account when selecting antibodies for specific applications.

| Antibody | Species | Immunogen/epitope |
|---|---|---|
| **S830** | Sheep | N-terminal of HTT aa 1-90, higher affinity for expanded polyglutamine lengths |
| **4C9** | Mouse | N-terminal proline rich region, aa 65-84 |
| **aa1-82 (N82)** | Mouse | N-terminal of HTT, aa 1-82 |
| **MW1** | Mouse | N-terminal polyQ region |
| **3B5H10** | Mouse | N-terminal fragment of 171 amino acids containing 65Q |
| **2B7** | Mouse | N-terminal HTT aa 1-17 |
| **ab109115** | Rabbit | N-terminal HTT aa 1-100 |
| **1H6** | Mouse | N- terminal aa 81-190 |
| **EM48** | Mouse | N-terminal HTT aa 1-256 (without PolyQ) |
| **MAB2166** | Mouse | HTT aa 181-810 |
| **D7F7** | Rabbit | Residues around HTT Pro 1220 |
| **MAB2170** | Mouse | HTT aa 1268-1666 |

**Table 5.1**: Table of HTT antibodies with corresponding presumed epitopes.

#### 5.5.1.1 Western blotting for HTT in HTT exon 1 ReNcellVM cells

Initial Western blotting for HTT exon 1 in the ReNcellVM lines was carried out using the S830 and 4C9 antibodies, and has been described previously. As can be seen from figure 3.23 (chapter 3), the signal for the 29Q HTT exon 1 was considerably fainter than for the 129Q HTT exon 1 line that was confirmed to have matched expression levels by an MSD assay. On many occasions it was not possible to see any signal at all for this product on Western blotting, despite observing a good signal on immunofluorescence studies. Further Western blotting was therefore carried out using a number of different HTT antibodies, in order to determine which recognised particular HTT species in the ReNcellVM lines. NSCs of the matched 29Q and 129Q lines were used, along with a highly expressing 29Q line (29Q-H) which was thawed for this purpose. The results are shown in figure 5.1.

S830 antibody detected the 129Q HTT exon 1 band at around 65 kDa as expected, and a relatively fainter 29Q HTT exon 1 band at 20 kDa. S830 is known to have preferential binding to mutant HTT and displays polyQ dependence, which may explain this finding. 4C9 antibody also detects both 129Q and 29Q exon 1, but the 29Q exon 1 band is again relatively faint. This is surprising as 4C9 antibody binds to the polyproline region on HTT exon 1, and therefore binds both wild-type and mutant HTT; is not known to be polyQ dependent. Western blotting with aa1-82 hardly picked up 29Q HTT exon 1 in the matched expressing line, despite binding to this product on immunofluorescence studies. MW1 and 3B5H10 antibodies, both of which are directed against mutant HTT, were able to detect 129Q HTT exon 1 but not 29Q HTT exon1, and in addition there is much non-specific background visible with MW1. Both D7F7

and 2B7 antibodies gave a good signal for the endogenous full-length HTT protein. 2B7 is directed against the extreme N-terminal of HTT and would be expected to detect both 29Q and 129Q HTT exon 1 equally well, however once again the 29Q HTT exon 1 product was not detected using this antibody. However the same 2B7 antibody was used in the MSD assay in the detection of *all* the HTT exon 1 products.

The lack of signal for the 29Q HTT exon 1 product on Western blotting raises the possibility that this product is being degraded in the cells, however its detection on both immunofluorescence studies and MSD assays rules this out. The Western blotting process involves steps that unfold the protein; therefore the epitope for antibody binding may be affected compared to immunofluorescence techniques that are more likely to preserve the native protein conformation. It is also possible that the 29Q HTT exon 1 protein may not transfer well, or only bind the transfer membrane very weakly, being washed away during the staining and washing steps. The lack of reliable detection of the 29Q HTT exon 1 product on Western blotting precluded this method for making comparisons between lines in the HTT exon 1 panel.

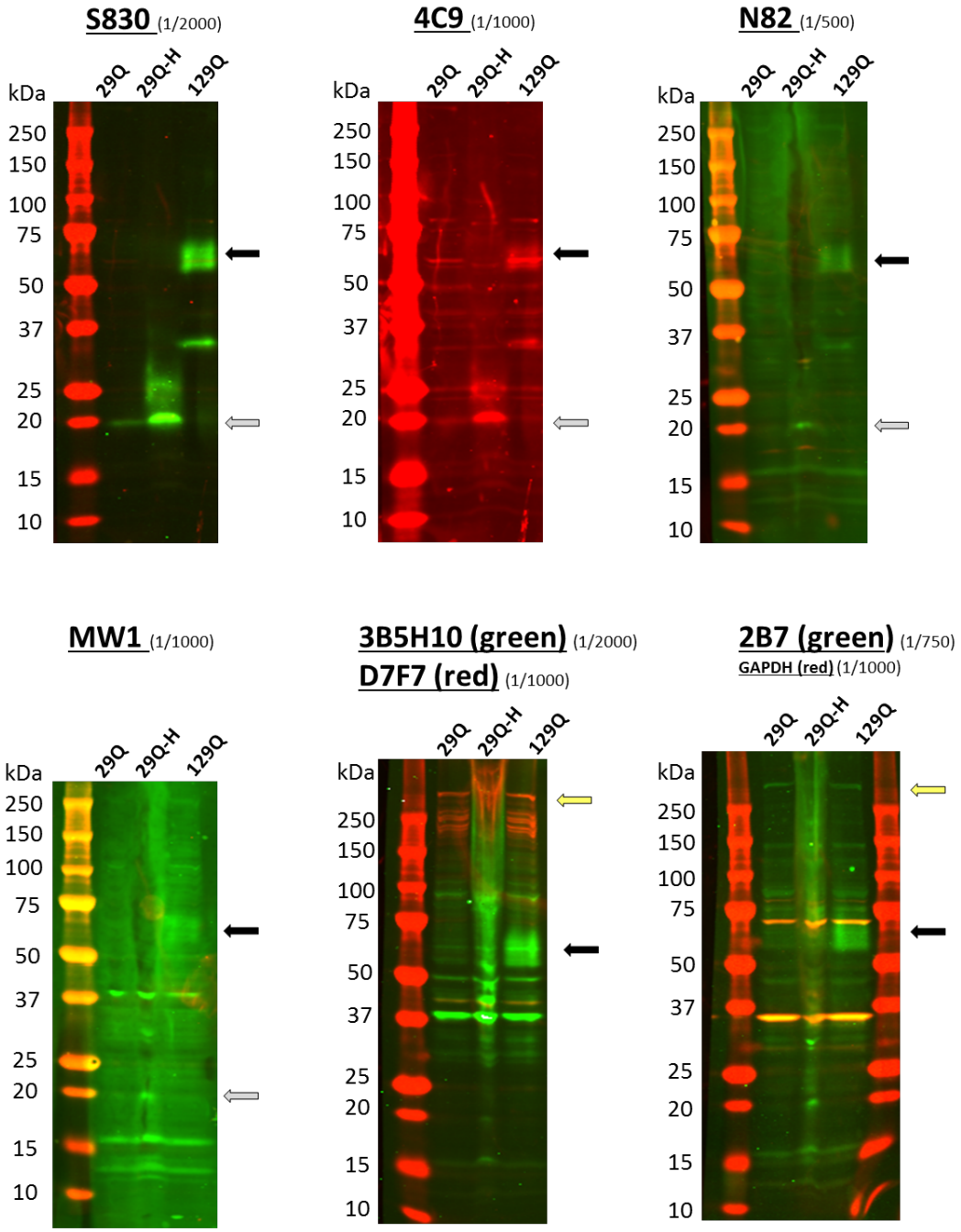


**Figure 5.1: Western blots with panel of HTT antibodies in HTT exon 1 29Q, 29Q-H (high expressor) and 129Q ReNcellVM NSCs.** Black arrow: 129Q exon 1, Grey arrow: 29Q exon 1, Yellow arrow: Full length endogenous HTT

#### 5.5.1.2 Immunofluorescence detection of HTT in HTT exon 1 ReNcellVM cells

A number of HTT antibodies were also tested for the immunofluorescence (IF) detection of HTT exon 1 in these lines, with the results shown below. EM48 is a well-known antibody used for the detection of mHTT inclusions on IF (Carty et al, 2015), and shows the presence of mHTT inclusions in the pathogenic 71Q-H line by day 14 of differentiation (dd14). S830 can also be seen to bind to these aggregates, confirming that they are indeed mHTT inclusion bodies (IBs). In addition, a diffuse cytoplasmic stain is visible with S830 that is not seen in the GFP-only line (figure 5.2). This is likely to be soluble HTT exon 1, not incorporated into inclusions. S830 antibody does not seem to detect wild-type HTT.

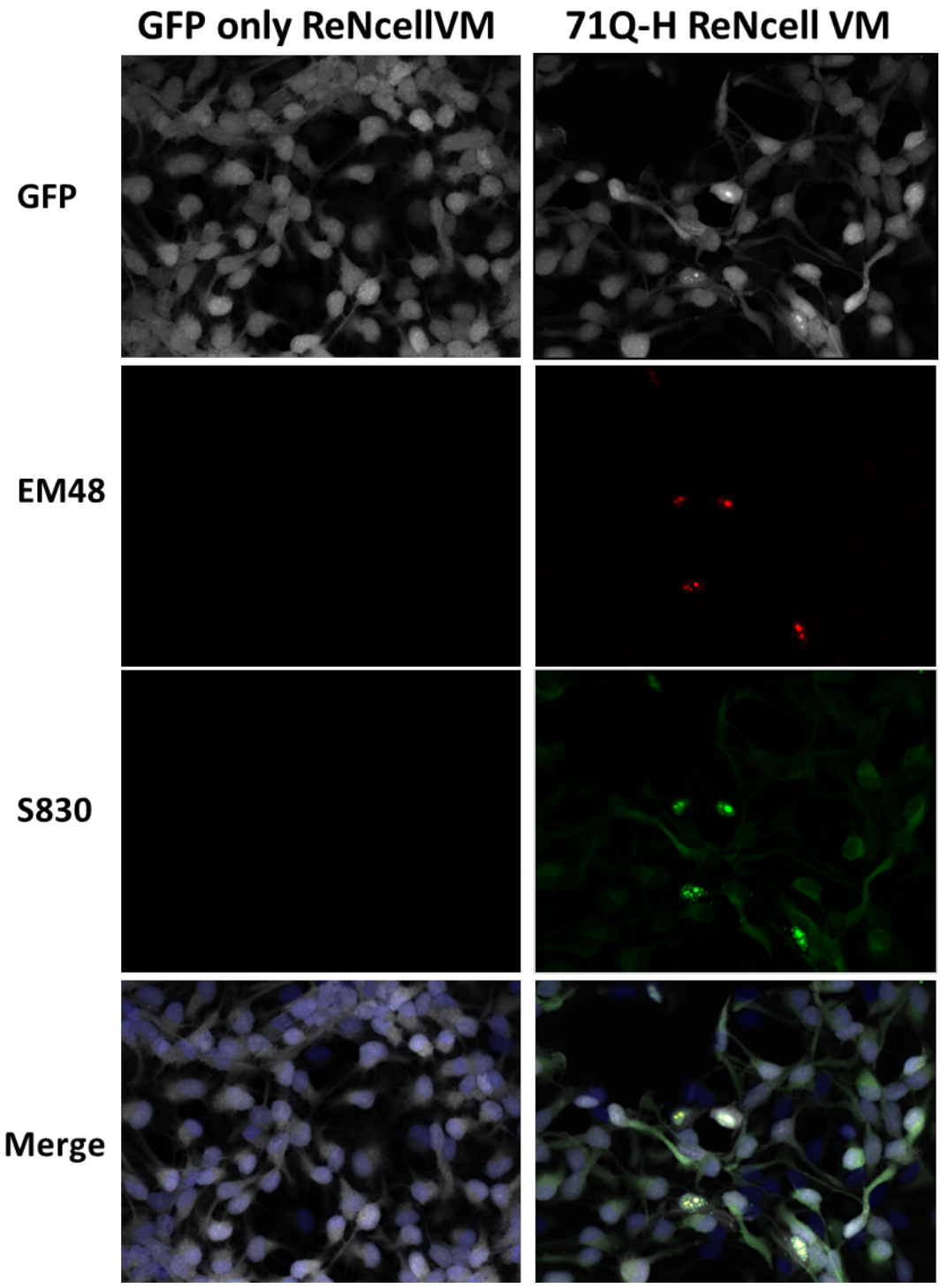


**Figure 5.2: Immunofluorescence co-stain of dd14 GFP only and 71Q-H HTT exon 1 ReNcellVM cells with EM48 and S830 antibody.** Both antibodies are seen to bind to HTT inclusions in the 71Q-H line, and in addition, S830 detects soluble cytoplasmic mHTT exon 1. Green – S830, Red – EM48, White – GFP, Blue - Hoescht.

Different HTT antibodies have the potential to recognise different HTT species, depending on protein conformation. A series of co-stains with S830 antibody was therefore carried out, with findings as follows (figure 5.3):

1. 4C9 antibody displays a similar pattern of staining to S830, however is less sensitive than S830 (when tested on the GFP-only line, 4C9 did not detect to wild-type endogenous HTT.

2. Both MW1 and 3B5H10 stain soluble mutant exon 1 and not aggregates. 3B5H10 is thought to specifically recognise a monomeric species that predicts neurodegeneration, whereas MW1 recognises an extended unfolded PolyQ “linear lattice” (Miller et al, 2011). High levels of non-specific background staining were observed with both these antibodies.

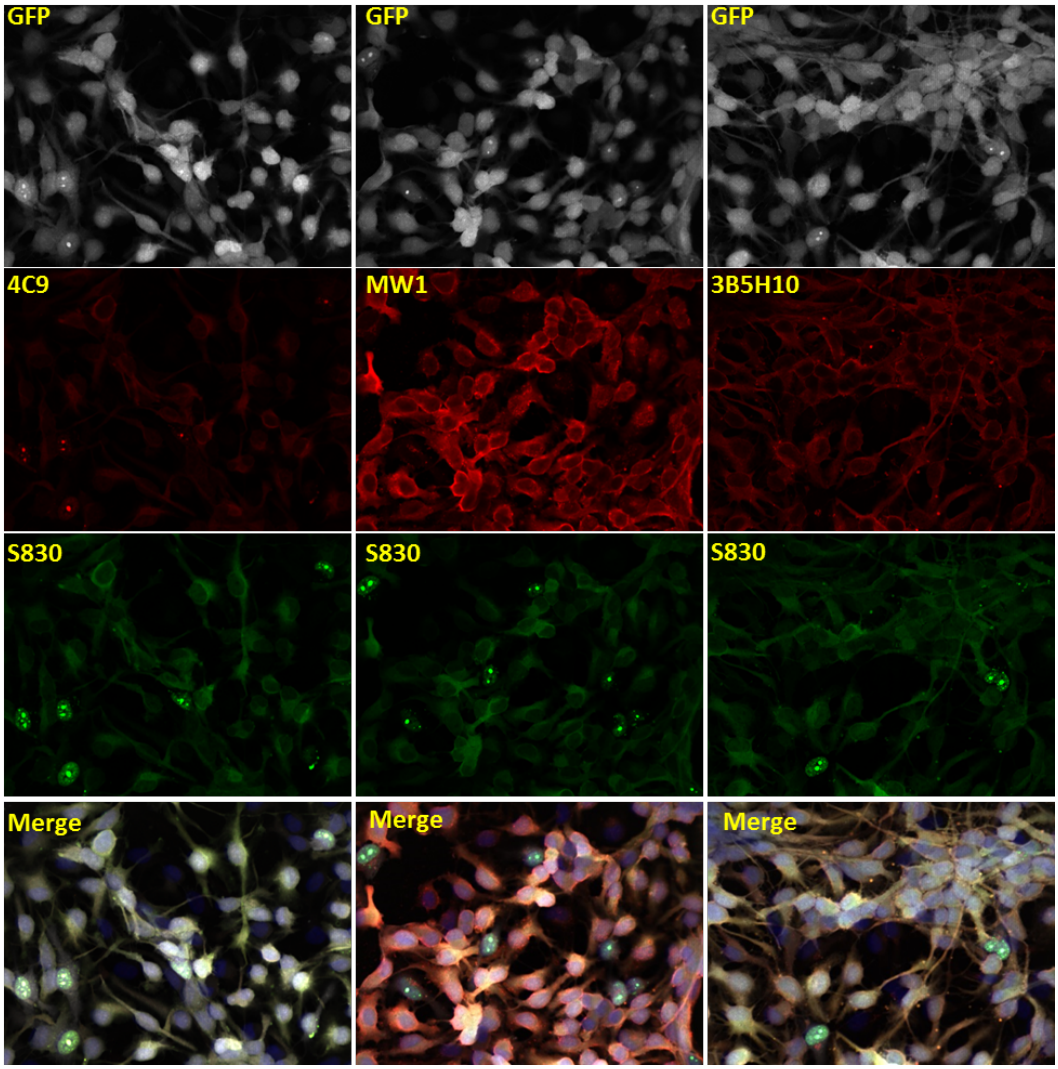


**Figure 5.3: Immunofluorescence co-staining of dd14 HTT exon 1 71Q-H ReNcellVM cells S830 and another HTT antibody as shown** (from left to right 4C9, MW1, 3B5H10). 4C9 displays a similar pattern of staining to S830, but appears less sensitive. Both MW1 and 3B5H10 stain soluble mutant exon 1 and not aggregates. Green – S830, Red – HTT antibody as shown, White – GFP, Blue - Hoescht.

Due to the restricted supply of S830 and 4C9 antibody, the commercially available aa1-82 antibody was also tested (figure 5.4). It also binds to inclusions, though is also less sensitive than S830. Cytoplasmic HTT exon 1 staining also appears to have a more granular appearance.

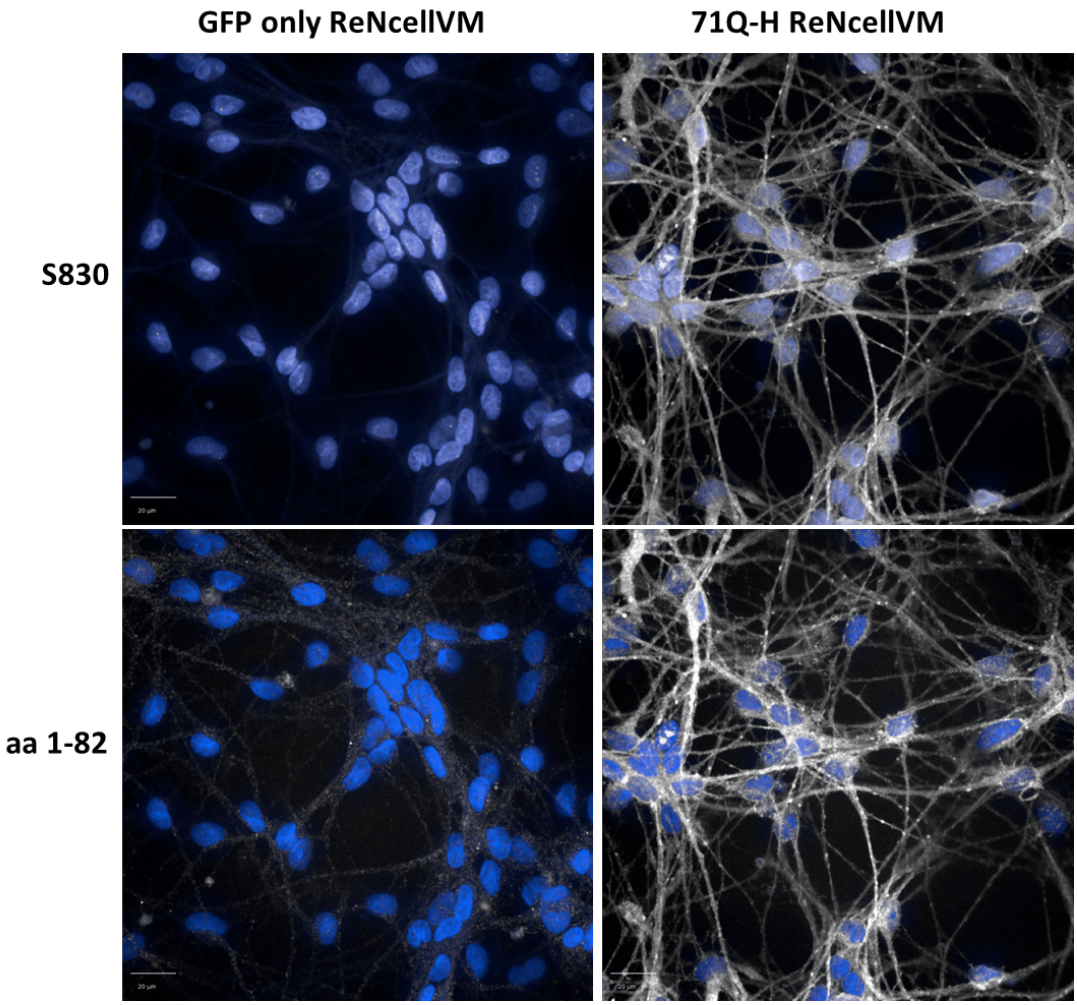


**Figure 5.4: Immunofluorescence co-stain of dd14 GFP only and 71Q-H HTT exon 1 ReNcellVM cells with S830 and aa 1-82 antibody.** aa 1-82 binds to HTT inclusions but is less sensitive than S830 and appears to produce more granular cytoplasmic HTT exon 1 staining. Blue – Hoescht, White – S830 or aa 1-82 as labelled.

The anti-HTT 2170 antibody recognises full length wild-type HTT in the cells and displayed diffuse cytoplasmic staining in both GFP only and 71Q-H lines. It does not bind to HTT exon 1 which lacks this more C-terminal epitope. There was no co-localisation with inclusions, suggesting that the IBs are not binding or sequestering the wild-type protein (figure 5.5). The extremely N-terminal antibody 2B7, which had worked well in detecting full length endogenous HTT on Western blotting, was not effective when used for immunocytochemistry in HTT exon 1 ReNcellVM cells.

Therefore it is possible to specifically detect mHTT inclusion bodies, soluble mutant HTT exon 1 and wild-type HTT in these cells.

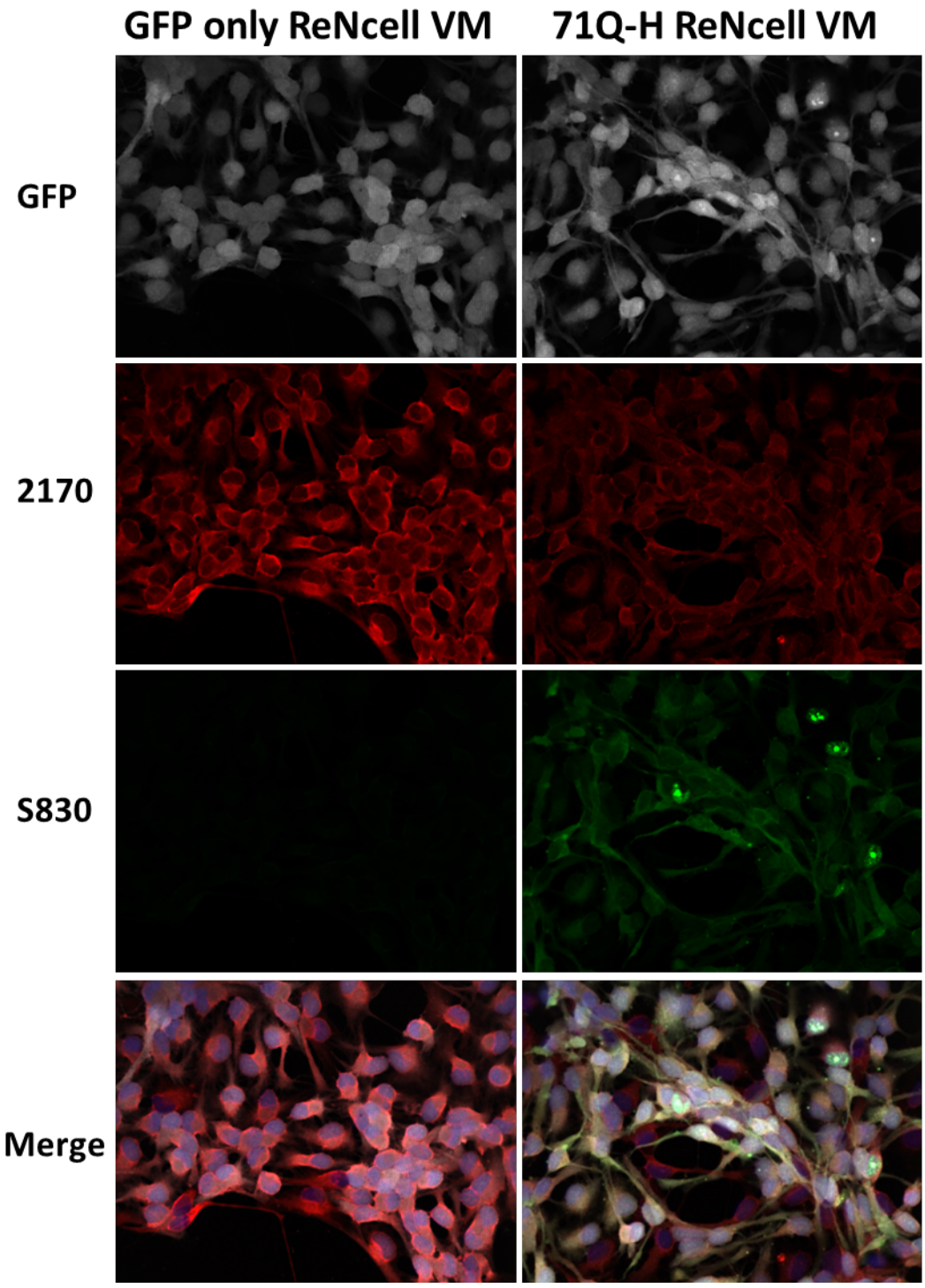


**Figure 5.5: Immunofluorescence co-stain of dd14 GFP only and 71Q-H HTT exon 1 ReNcellVM cells with S830 and 2170 antibody.** 2170 antibody recognises full length wild-type HTT in the cells and displays diffuse cytoplasmic staining in both lines. There is no co-localisation with inclusions. Green – S830, Red – HTT antibody 2170, White – GFP, Blue - Hoescht.

#### 5.5.1.3 Alternative methods for imaging HTT inclusions in HTT exon 1 ReNcellVM cells

Previous studies have reported that HTT inclusions form a heterogenous population, and different species may have different effects within neurons (Caron et al, 2014). In this particular study Thioflavin T (ThioT) was used to demonstrate the existence of at least two inclusion types: fibrillar or globular. ThioT is an amyloid dye which binds to β-sheet structures and fluoresces green (482 nm) on excitation. Following the staining of dd14 HTT exon 1 129Q ReNcellVM cells with S830, ThioT was used as per protocol to visualise any amyloid-like inclusions formed by HTT exon 1. It was hoped that any such structures would fluoresce in the green channel more brightly than the background GFP, in order to allow visualisation. Unfortunately no bright green spot-like structures were seen and ThioT was deemed not to be useful for further experiments in these cells (Figure 5.6). Another fluorescent probe specific for β-sheet structures is NIAD-4, which binds to amyloid-β and displays far-red emission (Woerner et al, 2016). This dye was also tested on these cells, but again did not bind to any HTT inclusions in the cells, as can be seen from the complete lack of any detection in the far red channel (figure 5.6). The lack of binding of both these dyes may indicate that the inclusions formed by mHTT exon 1 in these lines are not amyloid in nature.

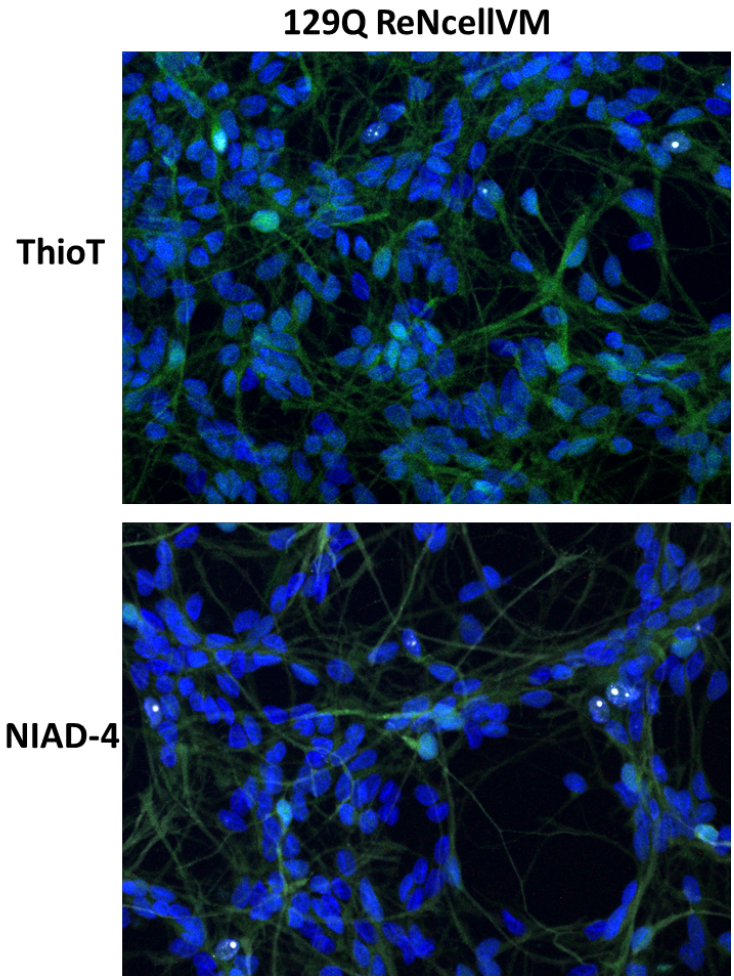


**Figure 5.6: Amyloid staining in dd14 HTT exon 1 129Q ReNcellVM cells.** Neither thioflavin T (top panel) nor NIAD-4 (bottom panel) reveals the presence of amyloid, suggesting that HTT inclusions in ReNcellVM do not contain β-sheet structures. Blue – Hoescht, Green – GFP, White – S830.

### 5.5.2 HTT inclusions in HTT exon 1 ReNcellVM cells

Having tested a range of HTT antibodies, it was decided that S830 was the most suitable to use for further analysis of mHTT inclusion formation; this is due to its sensitivity in detecting mHTT IBs, and also its ability to detect at least one other form of HTT exon 1 (soluble HTT exon 1, corresponding to the diffuse cytoplasmic staining). The full HTT exon 1 ReNcellVM panel was fixed and stained with S830 and B3-tubulin, both in NSC form and at dd14 (figure 5.7). From these representative images it can be observed that NSCs do not contain inclusions, except in the mostly highly pathogenic HTT exon 1 71Q-H ReNcellVM "positive control" line. In addition, upon differentiation IBs form in a small proportion of the matched expressing pathogenic HTT exon 1 (71Q and 129Q) ReNcellVM lines too.

The different patterns of S830 staining in the pathogenic 71Q-H line are shown in Figure 5.8. It is notable that when present inclusions are mostly found within the nucleus, but in some cells a cluster of smaller peri-nuclear inclusions can be seen. Inclusion formation appears to be an "all or nothing" phenomenon; cells either contain a number of intranuclear IBs or none at all. The diffuse cytoplasmic stain is again observed, thought to be soluble HTT exon 1. Cells with intra-nuclear IBs are found to have lower levels of this this diffuse cytoplasmic staining, suggesting that in those cells most HTT exon 1 present has entered the nucleus and been incorporated into inclusions.

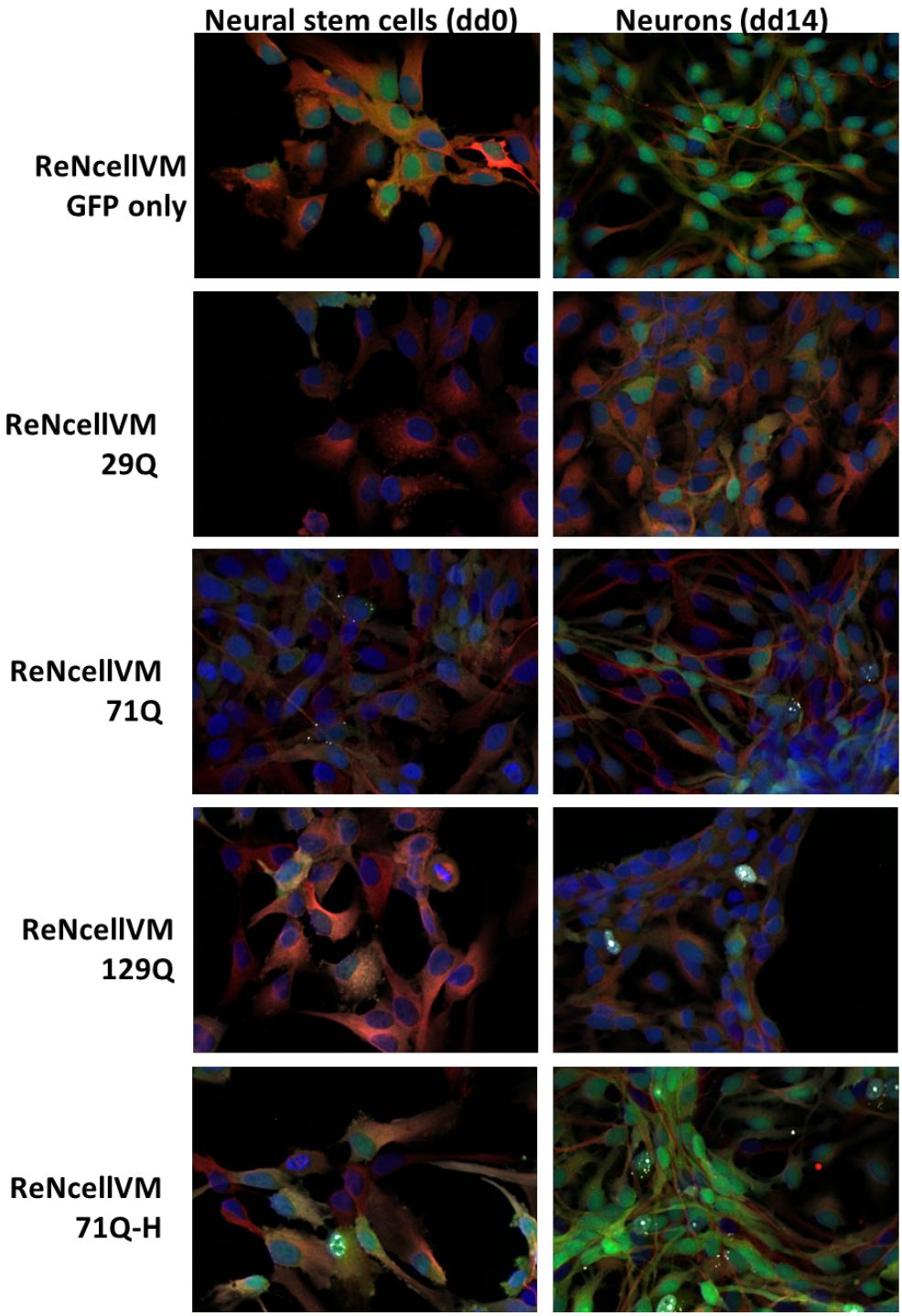


**Figure 5.7: HTT inclusion formation in full HTT exon 1 ReNcellVM panel at dd0 and dd14.** Neural stem cell IBs are only found in the HTT exon 1 71Q-H ReNcellVM cells. In addition, upon differentiation IBs form in a small proportion of HTT exon 1 71Q and 129Q ReNcellVM lines. Blue: Hoescht, Green – GFP, Red – B3-tubulin, White – S830 HTT antibody.

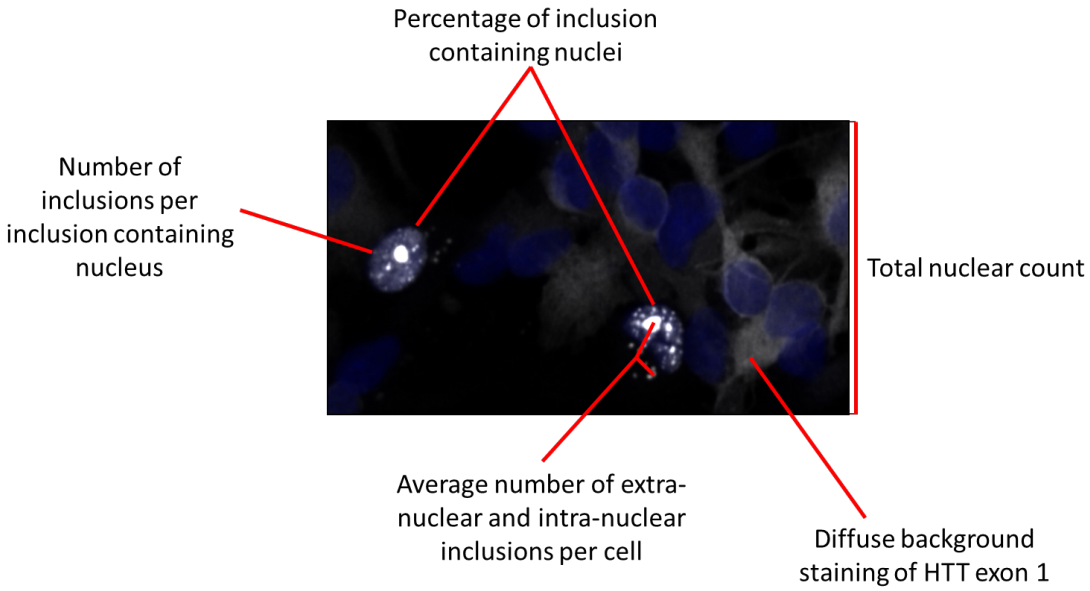


**Figure 5.8: Different patterns of HTT staining in dd14 HTT exon 1 71Q-H ReNcellVM cells labelled with S830 HTT antibody.** Blue: Hoescht, White – S830 HTT antibody.

### 5.5.2.1 Time-course of mHTT inclusion formation

In order to further analyse the formation of mHTT inclusions over time in the HTT exon 1 lines, the full panel was seeded into three 96 well plates and fixed at dd0 (NSC stage), dd7 and dd14 respectively, with 16 wells per cell line (technical replicates). Following staining with S830, plates were imaged on the Opera LX high content imaging microscope. Image analysis was carried out in conjunction with Dr. Janos Kristen-Vizi, using ImageJ and R. Further statistical analysis was carried out using GraphPad Prism software, with results as shown below.

*Intra-nuclear inclusions*

Following differentiation the pathogenic lines (71Q, 129Q and 71Q-H) started to form S830 positive intra-nuclear HTT inclusions (figure 5.9), and by day 7 (dd7) significant CAG-repeat length dependent differences were seen, as neither the matched expressing HTT exon 1 29Q line nor the GFP-only line contain IBs (figure 5.10). In the NSC state, only the 71Q-H line has significant numbers of inclusion containing nuclei (though occasional abnormal nuclei are seen in the 71Q and 129Q lines of the matched panel too) (figure 5.9). The increase in IB containing cells over time in the pathogenic lines is not due to a corresponding drop/death of cells without IBs (figure 5.11). Overall, the percentage of dd14 neurons that contains IBs is low, ranging from 0.5-1.0% in the 71Q and 129Q lines, and increasing to 3.0% in the 71Q-H line. Thus inclusion formation can be found to be proportional to CAG-repeat length and the level of HTT exon 1 expression, as has been found in other studies (Scherzinger et al, 1999).

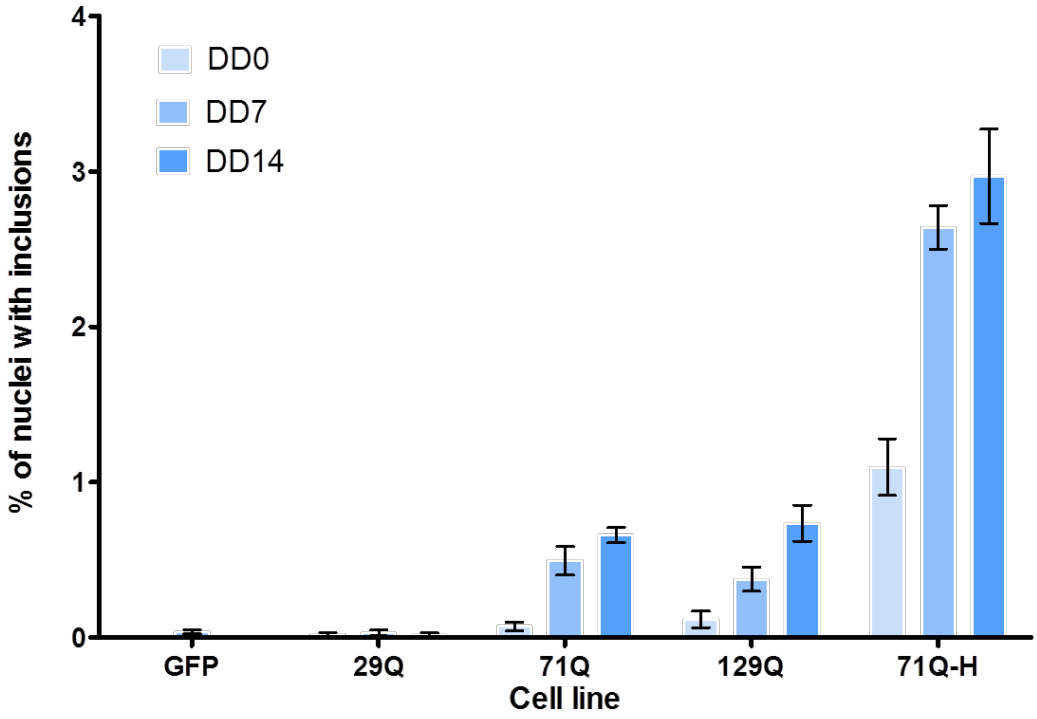


| Two way ANOVA with Bonferroni's correction | | | | | |
|---|---|---|---|---|---|
| DD0 vs DD7 | | DD0 vs DD14 | | DD7 vs DD14 | |
| GFP | ns | GFP | ns | GFP | ns |
| 29Q | ns | 29Q | ns | 29Q | ns |
| 71Q | P<0.05 | 71Q | ns | 71Q | ns |
| 129Q | ns | 129Q | P<0.01 | 129Q | ns |
| 71Q-H | P<0.01 | 71Q-H | P<0.01 | 71Q-H | ns |

**Figure 5.9: Development of nuclear inclusions over time in HTT exon 1 ReNcellVM cells.** The percentage of cells with nuclear IBs increases over time in the pathogenic lines (71Q, 129Q and 71Q-H). Two-way ANOVA with Bonferroni's correction as shown, n=16 per condition.

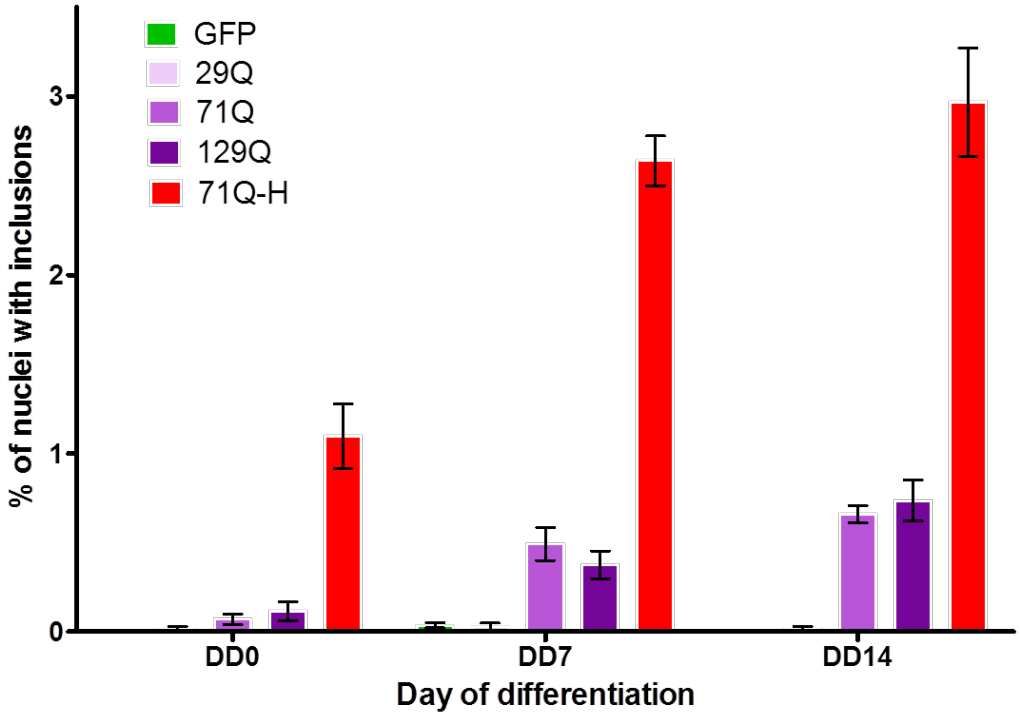


| Two way ANOVA with Bonferroni's correction | | | | | |
|---|---|---|---|---|---|
| GFP vs 71Q | DD7 | P<0.05 | 29Q vs 71Q -H | DD0 | P<0.001 |
| | DD14 | P<0.001 | | DD7 | P<0.001 |
| GFP vs 129Q | DD14 | P<0.001 | | DD14 | P<0.001 |
| GFP vs 71Q-H | DD0 | P<0.001 | 71Q vs 71Q-H | DD0 | P<0.001 |
| | DD7 | P<0.001 | | DD7 | P<0.001 |
| | DD14 | P<0.001 | | DD14 | P<0.001 |
| 29Q vs 71Q | DD7 | P<0.01 | 129Q vs 71Q-H | DD0 | P<0.001 |
| | DD14 | P<0.001 | | DD7 | P<0.001 |
| 29Q vs 129Q | DD14 | P<0.001 | | DD14 | P<0.001 |

**Figure 5.10: Formation of nuclear IBs in HTT exon 1 ReNcellVM cells is CAG-repeat length dependent.** By dd7, differences between lines in the percentage of cells with inclusions appear, with only the 71Q, 129Q and 71Q-H lines developing nuclear IBs. The 71Q-H line forms a significantly higher percentage of nuclear IB containing cells than all other lines. Two-way ANOVA with Bonferroni's correction as shown, n=16 per condition (all other comparisons were not significant).

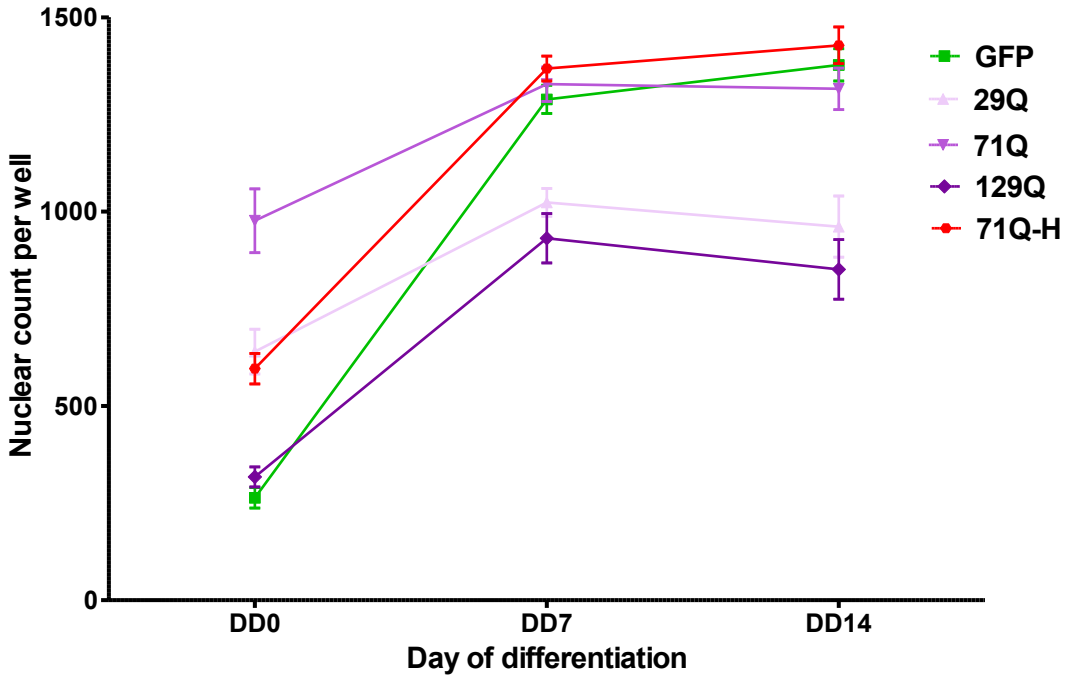


**Figure 5.11: Total nuclear count per well over time in HTT exon 1 ReNcellVM cells.** Two-way ANOVA with Bonferroni's correction confirms no significant difference between DD7 and DD14 in any cell line (n=16 per condition).

The number of inclusions per inclusion-containing nucleus is also higher in the positive control 71Q-H line compared to both the other pathogenic lines, with a trend towards increased number in the 129Q compared to the matched 71Q line (though this did not reach significance) (figure 5.12). This measurement also significantly increased over time in the 71Q and 129Q lines, but not in the positive control line (figure 5.13).

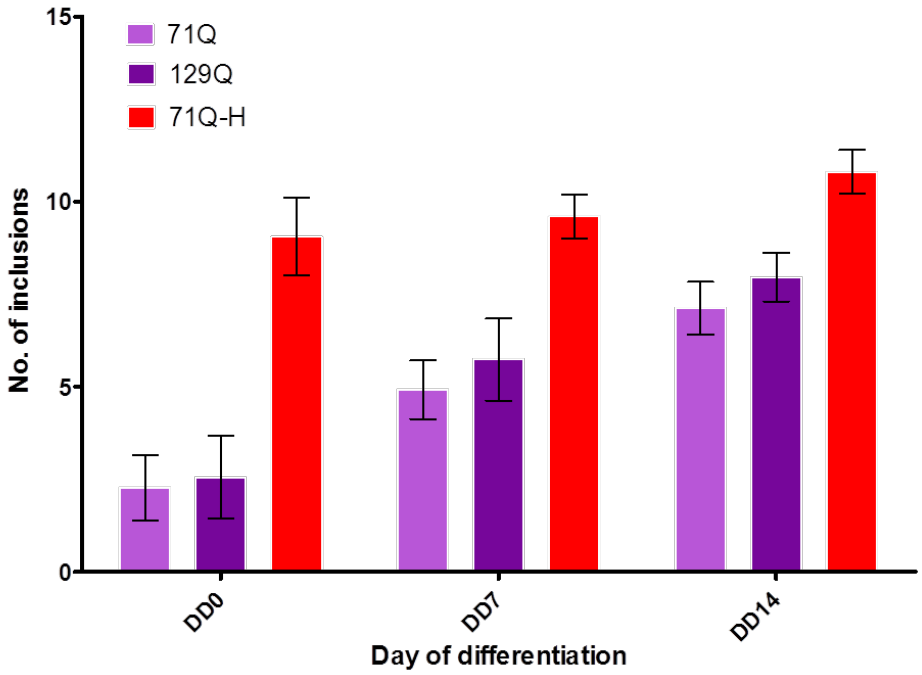


| Two way ANOVA with Bonferroni's correction | | |
|---|---|---|
| 71Q vs 129Q | DD0 | ns |
| | DD7 | ns |
| | DD14 | ns |
| 71Q vs 71Q-H | DD0 | P<0.001 |
| | DD7 | P<0.001 |
| | DD14 | P<0.01 |
| 129Q vs 71Q-H | DD0 | P<0.001 |
| | DD7 | P<0.01 |
| | DD14 | ns |

**Figure 5.12: Number of IBs per inclusion containing nucleus** in pathogenic HTT exon 1 ReNcellVM lines is highest in the 71Q-H line, which has the highest concentration of mHTT exon 1. The increasing trend between 71Q and 129Q lines is not statistically significant. Two-way ANOVA with Bonferroni's correction as shown, n=16 per condition.

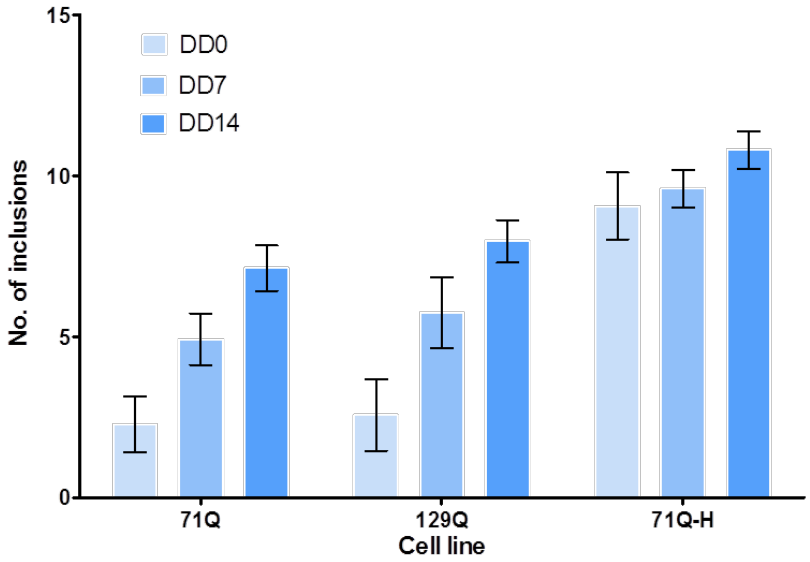


| Two way ANOVA with Bonferroni's correction | | |
|---|---|---|
| DD0 vs DD7 | 71Q | ns |
| | 129Q | P<0.05 |
| | 71Q-H | ns |
| DD0 vs DD14 | 71Q | P<0.001 |
| | 129Q | P<0.001 |
| | 71Q-H | ns |
| DD7 vs DD14 | 71Q | ns |
| | 129Q | ns |
| | 71Q-H | ns |

**Figure 5.13: Number of IBs per inclusion containing nucleus increases over time in the pathogenic HTT exon 1 ReNcellVM lines**, although this measure does not reach statistical significance in the 71Q-H line. Two-way ANOVA with Bonferroni's correction as shown, n=16 per condition.

*Peri-nuclear inclusions*

In line with the increase in intra-nuclear IBs on differentiation, the number of peri-nuclear inclusions decreases in the two most pathogenic lines (129Q and 71Q-H) (figure 5.14). However this has not been found in the 71Q line, and this result may be affected by the difficulty in setting up accurate spot counting algorithms for peri-nuclear inclusions on ImageJ, as generally the peri-nuclear inclusions have a much smaller area than intra-nuclear inclusions and counts can be spuriously increased by non-specific background staining artifact.

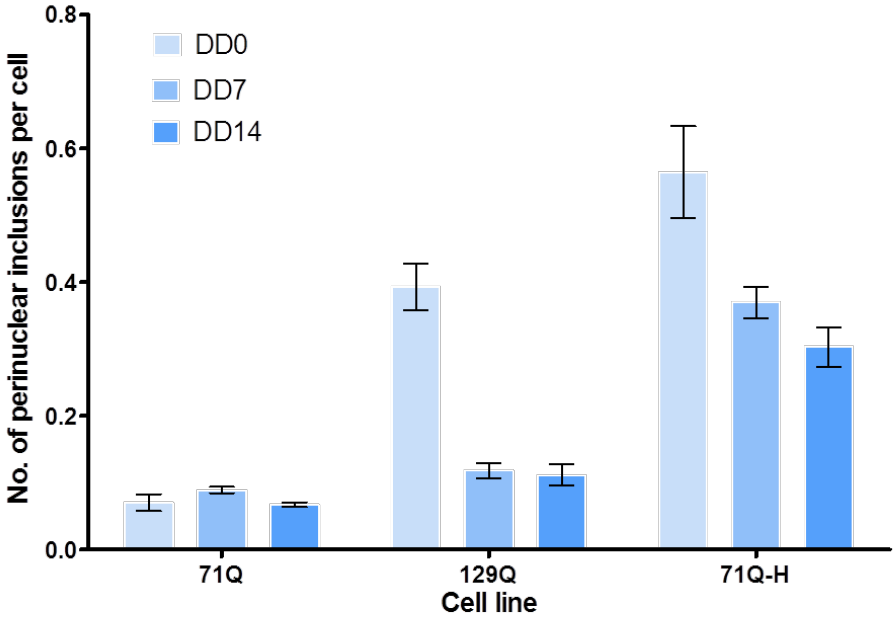


| Two way ANOVA with Bonferroni's correction | | | | | |
|---|---|---|---|---|---|
| DD0 vs DD7 | | DD0 vs DD14 | | DD7 vs DD14 | |
| 71Q | ns | 71Q | ns | 71Q | ns |
| 129Q | P<0.001 | 129Q | P<0.001 | 129Q | ns |
| 71Q-H | P<0.001 | 71Q-H | P<0.001 | 71Q-H | ns |

**Figure 5.14: The number of perinuclear inclusions decreases over time in the two most pathogenic 71Q-H and 129Q HTT exon 1 ReNcellVM lines**, however this has not been found in the 71Q line. Two-way ANOVA with Bonferroni's correction as shown, n=16 per condition.

*Soluble HTT exon 1*

Diffuse cytoplasmic S830 staining (thought to represent soluble HTT exon 1) increases over time, particularly in the pathogenic lines (Figure 5.15). Again, this was found to be less prominent, or absent, in cells which have inclusion containing nuclei.

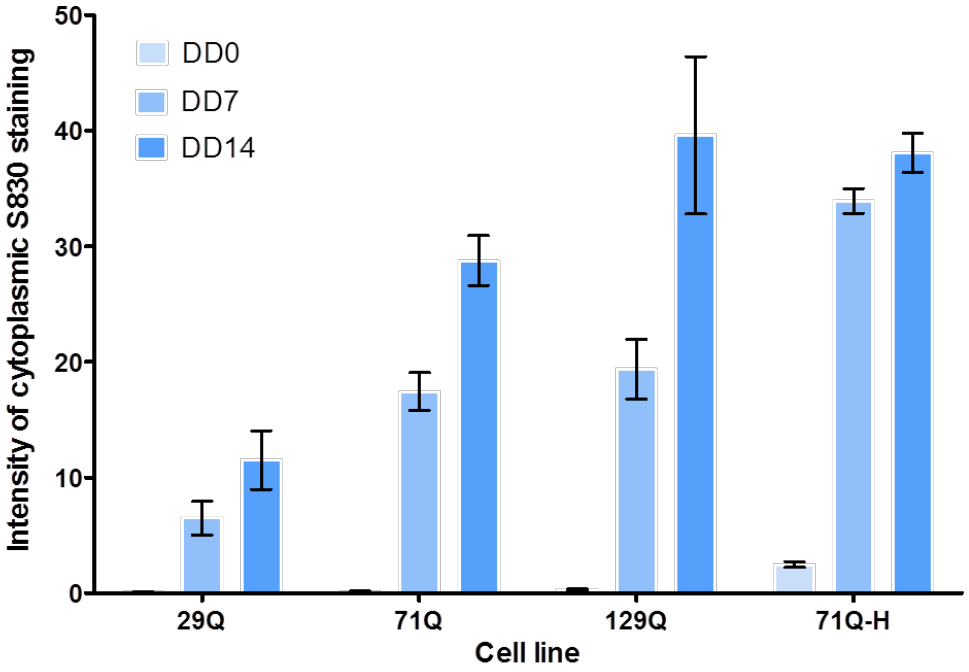


| Two way ANOVA with Bonferroni's correction | | | | | |
|---|---|---|---|---|---|
| DD0 vs DD7 | | DD0 vs DD14 | | DD7 vs DD14 | |
| 29Q | ns | 29Q | P<0.01 | 29Q | ns |
| 71Q | P<0.001 | 71Q | P<0.001 | 71Q | P<0.01 |
| 129Q | P<0.001 | 129Q | P<0.001 | 129Q | P<0.001 |
| 71Q-H | P<0.001 | 71Q-H | P<0.001 | 71Q-H | ns |

**Figure 5.15: Cytoplasmic soluble HTT exon 1 increases over time in the HTT exon 1 ReNcellVM cells**, particularly in the pathogenic 71Q, 129Q and 71Q-H lines. Soluble HTT exon 1 is thought to correspond to diffuse cytoplasmic staining of S830 antibody, which is not present in the GFP only line. Two-way ANOVA with Bonferroni's correction as shown, n=16 per condition.

### 5.5.2.2 The effect of mHTT inclusions on neurons

As mentioned, the overall proportion of cells containing mHTT inclusions was low, even in the 71Q-H line. Therefore it was not possible to ascertain their effect globally on the neuronal culture. However, it could be seen on immunofluorescence that cells containing nuclear IBs often had reduced expression of cell type markers and abnormal morphology, with a more rounded cellular appearance compared to the surrounding neuronal culture (figure 5.16). This finding was supported by high content image analysis (Columbus) which revealed that the intensity of B3-tubulin staining in the pathogenic lines was significantly reduced in nuclear IB containing cells compared to cells without nuclear IBs (two-tailed t-test, $p<0.05$).

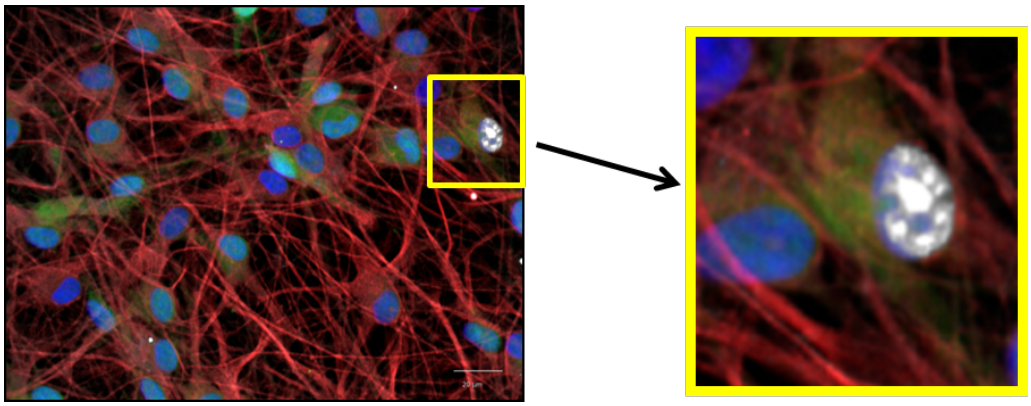

**Figure 5.16: Cells with nuclear inclusions have reduced expression of cell markers** as shown by immunocytochemistry of dd14 129Q ReNcellVM cells. A more rounded cell morphology is also observed.
White – S830 antibody; Red – B3-tubulin; Green – GFP; Blue - Hoescht

It was difficult to co-stain with S830 and markers of cell toxicity, due to the GFP expression blocking the 488 nm channel in these lines. HTT is intracellular and therefore it is necessary to permeabilise cells post-fixing in order to expose antigens for HTT-antibody binding. The permeabilisation procedure caused any cell viability markers added to live cells (such as propidium iodide), to leach out. However, it can be seen from figure 5.17 that there was no obvious effect of nuclear IB formation on Hoescht staining, in terms of abnormal nuclear morphology or formation of apoptotic bodies. This was confirmed using anti-activated caspase 3 staining, which was not present in untreated/unstressed cells with nuclear inclusions.

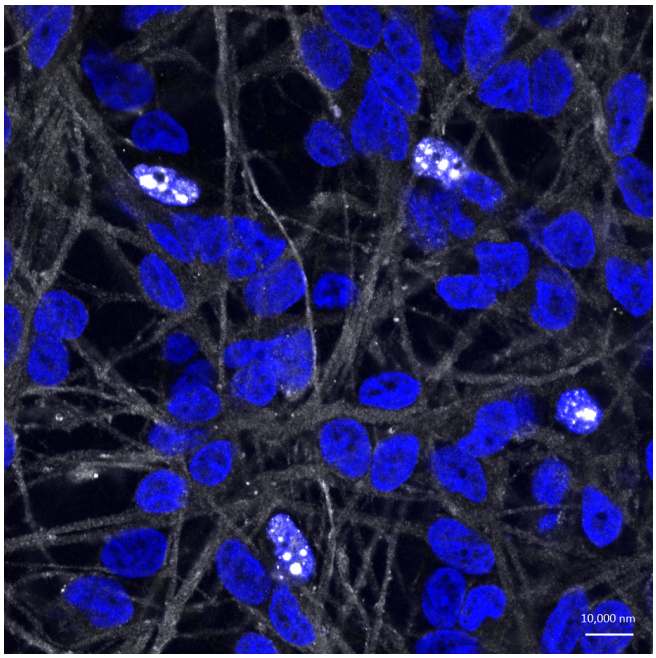


**Figure 5.17: Nuclei containing inclusion bodies have normal morphology** as demonstrated in dd21 HTT exon 1 71Q-H ReNcellVM cells at x60 magnification. Blue – Hoescht, White – S830.

However high content image analysis (Columbus) with measurement of nuclear area revealed that nuclei with inclusions are slightly bigger than those without (figure 5.18).

This may be simply the spatial effect of the inclusions themselves, or may be due to an osmotic effect, drawing water into the nuclei and expanding their size. This in turn may lead to impaired nuclear functioning, including transcriptional dysregulation that is known to occur in HD.

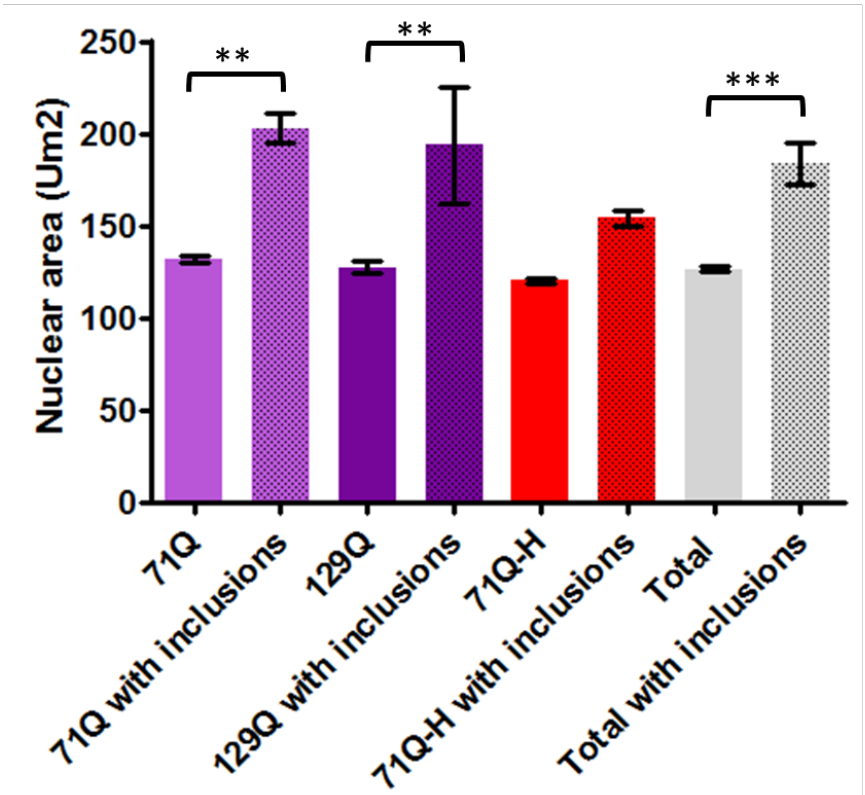


**Figure 5.18: Nuclear area in pathogenic HTT exon 1 ReNcellVM lines.** Columbus analysis of nuclear size in dd14 71Q, 129Q, 71Q-H stained with Hoesht and anti-HTT S830 antibody revealed significantly increased size of nuclei containing inclusion bodies.

One-way ANOVA with Bonferroni correction. **=p<0.01, ***=p<0.001. n=16 per cell line (with and without inclusions)

### 5.5.3 Super-resolution imaging of HTT exon 1 ReNcellVM lines

In order to examine the nuclear inclusions in more detail, and to further ascertain the nature of the diffuse cytoplasmic staining, super-resolution imaging of the HTT exon 1 ReNcellVM lines was carried out. Cells were differentiated on specific glass plates (0.17mm thickness) for imaging, fixed and stained using S830. Imaging was carried out with Dr. Ed Smith at the King's Nikon Centre, using the N-SIM Super Resolution System with corresponding N-SIM software. This achieves resolution of 100-120 nm and the results are shown in figure 5.19.

These images reveal smaller intra-nuclear inclusions not previously seen on standard confocal microscopy, and a range of IB size is observed. This is consistent with a previous super-resolution study which suggests that IBs increase in size over time with the addition of more huntingtin monomers, and a range of sizes are therefore present at the same time (Duim et al, 2014). The all-or-nothing nature of inclusion formation is again highlighted, with the majority of nuclei completely clear, but affected nuclei full of inclusions. The cytoplasmic diffuse S830 is still seen in all lines except for the GFP only line, and therefore likely corresponds to soluble HTT exon 1. This is confirmed to be absent in cells with nuclear IBs.

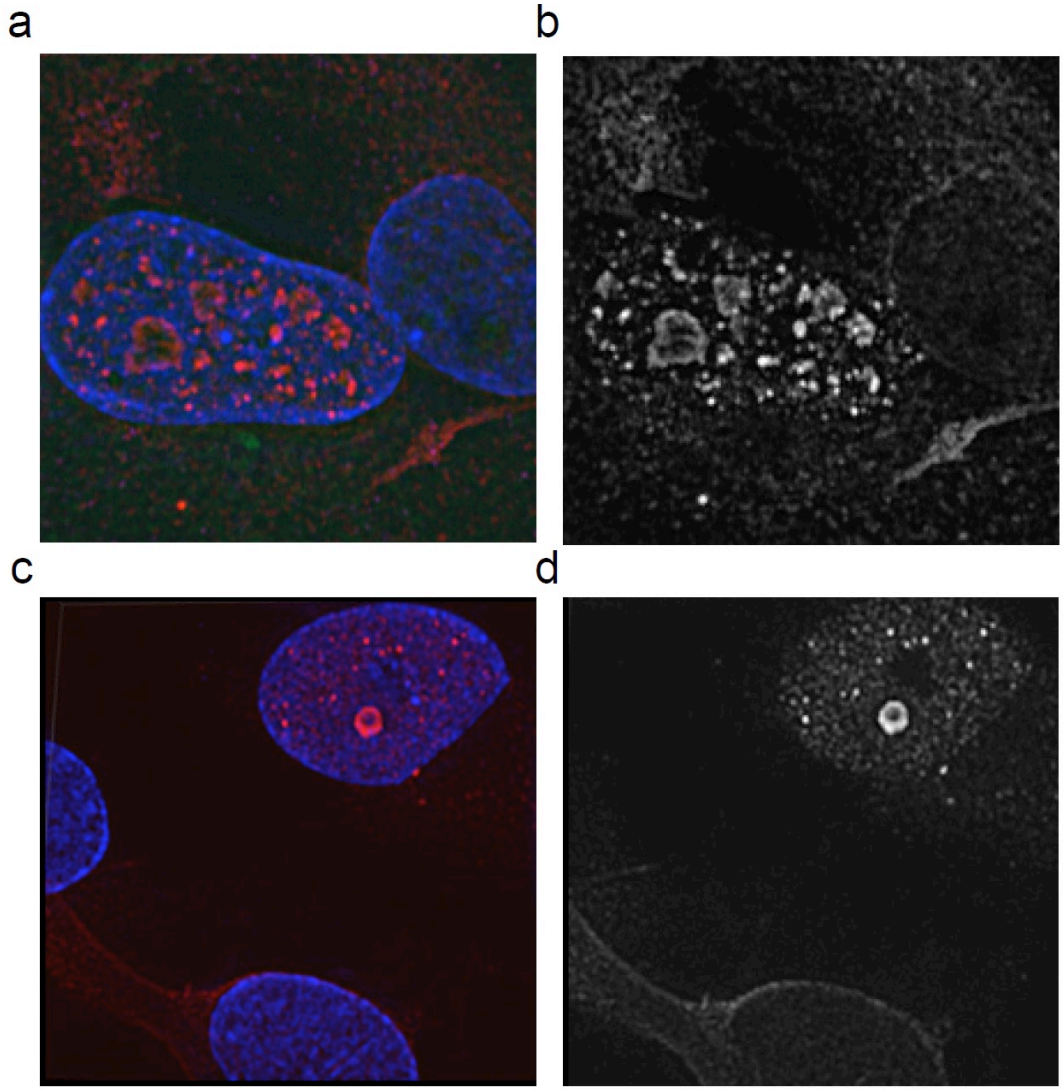


**Figure 5.19: Structured illumination microscopy images of dd21 HTT exon 1 71Q-H ReNcellVM.** (a,b) Multiple smaller nuclear inclusions not previously appreciated with standard confocal microscopy can be seen. (c,d) Cytoplasmic HTT staining is less prominent in cells with nuclear inclusions.

Blue - Hoescht; Red - S830; White - S830. Scale: Width 31.94 µm, Height 31.94 µm, Depth 5.00 µm

### 5.5.4 Effect of proteostasis modulators on mHTT in ReNcellVM lines

#### 5.5.4.1 Effect of MG132 and Bafilomycin on distribution of HTT exon 1

The panel of HTT exon 1 cells was seeded onto 96 well plates for imaging, and after 14 days of differentiation, cells were treated with 200 μM MG132, 1 μM bafilomycin or DMSO control for 24 hours with 8 wells (technical replicates) tested per line for each treatment. Due to the restricted supply of S830 antibody, plates were fixed and stained with HTT antibody aa1-82, imaged on the Opera Phenix and analysed using Columbus software. Example images from these plates are shown in figure 4.24 (chapter 4), with further images of the 129Q line shown below (figure 5.20).

It is clear that MG132 and bafilomycin both alter the distribution of HTT in the 129Q cells. As expected, the effect of autophagy inhibition with bafilomycin serves to increase the amount of mHTT in the neurons, with higher levels of aa1-82 staining observed both in the nucleus and axons. However proteasomal inhibition with MG132 appears to cause increased HTT levels in the nuclear and perinuclear regions of only a few cells, with very little HTT observed in axons.

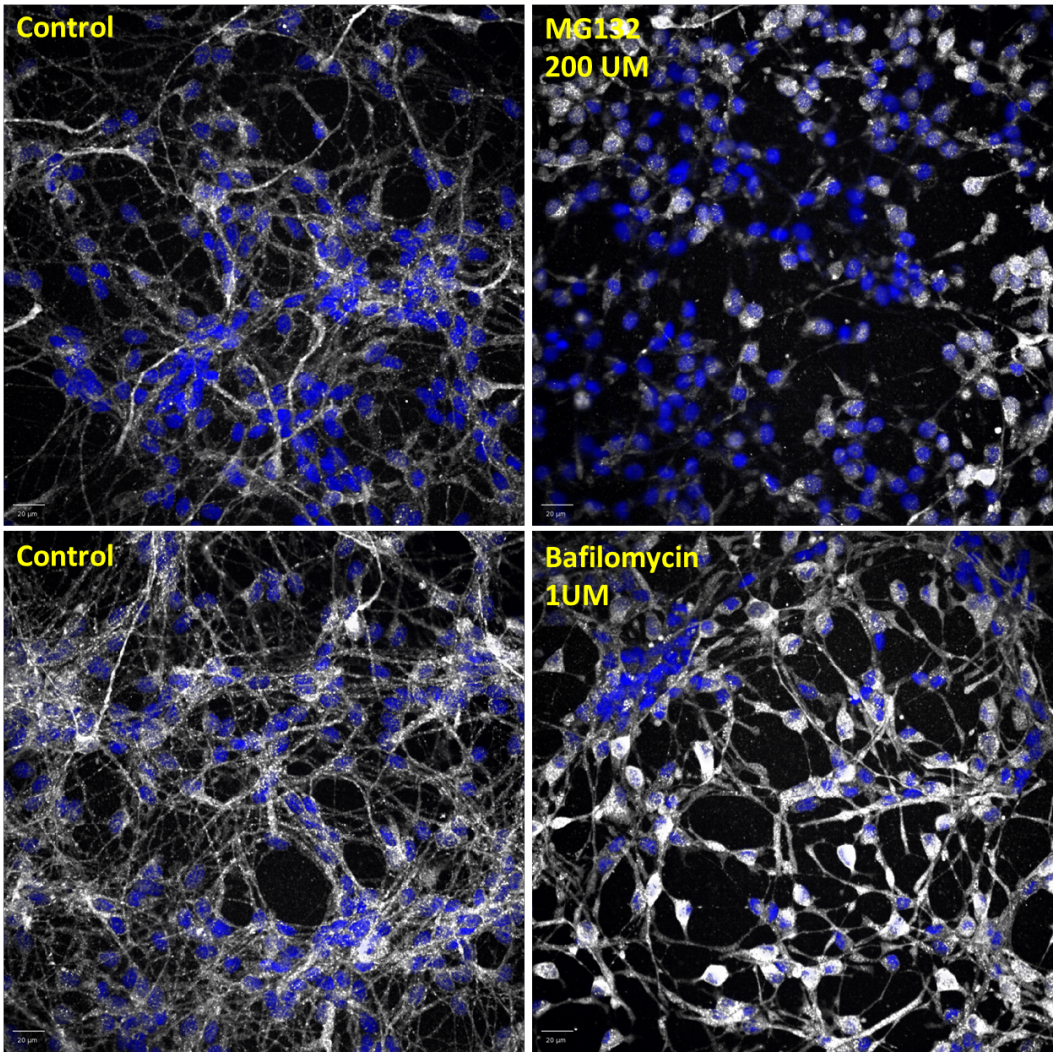


**Figure 5.20: Distribution of mHTT exon 1 following treatment with MG132 and bafilomycin** in dd14 HTT exon 1 129Q ReNcellVM cells.

Blue – Hoescht, White – aa1-82 antibody.

Quantification of HTT staining using Columbus proved difficult. The plates displayed enormous variability in cell number between different fields of view (fov), even within the same well. This is due to the “honeycomb” effect mentioned previously. Many fields of view had no cells at all. Therefore when calculating the measure of aa1-82 staining intensity by dividing the overall intensity per fov by the nuclear count (for normalisation), the zero value divisor led to an infinite error result. This was discussed with engineers from Perkin Elmer, in order to find a way of excluding such fields of view from the analysis. However, ultimately the software was not able to perform this function. An alternative method of aa1-82 staining analysis was suggested, by creating a nuclear mask around each nucleus and measuring the average (mean) intensity in this area. This method was used to quantify the treatment effect of MG132 and bafilomycin in the cells, with results as shown in figure 5.21. Baseline levels of HTT in the GFP only line appear to be much higher than expected and are not as high as expected in the 71Q-H line. This is likely to be because the quantification method used misses the aa1-82 staining in the axons. However, within line comparisons of the treatment effect show that MG132 does not significantly alter the total levels of HTT within the cell, whereas bafilomycin does lead to a significant increase in all lines.

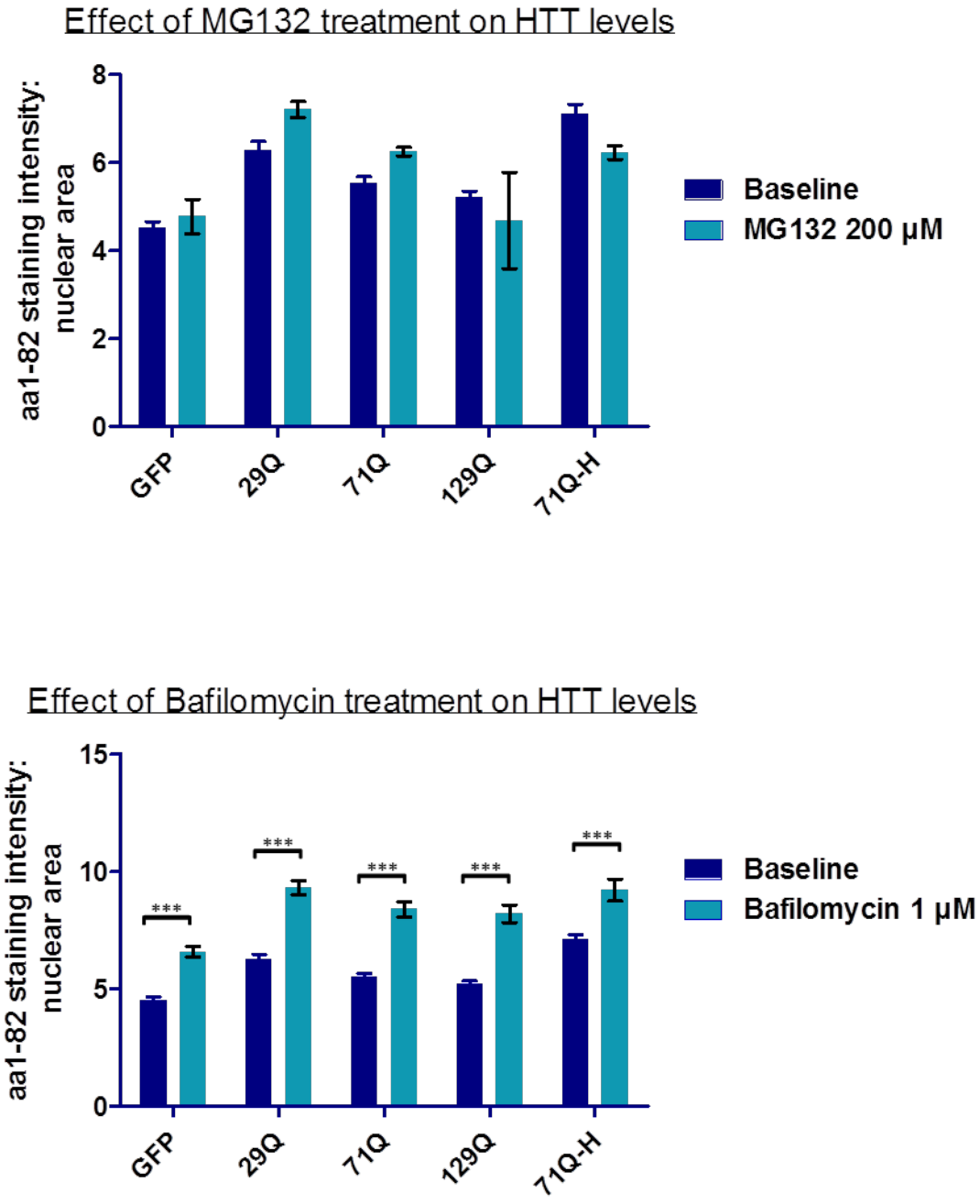


**Figure 5.21: Quantification of total HTT staining in the HTT exon 1 ReNcellVM lines following administration of proteasomal inhibitor MG132 and autophagy inhibitor bafilomycin** was carried out using Columbus software. Treatment with MG132 (top panel) has no significant effect on the total levels of HTT; Two-way ANOVA with Bonferroni's correction. Treatment with Bafilomycin (bottom panel) significantly increases total HTT levels in all lines; Two-way ANOVA with Bonferroni's correction (***=p<0.001), n=8 per condition.

### 5.5.4.2 mHTT exon 1 clearance by proteasomal activators

Upregulation of the UPS is an attractive therapeutic option in HD. In a collaboration with Proteostasis Therapeutics Inc (PTI), a number of USP14 inhibitors were tested for their ability to clear HTT exon 1 from ReNcellVM neurons. PTI supplied five active compounds and one scrambled control, which was initially blinded to us. On receipt, the compounds were reconstituted in DMSO to achieve a final concentration of 5 mM. Following guidance from PTI, final doses of 1 μM, 3 μM and 10 μM were tested for each compound.

Initially as a preliminary experiment only the 129Q line was tested; cells were differentiated in 6-well plates to dd14, followed by the addition of test compounds for 48 hours. Cells were then harvested and samples prepared for Western blotting with measurement of total protein levels. Twenty micrograms of total protein was loaded per lane and blotting was carried out for HTT exon 1 (using aa1-82 antibody) and actin as a loading control. The membrane was then stripped and reprobed with HTT antibody 4C9 and PSMb5 (a subunit of the 20S proteasome complex) as loading control. Results are shown in figure 5.22 below.

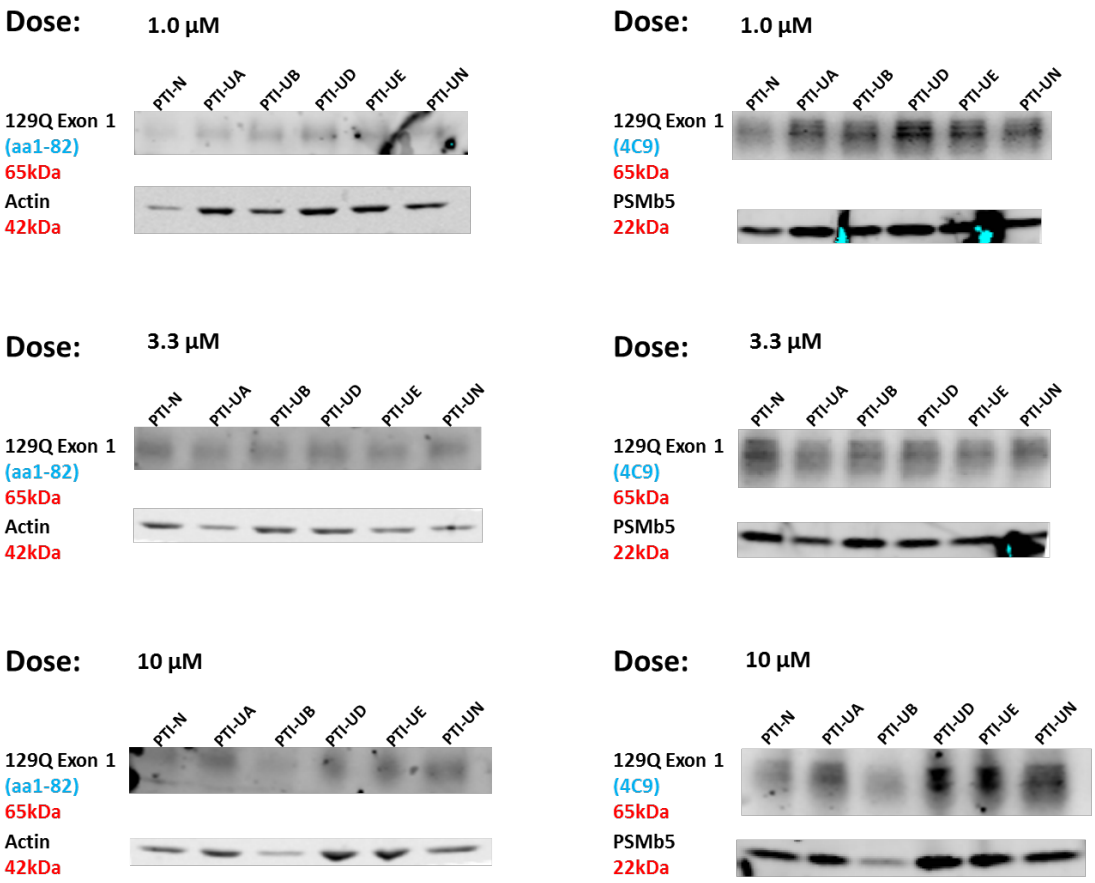


**Figure 5.22: Western blotting of dd14 HTT exon 1 129Q ReNcellVM cells following treatment with PTI compounds at doses as shown.** Detection of HTT exon 1 was carried out using HTT antibody aa1-82 (left), and 4C9 (right). A comparison of actin loading control (left) and the 20S proteasome subunit PSMb5 (right) is also shown.

Densitometry was carried out and aa1-82:4C9 ratio was normalised to compound PTI-N (as instructed by collaborators PTI). The same procedure was carried out for 4C9:PSMb5 ratio, but with some missing data due to the reduced quality of the re-probed membrane. However from comparing these preliminary results at the 10 µM dose it can be seen that both methods give rise to similar findings (figure 5.23).

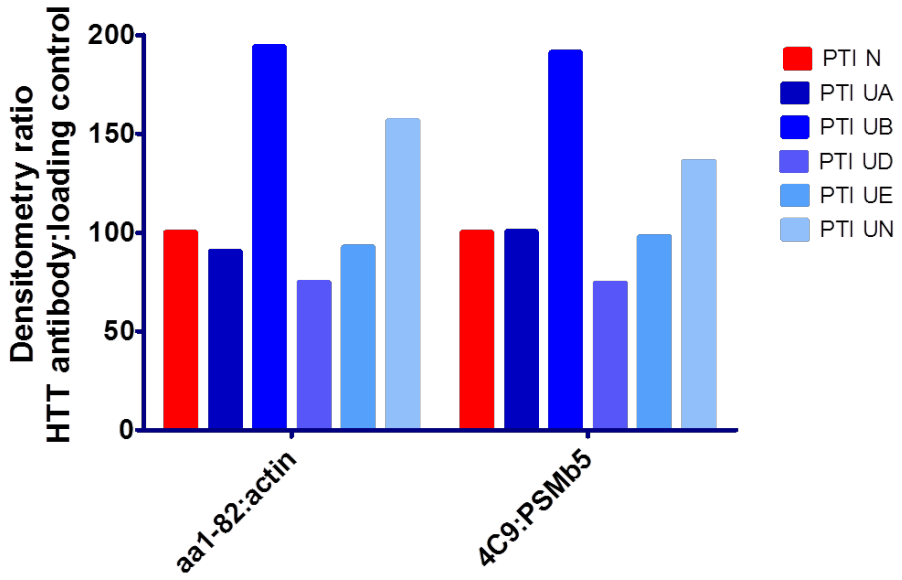


**Figure 5.23: Densitometry of bands at 10 µM PTI compound dose** from Western blots shown in Figure 5.22. This preliminary experiment shows that both methods using anti-HTT aa1-82 and 4C9 antibody give rise to similar results.

It was therefore decided to carry out a full experiment testing all compounds and doses on 71Q, 129Q and 71Q-H lines at dd14 (figure 5.24). Densitometry of bands in shown in figure 5.25, with results normalised to PTI-UB which was revealed by PTI to be the control scrambled compound.

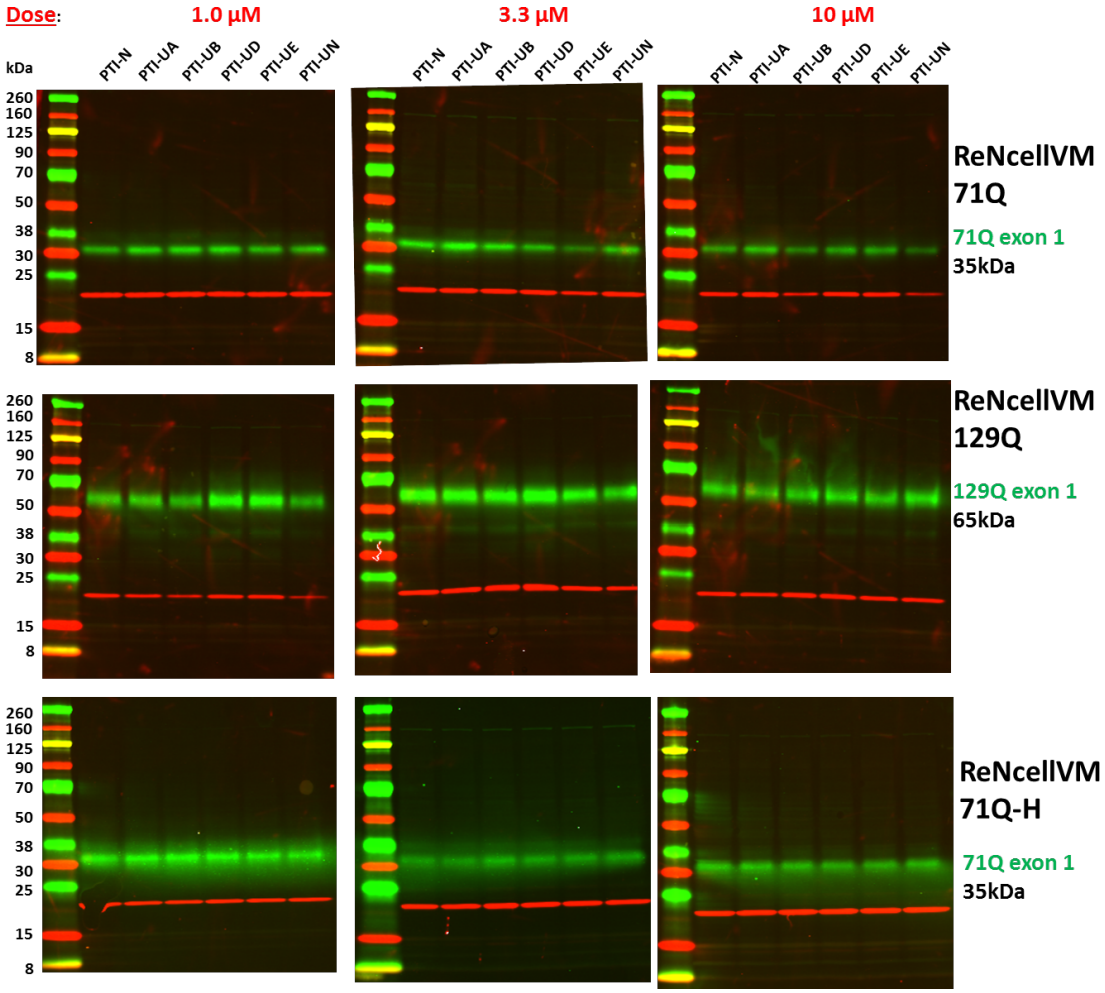


**Figure 5.24:** Western blots of HTT exon 1 detected by 4C9 antibody (green), and PSMb5 (red) across the three pathogenic HTT exon 1 ReNcellVM lines (71Q, 129Q, 71Q-H) following 48 hours of treatment with PTI compounds as doses shown above.

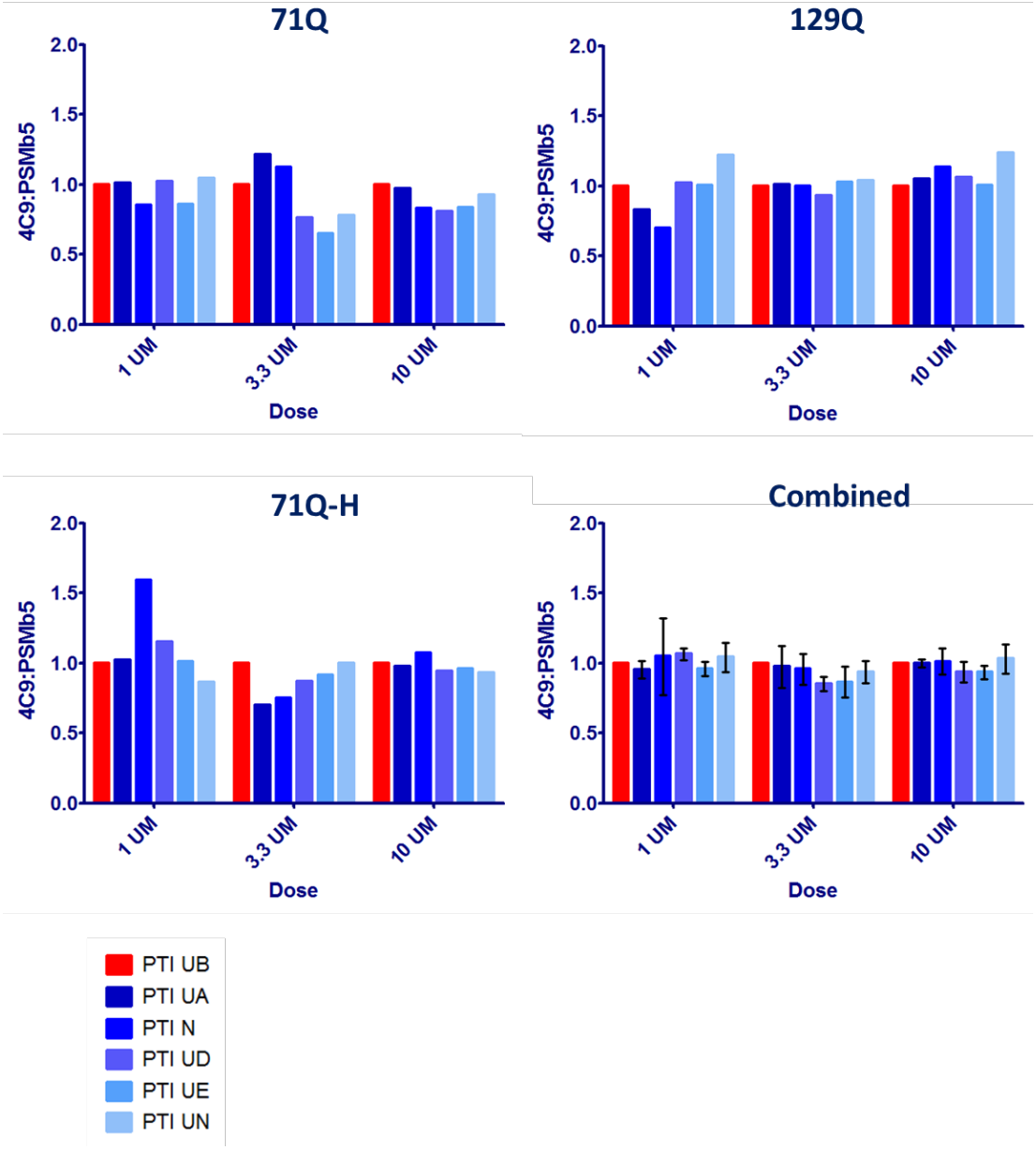


**Figure 5.25**: Densitometry results of Western blots shown in Figure 5.24, normalised to PTI-UB control. Bottom right panel shows combined results (mean+SEM) of all three pathogenic lines. Two-way ANOVA with Bonferroni's correction shows no significant difference between the compounds at any of the doses tested.

These results were discussed with the PTI scientific team, who were hopeful that in the 71Q line there had been a lowering of 71Q exon 1 with their newer USP14 inhibitors PTI UD/UE and UN. These compounds had previously only been tested in transiently transfected cells, and not in a system with steady state levels of pathogenic protein. The possibility of the compounds not working to clear the longer 129Q exon 1 or being "swamped" by the high expression of 71Q exon 1 in the 71Q-H line was suggested. Therefore, two further Western blots of the 71Q line treated with the PTI compounds at 3.3 µM were carried out (technical replicates) (figure 5.26), with corresponding densitometry in figure 5.27. This showed that treatment with PTI-UE at 3.3 µM significantly lowered levels of 71Q exon 1 in this line.

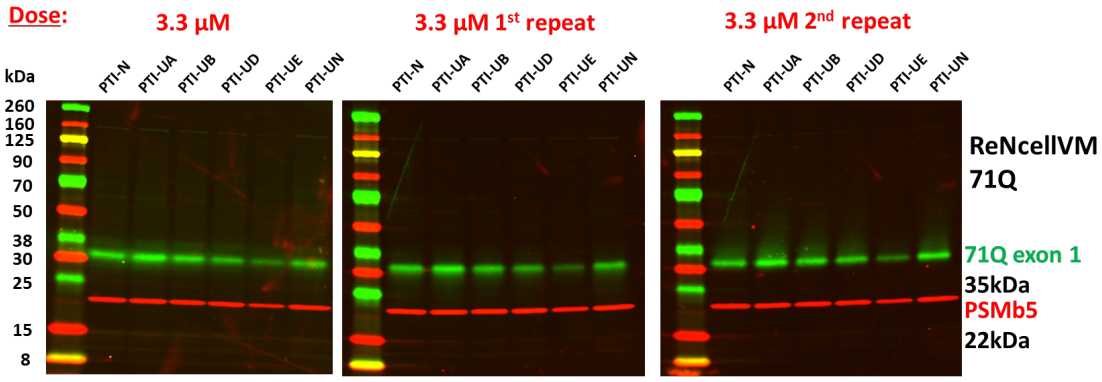


**Figure 5.26**: Further Western blotting (technical replicates) of HTT exon 1 71Q ReNcellVM line treated with 3.3 µM dose of PTI compounds.

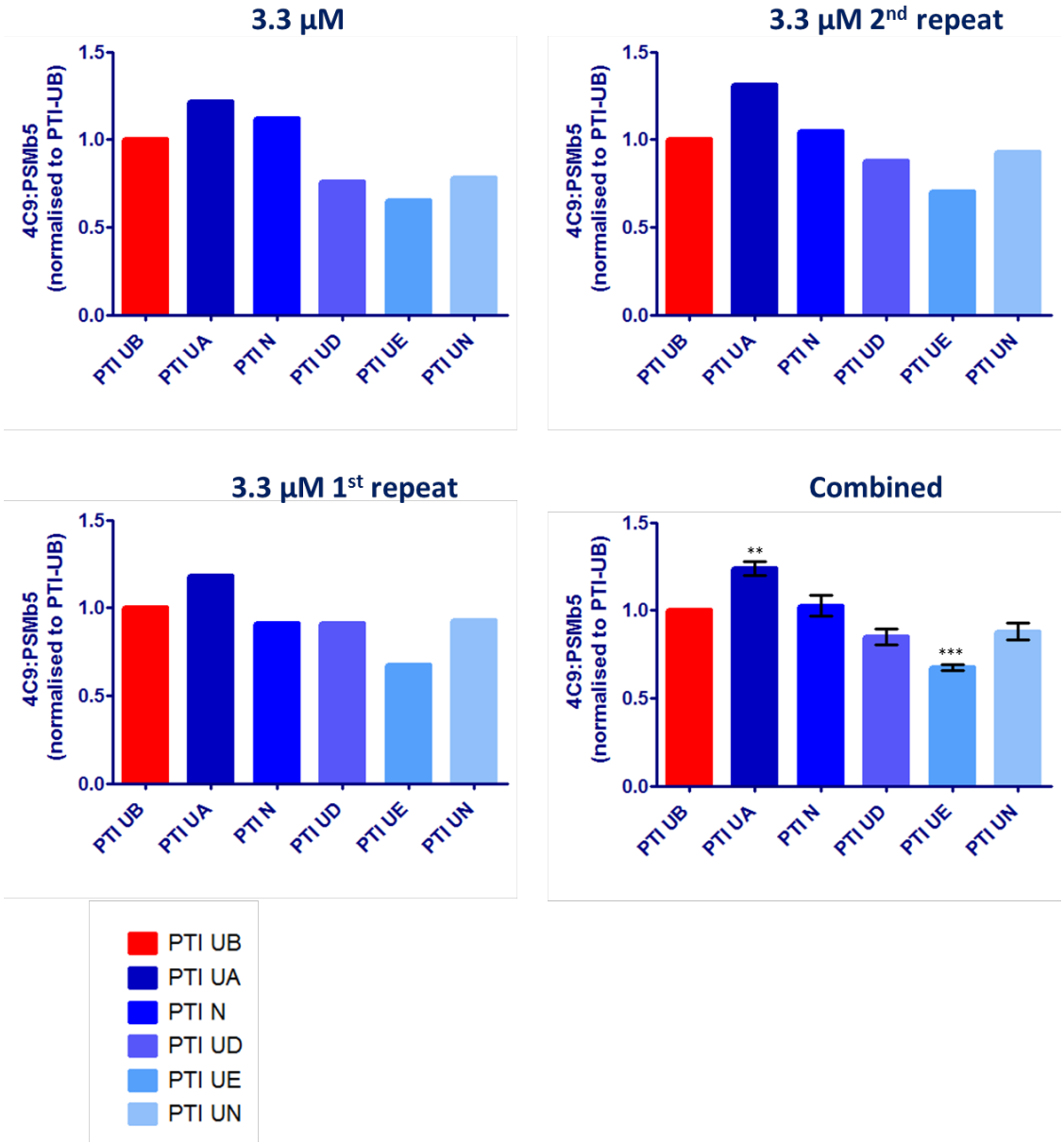


**Figure 5.27**: Densitometry of Western blots of HTT exon 1 71Q ReNcellVM line treated with 3.3 µM dose of PTI compounds (shown in figure 5.26). Combined results (bottom right panel) show mean+SEM. PTI-UE is found to significantly lower 71Q exon 1 levels in these cells (One-way ANOVA with Bonferroni's correction, **=p≤0.01, ***=p≤0.001, n=3).

Based on these results, three further 6-well plates of the 71Q line were differentiated and treated with DMSO (control), 3.3 µM PTI-UB (control), PTI-UD, PTI-UE and PTI-UN as well as a media only control. The results are shown in figure 5.28 and figure 5.29 respectively.

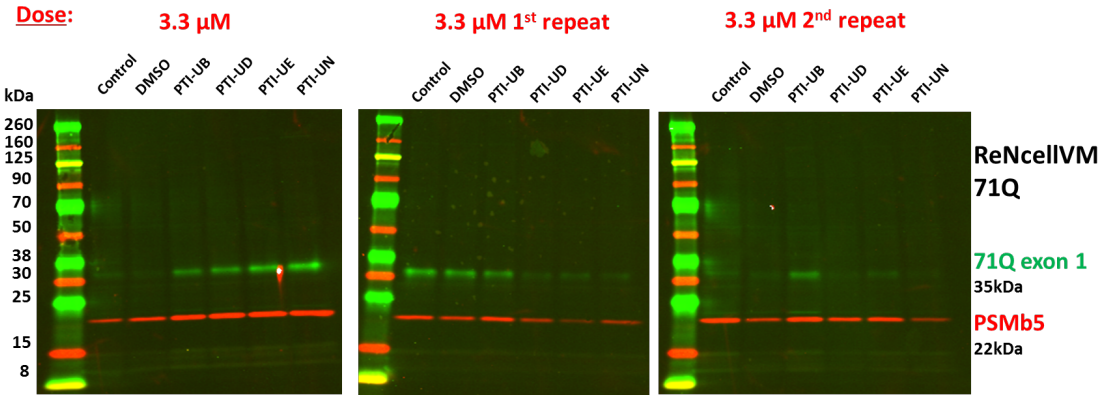


**Figure 5.28:** Western blotting of further HTT exon 1 71Q ReNcellVM cells (biological replicates) treated with 3.3 µM dose of PTI compounds.

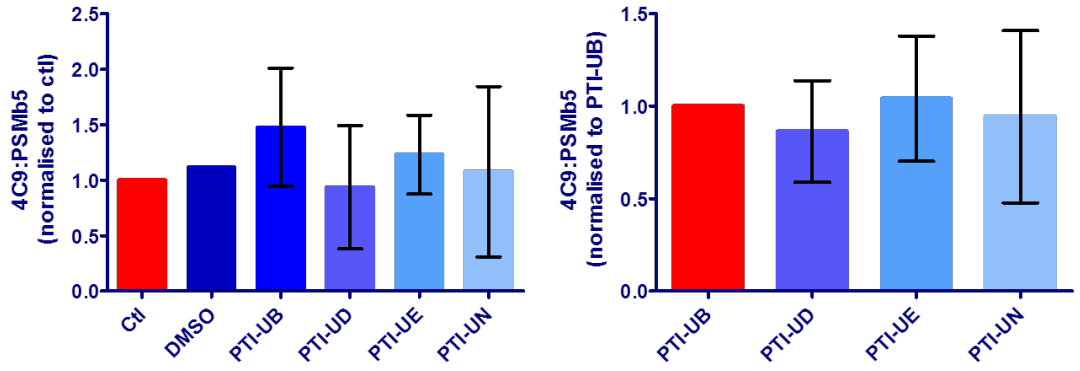


**Figure 5.29:** Densitometry of Western blots of HTT exon 1 71Q ReNcellVM line treated with 3.3 µM dose of PTI compounds (figure 5.28). Results show mean+SEM. Left panel: results normalised to media only control, Right panel: results normalised to PTI-UB control. In both panels, analysis of results with one-way ANOVA showed no significant differences between treatments (n=3).

The results were also combined with the 71Q line results from the previous experiment, in order to increase to n=4, however this made no difference to the overall results. **Therefore the USP14 inhibitors supplied did not lower levels of HTT exon 1 in this cell model, and were not tested further.**

## 5.6 Discussion

Increasing CAG repeat length in HTT exon 1 in ReNcellVM cells was found to cause nuclear inclusion body (IB) formation in the pathogenic lines. The number of cells containing IBs increased on differentiation, and was highest amongst the matched expressing lines in the 129Q line (the longest CAG-repeat length). Raised expression levels of HTT exon 1 also led to increased IB formation, with the 71Q-H line displaying the most inclusion forming cells by two weeks. Thus the development of inclusion containing cells can be seen to be proportional to CAG-repeat length and the level of HTT exon 1 expression in these lines, as has been previously shown in vitro (Scherzinger et al, 1999).

Overall, only a small proportion of cells (up to 3% in the highly expressing 71Q-H line) developed intra-nuclear IB. It is not clear why some cells in particular were susceptible to inclusion formation, particularly since it could be seen from the GFP expression that cells with IBs were not more highly expressing mHTT exon 1 than the surrounding culture (the mHTT exon 1 construct is linked via an IRES site to GFP and therefore GFP expression is proportional to mHTT exon 1 expression). SIM imaging confirmed that nuclear inclusion formation appears to be an “all-or-nothing” process in these cells

and that the soluble cytoplasmic HTT exon 1 is reduced or absent in cells with nuclear IBs. Hence there looks to be a shift in mHTT exon 1 distribution from cytoplasm to nucleus, with associated IB formation, in a small number of cells. It is possible that on prolonged culture greater numbers of cells would accumulate inclusions, as HD is a progressive disease with onset generally in adult-life. Post-mortem studies of HD brain cortex have found neuronal inclusions in 3-6% of neurons in adult-onset patients and 38-52% in JHD patients. Cortex from a patient with pre-symptomatic HD had no nuclear inclusions (DiFiglia et al, 1997).

In this study inclusion formation was not associated with cell death, as there was no drop in cell count over time. Nuclei containing IBs did not appear to have abnormal morphology (except for a slight increase in overall nuclear area), and cells with inclusions did not have higher levels of activated caspase-3 staining. However it was not possible to track inclusion formation in specific neurons longitudinally over time and so the possibility that IB containing cells die and are replaced by others cannot be excluded. A longitudinal study tracking live cells over time has previously been carried out and did not find that inclusion formation led to cell death, rather it has a protective effect in neurons, possibly by reducing levels of soluble diffuse mHtt which was thought to be the toxic species (Arrasate et al, 2004).

Immunofluorescence studies of the ReNcellVM lines showed that IBs do not recruit or bind full length endogenous mHTT. Cells with nuclear IBs were however noted on to be more rounded in shape and have reduced expression of cell markers, which was confirmed on image quantification with Columbus. This may suggest that cells with nuclear IBs become “inert” and do not differentiate as well as the surrounding culture.

This would be consistent with recent studies suggesting that inclusion formation is neither harmful nor protective but triggers a state of cellular quiescence, and shifts cells from a fast cell death by apoptosis due to soluble mHtt exon 1, to a slow death by necrosis due to co-aggregation with other proteins (Ramdzan et al, 2017). For future work to ascertain the effect of nuclear IBs on cells, or to determine which cellular factors favour IB formation, it would be useful to develop a method of separating such cells from the surrounding culture. This has previously been achieved in Neuro2a (N2a) cells expressing fluorescently tagged mHTT exon 1, using pulse-shape analysis (PulSA) by flow cytometry (Ramdzan et al, 2012), however mHTT exon 1 in the ReNcellVM cells does not contain a tag.

A wide range of nuclear IB sizes was observed in the cells. This is consistent with previous studies suggesting that IBs are comprised of a heterogeneous population, including amyloid aggregates with a β-sheet structure (Caron et al, 2014; Nekooki-Machida et al, 2009), and inclusions at various stages of maturity (Duim et al, 2014). In the ReNcellVM, inclusions did not stain with NIAD-4 (or Thioflavin T) suggesting that they do not contain amyloid. However, intracellular inclusions may be difficult for these dyes to access, and variable response of in vitro amyloid to ThioT has been reported (Chen et al, 2002). The intracellular location of mHTT inclusions also precluded live-cell imaging of inclusion formation in the ReNcellVM lines. Many previous studies have utilised fluorescent proteins such as GFP tagged or fused onto the HTT protein, however, the presence of the tag may affect the behaviour of the protein of interest and therefore this approach was not used.

Having determined that mHTT exon 1 exists in a number of forms in the HTT exon 1 ReNcellVM lines, the impact of proteostasis modulation on the accumulation, distribution and clearance of mHTT exon 1 was then investigated. Bafilomycin A1 is a vacuolar ATPase inhibitor which interferes with the autophagosome–lysosome fusion, possibly because lysosomal acidification is required for this step (Yamamoto et al, 1998). Treatment with bafilomycin resulted in increased HTT staining throughout the whole neuron (nucleus, cytoplasm and axons) across all ReNcellVM lines. This was also confirmed on high content image analysis with Columbus. This suggests that autophagy is at least partly responsible for the clearance of mHTT from these cells, and is in support of a previous finding that the degradation of polyQ expanded peptides is particularly dependent on autophagy (Tsvetkov et al, 2013).

Surprisingly proteasomal inhibition with MG132 did not lead to increased levels of HTT in the ReNcellVM lines. However, on visual inspection of the images a striking redistribution of HTT exon 1 could be seen, with increased staining in nuclear and perinuclear regions, with no axonal/cytoplasmic signal. This may suggest that clearance of mHTT occurs via different mechanisms in different cellular compartments (Zhao et al, 2016), and is particularly UPS dependent in nuclear/perinuclear areas rather than axonal or cytoplasmic regions. There is also the possibility that MG132 affects the mechanisms that govern the trafficking of the HTT protein itself within neurons.

Proteasomal enhancement is a potential therapeutic avenue in HD and the overexpression of ubiquitin E3 ligase decreased mHTT aggregates in the brains of HD mice (Bhat et al, 2014). However, the USP14 inhibitors provided by Proteostasis

Therapeutics Inc (PTI) did not clear HTT exon 1 from the pathogenic ReNcellVM lines. There are many potential reasons for this including lack of target (USP14) engagement, or overwhelming the UPS by a general increase in ubiquitinated proteins. Another possibility is that mitochondrial dysfunction (which is known to occur in HD models) may preclude proteasomal enhancement because the UPS is a highly ATP-dependent system. Indeed, mitochondrial deficits have been observed in the ReNcellVM HTT exon 1 lines by Dr. Wood-Kaczmar (unpublished data).

## 5.7 Summary

HTT exon 1 ReNcellVM neurons developed nuclear inclusion bodies in a manner proportional to CAG-repeat length and the level of mHTT exon 1 overexpression. Cells containing nuclear IBs displayed decreased or absent soluble cytoplasmic mHTT exon 1, and reduced expression of cell markers. Although autophagy and proteasomal inhibition altered the distribution of mHTT within neurons, enhancement of the UPS with USP14 inhibitors had no effect on the clearance of mHTT exon 1 from ReNcellVM neurons.

# 6 Trafficking of huntingtin in HTT exon 1 ReNcellVM neurons and in iPSC-derived medium spiny neurons

## 6.1 Background

Mutant huntingtin exerts a dominant toxic effect through a multitude of pathogenic mechanisms; among others, these include transcriptional dysregulation, abnormal mitochondrial transport and function, and impaired vesicular trafficking. It is not clear which of these pathways lends the greatest contribution to neurodegeneration in Huntington's disease, particularly to the loss of striatal medium spiny neurons (MSNs) that is characteristic of HD. An understanding of the trafficking of the HTT protein itself, and how this is altered by the polyglutamine expansion mutation, might shed light on which of these mechanisms is the most important. Aberrant trafficking of the mutant protein may also play a role in pathogenesis.

Initial studies of subcellular localisation of HTT and mHTT were hampered by the lack of well characterised HTT antibodies or human neuronal cell models, and yielded conflicting results. N-terminal fragments of mHTT formed aggregates in the cytoplasm and nucleus, but full length HTT (both wild-type and mutant) was only found in the cytoplasm (Cooper et al, 1998). An absence (or near absence) of nuclear HTT was also reported by other groups (Persichetti et al, 1995; Trottier et al, 1995). However

further immunofluorescence studies found that full-length wild type HTT could be detected in the nucleus of multiple mammalian cell lines (De Rooij et al, 1996; Dorsman et al, 1999), although neuronal intra-nuclear inclusions could only be detected by N-terminal antibodies in HD autopsy brain (Dorsman et al, 1999).

More recent studies have suggested that the trafficking of HTT is dependent on the cell context. Under basal conditions, huntingtin is thought to be an endoplasmic reticulum (ER)-associated protein, which attaches through its N-terminal membrane binding domain. On ER stress, HTT can dissociate and translocate to and from the nucleus. Loss of ER targeting of mHTT results in increased nuclear entry of mHTT and increased toxicity (Atwal et al, 2007). This has also been found to occur in response to reactive oxygen species (ROS) stress, which triggers structural change of the N17 domain resulting in HTT dissociation from the ER membrane, increased N17 phosphorylation, and nuclear targeting (DiGiovanni et al, 2016). Using novel chromobodies, HTT was shown to localise to sites of DNA damage within the nucleus of retinal epithelial cells, where it acts as a scaffold for proteins of the DNA damage response pathway, in a process which is deficient in HD patient fibroblasts (Maiuri et al, 2017). HTT also localises to early endosomes and forms cytosolic puncta, termed huntingtin stress bodies (HSBs) as part of a rapid cell stress response, and this is associated with the arrest of endosomal trafficking which conserves ATP use. Mutant HTT displays defective recovery from this stress response (Nath et al, 2015).

Nuclear huntingtin also increases at certain points during the cell cycle (Martín-Aparicio et al, 2002), and localises to the mitotic spindle during cell division (Godin et al, 2010). Within the nucleus, huntingtin has been localised to chromatin (Benn et al, 2008).

Stress dependent phosphorylation at Ser13 and Ser16 targets full-length HTT to chromatin-dependent sub-regions of the nucleus, the mitotic spindle and cleavage furrow during cell division (Atwal et al, 2011). Huntingtin has also been shown to transport to the nuclear compartment during the meiotic stage of spermatogenesis (Im et al, 2014).

The entry or exit of proteins to and from the nucleus is a tightly controlled process. Smaller proteins (50-60kDa) may pass by passive diffusion though the nuclear pore complex (NPC), but larger proteins require a nuclear localisation signal (NLS) to enter via a facilitated diffusion mechanism. The NPC spans the nuclear envelope and is the main transport conduit between the nucleus and cytoplasm. It is made up of many subunit proteins called nucleoporins (NUPs), which have functions including nuclear import and export, RNA export and membrane anchoring. NUPs have been shown to be severely mislocalised in a number of HD cell models, leading to general deficits in both active and passive nucleocytoplasmic transport (Grima et al, 2017). Conversely, HTT itself is known to contain a nuclear localisation signal (NLS) near its N-terminus, between aa 174-207 (Desmond et al, 2012), and two nuclear export signals (NES), one at its C-terminus (Xia et al, 2003) and one within the N17 domain (Maiuri et al, 2013). This may explain the rapid pathology in the R6/2 mouse, which expresses aa 1-81 of Htt and does not contain the NLS; this small N-terminal fragment therefore can pass unrestricted into the nucleus by passive diffusion through the NPC. With CAG repeat lengths >335 in the R6/2 mouse a larger N-terminal fragment is generated, which cannot pass through the NPC by passive diffusion, and also does not contain the NLS; therefore cytoplasmic rather than nuclear inclusions are formed which may account for the striking improvement in phenotype that is seen (Dragatsis et al, 2009).

Hence multiple lines of evidence suggest that alterations in the trafficking of mutant HTT may play a role in disease pathogenesis. Therefore using an approach of subcellular fractionation followed by measurement of HTT levels in different cell compartments, the trafficking of HTT was studied in HTT exon 1 overexpressing ReNcellVM neurons and also in iPSC-derived MSNs. By studying both cell models, comparisons between the behaviour of HTT exon 1 and endogenous full length HTT could be made, in addition to evaluating differences any between mutant and wild-type HTT.

## 6.2 Aims

1. To determine any differences in the subcellular trafficking of control (29Q) and mutant length (129Q) HTT exon 1 in HTT exon 1 overexpressing ReNcellVM neurons.

2. To determine any differences in subcellular trafficking between wild type and mutant HTT in iPSC-derived MSNs.

## 6.3 Methods

HTT exon 1 overexpressing ReNcellVM cells and iPSC-derived MSNs were differentiated as described in section 2.1.3 and 2.2.6 respectively. In order to ensure correct differentiation of MSNs, immunocytochemistry was carried out (section 2.7.1)

with images taken on the Opera Phenix microscope as previously described (section 2.7.2). Subcellular fractionation was carried out as per the protocol outlined by Thermo (section 2.9). A sample of each fraction was used to check for adequate separation using Western blotting (section 2.4.2) with antibodies to various compartment markers (appendix table A.1). Measurement of mutant and total HTT levels was carried out at Evotec, using the Erenna Singulex human huntingtin protein detection assay (section 2.5). Graphical representation and statistical analysis was carried out using Prism software (section 2.10).

## 6.4 Contributions

The work described in this chapter was carried out by Dr. Rhia Ghosh, with the following exceptions:

The measurement of HTT levels using the Erenna Singulex assay was carried out at Evotec by Drs Frank Herrman, Michaela Pirsch and Chantal Bazenet.

The antibody staining and imaging of cells displayed in Figures 6.5 and 6.6 was carried out by Dr. Alison Wood-Kaczmar (due to Dr. Rhia Ghosh commencing maternity leave).

## 6.5 Results

### 6.5.1 Trafficking of huntingtin protein in HTT exon 1 overexpressing ReNcellVM neurons

To study the trafficking of HTT exon 1 in ReNcellVM neurons, subcellular fractionation was carried out in dd14 neurons in the 29Q (control) and 129Q (mutant) lines, followed by measurement of total and mutant HTT levels in the resulting fractions with the Erenna Singulex human huntingtin protein detection assay.

#### 6.5.1.1 Subcellular fractionation of HTT exon 1 overexpressing ReNcellVM neurons

Subcellular fractionation was used to separate ReNcellVM neurons into cytoplasmic, membrane-bound, soluble nuclear, chromatin bound and cytoskeletal fractions. This was followed by Western blotting to check for the presence of respective compartment markers in each fraction, to ensure satisfactory separation. Initial fractionation attempts produced very little material in each fraction (due to loss of material at each separation stage), with incomplete separation of nuclear, chromatin bound and cytoskeletal fractions. To compensate for this, the amount of starting material was increased to one confluent T175 flask. Solution buffers were doubled from the nuclear fractionation stage onwards, with the addition of an incubation step with 1 Ul benzonase to encourage separation of the chromatin bound fraction from the soluble nuclear fraction. It was decided that the cytoskeletal fraction (the final product after completion of the protocol) was not of sufficient purity to warrant further study.

Following optimisation of the fractionation protocol, ReNcellVM 29Q and 129Q cells were differentiated to dd21. A proportion of these cells were used to prepare whole cell pellets. The remainder underwent cell fractionation, of which a proportion of each fraction was used for Western blotting to ensure adequacy of separation. Results are shown in figure 6.1 and figure 6.2. ReNcellVM 29Q fractions displayed appropriate enrichment of compartment markers in each fraction on Western blotting. ReNcellVM 129Q fractions were also well separated, however there was no signal for the nuclear compartment marker PMS2 (a mismatch repair endonuclease) in the soluble nuclear fraction. This may be because of the limited sample availability for this particular fraction (the majority of which was reserved for testing of HTT levels).

Whole cell pellets and fractions of cytoplasm, membrane-bound, nuclear and chromatin bound samples for the HTT exon 1 ReNcellVM 29Q and 129Q lines were sent to Evotec for quantitative measurement of HTT levels.

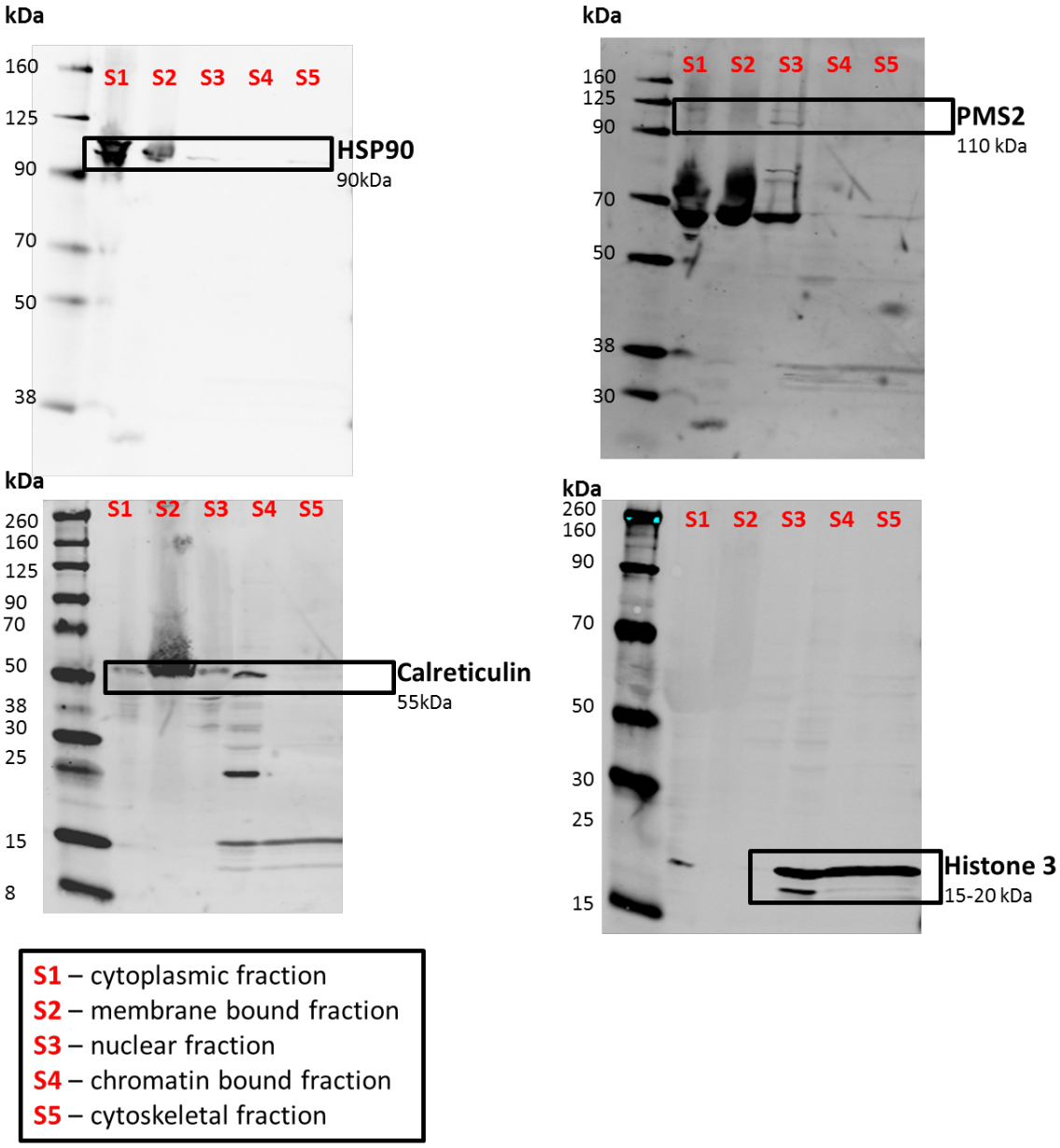


**Figure 6.1: Subcellular fractionation of dd21 ReNcellVM 29Q neurons.** Western blotting with cell compartment markers shows good separation of the cytoplasmic marker HSP90 in lane S1, the membrane bound compartment marker calreticulin in lane S2, the nuclear marker PMS2 in lane S3, and the chromatin bound compartment marker histone 3 in lane S4. There is some overlap between fractions, which is to be expected.

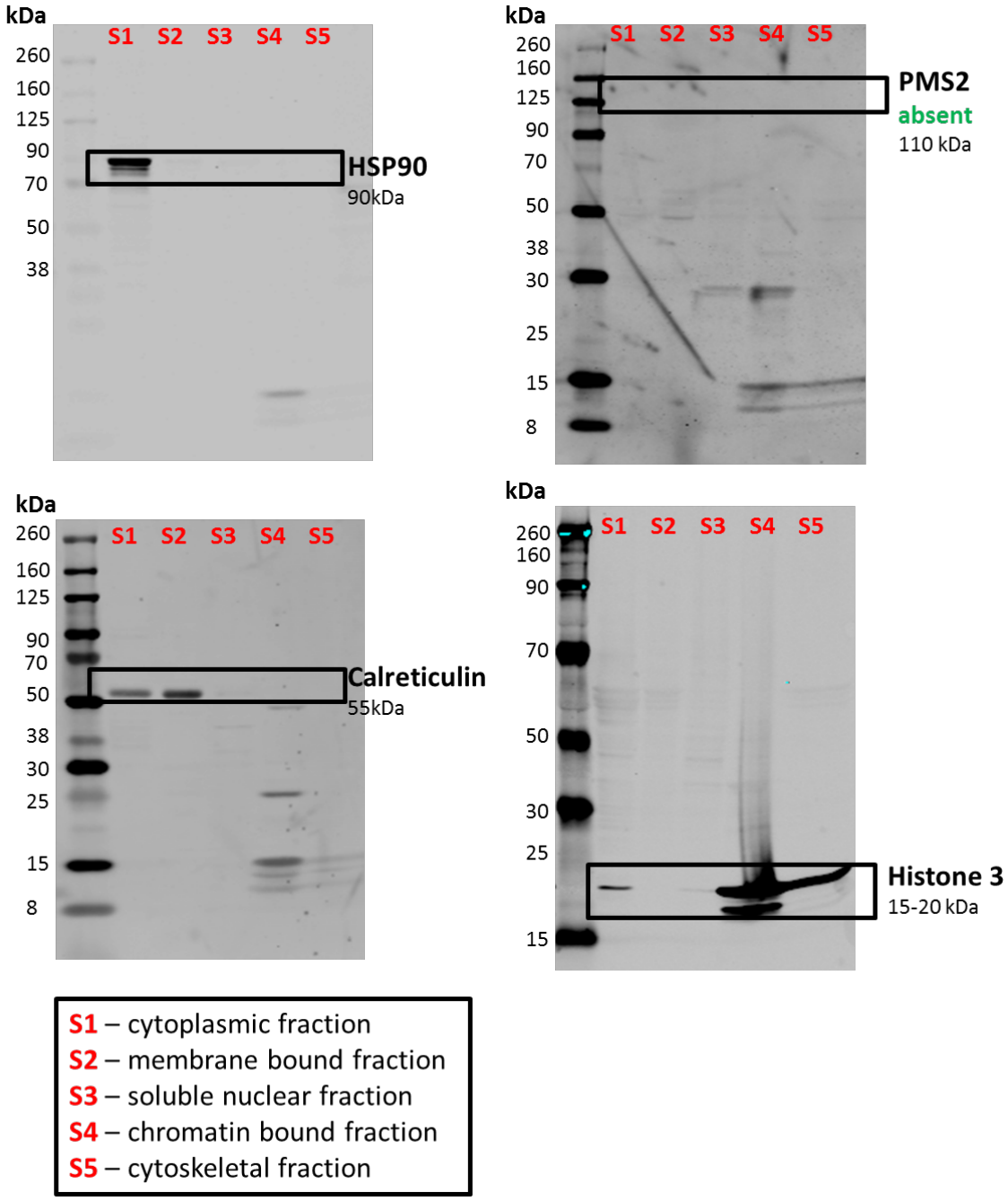


**Figure 6.2: Subcellular fractionation of dd21 ReNcellVM 129Q neurons.** Western blotting with cell compartment markers shows good separation of fractions with HSP90 (cytoplasmic marker), calreticulin (membrane bound compartment marker) and histone 3 (chromatin bound) enriched in respective lanes. However the nuclear marker PMS2 cannot be visualised in lane S3 – this is likely due to the small amount of material isolated for this fraction.

#### 6.5.1.2 Measurement of total and mHTT levels in HTT exon 1 ReNcellVM neurons and cell fractions

The Erenna Singulex human huntingtin protein detection assay was used to quantify levels of soluble total and mHTT in whole cell pellets and cell fractions of 29Q and 129Q ReNcellVM dd21 neurons. This ultrasensitive single-molecule counting (SMC) mHTT immunoassay has previously been used to detect femtomolar levels of mHTT in the CSF of premanifest HD gene carriers (Wild et al, 2015). The antibody pair 2B7/MW1 is used to detect levels of mutant HTT, and 2B7/4C9 is used to detect levels of total HTT. The latter is known to be the less sensitive assay. Readings were taken in triplicate for each line and results are shown in figure 6.3 and figure 6.4 respectively.

As expected, mHTT exon 1 is detected in the ReNcellVM 129Q line, but not in the control ReNcellVM 29Q line. mHTT is found in all compartments in the mutant line, and the concentration of mHTT in the nucleus is seen to be extremely low in comparison to the cytoplasm and membrane-bound compartments. This is consistent with observations from immunofluorescence studies (chapter 5), particularly since this assay detects only soluble and not aggregated forms of mHTT.

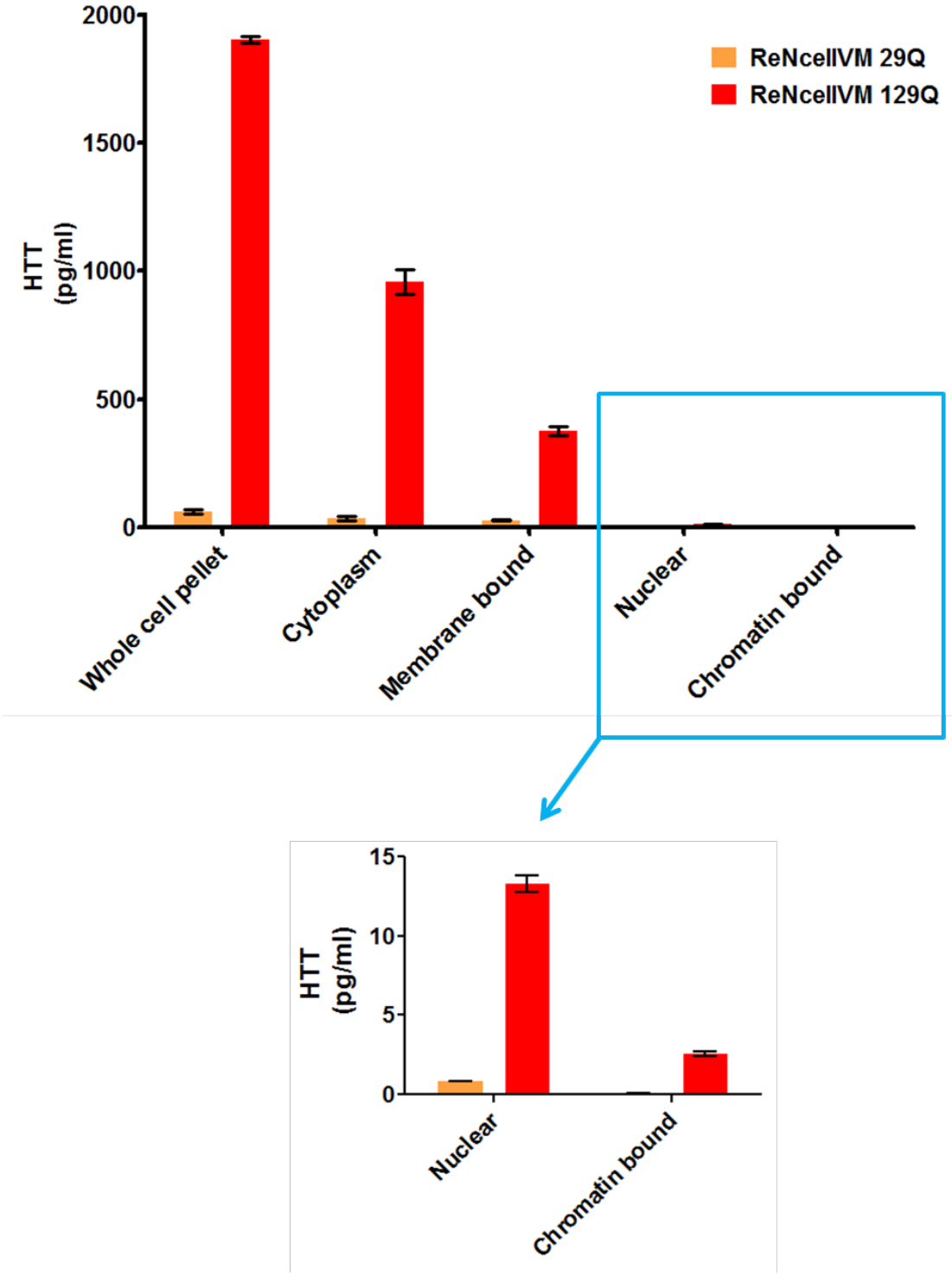


**Figure 6.3: Mutant HTT levels in ReNcellVM 29Q and 129Q neurons and cell fractions.** Using the 2B7/MW1 Singulex assay mHTT exon 1 is detected in all fractions of the mutant 129Q line, but not in the control 29Q (as is expected). The concentration of mHTT in the nucleus is extremely low in comparison to the cytoplasm and membrane-bound compartments. (n=3, technical replicates).

Measurement of total HTT levels again shows the presence of HTT in all fractions of the 129Q line (this is likely to be mostly HTT exon 1, though this assay would also detect endogenous full-length HTT). HTT is also seen in the cytoplasmic, membrane bound, and nuclear fractions of the control 29Q line.

The total HTT concentration in the cell (whole cell pellet) was significantly higher in the 129Q line than the 29Q line (unpaired t-test). This was surprising as these lines were initially confirmed to have very closely matched expression levels of HTT exon 1 on MSD assay (chapter 3, section 3.5.3.2). Due to this difference in whole cell HTT concentration in 29Q and 129Q lines, further between-line comparisons of compartmental HTT concentration were not made. As a proportion of whole cell HTT levels, the nuclear HTT concentration is lower in the 29Q than the 129Q line (2.6% vs 5.5%). This may suggest that mHTT 129Q HTT exon 1 accumulates in the nucleus more readily than control length 29Q HTT exon 1.

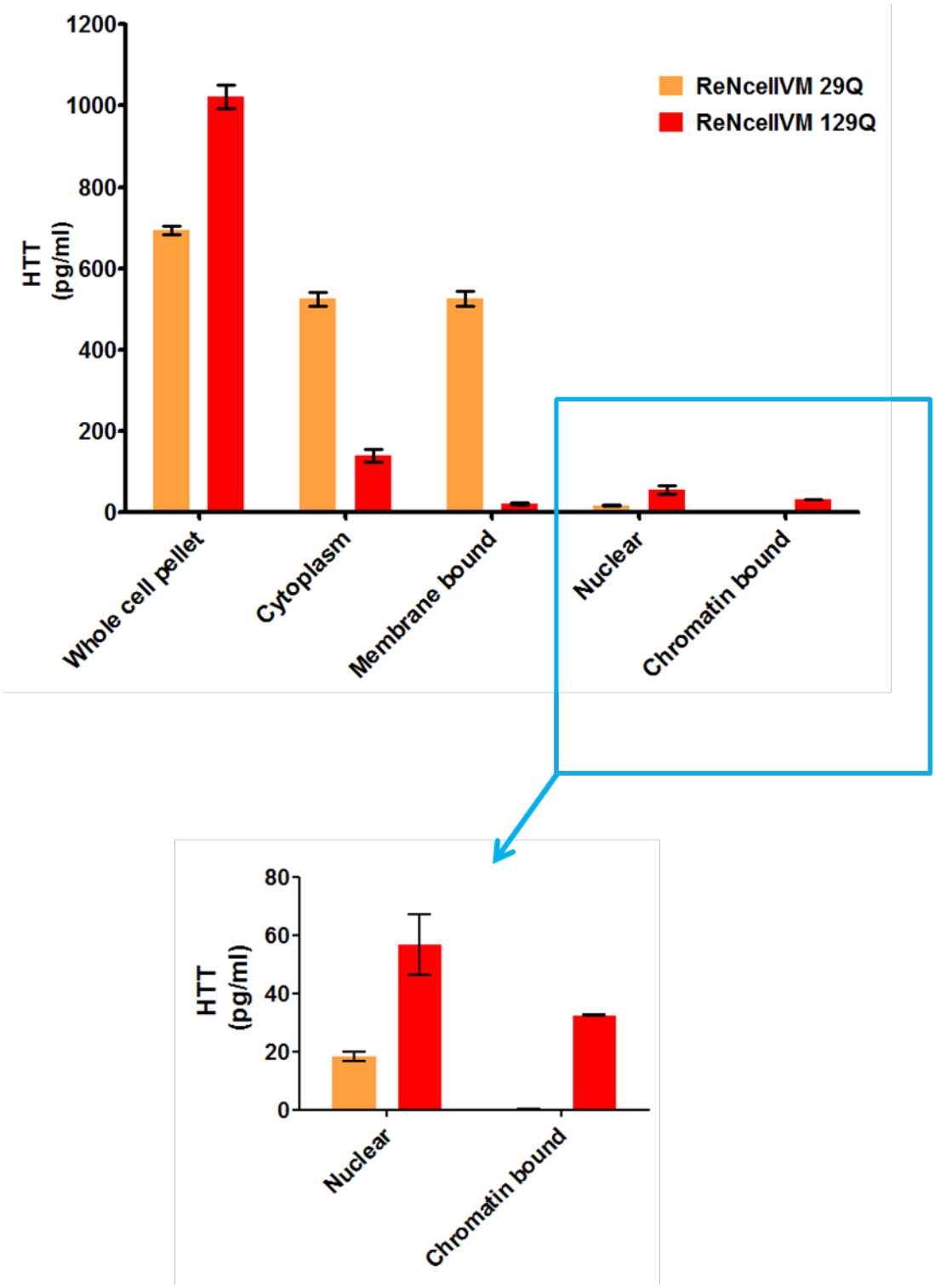


**Figure 6.4: Total HTT levels in ReNcellVM 29Q and 129Q neurons and cell fractions.** Using the 2B7/4C9 Singulex assay HTT exon 1 is detected in all 129Q fractions, including nuclear and chromatin bound fractions. The presence of HTT is also confirmed in the nucleus of the control 29Q line. n=3 (technical replicates).

### 6.5.2 Trafficking of huntingtin protein in iPSC-derived MSNs

The trafficking of HTT protein in iPSC-derived MSNs was then studied using the same approach as for the HTT exon 1 ReNcellVM neurons. In this case, MSNs express HTT from the endogenous locus only, so HTT levels would be expected to be much lower. Control length (20Q) and the longest mutant length (73Q) iPSCs were utilised to enhance the chance of observing mutant HTT driven differences between the lines. Three clones of each line were used as biological replicates to account for clonal variability. After differentiation of iPSCs into MSNs, subcellular fractionation was carried out, followed by measurement of total and mutant HTT levels as previously described.

#### 6.5.2.1 Differentiation of iPSC-derived MSNs

Three clones of the control iPSC line (designated 20Q clone 1, 20Q clone 2 and 20Q clone 3) and mutant 73Q iPSC line (designated 73Q clone 1, 73Q clone 2 and 73Q clone 3) were differentiated in 10 cm dishes to generate sufficient material. A proportion of cells were grown in Ibidi glass-bottom wells for imaging purposes. These iPSC lines were derived from a related family as described in chapter 3; in the case of these two particular lines, an unaffected mother (control) and affected son (carrying an *HTT* mutation with 73 CAG repeats). MSN differentiation was carried out for at least 36 days (as per protocol), and cultures have been shown to be comprised of 50% MSNs from this time (Arber et al, 2015). A portion of cells were fixed and stained to ensure correct differentiation, with results of one control and one mutant (73Q) clone as shown in figure 6.5 and figure 6.6. Work is currently on-going in the lab to quantify the proportion of MSNs generated using high-content imaging.

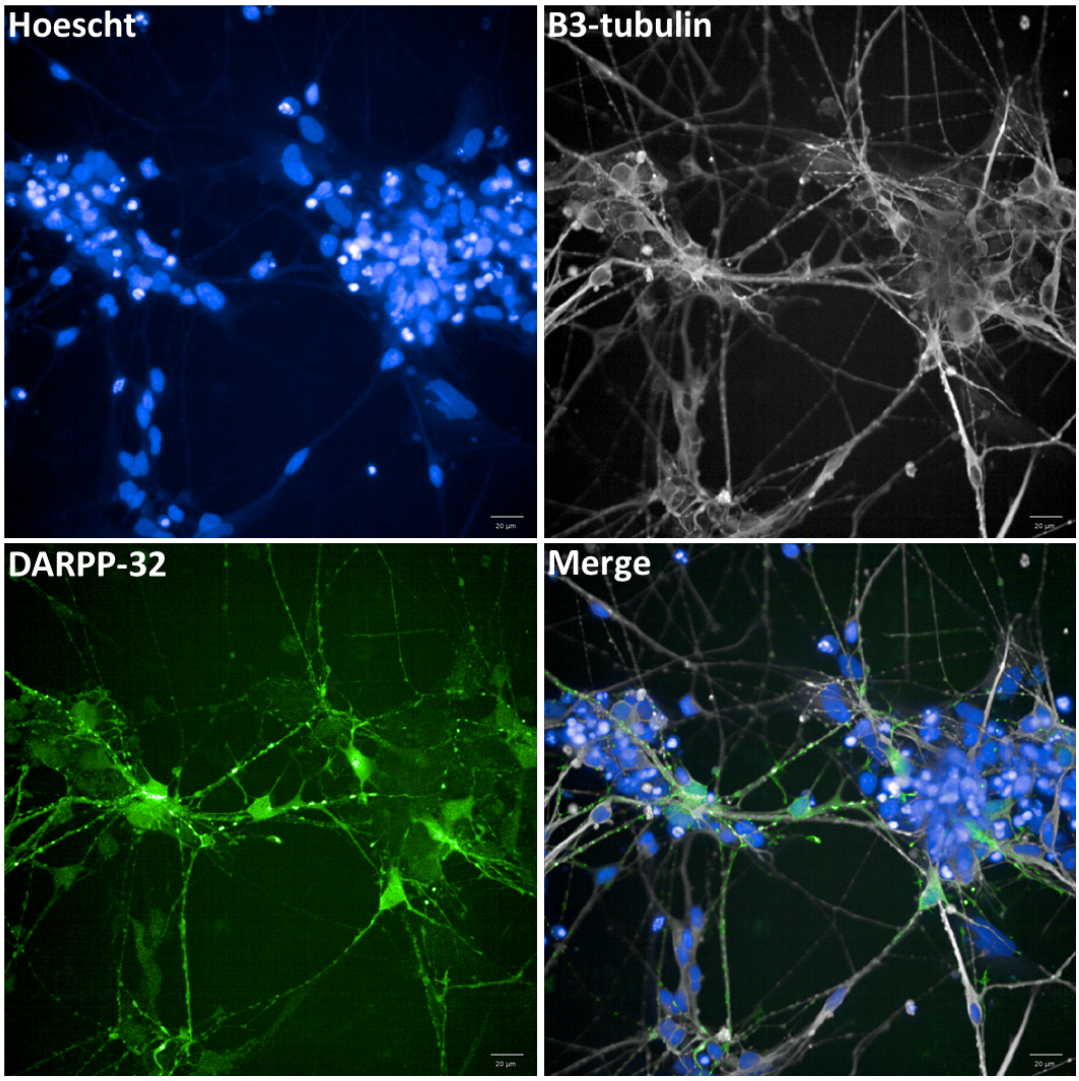


**Figure 6.5: Immunocytochemistry of control 20Q clone 2 cell cultures at dd36.** Many cells display DARPP-32 staining with characteristic MSN morphology. High densities of clustered nuclei are observed, due to ongoing cell proliferation during differentiation. Prominent B3-tubulin staining confirms that the majority of the culture is neuronal. Blue – Hoescht (nuceli), White – anti-B3-tubulin antibody, Green – anti-DARPP-32 antibody.

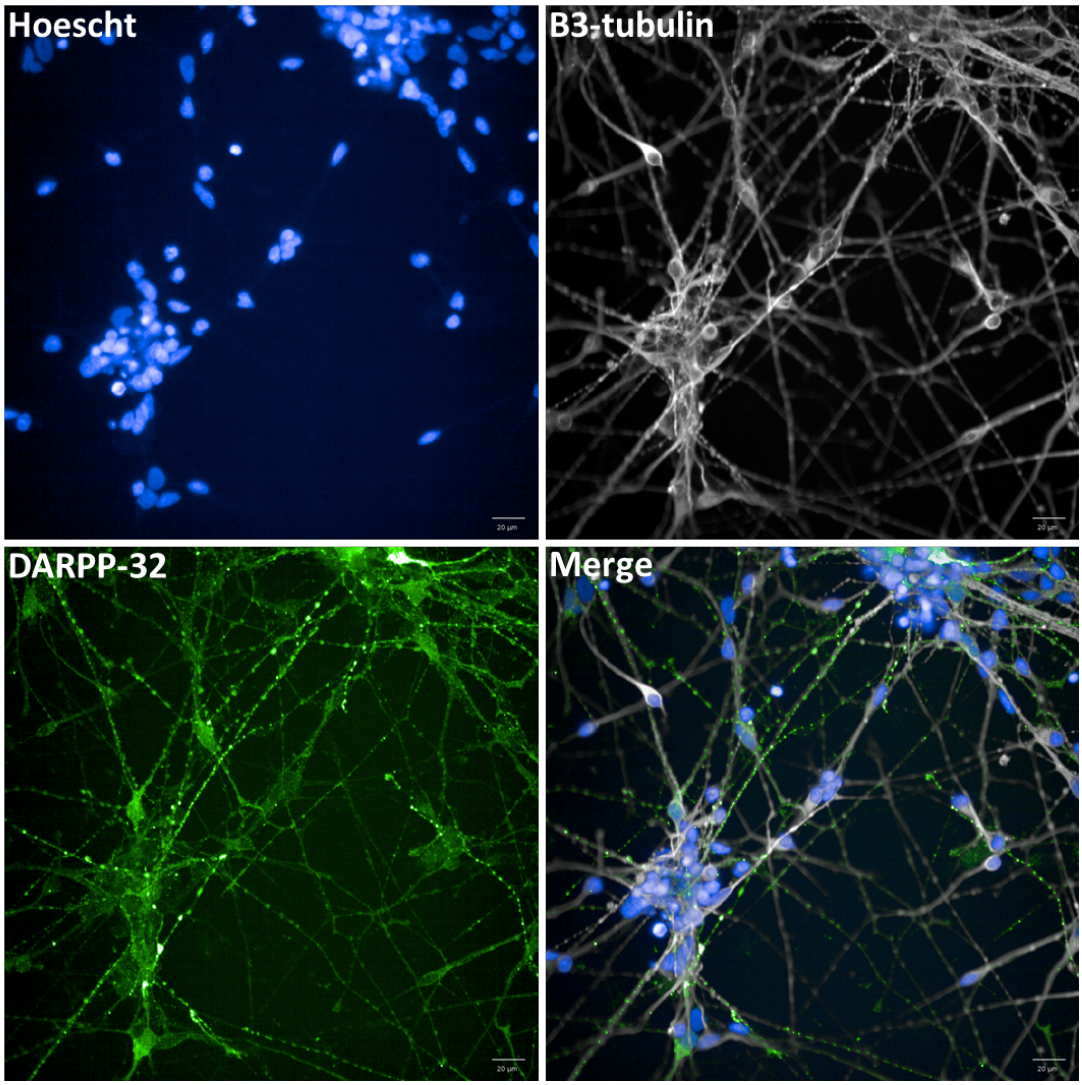


**Figure 6.6: Immunocytochemistry of mutant 73Q clone 2 cell cultures at dd36.** Mutant neurons also display DARPP-32 staining, confirming that they also differentiate into a predominantly neuronal culture with a high proportion of MSNs. Clusters of nuclei are observed, due to ongoing cell proliferation during differentiation. Blue – Hoescht (nuceli), White – anti-B3-tubulin antibody, Green – anti-DARPP-32 antibody.

### 6.5.2.2 Subcellular fractionation of iPSC-derived MSNs

Subcellular fractionation was carried out using the optimised protocol, and Western blotting with compartment markers carried out to ensure adequate separation of cytoplasmic, membrane-bound, nuclear and chromatin-bound fractions. Results are shown in figures 6.7 - 6.12. Whole cell pellets were also prepared.

20Q clone 1 and 2, and 73Q clone 2 and 3 MSN fractions displayed appropriate enrichment of compartment markers on Western blotting, suggestive of good separation of the different fractions. 20Q clone 3 and 73Q clone 1 MSN fractions also showed good separation of all fractions except for the nuclear fraction, which showed no signal on Western blotting with nuclear compartment markers PMS2 or MLH1. This is likely due to the limited amount of sample produced during nuclear fractionation, of which the majority therefore was reserved for the quantification of HTT levels.

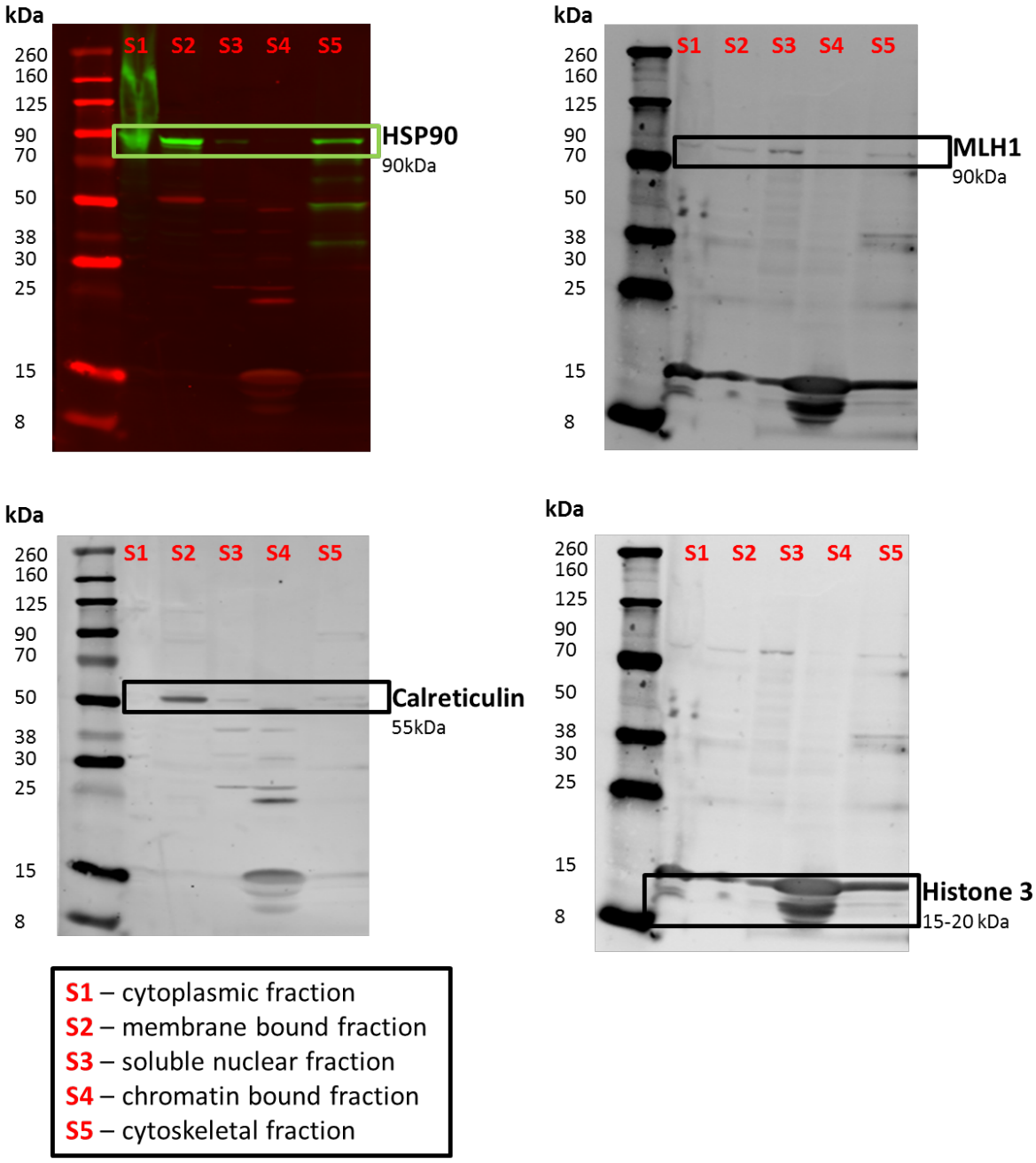


**Figure 6.7: Subcellular fractionation of 20Q clone 1 MSNs (dd49).** Western blotting with cell compartment markers shows enrichment of the cytoplasmic marker HSP90 in lane S1, the membrane bound compartment marker calreticulin in lane S2, the nuclear marker MLH1 in lane S3, and the chromatin bound compartment marker histone 3 in lane S4.

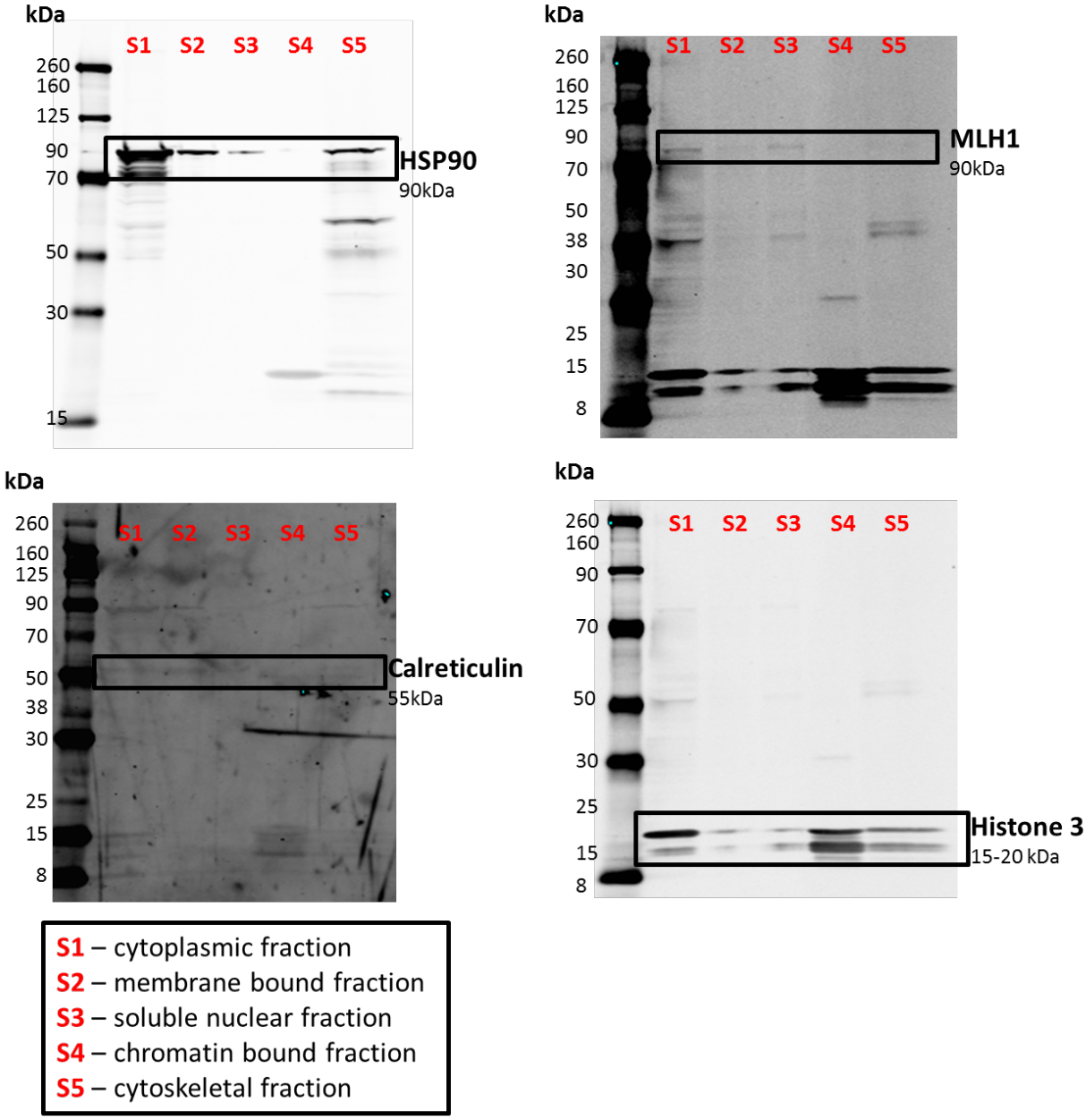


**Figure 6.8: Subcellular fractionation of 20Q clone 2 MSNs (dd43):** Western blotting with cell compartment markers shows enrichment of the cytoplasmic marker HSP90 in lane S1, the presence of membrane bound compartment marker calreticulin in lane S2, the nuclear marker MLH1 in lane S3, and the enrichment of chromatin bound compartment marker histone 3 in lane S4.

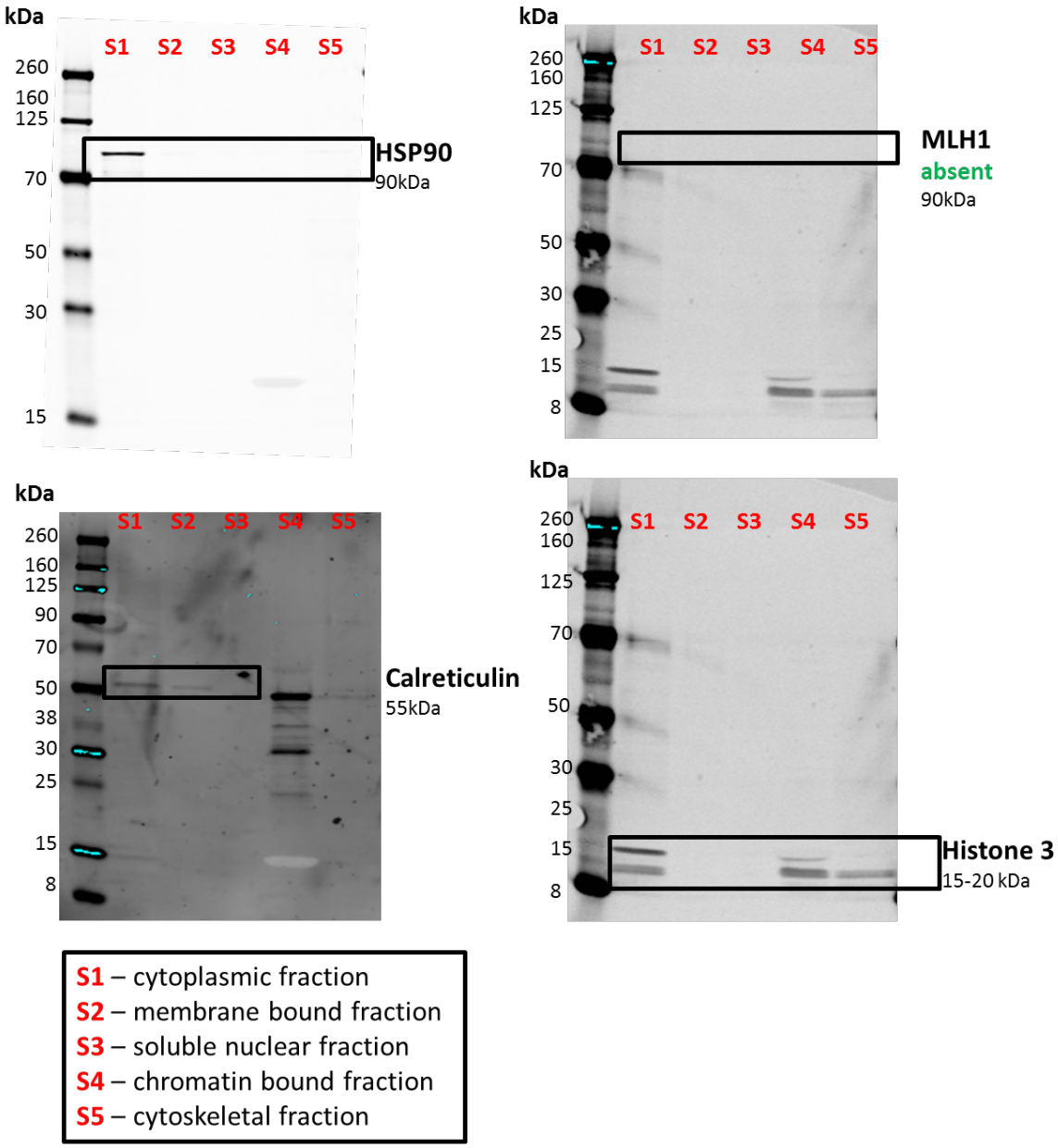


**Figure 6.9: Subcellular fractionation of 20Q clone 3 MSNs (dd39).** Western blotting with cell compartment markers shows enrichment of the cytoplasmic marker HSP90 in lane S1, the presence of membrane bound compartment marker calreticulin in lane S2, and the enrichment of chromatin bound compartment marker histone 3 in lane S4. No signal with nuclear marker MLH1 was obtained, and this was also found to be the case with PMS2 antibody. No other compartment markers are visible in lane S3 which suggests that insufficient material was loaded for Western blotting.

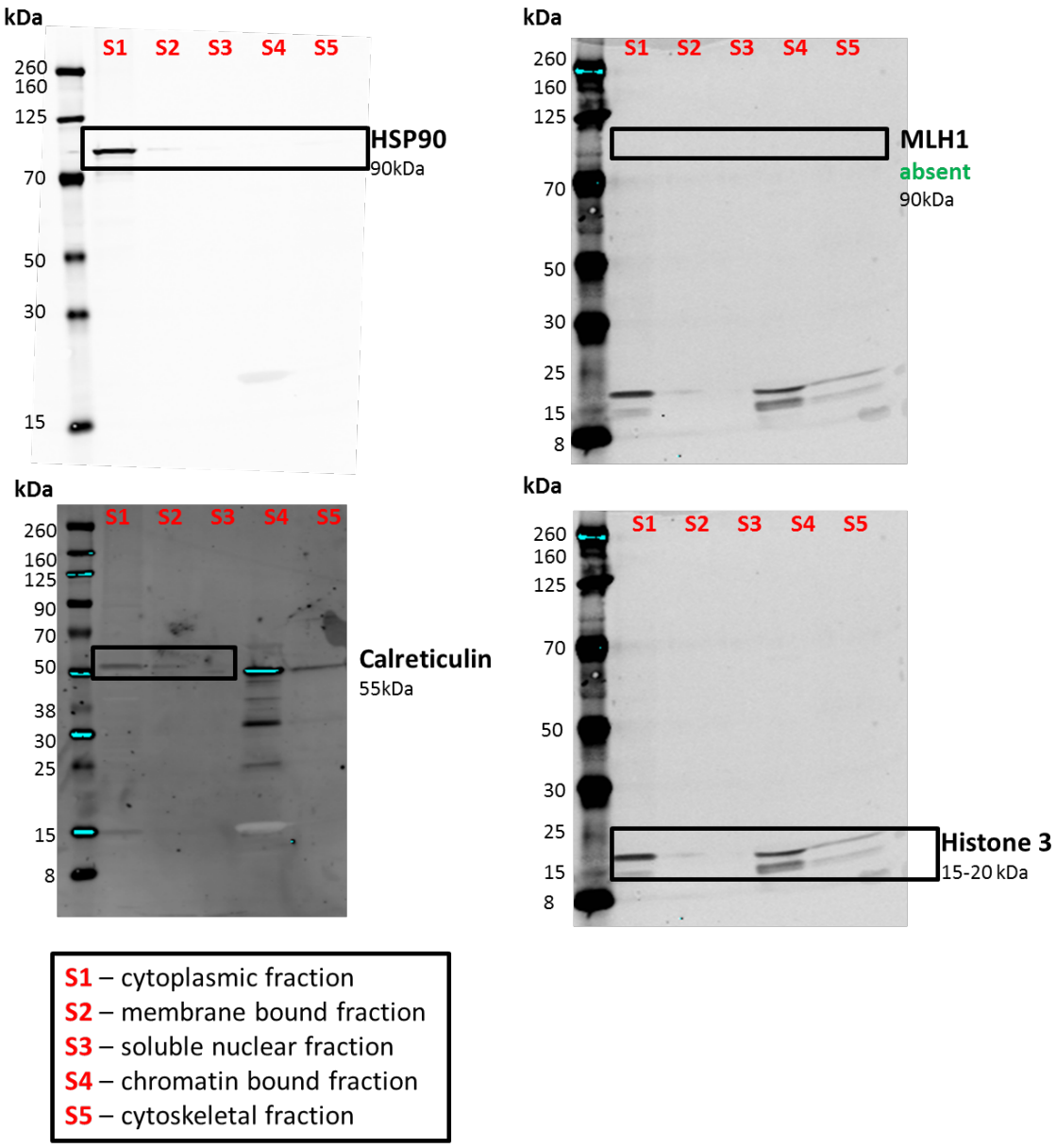


**Figure 6.10: Subcellular fractionation of 73Q clone 1 MSNs (dd38).** Western blotting with cell compartment markers shows enrichment of the cytoplasmic marker HSP90 in lane S1, the presence of membrane bound compartment marker calreticulin in lane S2, and the enrichment of chromatin bound compartment marker histone 3 in lane S4. No signal with nuclear marker MLH1 was obtained, and this was also found to be the case with PMS2 antibody. No other compartment markers are visible in lane S3 which suggests that insufficient material was loaded for Western blotting.

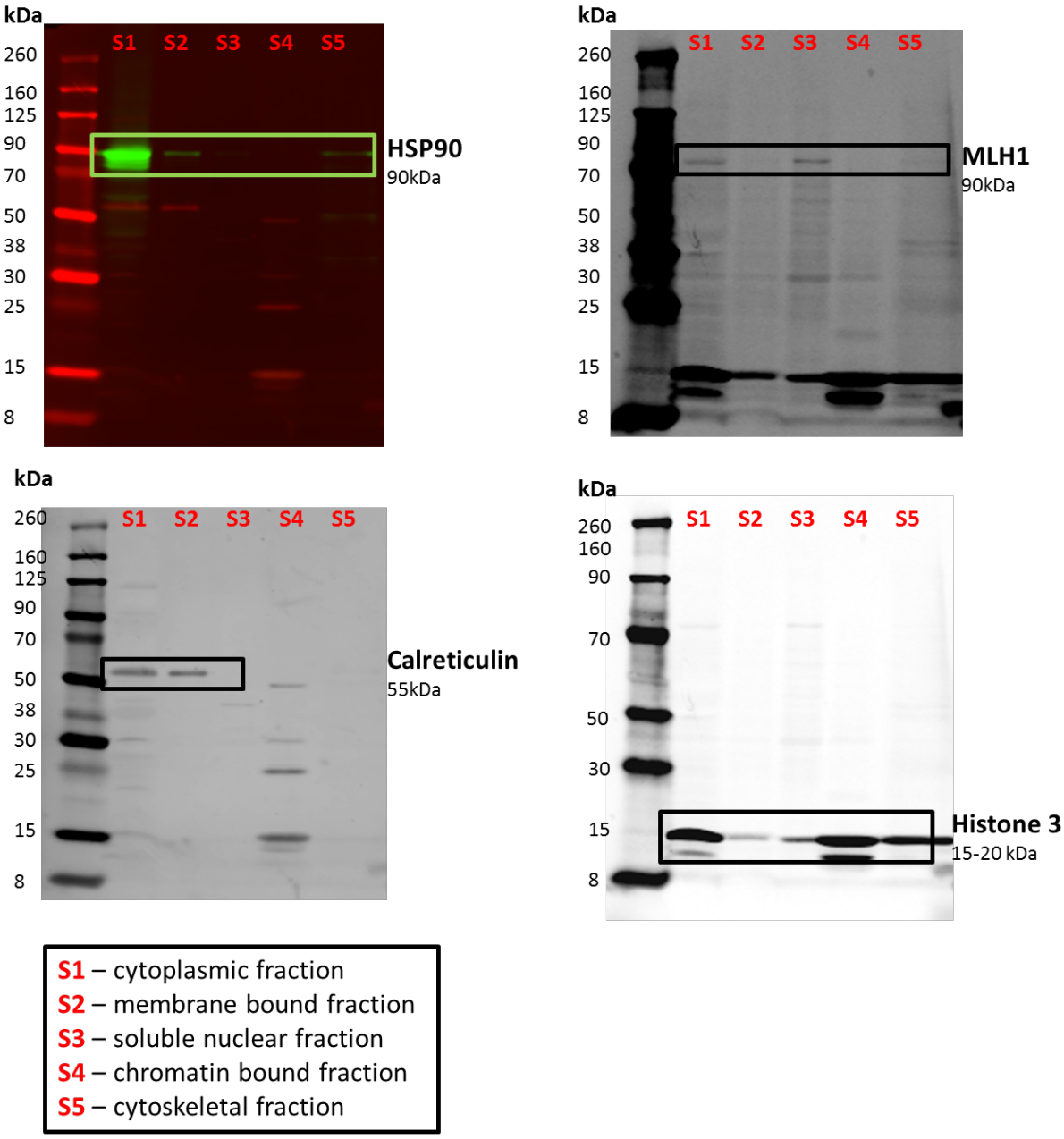


**Figure 6.11: Subcellular fractionation of 73Q clone 2 MSNs (dd45).** Western blotting with cell compartment markers shows enrichment of the cytoplasmic marker HSP90 in lane S1, the membrane bound compartment marker calreticulin in lane S2, the nuclear marker MLH1 in lane S3, and the chromatin bound compartment marker histone 3 in lane S4.

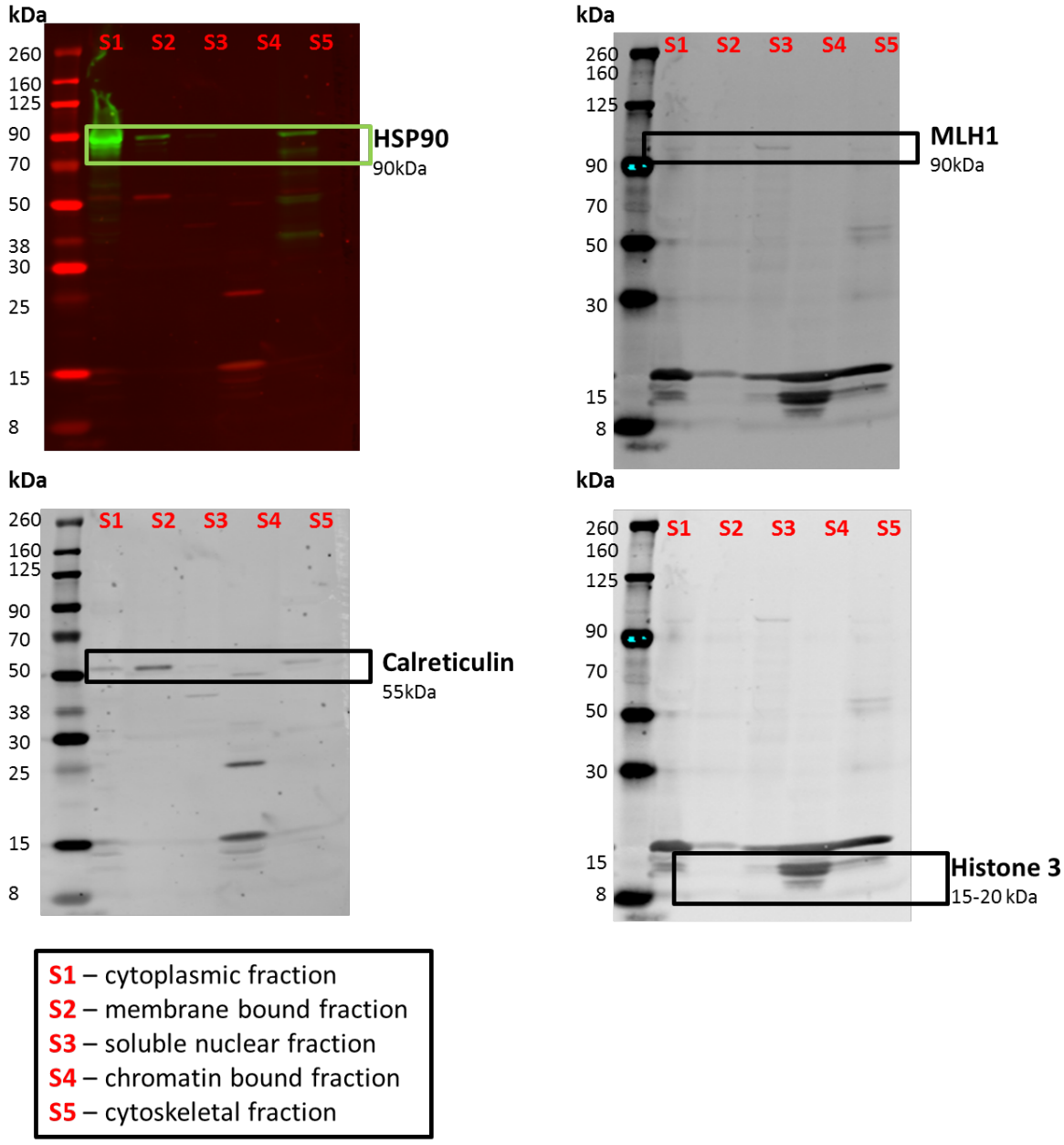


**Figure 6.12: Subcellular fractionation of 73Q clone 3 MSNs (dd47).** Western blotting with cell compartment markers shows enrichment of the cytoplasmic marker HSP90 in lane S1, the membrane bound compartment marker calreticulin in lane S2, the nuclear marker MLH1 in lane S3, and the chromatin bound compartment marker histone 3 in lane S4.

#### 6.5.2.3 Measurement of total and mHTT levels in iPSC-derived MSNs and cell fractions

The Erenna Singulex human huntingtin protein detection assay was used to quantify levels of total and mHTT in whole cell pellets and cell fractions of MSN control 20Q and mutant 73Q lines. The three epistemic replicates (clones) of the control 20Q and 73Q line were analysed, with the results as shown in figure 6.13 (mHTT) and figure 6.14 (total HTT).

Mutant huntingtin is confirmed to be present in the 73Q line but not in the control line. Within the 73Q line, mHTT is present in all fractions tested although the concentration detected in the chromatin bound fraction is low enough to be considered background noise. The presence of endogenous soluble mutant huntingtin is observed in the nucleus of human HD MSNs, where it is found at a much lower concentration than seen in cytoplasm and membrane-bound compartments, a pattern that was also observed in the 129Q HTT exon 1 mutant ReNcellVM line.

The total HTT assay detects wild-type HTT in the control MSN line, and both mutant and wild-type HTT in the 73Q MSN line. Results show that the highest concentration of HTT is in the cytoplasm and membrane-bound fractions in both lines. Soluble HTT is again found in the nuclear fraction of both control and mutant MSN lines, at a much lower level, and suggests the presence of soluble wild-type huntingtin in the nucleus of human control MSNs.

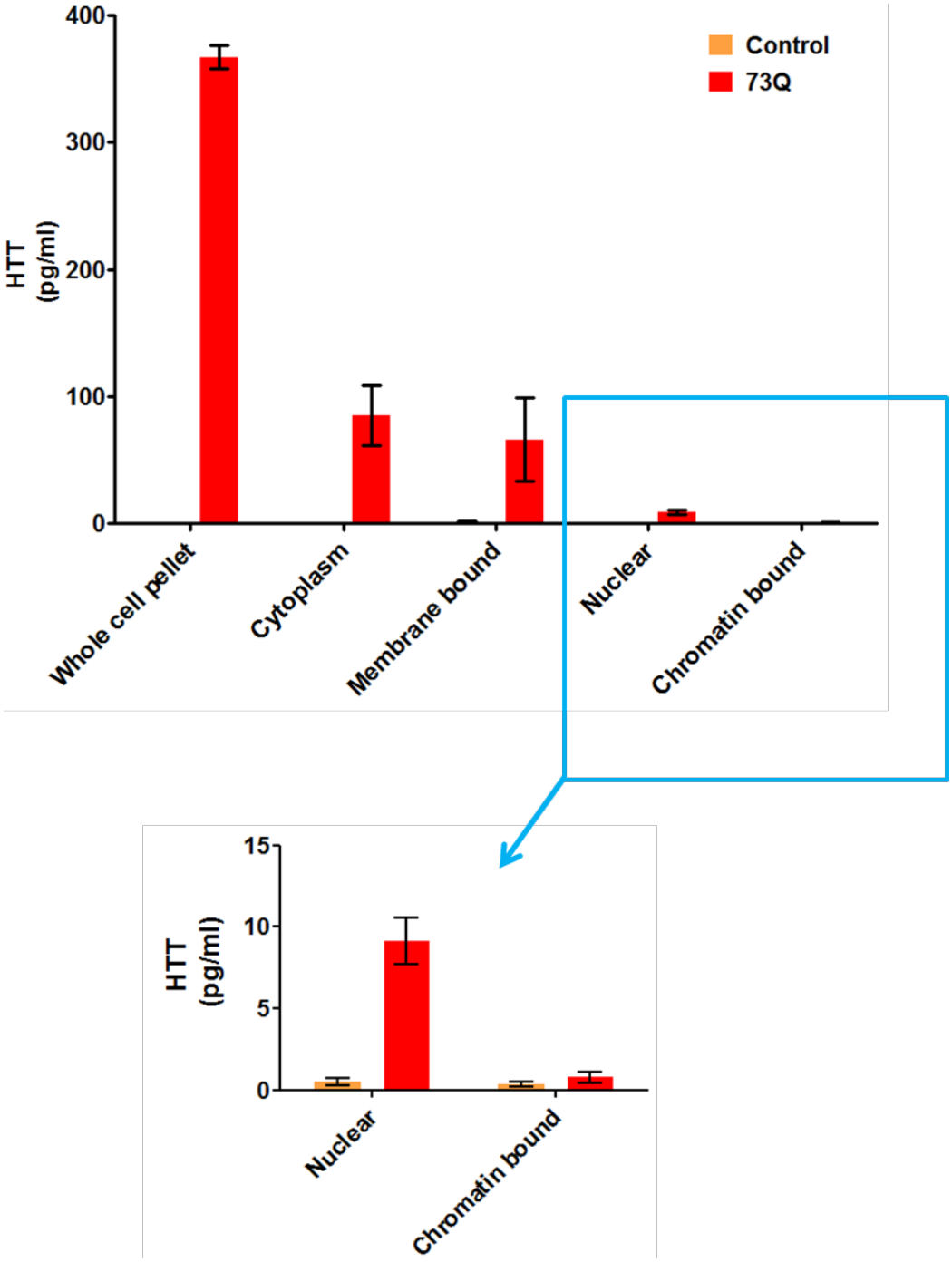


**Figure 6.13: Mutant HTT levels in control and 73Q MSNs and MSN cell fractions.** mHTT is detected in all fractions of the mutant 73Q line, though levels shown in the chromatin-bound fraction are likely to be background noise. As expected, no mHTT is found in the control MSN line. The concentration of mHTT in the nucleus is extremely low in comparison to the cytoplasm and membrane-bound compartments. (n=3, biological replicates).

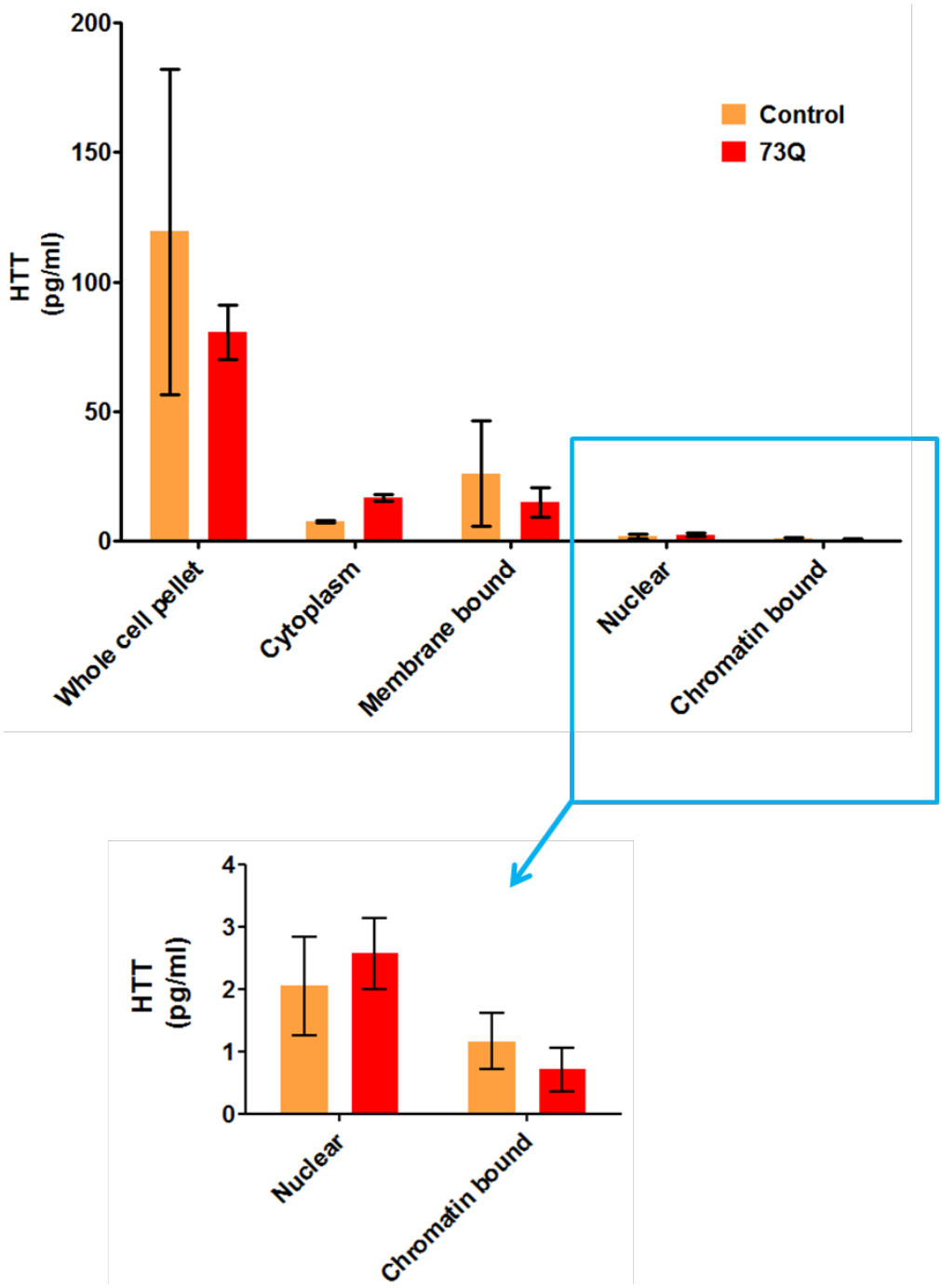


**Figure 6.14: Total HTT levels in control and 73Q MSNs and MSN cell fractions.** HTT is detected in both line in all fractions, though ultra-low levels in the chromatin bound fraction is likely to be background noise. The concentration of soluble HTT is highest in cytoplasm and membrane-bound compartments, with much lower levels found in the nucleus. There are no significant differences between the two lines in any of the cell fractions (Two-way ANOVA with Bonferroni's correction, n=3 (biological replicates)).

The total HTT assay uses a combination of 2B7 and 4C9 antibodies to detect all HTT present, both mutant and wild-type (provided the N-terminal is present). 4C9 binds to the polyproline region on the N-terminal and is not polyQ length dependent – therefore between-line comparisons can be made and statistical analysis carried out. Two-way ANOVA of the results revealed no significant difference between the HTT concentration of control and 73Q MSNs in any of the fractions tested.

The total HTT concentration was much lower (at least ten-fold in the case of control lines and 20-30 fold in the case of the mutant lines) in the nucleus of the MSN samples compared to the HTT exon 1 ReNcellVM lines, suggesting that in both control and mutant ReNcellVM lines, the HTT exon 1 protein is the principle component of the nuclear fraction.

## 6.6 Discussion

Subcellular fractionation followed by the measurement of HTT levels using the Erenna Singulex assay was used to study the trafficking of HTT in HTT exon 1 overexpressing ReNcellVM neurons and in iPSC-derived MSNs. Using this approach, some soluble wild-type HTT was found in the nucleus of human MSNs, and soluble mHTT was detected in human HD MSNs. A similar pattern was found in the HTT exon 1 overexpressing ReNcellVM line, with both soluble 29Q HTT exon 1 (control) and 129Q HTT exon 1 (mutant) present in the nucleus. In all cases, the concentration of nuclear HTT was considerably lower than that in the cytoplasm. This finding is consistent with previous studies that have shown the presence of wild-type and mutant HTT in the

nucleus of mammalian cell lines, but at a lower concentration than in the cytoplasm (De Rooij et al, 1996; Dorsman et al, 1999).

In the ReNcellVM lines, the concentration of nuclear mutant 129Q HTT exon 1 was over double that of 29Q HTT exon 1 (as measured by the total HTT 2B7/4C9 assay, as a proportion of the whole cell pellet HTT level). This would suggest that mutant HTT exon 1 accumulates more readily in the nucleus than control HTT exon 1, although it should be noted that the presence of "wild-type" HTT exon 1 (in contrast to full-length HTT) has never been confirmed in control human neurons. This assay does not detect aggregates or inclusions, but it is possible that mHTT oligomers that are formed along the pathway to IB generation in the 129Q line are detected by this assay. Mutant HTT oligomeric species may not be able to exit the nucleus (due to increased size/conformation), and therefore the concentration of soluble mHTT is higher in the nuclear compartment of the 129Q line compared to the 29Q control. Another possibility is that due to a conformational change in the 129Q HTT exon 1, the N17 nuclear export signal (Maiuri et al, 2013) is less accessible. A previous study has found that small N-terminal HTT fragments interact with the nuclear pore protein translocated promoter region (Tpr), which is involved in nuclear export. PolyQ expansion and aggregation decreases this interaction, impairs nuclear export of N-terminal mHTT and increases the nuclear accumulation of mHTT (Cornett et al, 2005).

No significant differences were found between the trafficking of wild-type and mutant HTT in the control and mutant MSN lines, with the distribution of soluble HTT similar across all cell compartments in both cases. This may suggest that the pathogenic pathways triggered by mHTT are due to its aberrant interactions within key cellular

pathways, rather than any deficit or alteration in the trafficking of the HTT protein itself. Another possibility is that differences in HTT trafficking are only apparent in the context of cell stress and this experiment was performed in unstressed neurons. Multiple lines of evidence now suggest that nuclear localisation of wild-type HTT occurs in response to cell stress (Atwal et al, 2007; DiGiovanni et al, 2016), where it localises to sites of DNA damage and acts as a scaffold for proteins of the DNA repair pathway, in a process that is impaired in HD cells (Maiuri et al, 2017). Localisation of wild-type HTT to early endosomes also occurs as part of a rapid stress response and mutant HTT displays defective recovery from this (Nath et al, 2015).

It is notable that although mutant 129Q HTT exon 1 seems to accumulate in the nucleus more readily than control 29Q HTT exon 1, the levels of total HTT were not higher in the nuclei of mutant compared to control MSNs. This may be due to the fact that N-terminal HTT overexpression models exhibit phenotypes on a much faster timescale than full-length HTT models. Mutant HTT exon 1 is considerably smaller than full length mHTT and may enter the nucleus more readily, with higher expression levels leading to faster build-up. Alternative splicing is thought to lead to the generation of mHTT exon 1 from full-length mHTT, a process that may be occurring in the 73Q MSN line (Neueder et al, 2017; Sathasivam et al, 2013); however it is possible that more time would be needed to accumulate biologically significant levels of mHTT exon 1 in this manner.

One issue that was encountered in using this approach to study HTT trafficking was that the technical replicates of HTT measurement using the Erenna Singulex assay showed some variability, and in the case of the MSNs, there was also variation

between clones. This variation was present even in the whole cell pellets and therefore is not due to the fractionation technique. In addition, subcellular fractionation is not completely precise, with loss of cell material during the fractionation steps. In making between-lines comparisons however, this effect is partly mitigated.

Another issue is that the proportion of MSNs generated in culture was not quantified prior to subcellular fractionation of the global culture. This work is currently on-going in the lab, but previous studies have reported that this differentiation protocol generates cultures with 50% MSNs (Arber et al, 2015). MSNs are GABAergic striatal projection neurons derived from the progenitor zone of the lateral ganglionic eminence (LGE); LGE progenitors may be defined by the combinatorial expression of several transcription factors including FoxP1, FoxP2, CTIP2, Nolz1, Dlx2 and Gsx2, all of which regulate fate specification of MSNs. The presence of mature MSNs is generally demonstrated by the presence of DARPP-32 staining, but mature MSNs also express CTIP2, GAD 65/67; neuronal identity can be confirmed by co-staining with MAP2 or NeuN markers. MSNs also have a distinct appearance comprising a branching, multipolar morphology with numerous spines. Quantification of MSNs using immunofluorescence staining with combinations of markers, prior to fractionation, would have been useful to understand the degree to which this study represents the trafficking of HTT within actual MSNs, as it is not possible currently to separate these MSNs from the surrounding culture prior to experimentation.

Live-cell imaging would be a useful approach to study HTT trafficking in neurons; however in both the HTT exon 1 overexpressing ReNcellVM neurons and the iPSC-derived MSNs, there is no fluorescent tag to allow visualisation of the HTT protein. The

presence of such a tag fused onto the HTT protein may also alter its dynamics, and would not in any case allow visualisation of the endogenous HTT within the MSNs. Recently a novel approach using HTT intrabodies fused to fluorescent proteins has been utilised to study HTT trafficking in human retinal epithelial cells; intrabodies are expressed within the cell and can be manipulated to bind to HTT within particular cell compartments (Maiuri et al, 2017). In the future, such a method may allow the visualisation of endogenous wild-type and mHTT within patient derived cells.

## 6.7 Summary

A study of HTT trafficking in the HTT exon 1 overexpressing ReNcellVM lines has shown that mutant (129Q) HTT exon 1 accumulates in the nucleus more readily than control (29Q) HTT exon 1. However, there were no significant differences between the trafficking of wild-type and mHTT in the control and mutant iPSC-derived MSN lines. Soluble HTT, both wild-type and mutant, was detected in the nucleus of control and HD MSNs respectively.

# 7 Conclusions and future work

Over thirty years have passed since the discovery of the causative genetic mutation in Huntington's disease (Huntington's Disease Collaborative Research Group, 1993), but a full understanding of the mechanisms by which the consequent neuronal degeneration occurs remains incomplete. *HTT* CAG-repeat length is the key determinant of disease status and is inversely correlated with age at disease onset; an understanding of how increasing CAG-repeat length drives increasing neurotoxicity will likely further our knowledge of HD pathogenesis and help to guide research efforts in HD therapeutics. This thesis describes the development of novel *HTT* allelic series human neuronal cell models of HD, and subsequent experiments to determine the effect of CAG-repeat length on neuronal phenotypes and on the HTT protein itself.

## 7.1 Conclusions and main findings

### 7.1.1 Generating a HTT allelic series neuronal cell model of Huntington's disease

HD is a human neurodegenerative disease and therefore it is likely that cell culture models comprising human neurons are most likely to recapitulate the true pathogenic mechanisms underpinning disease. Increasing *HTT* CAG-repeat length on an otherwise constant genetic background eliminates any genetic heterogeneity that might

also affect disease-associated phenotypes. Consequently attempts were made here to create an isogenic HTT allelic series in the human neural stem cell (NSC) ReNcellVM line using rAAV vectors to knock in increasing CAG repeat lengths into the endogenous *HTT* locus. For a number of potential reasons this approach was not successful; the rate of homologous recombination in the ReNcellVM line was much lower than expected (Khan et al, 2011; Khan et al, 2010) and it is possible that the length of the desired insertion sequence may have been too long relative to the length of the guidance homology arms. In addition, pools of cells initially containing the positively integrated vector lost this over subsequent passages or freeze/thaw, perhaps due to a selective advantage of wild-type cells in the speed of cell division/doubling time and/or in their tolerance of cell stress. Indeed there is evidence that mHTT affects mitotic spindle formation (Godin et al, 2010) and cells expressing mHTT are known to be more sensitive to stress (Zhang et al, 2010).

Next, efforts were made to optimise and characterise a human neural stem cell HTT exon 1 overexpression model of HD. An allelic series containing HTT exon 1 with 29Q, 71Q and 129Q repeats with relatively matched expression levels was generated in ReNcellVM NSCs. This panel was shown to differentiate into B3-tubulin positive cells, a proportion of which displayed HTT inclusion bodies in the pathogenic lines (71Q and 129Q). HTT exon 1 and N-terminal fragment models of HD have many advantages over full-length HTT models. Mutant phenotypes develop over a much faster timescale and are therefore more amenable for study, as has been demonstrated by the R6/2 mouse model (Mangiarini et al, 1996), and HTT exon 1 cell models of rat striatal progenitors (Colby et al, 2006) and human neuroblastoma cells (Ho et al, 2001). An abnormal splicing mechanism (Sathasivam et al, 2013) for the generation of mHTT

exon 1 has been shown in patient derived fibroblasts and post-mortem human brain tissue (Neueder et al, 2017), and many studies have indicated the importance of HTT exon 1 in HD pathogenesis (DiFiglia et al, 1997); (Barbaro et al, 2015; Landles et al, 2010).

To complement this HTT exon 1 model, a full length HTT model was also generated in iPSCs derived from a genetically related HD family comprising three siblings with juvenile HD carrying *HTT* with 56, 67 and 73 CAG repeats respectively, and their unaffected mother (as control). These lines were shown to differentiate into a high proportion of MSNs, the predominant cell type that is affected in HD. Induced PSCs derived from patients are the most genetically precise disease model, but comparison between control and HD lines may be hampered by background genetic heterogeneity of the donors. In generating new HD-iPSC lines using fibroblasts from the same family, it was hoped that the impact of genetic heterogeneity would be diminished when making between-line comparisons of neuronal phenotypes. Previous studies in HD-iPSC derived neurons have reported subtle differences compared to control iPSCs in terms of protein expression, differentiation efficiency and neurite length (Chae et al, 2012), as well as in lysosomal function (Camnasio et al, 2012) and caspase 3/7 activity (Zhang et al, 2010). In addition, HD-iPSC lines have been shown to display neurodevelopmental abnormalities on differentiation (Conforti et al, 2018).

In recent years, advances in iPSC research have led to improvements in reprogramming techniques (Fusaki et al, 2009) and neuronal differentiation protocols (Arber et al, 2015). In addition, the development of CRISPR (clustered regularly

interspaced short palindromic repeats)/Cas9 (CRISPR-associated system 9) nuclease for precision genome editing has revolutionised the field of molecular biology. Indeed this technique has recently been used to create the first isogenic HTT allelic series in human embryonic stem cells (hESCs) (Ruzo et al, 2018). Use of CRISPR/Cas9 to create an isogenic HTT allelic series in the ReNcellVM line is also feasible, and such a line would be highly suitable for high content screening of therapeutic compounds due to its robust and rapid neuronal differentiation.

### 7.1.2 Effect of increasing HTT exon 1 CAG repeat length on human neuronal phenotypes

Having optimised a HTT exon 1 overexpressing allelic series in the ReNcellVM line, the effect of increasing CAG-repeat length on neuronal phenotype and the response to cell stress was then studied. A small decrease in B3-tubulin positive cells was seen in the 129Q ReNcellVM on neuronal differentiation, and there was a marginal increase in anti-activated caspase 3 staining in the highly expressing 71Q-H ReNcellVM line, as detect by high content imaging and analysis. Surprisingly, the HTT exon 1 ReNcellVM allelic series did not display overt neuronal toxicity or increased vulnerability to toxins in the pathogenic lines.

The lack of obvious overt pathogenic neuronal phenotypes in this line may reflect the fact that the symptoms of HD take many years to manifest, even in patients who have juvenile HD. Neuronal cultures derived from the HTT exon 1 ReNcellVM lines displayed persistent GFAP and nestin staining and were therefore relatively immature/not true neurons (section 3.5.3.3), and it is possible that an extended period of cell

culture/aging is needed before neuronal toxicity is evident the pathogenic lines. In addition, the HTT exon 1 ReNcellVM lines have relatively low levels of HTT exon 1 overexpression (levels are often not published in papers using other transgenic HTT exon 1 models) and wild-type huntingtin is known to have a neuroprotective effect (Rigamonti et al, 2001).

The finding that B3-tubulin expression is slightly reduced in the 129Q ReNcellVM line may hint towards adverse neuronal differentiation in this line, although the finding that none of these cell lines differentiated into true neurons should be borne in mind. In support of this, recent papers have described an effect of mutant HTT on early neurodevelopment, in terms of chromosomal instability and failed cytokinesis (Ruzo et al, 2018), as well as impaired neuro-ectodermal acquisition and disrupted cytoarchitecture (Conforti et al, 2018). The increased anti-activated caspase 3 staining in the highly expressing 71Q-H ReNcellVM line is backed by studies showing that caspase 3 activation is detected on Western blotting of cell lysates after 24 hours of mutant but not control length HTT exon 1 expression in PC12 cells (Sahoo et al, 2016). Activated caspase 3 is a key effector of apoptosis and its increased presence in 71Q-H ReNcellVM cells may be a marker of early toxicity in this line.

### 7.1.3 The effect of increasing CAG repeat length on HTT exon 1 protein in human neuronal cells

HTT exon 1 ReNcellVM neurons developed nuclear HTT inclusion bodies (IBs) in a manner proportional to CAG-repeat length and the level of HTT exon 1 overexpression, confirming previous findings (Scherzinger et al, 1999). Interestingly, only a small

percentage of cells developed IBs, even in the highly expressing 71Q-H line. Super-resolution imaging confirmed that nuclear inclusion formation is an “all-or-nothing” process with an apparent shift in HTT exon 1 distribution from cytoplasm to nucleus that accompanies IB formation. Why certain cells should be susceptible to this process is not clear, however it is possible that on prolonged culture greater numbers of cells would accumulate IBs as HD is generally an adult-onset, progressive disease.

Neuronal inclusion formation was not associated with cell death or increased levels of activated caspase-3 staining, suggesting that they are not intrinsically harmful (Arrasate et al, 2004). Cells with nuclear IBs were however noted to be more rounded in shape and have reduced expression of cell markers, suggesting that cells with nuclear IBs become “inert” and do not differentiate as well as the surrounding culture. This is consistent with recent studies suggesting that inclusion formation is neither harmful nor protective but triggers a state of cellular quiescence (Ramdzan et al, 2017). A wide range of nuclear IB size was observed in the ReNcellVM cells, supporting previous studies which suggest that IBs are comprised of a heterogeneous population including amyloid aggregates with a β-sheet structure (Caron et al, 2014; Nekooki-Machida et al, 2009) and inclusions at various stages of maturity (Duim et al, 2014).

Having determined that mHTT exon 1 exists in a number of forms in the HTT exon 1 ReNcellVM lines, the impact of proteostasis modulation on the accumulation, distribution and clearance of mHTT exon 1 was investigated. Treatment with the autophagy inhibitor bafilomycin resulted in increased HTT staining throughout the whole neuron (nucleus, cytoplasm and axons), whereas proteasomal inhibition with MG132 led to a striking redistribution of HTT exon 1, with increased staining in nuclear

and perinuclear regions, and no axonal/cytoplasmic signal. This may suggest that clearance of mHTT occurs via both autophagy and the UPS, and is particularly UPS dependent in nuclear/perinuclear areas. Alternatively, MG132 may be affecting HTT trafficking, either directly or indirectly. Unfortunately, proteasomal enhancement with USP14 inhibitors provided by Proteostasis Therapeutics Inc (PTI) did not clear mHTT exon 1 from the pathogenic ReNcellVM lines, despite previous studies suggesting this as a promising therapeutic approach in HD (Bhat et al, 2014). This may be due to a lack of target (USP14) engagement in these cells, or overwhelming the UPS with a general increase in ubiquitinated proteins.

### 7.1.4 Trafficking of huntingtin in HTT exon 1 ReNcellVM neurons and in iPSC-derived medium spiny neurons

The trafficking of HTT between different cellular compartments in HTT exon 1 overexpressing ReNcellVM neurons was studied using subcellular fractionation followed by the measurement of soluble HTT levels using the Erenna Singulex assay. This revealed that mutant (129Q) HTT exon 1 accumulated in the nucleus more readily than control (29Q) HTT exon 1, but in both cases the concentration of nuclear HTT was considerably lower than that of the cytoplasm. This finding was not unexpected (De Rooij et al, 1996; Dorsman et al, 1999); mutant HTT exon 1 may be less readily exported from the nucleus due to its propensity to form mHTT oligomers en route to IB generation. PolyQ expansion and aggregation has been previously shown to decrease the interaction of small N-terminal HTT fragments with the nuclear pore protein, leading to impaired nuclear export and nuclear accumulation of mHTT (Cornett et al, 2005).

The same experimental approach was used in control and mutant (73Q) iPSC-derived MSNs and revealed no significant difference between the trafficking of full-length wild-type and mHTT in these cells. Soluble HTT, both wild-type and mutant, was detected in the nucleus of control and HD MSNs respectively, again at a much lower concentration than that of the cytoplasm. However it is worth noting that the MSNs that were studied using this approach were part of a global cell culture, and were not quantified prior to subcellular fractionation. Previous studies have suggested this differentiation protocol generates 50% MSNs as defined by DARPP-32 staining (Arber et al, 2015); however even at this proportion any MSN specific findings may be missed and at present it is not possible to separate intact MSNs from the surrounding culture. Future experiments on these iPSC lines will require some form of immunofluorescence quantification in order to ascribe differences to MSNs specifically.

It is possible that differences in HTT trafficking between wild-type and mutant protein may only be apparent under conditions of cell stress; wild-type HTT undergoes nuclear localisation in response to cell stress (Atwal et al, 2007; DiGiovanni et al, 2016), where it localises to sites of DNA damage and acts as a scaffold for proteins of the DNA repair pathway, in a process that is impaired in HD cells (Maiuri et al, 2017). Wild-type HTT also localises to early endosomes as part of a rapid stress response and mutant HTT displays defective recovery from this (Nath et al, 2015).

The utility of using both HTT exon 1 and full-length HTT iPSC-derived models is highlighted by this study of HTT trafficking, in which different results were observed in each model. The ReNcellVM HTT exon 1 model exhibited a mutant trafficking phenotype by two weeks of differentiation, whereas this was absent in the more

genetically precise iPSC-derived MSN model. This may reflect the fact that N-terminal HTT overexpression models exhibit phenotypes on a much faster timescale than full-length HTT models. However, there is also the possibility that HTT exon 1 cell models exhibit phenotypes that are not present or different in full-length HTT cell models; repeating this experiment in MSNs following prolonged culture would distinguish between these two possibilities.

## 7.2 Insights and future work

Over ten years have passed since the discovery that iPSCs could be generated by the expression of four key factors in somatic cells (Takahashi et al, 2007). Since that time iPSC models have been generated for many neurodegenerative diseases, and differentiation protocols have been optimised to generate a range of neuronal cell types (Arber et al, 2015; Shi et al, 2012). The advantages of iPSC based modelling are that the cells represent one of the most genetically precise cell models to date, and that once generated, they form a renewable resource for the entire research community. They may in the future also provide a source of neurons for transplantation into patients, either from healthy donor cells or from autologous fibroblasts modified to correct the causative genetic mutation. However, neuronal differentiation protocols are generally still long and complex, as they attempt to recapitulate various stages of neuronal development. In addition they do not display overt mutant phenotypes on timescales compatible with standard research protocols, though they may allow the study of some of the earlier, subtler phenotypes that precede neurodegeneration.

Recently the direct reprogramming of human fibroblasts into striatal MSNs has been achieved through the ectopic expression of brain-enriched microRNAs (miRNAs) miR-9/9* and miR-124 (miR-9/9*-124), co-expressed with transcription factors enriched in the developing striatum (Victor et al, 2014). The method has also been applied to HD patient fibroblasts, and the resulting HD MSNs readily displayed HD-associated phenotypes, including the formation of mHTT aggregates, DNA damage, spontaneous neuronal death in culture, and a decline in mitochondrial function (Victor et al, 2018). Unlike iPSC-derived MSNs, HD-associated phenotypes are thought to result from the retention of the cellular age-related features when directly reprogramming cells; this includes epigenetic changes, oxidative stress, and any DNA damage already sustained by the donor cell. These elements are lost when reprogramming fibroblasts into iPSCs by traditional means.

In the case of HD, there remains a role for HTT exon 1 or N-terminal fragment overexpression models that overcome some of these limitations of iPSCs. In particular, such models lend themselves to high content screening of therapeutics as they can be easily generated in cells that are amenable to high throughput cell culture and generally have more overt disease phenotypes. However many potential therapeutic agents show promise in early stages of drug testing and then fail in human trials, and this may in part be because the models used for testing are not fully representative of the disease state. A combined approach using HTT exon 1 models for initial compound screening, followed by more targeted iPSC-based experiments may be the most suitable approach for the future.

Technology for high content screening (HCS) has advanced rapidly in recent years. HCS refers to the automated and rapid measurement of multiple cell parameters with cell imaging, in a high throughput manner. Most commonly HCS is used in drug discovery to visually identify phenotypic changes in response to various test compounds. However HCS can also be used to identify and quantify biological and pathogenic processes (Carty et al, 2015), and in this thesis was used to demonstrate CAG-repeat length dependent changes in IB formation in the ReNcellVM line. The acquisition of thousands of images in an automated manner allows for objective and robust statistical analysis of the results, and can identify rarer phenotypes in a small percentage of cells. The disadvantage is the need to optimize differentiation of cells in 96- or 384-well plates that are amenable to confocal imaging, however with improvements in general cell culture protocols, this will likely be overcome in the near future.

The long-standing debate over the role of HTT inclusions in the pathogenesis of HD has still not been fully resolved, with studies suggesting that they may be harmful, protective or neutral. In this study IBs were found to be associated with increased nuclear size and reduced expression of cell markers but not with increased cell death. As HTT is an intracellular protein, it was not possible to visualize inclusion formation in living ReNcellVM cells, or to separate IB containing cells from the surrounding culture. Previous studies have achieved this using cell models containing fluorescently tagged HTT exon 1 with pulse-shape analysis (PulSA) by flow cytometry (Ramdzan et al, 2012), however it is possible that the presence of a tag affects the behaviour and dynamics of the HTT protein. Recently a novel approach using HTT intrabodies fused to fluorescent proteins has been utilised to study HTT trafficking in human retinal epithelial cells (Maiuri et al, 2017). This approach could be used to study inclusion

formation in the HTT exon 1 ReNcellVM line, and also in iPSC-derived MSNs. Combined with live-cell imaging techniques, HTT intrabodies could also be an alternative method to study HTT trafficking in the MSN lines in the future.

It is clear that HD pathogenesis involves a variety of cellular mechanisms and a number of key questions remain; this includes the reason for the specific striatal degeneration that is observed, why only certain cells develop HTT inclusions, and the factors that trigger the actual onset of disease or neurodegeneration in patients after a period of clinically normal neurodevelopment and brain function. The answer to these questions and further insights into HD pathogenesis may provide alternative avenues to therapies for HD, as there are currently no disease-modifying treatments available. However a promising approach that is currently undergoing clinical trials in patients is the lowering of HTT levels using anti-sense oligonucleotides delivered by intra-thecal injection. This would minimise all the downstream negative effects of mHTT protein expression, and the drug has been shown to be safely tolerated in a Phase 1/2a trial in early stage HD patients (Tabrizi et al). Whilst the search for small molecule therapeutics continues, HTT lowering offers real hope to HD patients for a viable treatment in the coming years.

# Appendix

## A.1 Media components

Unless stated otherwise, all cell culture reagents were from purchased Gibco and supplementary chemicals were from Sigma-Aldrich.

### A.1.1 Neural stem cell medium

NSC medium comprised Dulbecco's Modified Eagle's Medium (DMEM): Nutrient Mixture F-12 (F12) supplemented with:

0.03% Human albumin solution

5 µg/ml Transferrin (human recombinant)

16.2 µg/ml Putrescine dihydrochloride

5 µg/ml Insulin (human recombinant)

400 ng/ml L-thyroxine

337 ng/ml Tri-iodo-thyronine

60 ng/ml Progesterone

2mM L-glutamine

40 ng/ml Sodium selenite

10 Units/ml Heparin sodium

10 ng/ml Corticosterone

10 ng/ml basic Fibroblast growth factor (bFGF) [Peprotech]

20 ng/ml Epidermal growth factor (EGF) [Peprotech]

### A.1.2 Neural differentiation medium

The basic neural differentiation medium was the same as the NSC medium listed above, but without bFGF or EGF. For ReNcell VM differentiation, the concentration of L-glutamine was reduced to 0.5 mM after 2 weeks.

### A.1.3 HEK culture medium

HEK culture medium comprised DMEM:F12 with:

2 mM L-glutamine

10% fetal bovine serum (FBS) [Invitrogen]

100 U/ml penicillin 0.1 mg/ml streptomycin [Invitrogen]

### A.1.4 HCT116 culture medium

This comprised McCoy's 5A modified medium with:

2 mM L-glutamine

10% FBS

50 U/ml penicillin 50 ug/ml streptomycin

### A.1.5 Fibroblast culture medium

Fibroblast culture medium comprised DMEM with glutamax and 4.5g/L of glucose and 1mM pyruvate with:

10% foetal bovine serum (FBS)

50 U/ml penicillin, 50 ug/ml streptomycin

2.5 ml/L amphotericin B

The amphotericin was added just prior to use for the first two weeks of cell culture, after which its addition was no longer required.

### A.1.6 N2B27 differentiation medium for MSNs

This comprised 2/3 volume DMEM:F12 medium and 1/3 volume Neurobasal with:

1:100 L-Glutamine

1:150 N2

1:150 B27 (without vitamin A until dd26 and with vitamin A post dd26)

0.1 mM B-mercaptoethanol

## A.2 Antibodies for Western blotting and confocal microscopy

### A.2.1 Western blotting

**Appendix Table A.1:** Primary and secondary antibodies used in Western blotting

| Primary antibody | Dilution | Species | Supplier |
|---|---|---|---|
| S830 (Anti-HTT) | 1:2000 | Sheep | Bates (in house) |
| 4C9 (Anti-HTT) | 1:1000 | Mouse | CHDI |
| aa 1-82 (N82) (Anti-HTT) | 1:500 | Mouse | Merck |
| MW1 (Anti-HTT) | 1:1000 | Mouse | Merck |
| 3B5H10 (Anti-HTT) | 1:2000 | Mouse | Merck |
| D7F7 (Anti-HTT) | 1:1000 | Rabbit | Cell Signaling Technology |
| 2B7 (Anti-HTT) | 1:750 | Mouse | CHDI |
| MAB2166 (Anti-HTT) | 1:1000 | Mouse | Merck |

| | | | |
|---|---|---|---|
| Green fluorescent protein (GFP) | 1:2000 | Rabbit | Santa-Cruz |
| Glyceraldehyde 3-phosphate dehydrogenase (GAPDH) | 1:10,000 | Rabbit | Merck |
| Beta-actin | 1:10,000 | Mouse | Merck |
| Beta-actin | 1:5000 | Rabbit | Merck |
| Beta 3 tubulin (B3T) | 1:5000 | Rabbit | Abcam |
| Glial fibrillary acidic protein (GFAP) | 1:5000 | Rabbit | Abcam |
| Nestin | 1:5000 | Mouse | Abcam |
| Microtubule-associated protein 2 (MAP2) | 1:1000 | Rabbit | Merck |
| Human HuD neuronal protein (HuD) | 1:500 | Rabbit | Merck |
| Oligodendrocyte transcription factor 1 (Olig 1) | 1:250 | Mouse | Merck |
| Neurofilament (NF200) | 1:250 | Mouse | Merck |
| Heat shock protein 90 (HSP90) | 1:1000 | Mouse | Abcam |
| Calreticulin | 1:500 | Rabbit | Abcam |
| Mismatch repair endonuclease PMS2 (PMS2) | 1:200 | Rabbit | Merck |
| MutL homolog 1 (MLH1) | 1:1000 | Mouse | Merck |
| Histone 3 (H3) | 1:5000 | Mouse | Cell Signaling Technology |
| Secondary antibody | Dilution | Species | Supplier |
| IRDye 800CW anti-goat | 1:10,000 | Donkey | LI-COR |
| IRDye 680LT anti-mouse | 1:10,000 | Goat | LI-COR |
| IRDye 680LT anti-rabbit | 1:10,000 | Goat | LI-COR |
| IRDye 800CW anti-mouse | 1:10,000 | Goat | LI-COR |
| IRDye 800CW anti-rabbit | 1:10,000 | Goat | LI-COR |

### A.2.2 Confocal microscopy (including high content screening)

**Appendix Table A.2:** Primary and secondary antibodies used for confocal microscopy and high content screening

| **Primary antibody** | **Dilution** | **Species** | **Supplier** |
|---|---|---|---|
| S830 (Anti-HTT) | 1:250-500 | Sheep | Bates (in house) |
| EM48 (Anti-HTT) | 1:50-100 | Mouse | Merck |
| aa 1-82 (Anti-HTT) | 1:200-500 | Mouse | Merck |
| 4C9 (Anti-HTT) | 1:500 | Mouse | CHDI |
| MW1 (Anti-HTT) | 1:500 | Mouse | Merck |
| 3B5H10 (Anti-HTT) | 1:500 | Mouse | Merck |
| MAB2170 (Anti-HTT) | 1:500 | Mouse | Merck |
| Beta 3 tubulin (B3T) | 1:500 | Rabbit | Abcam |
| Glial fibrillary acidic protein (GFAP) | 1:500 | Rabbit | Abcam |
| Nestin | 1:600 | Mouse | Abcam |
| Caspase 3 | 1:100 | Rabbit | Abcam |
| Microtubule-associated protein 2 (MAP2) | 1:200 | Rabbit | Sigma |
| Dopamine- and cAMP-regulated phosphoprotein, 32 kDa (DARPP-32) | 1:500 | Rabbit polyclonal | Abcam |
| Forkhead box protein P1 (FOXP1) | 1:500 | Mouse monoclonal | Abcam |
| **Secondary antibody** | **Dilution** | **Species** | **Supplier** |
| Anti-goat IgG (H+L) Alexa Fluor 546 | 1:10000 | Donkey | Thermo |
| Anti-rabbit IgG (H+L) Alexa Fluor 633 | 1:10000 | Goat | Abcam |

| | | | |
|---|---|---|---|
| Anti-rabbit IgG (H+L) Alexa Fluor 488 | 1:10000 | Goat | Abcam |
| Anti-rabbit IgG (H+L) Alexa Fluor 568 | 1:10000 | Goat | Abcam |
| Anti-mouse IgG (H+L) Alexa Fluor 568 | 1:10000 | Donkey | Abcam |
| Anti-mouse IgG (H+L) Alexa Fluor 633 | 1:10000 | Goat | Abcam |
| Anti-mouse IgG1 Alexa Fluor 488 | 1:10000 | Goat | Abcam |
| Anti-mouse IgG2 Alexa Fluor 568 | 1:10000 | Goat | Abcam |

## A.3 Solutions and buffers

**Lysis buffer** to prepare Exon 1 overexpressing ReNcells for Western blotting:

PBS

1% Triton X-100

0.5% sodium deoxycholate (SDS)

1x protease inhibitor cocktail [Roche] (1 tablet diluted in 500 µl of $H_20$ makes a 100x solution that can be kept for 2 weeks at -20°C)

**5x sample buffer** to prepare lystaes for Western blottin):

0.625M Tris pH 6.8

50% glycerol

10% (w/v) SDS

Trace Bromophenol blue

10% β-mercaptoethanol (added in the fume hood)

This 5x sample buffer can be stored at -20°C and freeze-thawed. The solution is diluted in water to make 1x sample buffer.

**10x running buffer** for Western blotting:

0.25M Tris pH 8.6

1.92M Glycine

1% SDS

The solution is diluted in water to make 1x running buffer.

**1x transfer buffer** for Western blotting. To make 1 L:

100 ml of 10x transfer buffer:

0.25M Tris pH 8.6

1.92M Glycine

200 ml methanol

700 ml dd$H_20$

# References

(1993) A novel gene containing a trinucleotide repeat that is expanded and unstable on Huntington's disease chromosomes. The Huntington's Disease Collaborative Research Group. *Cell*, 72(6), 971-83.

(1994) Guidelines for the molecular genetics predictive test in Huntington's disease. International Huntington Association (IHA) and the World Federation of Neurology (WFN) Research Group on Huntington's Chorea. *Neurology*, 44(8), 1533-6.

Almqvist, E. W., Elterman, D. S., MacLeod, P. M. & Hayden, M. R. (2001) High incidence rate and absent family histories in one quarter of patients newly diagnosed with Huntington disease in British Columbia. *Clin Genet*, 60(3), 198-205.

An, M. C., O'Brien, R. N., Zhang, N., Patra, B. N., De La Cruz, M., Ray, A. & Ellerby, L. M. (2014) Polyglutamine Disease Modeling: Epitope Based Screen for Homologous Recombination using CRISPR/Cas9 System. *PLoS Curr*, 6.

An, M. C., Zhang, N., Scott, G., Montoro, D., Wittkop, T., Mooney, S., Melov, S. & Ellerby, L. M. (2012) Genetic correction of Huntington's disease phenotypes in induced pluripotent stem cells. *Cell Stem Cell*, 11(2), 253-63.

Andrew, S. E., Goldberg, Y. P., Kremer, B., Telenius, H., Theilmann, J., Adam, S., Starr, E., Squitieri, F., Lin, B. & Kalchman, M. A. (1993) The relationship between trinucleotide (CAG) repeat length and clinical features of Huntington's disease. *Nat Genet*, 4(4), 398-403.

Apostol, B. L., Illes, K., Pallos, J., Bodai, L., Wu, J., Strand, A., Schweitzer, E. S., Olson, J. M., Kazantsev, A., Marsh, J. L. & Thompson, L. M. (2006) Mutant huntingtin alters MAPK signaling pathways in PC12 and striatal cells: ERK1/2 protects against mutant huntingtin-associated toxicity. *Hum Mol Genet*, 15(2), 273-85.

Apostol, B. L., Simmons, D. A., Zuccato, C., Illes, K., Pallos, J., Casale, M., Conforti, P., Ramos, C., Roarke, M., Kathuria, S., Cattaneo, E., Marsh, J. L. & Thompson, L. M. (2008) CEP-1347 reduces mutant huntingtin-associated neurotoxicity and restores BDNF levels in R6/2 mice. *Mol Cell Neurosci*, 39(1), 8-20.

Arber, C., Precious, S. V., Cambray, S., Risner-Janiczek, J. R., Kelly, C., Noakes, Z., Fjodorova, M., Heuer, A., Ungless, M. A., Rodríguez, T. A., Rosser, A. E., Dunnett, S. B. & Li, M. (2015) Activin A directs striatal projection neuron differentiation of human pluripotent stem cells. *Development*, 142(7), 1375-86.

Arrasate, M. & Finkbeiner, S. (2012) Protein aggregates in Huntington's disease. *Exp Neurol*, 238(1), 1-11.

Arrasate, M., Mitra, S., Schweitzer, E. S., Segal, M. R. & Finkbeiner, S. (2004) Inclusion body formation reduces levels of mutant huntingtin and the risk of neuronal death. *Nature*, 431(7010), 805-10.

Atwal, R. S., Desmond, C. R., Caron, N., Maiuri, T., Xia, J., Sipione, S. & Truant, R. (2011) Kinase inhibitors modulate huntingtin cell localization and toxicity. *Nat Chem Biol*, 7(7), 453-60.

Atwal, R. S., Xia, J., Pinchev, D., Taylor, J., Epand, R. M. & Truant, R. (2007) Huntingtin has a membrane association signal that can modulate huntingtin aggregation, nuclear entry and toxicity. *Hum Mol Genet*, 16(21), 2600-15.

Aylward, E. H., Nopoulos, P. C., Ross, C. A., Langbehn, D. R., Pierson, R. K., Mills, J. A., Johnson, H. J., Magnotta, V. A., Juhl, A. R., Paulsen, J. S. & Group, P.-H. I. a. C. o. H. S. (2011) Longitudinal change in regional brain volumes in prodromal Huntington disease. *J Neurol Neurosurg Psychiatry*, 82(4), 405-10.

Bachoud-Lévi, A. C., Gaura, V., Brugières, P., Lefaucheur, J. P., Boissé, M. F., Maison, P., Baudic, S., Ribeiro, M. J., Bourdet, C., Remy, P., Cesaro, P., Hantraye, P. & Peschanski, M. (2006) Effect of fetal neural transplants in patients with Huntington's disease 6 years after surgery: a long-term follow-up study. *Lancet Neurol*, 5(4), 303-9.

Bachoud-Lévi, A. C., Rémy, P., Nguyen, J. P., Brugières, P., Lefaucheur, J. P., Bourdet, C., Baudic, S., Gaura, V., Maison, P., Haddad, B., Boissé, M. F., Grandmougin, T., Jény, R., Bartolomeo, P., Dalla Barba, G., Degos, J. D., Lisovoski, F., Ergis, A. M., Pailhous, E., Cesaro, P., Hantraye, P. & Peschanski, M. (2000) Motor and cognitive improvements in patients with Huntington's disease after neural transplantation. *Lancet*, 356(9246), 1975-9.

Baig, S. S., Strong, M., Rosser, E., Taverner, N. V., Glew, R., Miedzybrodzka, Z., Clarke, A., Craufurd, D., Disease Prediction Consortium, U. H. & Quarrell, O. W. (2016) 22 Years of predictive testing for Huntington's disease: the experience of the UK Huntington's Prediction Consortium. *Eur J Hum Genet*, 24(10), 1515.

Barbaro, B. A., Lukacsovich, T., Agrawal, N., Burke, J., Bornemann, D. J., Purcell, J. M., Worthge, S. A., Caricasole, A., Weiss, A., Song, W., Morozova, O. A., Colby, D. W. & Marsh, J. L. (2015) Comparative study of naturally occurring huntingtin fragments in Drosophila points to exon 1 as the most pathogenic species in Huntington's disease. *Hum Mol Genet*, 24(4), 913-25.

Barbeau, A. (1970) Parental ascent in the juvenile form of Huntington's chorea. *Lancet*, 2(7679), 937.

Barker, R. A., Mason, S. L., Harrower, T. P., Swain, R. A., Ho, A. K., Sahakian, B. J., Mathur, R., Elneil, S., Thornton, S., Hurrelbrink, C., Armstrong, R. J., Tyers, P., Smith, E., Carpenter, A., Piccini, P., Tai, Y. F., Brooks, D. J., Pavese, N., Watts, C., Pickard, J. D., Rosser, A. E., Dunnett, S. B. & collaboration, N.-U. (2013) The long-term safety and efficacy of bilateral transplantation of human fetal striatal tissue in patients with mild to moderate Huntington's disease. *J Neurol Neurosurg Psychiatry*, 84(6), 657-65.

Bates, G. P. & Landles, C. (2014) Preclinical Experimental Therapeutics, in Bates, G. P., Tabrizi, S. J. T. & Jones, L. (eds), *Huntington's Disease*, 4th edition. Oxford Monographs on Medical GeneticsOxford University Press.

Bañez-Coronel, M., Ayhan, F., Tarabochia, A. D., Zu, T., Perez, B. A., Tusi, S. K., Pletnikova, O., Borchelt, D. R., Ross, C. A., Margolis, R. L., Yachnis, A. T., Troncoso, J. C. & Ranum, L. P. (2015) RAN Translation in Huntington Disease. *Neuron*, 88(4), 667-77.

Beal, M. F., Kowall, N. W., Ellison, D. W., Mazurek, M. F., Swartz, K. J. & Martin, J. B. (1986) Replication of the neurochemical characteristics of Huntington's disease by quinolinic acid. *Nature*, 321(6066), 168-71.

Benn, C. L., Slow, E. J., Farrell, L. A., Graham, R., Deng, Y., Hayden, M. R. & Cha, J. H. (2007) Glutamate receptor abnormalities in the YAC128 transgenic mouse model of Huntington's disease. *Neuroscience*, 147(2), 354-72.

Benn, C. L., Sun, T., Sadri-Vakili, G., McFarland, K. N., DiRocco, D. P., Yohrling, G. J., Clark, T. W., Bouzou, B. & Cha, J. H. (2008) Huntingtin modulates transcription,

occupies gene promoters in vivo, and binds directly to DNA in a polyglutamine-dependent manner. *J Neurosci*, 28(42), 10720-33.

Bennett, E. J., Shaler, T. A., Woodman, B., Ryu, K. Y., Zaitseva, T. S., Becker, C. H., Bates, G. P., Schulman, H. & Kopito, R. R. (2007a) Global changes to the ubiquitin system in Huntington's disease. *Nature*, 448(7154), 704-8.

Bennett, E. J., Shaler, T. A., Woodman, B., Ryu, K. Y., Zaitseva, T. S., Becker, C. H., Bates, G. P., Schulman, H. & Kopito, R. R. (2007b) Global changes to the ubiquitin system in Huntington's disease. *Nature*, 448(7154), 704-8.

Bett, J. S., Benn, C. L., Ryu, K. Y., Kopito, R. R. & Bates, G. P. (2009a) The polyubiquitin Ubc gene modulates histone H2A monoubiquitylation in the R6/2 mouse model of Huntington's disease. *J Cell Mol Med*, 13(8B), 2645-57.

Bett, J. S., Cook, C., Petrucelli, L. & Bates, G. P. (2009b) The ubiquitin-proteasome reporter GFPu does not accumulate in neurons of the R6/2 transgenic mouse model of Huntington's disease. *PLoS One*, 4(4), e5128.

Bhat, K. P., Yan, S., Wang, C. E., Li, S. & Li, X. J. (2014) Differential ubiquitination and degradation of huntingtin fragments modulated by ubiquitin-protein ligase E3A. *Proc Natl Acad Sci U S A*, 111(15), 5706-11.

Biglan, K. M., Zhang, Y., Long, J. D., Geschwind, M., Kang, G. A., Killoran, A., Lu, W., McCusker, E., Mills, J. A., Raymond, L. A., Testa, C., Wojcieszek, J., Paulsen, J. S. & Group, P.-H. I. o. t. H. S. (2013) Refining the diagnosis of Huntington disease: the PREDICT-HD study. *Front Aging Neurosci*, 5, 12.

Bjorkqvist, M., Wild, E. J., Thiele, J., Silvestroni, A., Andre, R., Lahiri, N., Raibon, E., Lee, R. V., Benn, C. L., Soulet, D., Magnusson, A., Woodman, B., Landles, C., Pouladi, M. A., Hayden, M. R., Khalili-Shirazi, A., Lowdell, M. W., Brundin, P., Bates, G. P., Leavitt, B. R., Moller, T. & Tabrizi, S. J. (2008) A novel pathogenic pathway of immune activation detectable before clinical onset in Huntington's disease. *J Exp Med*, 205(8), 1869-77.

Bonelli, R. M. & Hofmann, P. (2007) A systematic review of the treatment studies in Huntington's disease since 1990. *Expert Opin Pharmacother*, 8(2), 141-53.

Bradford, J., Shin, J. Y., Roberts, M., Wang, C. E., Li, X. J. & Li, S. (2009) Expression of mutant huntingtin in mouse brain astrocytes causes age-dependent neurological symptoms. *Proc Natl Acad Sci U S A*, 106(52), 22480-5.

Browne, S. E., Ferrante, R. J. & Beal, M. F. (1999) Oxidative stress in Huntington's disease. *Brain Pathol*, 9(1), 147-63.

Brück, W., Pförtner, R., Pham, T., Zhang, J., Hayardeny, L., Piryatinsky, V., Hanisch, U. K., Regen, T., van Rossum, D., Brakelmann, L., Hagemeier, K., Kuhlmann, T., Stadelmann, C., John, G. R., Kramann, N. & Wegner, C. (2012) Reduced astrocytic NF-κB activation by laquinimod protects from cuprizone-induced demyelination. *Acta Neuropathol*, 124(3), 411-24.

Butler, R. & Bates, G. P. (2006) Histone deacetylase inhibitors as therapeutics for polyglutamine disorders. *Nat Rev Neurosci*, 7(10), 784-96.

Byrne, L. M., Rodrigues, F. B., Blennow, K., Durr, A., Leavitt, B. R., Roos, R. A. C., Scahill, R. I., Tabrizi, S. J., Zetterberg, H., Langbehn, D. & Wild, E. J. (2017) Neurofilament light protein in blood as a potential biomarker of neurodegeneration in Huntington's disease: a retrospective cohort analysis. *Lancet Neurol*, 16(8), 601-609.

Cahan, P. & Daley, G. Q. (2013) Origins and implications of pluripotent stem cell variability and heterogeneity. *Nat Rev Mol Cell Biol*, 14(6), 357-68.

Camnasio, S., Delli Carri, A., Lombardo, A., Grad, I., Mariotti, C., Castucci, A., Rozell, B., Lo Riso, P., Castiglioni, V., Zuccato, C., Rochon, C., Takashima, Y., Diaferia, G., Biunno, I., Gellera, C., Jaconi, M., Smith, A., Hovatta, O., Naldini, L., Di Donato, S., Feki, A. & Cattaneo, E. (2012) The first reported generation of several induced pluripotent stem cell lines from homozygous and heterozygous Huntington's disease patients demonstrates mutation related enhanced lysosomal activity. *Neurobiol Dis*, 46(1), 41-51.

Capetian, P., Knoth, R., Maciaczyk, J., Pantazis, G., Ditter, M., Bokla, L., Landwehrmeyer, G. B., Volk, B. & Nikkhah, G. (2009) Histological findings on fetal striatal grafts in a Huntington's disease patient early after transplantation. *Neuroscience*, 160(3), 661-75.

Caron, N. S., Desmond, C. R., Xia, J. & Truant, R. (2013) Polyglutamine domain flexibility mediates the proximity between flanking sequences in huntingtin. *Proc Natl Acad Sci U S A*, 110(36), 14610-5.

Caron, N. S., Hung, C. L., Atwal, R. S. & Truant, R. (2014) Live cell imaging and biophotonic methods reveal two types of mutant huntingtin inclusions. *Hum Mol Genet*, 23(9), 2324-38.

Carroll, J. B., Warby, S. C., Southwell, A. L., Doty, C. N., Greenlee, S., Skotte, N., Hung, G., Bennett, C. F., Freier, S. M. & Hayden, M. R. (2011) Potent and selective antisense oligonucleotides targeting single-nucleotide polymorphisms in the Huntington disease gene / allele-specific silencing of mutant huntingtin. *Mol Ther*, 19(12), 2178-85.

Carty, N., Berson, N., Tillack, K., Thiede, C., Scholz, D., Kottig, K., Sedaghat, Y., Gabrysiak, C., Yohrling, G., von der Kammer, H., Ebneth, A., Mack, V., Munoz-Sanjuan, I. & Kwak, S. (2015) Characterization of HTT inclusion size, location, and timing in the zQ175 mouse model of Huntington's disease: an in vivo high-content imaging study. *PLoS One*, 10(4), e0123527.

Chae, J. I., Kim, D. W., Lee, N., Jeon, Y. J., Jeon, I., Kwon, J., Kim, J., Soh, Y., Lee, D. S., Seo, K. S., Choi, N. J., Park, B. C., Kang, S. H., Ryu, J., Oh, S. H., Shin, D. A., Lee, D. R., Do, J. T., Park, I. H., Daley, G. Q. & Song, J. (2012) Quantitative proteomic analysis of induced pluripotent stem cells derived from a human Huntington's disease patient. *Biochem J*, 446(3), 359-71.

Chen, C. M., Wu, Y. R., Cheng, M. L., Liu, J. L., Lee, Y. M., Lee, P. W., Soong, B. W. & Chiu, D. T. (2007) Increased oxidative damage and mitochondrial abnormalities in the peripheral blood of Huntington's disease patients. *Biochem Biophys Res Commun*, 359(2), 335-40.

Chen, S., Berthelier, V., Hamilton, J. B., O'Nuallain, B. & Wetzel, R. (2002) Amyloid-like features of polyglutamine aggregates and their assembly kinetics. *Biochemistry*, 41(23), 7391-9.

Chiu, F. L., Lin, J. T., Chuang, C. Y., Chien, T., Chen, C. M., Chen, K. H., Hsiao, H. Y., Lin, Y. S., Chern, Y. & Kuo, H. C. (2015) Elucidating the role of the A2A adenosine receptor in neurodegeneration using neurons derived from Huntington's disease iPSCs. *Hum Mol Genet*, 24(21), 6066-79.

Cicchetti, F., Lacroix, S., Cisbani, G., Vallières, N., Saint-Pierre, M., St-Amour, I., Tolouei, R., Skepper, J. N., Hauser, R. A., Mantovani, D., Barker, R. A. & Freeman, T.

B. (2014) Mutant huntingtin is present in neuronal grafts in huntington disease patients. *Ann Neurol*, 76(1), 31-42.

Colby, D. W., Cassady, J. P., Lin, G. C., Ingram, V. M. & Wittrup, K. D. (2006) Stochastic kinetics of intracellular huntingtin aggregate formation. *Nat Chem Biol*, 2(6), 319-23.

Comi, G., Jeffery, D., Kappos, L., Montalban, X., Boyko, A., Rocca, M. A., Filippi, M. & Group, A. S. (2012) Placebo-controlled trial of oral laquinimod for multiple sclerosis. *N Engl J Med*, 366(11), 1000-9.

Conforti, P., Besusso, D., Bocchi, V. D., Faedo, A., Cesana, E., Rossetti, G., Ranzani, V., Svendsen, C. N., Thompson, L. M., Toselli, M., Biella, G., Pagani, M. & Cattaneo, E. (2018) Faulty neuronal determination and cell polarization are reverted by modulating HD early phenotypes. *Proc Natl Acad Sci U S A*, 115(4), E762-E771.

Consortium, G. M. o. H. s. D. G.-H. (2015) Identification of Genetic Factors that Modify Clinical Onset of Huntington's Disease. *Cell*, 162(3), 516-26.

Consortium, H. i. (2012) Induced pluripotent stem cells from patients with Huntington's disease show CAG-repeat-expansion-associated phenotypes. *Cell Stem Cell*, 11(2), 264-78.

Cooper, J. K., Schilling, G., Peters, M. F., Herring, W. J., Sharp, A. H., Kaminsky, Z., Masone, J., Khan, F. A., Delanoy, M., Borchelt, D. R., Dawson, V. L., Dawson, T. M. & Ross, C. A. (1998) Truncated N-terminal fragments of huntingtin with expanded glutamine repeats form nuclear and cytoplasmic aggregates in cell culture. *Hum Mol Genet*, 7(5), 783-90.

Cornett, J., Cao, F., Wang, C. E., Ross, C. A., Bates, G. P., Li, S. H. & Li, X. J. (2005) Polyglutamine expansion of huntingtin impairs its nuclear export. *Nat Genet*, 37(2), 198-204.

Cox, D. B., Platt, R. J. & Zhang, F. (2015) Therapeutic genome editing: prospects and challenges. *Nat Med*, 21(2), 121-31.

Craufurd, D., MacLeod, R., Frontali, M., Quarrell, O., Bijlsma, E. K., Davis, M., Hjermind, L. E., Lahiri, N., Mandich, P., Martinez, A., Tibben, A., Roos, R. A. & (EHDN), o. b. o. t. W. G. o. G. C. a. T. o. t. E. H. s. D. N. (2014) Diagnostic genetic testing for Huntington's disease. *Pract Neurol*.

Craufurd D, S. J. (2002) Neuropsychological and neuropsychiatric aspects of Huntington's disease, in Huntington's disease., in PS, H. (ed), *Huntington's disease*Oxford Medical Publications: Oxford.

Craufurd, D. & Tyler, A. (1992) Predictive testing for Huntington's disease: protocol of the UK Huntington's Prediction Consortium. *J Med Genet*, 29(12), 915-8.

Crotti, A., Benner, C., Kerman, B. E., Gosselin, D., Lagier-Tourenne, C., Zuccato, C., Cattaneo, E., Gage, F. H., Cleveland, D. W. & Glass, C. K. (2014) Mutant Huntingtin promotes autonomous microglia activation via myeloid lineage-determining factors. *Nat Neurosci*, 17(4), 513-21.

Datson, N. A., González-Barriga, A., Kourkouta, E., Weij, R., van de Giessen, J., Mulders, S., Kontkanen, O., Heikkinen, T., Lehtimäki, K. & van Deutekom, J. C. (2017) The expanded CAG repeat in the huntingtin gene as target for therapeutic RNA modulation throughout the HD mouse brain. *PLoS One*, 12(2), e0171127.

De Rooij, K. E., Dorsman, J. C., Smoor, M. A., Den Dunnen, J. T. & Van Ommen, G. J. (1996) Subcellular localization of the Huntington's disease gene product in cell lines by immunofluorescence and biochemical subcellular fractionation. *Hum Mol Genet*, 5(8), 1093-9.

Delli Carri, A., Onorati, M., Castiglioni, V., Faedo, A., Camnasio, S., Toselli, M., Biella, G. & Cattaneo, E. (2013) Human pluripotent stem cell differentiation into authentic striatal projection neurons. *Stem Cell Rev*, 9(4), 461-74.

Desmond, C. R., Atwal, R. S., Xia, J. & Truant, R. (2012) Identification of a karyopherin β1/β2 proline-tyrosine nuclear localization signal in huntingtin protein. *J Biol Chem*, 287(47), 39626-33.

Di Pardo, A., Maglione, V., Alpaugh, M., Horkey, M., Atwal, R. S., Sassone, J., Ciammola, A., Steffan, J. S., Fouad, K., Truant, R. & Sipione, S. (2012) Ganglioside GM1 induces phosphorylation of mutant huntingtin and restores normal motor behavior in Huntington disease mice. *Proc Natl Acad Sci U S A*, 109(9), 3528-33.

DiFiglia, M., Sapp, E., Chase, K. O., Davies, S. W., Bates, G. P., Vonsattel, J. P. & Aronin, N. (1997) Aggregation of huntingtin in neuronal intranuclear inclusions and dystrophic neurites in brain. *Science*, 277(5334), 1990-3.

DiGiovanni, L. F., Mocle, A. J., Xia, J. & Truant, R. (2016) Huntingtin N17 domain is a reactive oxygen species sensor regulating huntingtin phosphorylation and localization. *Hum Mol Genet*, 25(18), 3937-3945.

Ding, Q., Lewis, J. J., Strum, K. M., Dimayuga, E., Bruce-Keller, A. J., Dunn, J. C. & Keller, J. N. (2002) Polyglutamine expansion, protein aggregation, proteasome activity, and neural survival. *J Biol Chem*, 277(16), 13935-42.

Donato, R., Miljan, E. A., Hines, S. J., Aouabdi, S., Pollock, K., Patel, S., Edwards, F. A. & Sinden, J. D. (2007) Differential development of neuronal physiological responsiveness in two human neural stem cell lines. *BMC Neurosci*, 8, 36.

Dong, G., Callegari, E. A., Gloeckner, C. J., Ueffing, M. & Wang, H. (2012) Prothymosin-α interacts with mutant huntingtin and suppresses its cytotoxicity in cell culture. *J Biol Chem*, 287(2), 1279-89.

Dong, G., Ferguson, J. M., Duling, A. J., Nicholas, R. G., Zhang, D., Rezvani, K., Fang, S., Monteiro, M. J., Li, S., Li, X. J. & Wang, H. (2011) Modeling pathogenesis of Huntington's disease with inducible neuroprogenitor cells. *Cell Mol Neurobiol*, 31(5), 737-47.

Dorsman, J. C., Smoor, M. A., Maat-Schieman, M. L., Bout, M., Siesling, S., van Duinen, S. G., Verschuuren, J. J., den Dunnen, J. T., Roos, R. A. & van Ommen, G. J. (1999) Analysis of the subcellular localization of huntingtin with a set of rabbit polyclonal antibodies in cultured mammalian cells of neuronal origin: comparison with the distribution of huntingtin in Huntington's disease autopsy brain. *Philos Trans R Soc Lond B Biol Sci*, 354(1386), 1061-7.

Dragatsis, I., Efstratiadis, A. & Zeitlin, S. (1998) Mouse mutant embryos lacking huntingtin are rescued from lethality by wild-type extraembryonic tissues. *Development*, 125(8), 1529-39.

Dragatsis, I., Goldowitz, D., Del Mar, N., Deng, Y. P., Meade, C. A., Liu, L., Sun, Z., Dietrich, P., Yue, J. & Reiner, A. (2009) CAG repeat lengths > or =335 attenuate the phenotype in the R6/2 Huntington's disease transgenic mouse. *Neurobiol Dis*, 33(3), 315-30.

Dragileva, E., Hendricks, A., Teed, A., Gillis, T., Lopez, E. T., Friedberg, E. C., Kucherlapati, R., Edelmann, W., Lunetta, K. L., MacDonald, M. E. & Wheeler, V. C. (2009) Intergenerational and striatal CAG repeat instability in Huntington's disease knock-in mice involve different DNA repair genes. *Neurobiol Dis*, 33(1), 37-47.

Duff, K., Paulsen, J. S., Beglinger, L. J., Langbehn, D. R., Wang, C., Stout, J. C., Ross, C. A., Aylward, E., Carlozzi, N. E., Queller, S. & Group, P.-H. I. o. t. H. S. (2010) "Frontal" behaviors before the diagnosis of Huntington's disease and their relationship to markers of disease progression: evidence of early lack of awareness. *J Neuropsychiatry Clin Neurosci*, 22(2), 196-207.

Duim, W. C., Jiang, Y., Shen, K., Frydman, J. & Moerner, W. E. (2014) Super-resolution fluorescence of huntingtin reveals growth of globular species into short fibers and coexistence of distinct aggregates. *ACS Chem Biol*, 9(12), 2767-78.

Díaz-Hernández, M., Hernández, F., Martín-Aparicio, E., Gómez-Ramos, P., Morán, M. A., Castaño, J. G., Ferrer, I., Avila, J. & Lucas, J. J. (2003) Neuronal induction of the immunoproteasome in Huntington's disease. *J Neurosci*, 23(37), 11653-61.

El-Akabawy, G., Medina, L. M., Jeffries, A., Price, J. & Modo, M. (2011) Purmorphamine increases DARPP-32 differentiation in human striatal neural stem cells through the Hedgehog pathway. *Stem Cells Dev*, 20(11), 1873-87.

Evans, S. J., Douglas, I., Rawlins, M. D., Wexler, N. S., Tabrizi, S. J. & Smeeth, L. (2013) Prevalence of adult Huntington's disease in the UK based on diagnoses recorded in general practice records. *J Neurol Neurosurg Psychiatry*.

Finkel, R. S., Mercuri, E., Darras, B. T., Connolly, A. M., Kuntz, N. L., Kirschner, J., Chiriboga, C. A., Saito, K., Servais, L., Tizzano, E., Topaloglu, H., Tulinius, M., Montes, J., Glanzman, A. M., Bishop, K., Zhong, Z. J., Gheuens, S., Bennett, C. F., Schneider, E., Farwell, W., De Vivo, D. C. & Group, E. S. (2017) Nusinersen versus Sham Control in Infantile-Onset Spinal Muscular Atrophy. *N Engl J Med*, 377(18), 1723-1732.

Fornai, F., Lenzi, P., Gesi, M., Ferrucci, M., Lazzeri, G., Busceti, C. L., Ruffoli, R., Soldani, P., Ruggieri, S., Alessandri, M. G. & Paparelli, A. (2003) Fine structure and biochemical mechanisms underlying nigrostriatal inclusions and cell death after proteasome inhibition. *J Neurosci*, 23(26), 8955-66.

Frank, S. (2014) Treatment of Huntington's disease. *Neurotherapeutics*, 11(1), 153-60.

Fusaki, N., Ban, H., Nishiyama, A., Saeki, K. & Hasegawa, M. (2009) Efficient induction of transgene-free human pluripotent stem cells using a vector based on Sendai virus, an RNA virus that does not integrate into the host genome. *Proc Jpn Acad Ser B Phys Biol Sci*, 85(8), 348-62.

Gallina, P., Paganini, M., Lombardini, L., Mascalchi, M., Porfirio, B., Gadda, D., Marini, M., Pinzani, P., Salvianti, F., Crescioli, C., Bucciantini, S., Mechi, C., Sarchielli, E., Romoli, A. M., Bertini, E., Urbani, S., Bartolozzi, B., De Cristofaro, M. T., Piacentini, S., Saccardi, R., Pupi, A., Vannelli, G. B. & Di Lorenzo, N. (2010) Human striatal neuroblasts develop and build a striatal-like structure into the brain of Huntington's disease patients after transplantation. *Exp Neurol*, 222(1), 30-41.

Gandhi, S., Wood-Kaczmar, A., Yao, Z., Plun-Favreau, H., Deas, E., Klupsch, K., Downward, J., Latchman, D. S., Tabrizi, S. J., Wood, N. W., Duchen, M. R. & Abramov, A. Y. (2009) PINK1-associated Parkinson's disease is caused by neuronal vulnerability to calcium-induced cell death. *Mol Cell*, 33(5), 627-38.

Gauthier, L. R., Charrin, B. C., Borrell-Pagès, M., Dompierre, J. P., Rangone, H., Cordelières, F. P., De Mey, J., MacDonald, M. E., Lessmann, V., Humbert, S. & Saudou, F. (2004) Huntingtin controls neurotrophic support and survival of neurons by enhancing BDNF vesicular transport along microtubules. *Cell*, 118(1), 127-38.

Giampà, C., Laurenti, D., Anzilotti, S., Bernardi, G., Menniti, F. S. & Fusco, F. R. (2010) Inhibition of the striatal specific phosphodiesterase PDE10A ameliorates striatal and cortical pathology in R6/2 mouse model of Huntington's disease. *PLoS One*, 5(10), e13417.

Giampà, C., Montagna, E., Dato, C., Melone, M. A., Bernardi, G. & Fusco, F. R. (2013) Systemic delivery of recombinant brain derived neurotrophic factor (BDNF) in the R6/2 mouse model of Huntington's disease. *PLoS One*, 8(5), e64037.

Glickman, M. H. & Ciechanover, A. (2002) The ubiquitin-proteasome proteolytic pathway: destruction for the sake of construction. *Physiol Rev*, 82(2), 373-428.

Godin, J. D., Colombo, K., Molina-Calavita, M., Keryer, G., Zala, D., Charrin, B. C., Dietrich, P., Volvert, M. L., Guillemot, F., Dragatsis, I., Bellaiche, Y., Saudou, F., Nguyen, L. & Humbert, S. (2010) Huntingtin is required for mitotic spindle orientation and mammalian neurogenesis. *Neuron*, 67(3), 392-406.

Gong, B., Kielar, C. & Morton, A. J. (2012) Temporal separation of aggregation and ubiquitination during early inclusion formation in transgenic mice carrying the Huntington's disease mutation. *PLoS One*, 7(7), e41450.

Gourfinkel-An, I., Cancel, G., Trottier, Y., Devys, D., Tora, L., Lutz, Y., Imbert, G., Saudou, F., Stevanin, G., Agid, Y., Brice, A., Mandel, J. L. & Hirsch, E. C. (1997) Differential distribution of the normal and mutated forms of huntingtin in the human brain. *Ann Neurol*, 42(5), 712-9.

Gray, M., Shirasaki, D. I., Cepeda, C., André, V. M., Wilburn, B., Lu, X. H., Tao, J., Yamazaki, I., Li, S. H., Sun, Y. E., Li, X. J., Levine, M. S. & Yang, X. W. (2008) Full-length human mutant huntingtin with a stable polyglutamine repeat can elicit progressive and selective neuropathogenesis in BACHD mice. *J Neurosci*, 28(24), 6182-95.

Grima, J. C., Daigle, J. G., Arbez, N., Cunningham, K. C., Zhang, K., Ochaba, J., Geater, C., Morozko, E., Stocksdale, J., Glatzer, J. C., Pham, J. T., Ahmed, I., Peng, Q., Wadhwa, H., Pletnikova, O., Troncoso, J. C., Duan, W., Snyder, S. H., Ranum, L. P. W., Thompson, L. M., Lloyd, T. E., Ross, C. A. & Rothstein, J. D. (2017) Mutant Huntingtin Disrupts the Nuclear Pore Complex. *Neuron*, 94(1), 93-107.e6.

Grondin, R., Kaytor, M. D., Ai, Y., Nelson, P. T., Thakker, D. R., Heisel, J., Weatherspoon, M. R., Blum, J. L., Burright, E. N., Zhang, Z. & Kaemmerer, W. F. (2012) Six-month partial suppression of Huntingtin is well tolerated in the adult rhesus striatum. *Brain*, 135(Pt 4), 1197-209.

Gunawardena, S., Her, L. S., Brusch, R. G., Laymon, R. A., Niesman, I. R., Gordesky-Gold, B., Sintasath, L., Bonini, N. M. & Goldstein, L. S. (2003) Disruption of axonal transport by loss of huntingtin or expression of pathogenic polyQ proteins in Drosophila. *Neuron*, 40(1), 25-40.

Guo, Q., Bin Huang, Cheng, J., Seefelder, M., Engler, T., Pfeifer, G., Oeckl, P., Otto, M., Moser, F., Maurer, M., Pautsch, A., Baumeister, W., Fernández-Busnadiego, R. & Kochanek, S. (2018) The cryo-electron microscopy structure of huntingtin. *Nature*, 555(7694), 117-120.

Gusella, J. F., Wexler, N. S., Conneally, P. M., Naylor, S. L., Anderson, M. A., Tanzi, R. E., Watkins, P. C., Ottina, K., Wallace, M. R. & Sakaguchi, A. Y. (1983) A polymorphic DNA marker genetically linked to Huntington's disease. *Nature*, 306(5940), 234-8.

Gutekunst, C. A., Li, S. H., Yi, H., Mulroy, J. S., Kuemmerle, S., Jones, R., Rye, D., Ferrante, R. J., Hersch, S. M. & Li, X. J. (1999) Nuclear and neuropil aggregates in Huntington's disease: relationship to neuropathology. *J Neurosci*, 19(7), 2522-34.

Hackam, A. S., Singaraja, R., Wellington, C. L., Metzler, M., McCutcheon, K., Zhang, T., Kalchman, M. & Hayden, M. R. (1998) The influence of huntingtin protein size on nuclear localization and cellular toxicity. *J Cell Biol*, 141(5), 1097-105.

Hackam, A. S., Singaraja, R., Zhang, T., Gan, L. & Hayden, M. R. (1999) In vitro evidence for both the nucleus and cytoplasm as subcellular sites of pathogenesis in Huntington's disease. *Hum Mol Genet*, 8(1), 25-33.

Halliday, G. M., McRitchie, D. A., Macdonald, V., Double, K. L., Trent, R. J. & McCusker, E. (1998) Regional specificity of brain atrophy in Huntington's disease. *Exp Neurol*, 154(2), 663-72.

Harper, P. (2002) The epidemiology of Huntington's disease, *Huntington's disease*Oxford Medical Publications: Oxford.

Harper, S. Q., Staber, P. D., He, X., Eliason, S. L., Martins, I. H., Mao, Q., Yang, L., Kotin, R. M., Paulson, H. L. & Davidson, B. L. (2005) RNA interference improves motor and neuropathological abnormalities in a Huntington's disease mouse model. *Proc Natl Acad Sci U S A*, 102(16), 5820-5.

Harrington, D. L., Smith, M. M., Zhang, Y., Carlozzi, N. E., Paulsen, J. S. & Group, P.-H. I. o. t. H. S. (2012) Cognitive domains that predict time to diagnosis in prodromal Huntington disease. *J Neurol Neurosurg Psychiatry*, 83(6), 612-9.

Hauser, R. A., Furtado, S., Cimino, C. R., Delgado, H., Eichler, S., Schwartz, S., Scott, D., Nauert, G. M., Soety, E., Sossi, V., Holt, D. A., Sanberg, P. R., Stoessl, A. J. & Freeman, T. B. (2002) Bilateral human fetal striatal transplantation in Huntington's disease. *Neurology*, 58(5), 687-95.

Heng, M. Y., Duong, D. K., Albin, R. L., Tallaksen-Greene, S. J., Hunter, J. M., Lesort, M. J., Osmand, A., Paulson, H. L. & Detloff, P. J. (2010) Early autophagic response in a novel knock-in model of Huntington disease. *Hum Mol Genet*, 19(19), 3702-20.

Hensman Moss, D. J., Pardiñas, A. F., Langbehn, D., Lo, K., Leavitt, B. R., Roos, R., Durr, A., Mead, S., Holmans, P., Jones, L., Tabrizi, S. J., investigators, T.-H. & investigators, R. (2017) Identification of genetic variants associated with Huntington's disease progression: a genome-wide association study. *Lancet Neurol*, 16(9), 701-711.

Ho, L. W., Brown, R., Maxwell, M., Wyttenbach, A. & Rubinsztein, D. C. (2001) Wild type Huntingtin reduces the cellular toxicity of mutant Huntingtin in mammalian cell models of Huntington's disease. *J Med Genet*, 38(7), 450-2.

Hodges, A., Strand, A. D., Aragaki, A. K., Kuhn, A., Sengstag, T., Hughes, G., Elliston, L. A., Hartog, C., Goldstein, D. R., Thu, D., Hollingsworth, Z. R., Collin, F., Synek, B., Holmans, P. A., Young, A. B., Wexler, N. S., Delorenzi, M., Kooperberg, C., Augood, S. J., Faull, R. L., Olson, J. M., Jones, L. & Luthi-Carter, R. (2006) Regional and cellular gene expression changes in human Huntington's disease brain. *Hum Mol Genet*, 15(6), 965-77.

Hodgson, J. G., Smith, D. J., McCutcheon, K., Koide, H. B., Nishiyama, K., Dinulos, M. B., Stevens, M. E., Bissada, N., Nasir, J., Kanazawa, I., Disteche, C. M., Rubin, E. M. &

Hayden, M. R. (1996) Human huntingtin derived from YAC transgenes compensates for loss of murine huntingtin by rescue of the embryonic lethal phenotype. *Hum Mol Genet*, 5(12), 1875-85.

Hoffner, G. & Djian, P. (2014) Monomeric, oligomeric and polymeric proteins in huntington disease and other diseases of polyglutamine expansion. *Brain Sci*, 4(1), 91-122.

Holmberg, C. I., Staniszewski, K. E., Mensah, K. N., Matouschek, A. & Morimoto, R. I. (2004) Inefficient degradation of truncated polyglutamine proteins by the proteasome. *EMBO J*, 23(21), 4307-18.

Hoogeveen, A. T., Willemsen, R., Meyer, N., de Rooij, K. E., Roos, R. A., van Ommen, G. J. & Galjaard, H. (1993) Characterization and localization of the Huntington disease gene product. *Hum Mol Genet*, 2(12), 2069-73.

Hoop, C. L., Lin, H. K., Kar, K., Magyarfalvi, G., Lamley, J. M., Boatz, J. C., Mandal, A., Lewandowski, J. R., Wetzel, R. & van der Wel, P. C. (2016) Huntingtin exon 1 fibrils feature an interdigitated β-hairpin-based polyglutamine core. *Proc Natl Acad Sci U S A*, 113(6), 1546-51.

Horvath, P. & Barrangou, R. (2010) CRISPR/Cas, the immune system of bacteria and archaea. *Science*, 327(5962), 167-70.

Hu, B. Y., Weick, J. P., Yu, J., Ma, L. X., Zhang, X. Q., Thomson, J. A. & Zhang, S. C. (2010) Neural differentiation of human induced pluripotent stem cells follows developmental principles but with variable potency. *Proc Natl Acad Sci U S A*, 107(9), 4335-40.

Huang, S. S., He, J., Zhao, D. M., Xu, X. Y., Tan, H. P. & Li, H. (2010) Effects of mutant huntingtin on mGluR5-mediated dual signaling pathways: implications for therapeutic interventions. *Cell Mol Neurobiol*, 30(7), 1107-15.

Hughes, A. & Jones, L. (2014) Pathogenic mechanisms in Huntington's disease, in Bates, G. P., Tabrizi, S. J. & Jones, L. (eds), *Huntington's Disease*, 4th edition. Oxford Monographs on Medical GeneticsOxford University Press.

Huntington, G. (1872) On chorea., *Med Surg Report: Weekly J 26(15):317-321.* Available online: [Accessed.

Huntington's Disease Collaborative Research Group, T. (1993) A novel gene containing a trinucleotide repeat that is expanded and unstable on Huntington's disease chromosomes. *Cell*, 72(6), 971-83.

Igarashi, S., Morita, H., Bennett, K. M., Tanaka, Y., Engelender, S., Peters, M. F., Cooper, J. K., Wood, J. D., Sawa, A. & Ross, C. A. (2003) Inducible PC12 cell model of Huntington's disease shows toxicity and decreased histone acetylation. *Neuroreport*, 14(4), 565-8.

Im, W., Chung, J., Lee, S. T., Chu, K., Kim, M. W. & Kim, M. (2014) Nuclear localization of huntingtin during spermatogenesis. *Neurol Sci*, 35(3), 459-62.

Jacobsen, J. C., Bawden, C. S., Rudiger, S. R., McLaughlan, C. J., Reid, S. J., Waldvogel, H. J., MacDonald, M. E., Gusella, J. F., Walker, S. K., Kelly, J. M., Webb, G. C., Faull, R. L., Rees, M. I. & Snell, R. G. (2010) An ovine transgenic Huntington's disease model. *Hum Mol Genet*, 19(10), 1873-82.

Jeon, I., Lee, N., Li, J. Y., Park, I. H., Park, K. S., Moon, J., Shim, S. H., Choi, C., Chang, D. J., Kwon, J., Oh, S. H., Shin, D. A., Kim, H. S., Do, J. T., Lee, D. R., Kim, M.,

Kang, K. S., Daley, G. Q., Brundin, P. & Song, J. (2012) Neuronal properties, in vivo effects, and pathology of a Huntington's disease patient-derived induced pluripotent stem cells. *Stem Cells*, 30(9), 2054-62.

Jin, J., Albertz, J., Guo, Z., Peng, Q., Rudow, G., Troncoso, J. C., Ross, C. A. & Duan, W. (2013) Neuroprotective effects of PPAR-γ agonist rosiglitazone in N171-82Q mouse model of Huntington's disease. *J Neurochem*, 125(3), 410-9.

Jin, Y. N. & Johnson, G. V. (2010) The interrelationship between mitochondrial dysfunction and transcriptional dysregulation in Huntington disease. *J Bioenerg Biomembr*, 42(3), 199-205.

Joshi, P. R., Wu, N. P., André, V. M., Cummings, D. M., Cepeda, C., Joyce, J. A., Carroll, J. B., Leavitt, B. R., Hayden, M. R., Levine, M. S. & Bamford, N. S. (2009) Age-dependent alterations of corticostriatal activity in the YAC128 mouse model of Huntington disease. *J Neurosci*, 29(8), 2414-27.

Juenemann, K., Schipper-Krom, S., Wiemhoefer, A., Kloss, A., Sanz Sanz, A. & Reits, E. A. (2013) Expanded polyglutamine-containing N-terminal huntingtin fragments are entirely degraded by mammalian proteasomes. *J Biol Chem*, 288(38), 27068-84.

Keiser, M. S., Kordasiewicz, H. B. & McBride, J. L. (2016) Gene suppression strategies for dominantly inherited neurodegenerative diseases: lessons from Huntington's disease and spinocerebellar ataxia. *Hum Mol Genet*, 25(R1), R53-64.

Kennedy, L., Evans, E., Chen, C. M., Craven, L., Detloff, P. J., Ennis, M. & Shelbourne, P. F. (2003) Dramatic tissue-specific mutation length increases are an early molecular event in Huntington disease pathogenesis. *Hum Mol Genet*, 12(24), 3359-67.

Khan, I. F., Hirata, R. K. & Russell, D. W. (2011) AAV-mediated gene targeting methods for human cells. *Nat Protoc*, 6(4), 482-501.

Khan, I. F., Hirata, R. K., Wang, P. R., Li, Y., Kho, J., Nelson, A., Huo, Y., Zavaljevski, M., Ware, C. & Russell, D. W. (2010) Engineering of human pluripotent stem cells by AAV-mediated gene targeting. *Mol Ther*, 18(6), 1192-9.

Killoran, A., Biglan, K. M., Jankovic, J., Eberly, S., Kayson, E., Oakes, D., Young, A. B. & Shoulson, I. (2013) Characterization of the Huntington intermediate CAG repeat expansion phenotype in PHAROS. *Neurology*.

Kim, H. T. & Goldberg, A. L. (2017) The deubiquitinating enzyme Usp14 allosterically inhibits multiple proteasomal activities and ubiquitin-independent proteolysis. *J Biol Chem*, 292(23), 9830-9839.

Kim, M. W., Chelliah, Y., Kim, S. W., Otwinowski, Z. & Bezprozvanny, I. (2009) Secondary structure of Huntingtin amino-terminal region. *Structure*, 17(9), 1205-12.

Kim, Y. E., Hosp, F., Frottin, F., Ge, H., Mann, M., Hayer-Hartl, M. & Hartl, F. U. (2016) Soluble Oligomers of PolyQ-Expanded Huntingtin Target a Multiplicity of Key Cellular Factors. *Mol Cell*, 63(6), 951-64.

Kitamura, A., Kubota, H., Pack, C. G., Matsumoto, G., Hirayama, S., Takahashi, Y., Kimura, H., Kinjo, M., Morimoto, R. I. & Nagata, K. (2006) Cytosolic chaperonin prevents polyglutamine toxicity with altering the aggregation state. *Nat Cell Biol*, 8(10), 1163-70.

Kordasiewicz, H. B., Stanek, L. M., Wancewicz, E. V., Mazur, C., McAlonis, M. M., Pytel, K. A., Artates, J. W., Weiss, A., Cheng, S. H., Shihabuddin, L. S., Hung, G., Bennett, C. F. & Cleveland, D. W. (2012) Sustained therapeutic reversal of

Huntington's disease by transient repression of huntingtin synthesis. *Neuron*, 74(6), 1031-44.

Kremer, B. (2002) Clinical neurology of Huntington's disease, in Bates, G. P., Harper, P. & Jones, L. (eds), *Huntington's Disease*. Oxford: Oxford University Press.

Kremer, B., Almqvist, E., Theilmann, J., Spence, N., Telenius, H., Goldberg, Y. P. & Hayden, M. R. (1995) Sex-dependent mechanisms for expansions and contractions of the CAG repeat on affected Huntington disease chromosomes. *Am J Hum Genet*, 57(2), 343-50.

Kuemmerle, S., Gutekunst, C. A., Klein, A. M., Li, X. J., Li, S. H., Beal, M. F., Hersch, S. M. & Ferrante, R. J. (1999) Huntington aggregates may not predict neuronal death in Huntington's disease. *Ann Neurol*, 46(6), 842-9.

Kumar, A. & Ratan, R. R. (2016) Oxidative Stress and Huntington's Disease: The Good, The Bad, and The Ugly. *J Huntingtons Dis*, 5(3), 217-237.

Kyttälä, A., Moraghebi, R., Valensisi, C., Kettunen, J., Andrus, C., Pasumarthy, K. K., Nakanishi, M., Nishimura, K., Ohtaka, M., Weltner, J., Van Handel, B., Parkkonen, O., Sinisalo, J., Jalanko, A., Hawkins, R. D., Woods, N. B., Otonkoski, T. & Trokovic, R. (2016) Genetic Variability Overrides the Impact of Parental Cell Type and Determines iPSC Differentiation Potential. *Stem Cell Reports*, 6(2), 200-12.

La Spada, A. R. (2012) PPARGC1A/PGC-1α, TFEB and enhanced proteostasis in Huntington disease: defining regulatory linkages between energy production and protein-organelle quality control. *Autophagy*, 8(12), 1845-7.

Labbadia, J., Cunliffe, H., Weiss, A., Katsyuba, E., Sathasivam, K., Seredenina, T., Woodman, B., Moussaoui, S., Frentzel, S., Luthi-Carter, R., Paganetti, P. & Bates, G. P. (2011) Altered chromatin architecture underlies progressive impairment of the heat shock response in mouse models of Huntington disease. *J Clin Invest*, 121(8), 3306-19.

Labbadia, J., Novoselov, S. S., Bett, J. S., Weiss, A., Paganetti, P., Bates, G. P. & Cheetham, M. E. (2012) Suppression of protein aggregation by chaperone modification of high molecular weight complexes. *Brain*, 135(Pt 4), 1180-96.

Laforet, G. A., Sapp, E., Chase, K., McIntyre, C., Boyce, F. M., Campbell, M., Cadigan, B. A., Warzecki, L., Tagle, D. A., Reddy, P. H., Cepeda, C., Calvert, C. R., Jokel, E. S., Klapstein, G. J., Ariano, M. A., Levine, M. S., DiFiglia, M. & Aronin, N. (2001) Changes in cortical and striatal neurons predict behavioral and electrophysiological abnormalities in a transgenic murine model of Huntington's disease. *J Neurosci*, 21(23), 9112-23.

Landles, C., Sathasivam, K., Weiss, A., Woodman, B., Moffitt, H., Finkbeiner, S., Sun, B., Gafni, J., Ellerby, L. M., Trottier, Y., Richards, W. G., Osmand, A., Paganetti, P. & Bates, G. P. (2010) Proteolysis of mutant huntingtin produces an exon 1 fragment that accumulates as an aggregated protein in neuronal nuclei in Huntington disease. *J Biol Chem*, 285(12), 8808-23.

Langbehn, D. R., Brinkman, R. R., Falush, D., Paulsen, J. S., Hayden, M. R. & Group, I. H. s. D. C. (2004) A new model for prediction of the age of onset and penetrance for Huntington's disease based on CAG length. *Clin Genet*, 65(4), 267-77.

Langbehn, D. R., Hayden, M. R., Paulsen, J. S. & Group, P.-H. I. o. t. H. S. (2010) CAG-repeat length and the age of onset in Huntington disease (HD): a review and validation study of statistical approaches. *Am J Med Genet B Neuropsychiatr Genet*, 153B(2), 397-408.

Lanska, D. J., Lanska, M. J., Lavine, L. & Schoenberg, B. S. (1988) Conditions associated with Huntington's disease at death. A case-control study. *Arch Neurol*, 45(8), 878-80.

Laywell, E. D., Kearns, S. M., Zheng, T., Chen, K. A., Deng, J., Chen, H. X., Roper, S. N. & Steindler, D. A. (2005) Neuron-to-astrocyte transition: phenotypic fluidity and the formation of hybrid asterons in differentiating neurospheres. *J Comp Neurol*, 493(3), 321-33.

Li, H., Wyman, T., Yu, Z. X., Li, S. H. & Li, X. J. (2003) Abnormal association of mutant huntingtin with synaptic vesicles inhibits glutamate release. *Hum Mol Genet*, 12(16), 2021-30.

Li, S. H., Schilling, G., Young, W. S., Li, X. J., Margolis, R. L., Stine, O. C., Wagster, M. V., Abbott, M. H., Franz, M. L. & Ranen, N. G. (1993) Huntington's disease gene (IT15) is widely expressed in human and rat tissues. *Neuron*, 11(5), 985-93.

Lilienbaum, A. (2013) Relationship between the proteasomal system and autophagy. *Int J Biochem Mol Biol*, 4(1), 1-26.

Lin, C. H., Tallaksen-Greene, S., Chien, W. M., Cearley, J. A., Jackson, W. S., Crouse, A. B., Ren, S., Li, X. J., Albin, R. L. & Detloff, P. J. (2001) Neurological abnormalities in a knock-in mouse model of Huntington's disease. *Hum Mol Genet*, 10(2), 137-44.

Liu, K. Y., Shyu, Y. C., Barbaro, B. A., Lin, Y. T., Chern, Y., Thompson, L. M., James Shen, C. K. & Marsh, J. L. (2015) Disruption of the nuclear membrane by perinuclear inclusions of mutant huntingtin causes cell-cycle re-entry and striatal cell death in mouse and cell models of Huntington's disease. *Hum Mol Genet*, 24(6), 1602-16.

Lu, B. & Palacino, J. (2013) A novel human embryonic stem cell-derived Huntington's disease neuronal model exhibits mutant huntingtin (mHTT) aggregates and soluble mHTT-dependent neurodegeneration. *FASEB J*, 27(5), 1820-9.

Macdonald, D., Tessari, M. A., Boogaard, I., Smith, M., Pulli, K., Szynol, A., Albertus, F., Lamers, M. B., Dijkstra, S., Kordt, D., Reindl, W., Herrmann, F., McAllister, G., Fischer, D. F. & Munoz-Sanjuan, I. (2014) Quantification assays for total and polyglutamine-expanded huntingtin proteins. *PLoS One*, 9(5), e96854.

Maiuri, T., Mocle, A. J., Hung, C. L., Xia, J., van Roon-Mom, W. M. & Truant, R. (2017) Huntingtin is a scaffolding protein in the ATM oxidative DNA damage response complex. *Hum Mol Genet*, 26(2), 395-406.

Maiuri, T., Woloshansky, T., Xia, J. & Truant, R. (2013) The huntingtin N17 domain is a multifunctional CRM1 and Ran-dependent nuclear and cilial export signal. *Hum Mol Genet*, 22(7), 1383-94.

Mangiarini, L., Sathasivam, K., Seller, M., Cozens, B., Harper, A., Hetherington, C., Lawton, M., Trottier, Y., Lehrach, H., Davies, S. W. & Bates, G. P. (1996) Exon 1 of the HD gene with an expanded CAG repeat is sufficient to cause a progressive neurological phenotype in transgenic mice. *Cell*, 87(3), 493-506.

Marcellin, D., Abramowski, D., Young, D., Richter, J., Weiss, A., Marcel, A., Maassen, J., Kauffmann, M., Bibel, M., Shimshek, D. R., Faull, R. L., Bates, G. P., Kuhn, R. R., Van der Putten, P. H., Schmid, P. & Lotz, G. P. (2012) Fragments of HdhQ150 mutant huntingtin form a soluble oligomer pool that declines with aggregate deposition upon aging. *PLoS One*, 7(9), e44457.

Martinez-Vicente, M., Talloczy, Z., Wong, E., Tang, G., Koga, H., Kaushik, S., de Vries, R., Arias, E., Harris, S., Sulzer, D. & Cuervo, A. M. (2010) Cargo recognition failure is

responsible for inefficient autophagy in Huntington's disease. *Nat Neurosci*, 13(5), 567-76.

Martín-Aparicio, E., Avila, J. & Lucas, J. J. (2002) Nuclear localization of N-terminal mutant huntingtin is cell cycle dependent. *Eur J Neurosci*, 16(2), 355-9.

Mason, S. L. & Barker, R. A. (2009) Emerging drug therapies in Huntington's disease. *Expert Opin Emerg Drugs*, 14(2), 273-97.

Maynard, C. J., Böttcher, C., Ortega, Z., Smith, R., Florea, B. I., Díaz-Hernández, M., Brundin, P., Overkleeft, H. S., Li, J. Y., Lucas, J. J. & Dantuma, N. P. (2009) Accumulation of ubiquitin conjugates in a polyglutamine disease model occurs without global ubiquitin/proteasome system impairment. *Proc Natl Acad Sci U S A*, 106(33), 13986-91.

McBride, J. L., Pitzer, M. R., Boudreau, R. L., Dufour, B., Hobbs, T., Ojeda, S. R. & Davidson, B. L. (2011) Preclinical safety of RNAi-mediated HTT suppression in the rhesus macaque as a potential therapy for Huntington's disease. *Mol Ther*, 19(12), 2152-62.

Menalled, L. B., Kudwa, A. E., Miller, S., Fitzpatrick, J., Watson-Johnson, J., Keating, N., Ruiz, M., Mushlin, R., Alosio, W., McConnell, K., Connor, D., Murphy, C., Oakeshott, S., Kwan, M., Beltran, J., Ghavami, A., Brunner, D., Park, L. C., Ramboz, S. & Howland, D. (2012) Comprehensive behavioral and molecular characterization of a new knock-in mouse model of Huntington's disease: zQ175. *PLoS One*, 7(12), e49838.

Menalled, L. B., Sison, J. D., Dragatsis, I., Zeitlin, S. & Chesselet, M. F. (2003) Time course of early motor and neuropathological anomalies in a knock-in mouse model of Huntington's disease with 140 CAG repeats. *J Comp Neurol*, 465(1), 11-26.

Menzies, F. M., Fleming, A., Caricasole, A., Bento, C. F., Andrews, S. P., Ashkenazi, A., Füllgrabe, J., Jackson, A., Jimenez Sanchez, M., Karabiyik, C., Licitra, F., Lopez Ramirez, A., Pavel, M., Puri, C., Renna, M., Ricketts, T., Schlotawa, L., Vicinanza, M., Won, H., Zhu, Y., Skidmore, J. & Rubinsztein, D. C. (2017) Autophagy and Neurodegeneration: Pathogenic Mechanisms and Therapeutic Opportunities. *Neuron*, 93(5), 1015-1034.

Mercuri, E., Darras, B. T., Chiriboga, C. A., Day, J. W., Campbell, C., Connolly, A. M., Iannaccone, S. T., Kirschner, J., Kuntz, N. L., Saito, K., Shieh, P. B., Tulinius, M., Mazzone, E. S., Montes, J., Bishop, K. M., Yang, Q., Foster, R., Gheuens, S., Bennett, C. F., Farwell, W., Schneider, E., De Vivo, D. C., Finkel, R. S. & Group, C. S. (2018) Nusinersen versus Sham Control in Later-Onset Spinal Muscular Atrophy. *N Engl J Med*, 378(7), 625-635.

Mestre, T., Ferreira, J., Coelho, M. M., Rosa, M. & Sampaio, C. (2009) Therapeutic interventions for symptomatic treatment in Huntington's disease. *Cochrane Database Syst Rev*(3), CD006456.

Mielcarek, M., Landles, C., Weiss, A., Bradaia, A., Seredenina, T., Inuabasi, L., Osborne, G. F., Wadel, K., Touller, C., Butler, R., Robertson, J., Franklin, S. A., Smith, D. L., Park, L., Marks, P. A., Wanker, E. E., Olson, E. N., Luthi-Carter, R., van der Putten, H., Beaumont, V. & Bates, G. P. (2013) HDAC4 reduction: a novel therapeutic strategy to target cytoplasmic huntingtin and ameliorate neurodegeneration. *PLoS Biol*, 11(11), e1001717.

Miller, B. R., Dorner, J. L., Shou, M., Sari, Y., Barton, S. J., Sengelaub, D. R., Kennedy, R. T. & Rebec, G. V. (2008) Up-regulation of GLT1 expression increases glutamate

uptake and attenuates the Huntington's disease phenotype in the R6/2 mouse. *Neuroscience*, 153(1), 329-37.

Miller, J., Arrasate, M., Brooks, E., Libeu, C. P., Legleiter, J., Hatters, D., Curtis, J., Cheung, K., Krishnan, P., Mitra, S., Widjaja, K., Shaby, B. A., Lotz, G. P., Newhouse, Y., Mitchell, E. J., Osmand, A., Gray, M., Thulasiramin, V., Saudou, F., Segal, M., Yang, X. W., Masliah, E., Thompson, L. M., Muchowski, P. J., Weisgraber, K. H. & Finkbeiner, S. (2011) Identifying polyglutamine protein species in situ that best predict neurodegeneration. *Nat Chem Biol*, 7(12), 925-34.

Miller, J., Arrasate, M., Shaby, B. A., Mitra, S., Masliah, E. & Finkbeiner, S. (2010) Quantitative relationships between huntingtin levels, polyglutamine length, inclusion body formation, and neuronal death provide novel insight into huntington's disease molecular pathogenesis. *J Neurosci*, 30(31), 10541-50.

Miller, J. R. C., Pfister, E. L., Liu, W., Andre, R., Träger, U., Kennington, L. A., Lo, K., Dijkstra, S., Macdonald, D., Ostroff, G., Aronin, N. & Tabrizi, S. J. (2017) Allele-Selective Suppression of Mutant Huntingtin in Primary Human Blood Cells. *Sci Rep*, 7, 46740.

Miller, T. M., Pestronk, A., David, W., Rothstein, J., Simpson, E., Appel, S. H., Andres, P. L., Mahoney, K., Allred, P., Alexander, K., Ostrow, L. W., Schoenfeld, D., Macklin, E. A., Norris, D. A., Manousakis, G., Crisp, M., Smith, R., Bennett, C. F., Bishop, K. M. & Cudkowicz, M. E. (2013) An antisense oligonucleotide against SOD1 delivered intrathecally for patients with SOD1 familial amyotrophic lateral sclerosis: a phase 1, randomised, first-in-man study. *Lancet Neurol*, 12(5), 435-42.

Miniarikova, J., Evers, M. M. & Konstantinova, P. (2018) Translation of MicroRNA-Based Huntingtin-Lowering Therapies from Preclinical Studies to the Clinic. *Mol Ther*, 26(4), 947-962.

Morton, A. J., Glynn, D., Leavens, W., Zheng, Z., Faull, R. L., Skepper, J. N. & Wight, J. M. (2009) Paradoxical delay in the onset of disease caused by super-long CAG repeat expansions in R6/2 mice. *Neurobiol Dis*, 33(3), 331-41.

Myers, R. H., Sax, D. S., Koroshetz, W. J., Mastromauro, C., Cupples, L. A., Kiely, D. K., Pettengill, F. K. & Bird, E. D. (1991) Factors associated with slow progression in Huntington's disease. *Arch Neurol*, 48(8), 800-4.

Nasir, J., Floresco, S. B., O'Kusky, J. R., Diewert, V. M., Richman, J. M., Zeisler, J., Borowski, A., Marth, J. D., Phillips, A. G. & Hayden, M. R. (1995) Targeted disruption of the Huntington's disease gene results in embryonic lethality and behavioral and morphological changes in heterozygotes. *Cell*, 81(5), 811-23.

Nath, S., Munsie, L. N. & Truant, R. (2015) A huntingtin-mediated fast stress response halting endosomal trafficking is defective in Huntington's disease. *Hum Mol Genet*, 24(2), 450-62.

NCT02197130 *Randomized, Placebo Controlled Study Of The Efficacy And Safety Of PF-02545920 In Subjects With Huntington's Disease*Available online: [Accessed.

NCT02215616 *A Clinical Study in Subjects With Huntington's Disease to Assess the Efficacy and Safety of Three Oral Doses of Laquinimod (LEGATO-HD)*Available online: [Accessed.

Nekooki-Machida, Y., Kurosawa, M., Nukina, N., Ito, K., Oda, T. & Tanaka, M. (2009) Distinct conformations of in vitro and in vivo amyloids of huntingtin-exon1 show different cytotoxicity. *Proc Natl Acad Sci U S A*, 106(24), 9679-84.

Neueder, A., Landles, C., Ghosh, R., Howland, D., Myers, R. H., Faull, R. L. M., Tabrizi, S. J. & Bates, G. P. (2017) The pathogenic exon 1 HTT protein is produced by incomplete splicing in Huntington's disease patients. *Sci Rep*, 7(1), 1307.

Nirmaladevi, D., Venkataramana, M., Chandranayaka, S., Ramesha, A., Jameel, N. M. & Srinivas, C. (2014) Neuroprotective effects of bikaverin on H2O2-induced oxidative stress mediated neuronal damage in SH-SY5Y cell line. *Cell Mol Neurobiol*, 34(7), 973-85.

Novak, M. J. & Tabrizi, S. J. (2010) Huntington's disease. *BMJ*, 340, c3109.

Ossato, G., Digman, M. A., Aiken, C., Lukacsovich, T., Marsh, J. L. & Gratton, E. (2010) A two-step path to inclusion formation of huntingtin peptides revealed by number and brightness analysis. *Biophys J*, 98(12), 3078-85.

Pardo, R., Molina-Calavita, M., Poizat, G., Keryer, G., Humbert, S. & Saudou, F. (2010) pARIS-htt: an optimised expression platform to study huntingtin reveals functional domains required for vesicular trafficking. *Mol Brain*, 3, 17.

Park, I. H., Arora, N., Huo, H., Maherali, N., Ahfeldt, T., Shimamura, A., Lensch, M. W., Cowan, C., Hochedlinger, K. & Daley, G. Q. (2008) Disease-specific induced pluripotent stem cells. *Cell*, 134(5), 877-86.

Park, S. H., Kukushkin, Y., Gupta, R., Chen, T., Konagai, A., Hipp, M. S., Hayer-Hartl, M. & Hartl, F. U. (2013) PolyQ proteins interfere with nuclear degradation of cytosolic proteins by sequestering the Sis1p chaperone. *Cell*, 154(1), 134-45.

Paulsen, J. S., Langbehn, D. R., Stout, J. C., Aylward, E., Ross, C. A., Nance, M., Guttman, M., Johnson, S., MacDonald, M., Beglinger, L. J., Duff, K., Kayson, E., Biglan, K., Shoulson, I., Oakes, D., Hayden, M. & Group, P.-H. I. a. C. o. t. H. S. (2008) Detection of Huntington's disease decades before diagnosis: the Predict-HD study. *J Neurol Neurosurg Psychiatry*, 79(8), 874-80.

Paulsen, J. S., Nehl, C., Hoth, K. F., Kanz, J. E., Benjamin, M., Conybeare, R., McDowell, B. & Turner, B. (2005) Depression and stages of Huntington's disease. *J Neuropsychiatry Clin Neurosci*, 17(4), 496-502.

Pavese, N., Gerhard, A., Tai, Y. F., Ho, A. K., Turkheimer, F., Barker, R. A., Brooks, D. J. & Piccini, P. (2006) Microglial activation correlates with severity in Huntington disease: a clinical and PET study. *Neurology*, 66(11), 1638-43.

Peavy, G. M., Jacobson, M. W., Goldstein, J. L., Hamilton, J. M., Kane, A., Gamst, A. C., Lessig, S. L., Lee, J. C. & Corey-Bloom, J. (2010) Cognitive and functional decline in Huntington's disease: dementia criteria revisited. *Mov Disord*, 25(9), 1163-9.

Pecho-Vrieseling, E., Rieker, C., Fuchs, S., Bleckmann, D., Esposito, M. S., Botta, P., Goldstein, C., Bernhard, M., Galimberti, I., Müller, M., Lüthi, A., Arber, S., Bouwmeester, T., van der Putten, H. & Di Giorgio, F. P. (2014) Transneuronal propagation of mutant huntingtin contributes to non-cell autonomous pathology in neurons. *Nat Neurosci*, 17(8), 1064-72.

Persichetti, F., Ambrose, C. M., Ge, P., McNeil, S. M., Srinidhi, J., Anderson, M. A., Jenkins, B., Barnes, G. T., Duyao, M. P. & Kanaley, L. (1995) Normal and expanded Huntington's disease gene alleles produce distinguishable proteins due to translation across the CAG repeat. *Mol Med*, 1(4), 374-83.

Peskett, T. R., Rau, F., O'Driscoll, J., Patani, R., Lowe, A. R. & Saibil, H. R. (2018) A Liquid to Solid Phase Transition Underlying Pathological Huntingtin Exon1 Aggregation. *Mol Cell*, 70(4), 588-601.e6.

Pfister, E. L., Kennington, L., Straubhaar, J., Wagh, S., Liu, W., DiFiglia, M., Landwehrmeyer, B., Vonsattel, J. P., Zamore, P. D. & Aronin, N. (2009) Five siRNAs targeting three SNPs may provide therapy for three-quarters of Huntington's disease patients. *Curr Biol*, 19(9), 774-8.

Pollock, K., Stroemer, P., Patel, S., Stevanato, L., Hope, A., Miljan, E., Dong, Z., Hodges, H., Price, J. & Sinden, J. D. (2006) A conditionally immortal clonal stem cell line from human cortical neuroepithelium for the treatment of ischemic stroke. *Exp Neurol*, 199(1), 143-55.

Pratt, G. & Rechsteiner, M. (2008) Proteasomes cleave at multiple sites within polyglutamine tracts: activation by PA28gamma(K188E). *J Biol Chem*, 283(19), 12919-25.

Qi, L., Zhang, X. D., Wu, J. C., Lin, F., Wang, J., DiFiglia, M. & Qin, Z. H. (2012) The role of chaperone-mediated autophagy in huntingtin degradation. *PLoS One*, 7(10), e46834.

Qin, Z. H., Wang, Y., Kegel, K. B., Kazantsev, A., Apostol, B. L., Thompson, L. M., Yoder, J., Aronin, N. & DiFiglia, M. (2003) Autophagy regulates the processing of amino terminal huntingtin fragments. *Hum Mol Genet*, 12(24), 3231-44.

Ramdzan, Y. M., Polling, S., Chia, C. P., Ng, I. H., Ormsby, A. R., Croft, N. P., Purcell, A. W., Bogoyevitch, M. A., Ng, D. C., Gleeson, P. A. & Hatters, D. M. (2012) Tracking protein aggregation and mislocalization in cells with flow cytometry. *Nat Methods*, 9(5), 467-70.

Ramdzan, Y. M., Trubetskov, M. M., Ormsby, A. R., Newcombe, E. A., Sui, X., Tobin, M. J., Bongiovanni, M. N., Gras, S. L., Dewson, G., Miller, J. M. L., Finkbeiner, S., Moily, N. S., Niclis, J., Parish, C. L., Purcell, A. W., Baker, M. J., Wilce, J. A., Waris, S., Stojanovski, D., Böcking, T., Ang, C. S., Ascher, D. B., Reid, G. E. & Hatters, D. M. (2017) Huntingtin Inclusions Trigger Cellular Quiescence, Deactivate Apoptosis, and Lead to Delayed Necrosis. *Cell Rep*, 19(5), 919-927.

Ravikumar, B., Vacher, C., Berger, Z., Davies, J. E., Luo, S., Oroz, L. G., Scaravilli, F., Easton, D. F., Duden, R., O'Kane, C. J. & Rubinsztein, D. C. (2004) Inhibition of mTOR induces autophagy and reduces toxicity of polyglutamine expansions in fly and mouse models of Huntington disease. *Nat Genet*, 36(6), 585-95.

Rawlins, M. (2010) Huntington's disease out of the closet? *Lancet*, 376(9750), 1372-3.

Reddy, P. H. & Shirendeb, U. P. (2012) Mutant huntingtin, abnormal mitochondrial dynamics, defective axonal transport of mitochondria, and selective synaptic degeneration in Huntington's disease. *Biochim Biophys Acta*, 1822(2), 101-10.

Reuter, I., Tai, Y. F., Pavese, N., Chaudhuri, K. R., Mason, S., Polkey, C. E., Clough, C., Brooks, D. J., Barker, R. A. & Piccini, P. (2008) Long-term clinical and positron emission tomography outcome of fetal striatal transplantation in Huntington's disease. *J Neurol Neurosurg Psychiatry*, 79(8), 948-51.

Rigamonti, D., Sipione, S., Goffredo, D., Zuccato, C., Fossale, E. & Cattaneo, E. (2001) Huntingtin's neuroprotective activity occurs via inhibition of procaspase-9 processing. *J Biol Chem*, 276(18), 14545-8.

Rodrigues, F. B., Byrne, L., McColgan, P., Robertson, N., Tabrizi, S. J., Leavitt, B. R., Zetterberg, H. & Wild, E. J. (2016) Cerebrospinal fluid total tau concentration predicts clinical phenotype in Huntington's disease. *J Neurochem*, 139(1), 22-5.

Rosas, H. D., Reuter, M., Doros, G., Lee, S. Y., Triggs, T., Malarick, K., Fischl, B., Salat, D. H. & Hersch, S. M. (2011) A tale of two factors: what determines the rate of progression in Huntington's disease? A longitudinal MRI study. *Mov Disord*, 26(9), 1691-7.

Rosenblatt, A., Kumar, B. V., Mo, A., Welsh, C. S., Margolis, R. L. & Ross, C. A. (2012) Age, CAG repeat length, and clinical progression in Huntington's disease. *Mov Disord*, 27(2), 272-6.

Ross, C. A., Aylward, E. H., Wild, E. J., Langbehn, D. R., Long, J. D., Warner, J. H., Scahill, R. I., Leavitt, B. R., Stout, J. C., Paulsen, J. S., Reilmann, R., Unschuld, P. G., Wexler, A., Margolis, R. L. & Tabrizi, S. J. (2014) Huntington disease: natural history, biomarkers and prospects for therapeutics. *Nat Rev Neurol*, 10(4), 204-16.

Ross, C. A. & Tabrizi, S. J. (2011) Huntington's disease: from molecular pathogenesis to clinical treatment. *Lancet Neurol*, 10(1), 83-98.

Rosser, A. E., Barker, R. A., Harrower, T., Watts, C., Farrington, M., Ho, A. K., Burnstein, R. M., Menon, D. K., Gillard, J. H., Pickard, J., Dunnett, S. B. & NEST-UK (2002) Unilateral transplantation of human primary fetal tissue in four patients with Huntington's disease: NEST-UK safety report ISRCTN no 36485475. *J Neurol Neurosurg Psychiatry*, 73(6), 678-85.

Roux, J. C., Zala, D., Panayotis, N., Borges-Correia, A., Saudou, F. & Villard, L. (2012) Modification of Mecp2 dosage alters axonal transport through the Huntingtin/Hap1 pathway. *Neurobiol Dis*, 45(2), 786-95.

Rubinsztein, D. C., Leggo, J., Coles, R., Almqvist, E., Biancalana, V., Cassiman, J. J., Chotai, K., Connarty, M., Crauford, D., Curtis, A., Curtis, D., Davidson, M. J., Differ, A. M., Dode, C., Dodge, A., Frontali, M., Ranen, N. G., Stine, O. C., Sherr, M., Abbott, M. H., Franz, M. L., Graham, C. A., Harper, P. S., Hedreen, J. C. & Hayden, M. R. (1996) Phenotypic characterization of individuals with 30-40 CAG repeats in the Huntington disease (HD) gene reveals HD cases with 36 repeats and apparently normal elderly individuals with 36-39 repeats. *Am J Hum Genet*, 59(1), 16-22.

Ruzo, A., Croft, G. F., Metzger, J. J., Galgoczi, S., Gerber, L. J., Pellegrini, C., Wang, H., Fenner, M., Tse, S., Marks, A., Nchako, C. & Brivanlou, A. H. (2018) Chromosomal instability during neurogenesis in Huntington's disease. *Development*, 145(2).

Sahoo, B., Arduini, I., Drombosky, K. W., Kodali, R., Sanders, L. H., Greenamyre, J. T. & Wetzel, R. (2016) Folding Landscape of Mutant Huntingtin Exon1: Diffusible Multimers, Oligomers and Fibrils, and No Detectable Monomer. *PLoS One*, 11(6), e0155747.

Sapp, E., Schwarz, C., Chase, K., Bhide, P. G., Young, A. B., Penney, J., Vonsattel, J. P., Aronin, N. & DiFiglia, M. (1997) Huntingtin localization in brains of normal and Huntington's disease patients. *Ann Neurol*, 42(4), 604-12.

Sarkar, S., Ravikumar, B. & Rubinsztein, D. C. (2009) Autophagic clearance of aggregate-prone proteins associated with neurodegeneration. *Methods Enzymol*, 453, 83-110.

Sasazawa, Y., Sato, N., Umezawa, K. & Simizu, S. (2015) Conophylline protects cells in cellular models of neurodegenerative diseases by inducing mammalian target of rapamycin (mTOR)-independent autophagy. *J Biol Chem*, 290(10), 6168-78.

Sathasivam, K., Neueder, A., Gipson, T. A., Landles, C., Benjamin, A. C., Bondulich, M. K., Smith, D. L., Faull, R. L., Roos, R. A., Howland, D., Detloff, P. J., Housman, D.

E. & Bates, G. P. (2013) Aberrant splicing of HTT generates the pathogenic exon 1 protein in Huntington disease. *Proc Natl Acad Sci U S A*, 110(6), 2366-70.

Schaffar, G., Breuer, P., Boteva, R., Behrends, C., Tzvetkov, N., Strippel, N., Sakahira, H., Siegers, K., Hayer-Hartl, M. & Hartl, F. U. (2004) Cellular toxicity of polyglutamine expansion proteins: mechanism of transcription factor deactivation. *Mol Cell*, 15(1), 95-105.

Scherzinger, E., Sittler, A., Schweiger, K., Heiser, V., Lurz, R., Hasenbank, R., Bates, G. P., Lehrach, H. & Wanker, E. E. (1999) Self-assembly of polyglutamine-containing huntingtin fragments into amyloid-like fibrils: implications for Huntington's disease pathology. *Proc Natl Acad Sci U S A*, 96(8), 4604-9.

Schilling, G., Becher, M. W., Sharp, A. H., Jinnah, H. A., Duan, K., Kotzuk, J. A., Slunt, H. H., Ratovitski, T., Cooper, J. K., Jenkins, N. A., Copeland, N. G., Price, D. L., Ross, C. A. & Borchelt, D. R. (1999) Intranuclear inclusions and neuritic aggregates in transgenic mice expressing a mutant N-terminal fragment of huntingtin. *Hum Mol Genet*, 8(3), 397-407.

Schrader, E. K., Harstad, K. G. & Matouschek, A. (2009) Targeting proteins for degradation. *Nat Chem Biol*, 5(11), 815-22.

Semaka, A., Kay, C., Doty, C., Collins, J. A., Bijlsma, E. K., Richards, F., Goldberg, Y. P. & Hayden, M. R. (2013) CAG size-specific risk estimates for intermediate allele repeat instability in Huntington disease. *J Med Genet*, 50(10), 696-703.

Seo, H., Sonntag, K. C. & Isacson, O. (2004) Generalized brain and skin proteasome inhibition in Huntington's disease. *Ann Neurol*, 56(3), 319-28.

Seo, H., Sonntag, K. C., Kim, W., Cattaneo, E. & Isacson, O. (2007) Proteasome activator enhances survival of Huntington's disease neuronal model cells. *PLoS One*, 2(2), e238.

Shi, Y., Kirwan, P. & Livesey, F. J. (2012) Directed differentiation of human pluripotent stem cells to cerebral cortex neurons and neural networks. *Nat Protoc*, 7(10), 1836-46.

Shibata, M., Lu, T., Furuya, T., Degterev, A., Mizushima, N., Yoshimori, T., MacDonald, M., Yankner, B. & Yuan, J. (2006) Regulation of intracellular accumulation of mutant Huntingtin by Beclin 1. *J Biol Chem*, 281(20), 14474-85.

Shin, J. W., Kim, K. H., Chao, M. J., Atwal, R. S., Gillis, T., MacDonald, M. E., Gusella, J. F. & Lee, J. M. (2016) Permanent inactivation of Huntington's disease mutation by personalized allele-specific CRISPR/Cas9. *Hum Mol Genet*, 25(20), 4566-4576.

Shin, J. Y., Fang, Z. H., Yu, Z. X., Wang, C. E., Li, S. H. & Li, X. J. (2005) Expression of mutant huntingtin in glial cells contributes to neuronal excitotoxicity. *J Cell Biol*, 171(6), 1001-12.

Siddiqui, A., Rivera-Sánchez, S., Castro, M. e. R., Acevedo-Torres, K., Rane, A., Torres-Ramos, C. A., Nicholls, D. G., Andersen, J. K. & Ayala-Torres, S. (2012) Mitochondrial DNA damage is associated with reduced mitochondrial bioenergetics in Huntington's disease. *Free Radic Biol Med*, 53(7), 1478-88.

Siesling, S., Vegter-van de Vlis, M., Losekoot, M., Belfroid, R. D., Maat-Kievit, J. A., Kremer, H. P. & Roos, R. A. (2000) Family history and DNA analysis in patients with suspected Huntington's disease. *J Neurol Neurosurg Psychiatry*, 69(1), 54-9.

Simmons, D. A., Belichenko, N. P., Yang, T., Condon, C., Monbureau, M., Shamloo, M., Jing, D., Massa, S. M. & Longo, F. M. (2013) A small molecule TrkB ligand reduces

motor impairment and neuropathology in R6/2 and BACHD mouse models of Huntington's disease. *J Neurosci*, 33(48), 18712-27.

Sirinathsingh, E. (2009) *Generation of human stem cell models of Huntington's disease*. Doctor of Philosophy Guy's, King's and St Thomas's School of Medicine.

Slow, E. J., Graham, R. K., Osmand, A. P., Devon, R. S., Lu, G., Deng, Y., Pearson, J., Vaid, K., Bissada, N., Wetzel, R., Leavitt, B. R. & Hayden, M. R. (2005) Absence of behavioral abnormalities and neurodegeneration in vivo despite widespread neuronal huntingtin inclusions. *Proc Natl Acad Sci U S A*, 102(32), 11402-7.

Slow, E. J., van Raamsdonk, J., Rogers, D., Coleman, S. H., Graham, R. K., Deng, Y., Oh, R., Bissada, N., Hossain, S. M., Yang, Y. Z., Li, X. J., Simpson, E. M., Gutekunst, C. A., Leavitt, B. R. & Hayden, M. R. (2003) Selective striatal neuronal loss in a YAC128 mouse model of Huntington disease. *Hum Mol Genet*, 12(13), 1555-67.

Smith, R., Brundin, P. & Li, J. Y. (2005) Synaptic dysfunction in Huntington's disease: a new perspective. *Cell Mol Life Sci*, 62(17), 1901-12.

Snell, R. G., MacMillan, J. C., Cheadle, J. P., Fenton, I., Lazarou, L. P., Davies, P., MacDonald, M. E., Gusella, J. F., Harper, P. S. & Shaw, D. J. (1993) Relationship between trinucleotide repeat expansion and phenotypic variation in Huntington's disease. *Nat Genet*, 4(4), 393-7.

Song, C., Perides, G. & Liu, Y. F. (2002) Expression of full-length polyglutamine-expanded Huntingtin disrupts growth factor receptor signaling in rat pheochromocytoma (PC12) cells. *J Biol Chem*, 277(8), 6703-7.

Sontag, E. M., Joachimiak, L. A., Tan, Z., Tomlinson, A., Housman, D. E., Glabe, C. G., Potkin, S. G., Frydman, J. & Thompson, L. M. (2013) Exogenous delivery of chaperonin subunit fragment ApiCCT1 modulates mutant Huntingtin cellular phenotypes. *Proc Natl Acad Sci U S A*, 110(8), 3077-82.

Sontag, E. M., Lotz, G. P., Agrawal, N., Tran, A., Aron, R., Yang, G., Necula, M., Lau, A., Finkbeiner, S., Glabe, C., Marsh, J. L., Muchowski, P. J. & Thompson, L. M. (2012) Methylene blue modulates huntingtin aggregation intermediates and is protective in Huntington's disease models. *J Neurosci*, 32(32), 11109-19.

Southwell, A. L., Skotte, N. H., Kordasiewicz, H. B., Østergaard, M. E., Watt, A. T., Carroll, J. B., Doty, C. N., Villanueva, E. B., Petoukhov, E., Vaid, K., Xie, Y., Freier, S. M., Swayze, E. E., Seth, P. P., Bennett, C. F. & Hayden, M. R. (2014) In vivo evaluation of candidate allele-specific mutant huntingtin gene silencing antisense oligonucleotides. *Mol Ther*, 22(12), 2093-106.

Stanek, L. M., Sardi, S. P., Mastis, B., Richards, A. R., Treleaven, C. M., Taksir, T., Misra, K., Cheng, S. H. & Shihabuddin, L. S. (2014) Silencing mutant huntingtin by adeno-associated virus-mediated RNA interference ameliorates disease manifestations in the YAC128 mouse model of Huntington's disease. *Hum Gene Ther*, 25(5), 461-74.

Steffan, J. S., Kazantsev, A., Spasic-Boskovic, O., Greenwald, M., Zhu, Y. Z., Gohler, H., Wanker, E. E., Bates, G. P., Housman, D. E. & Thompson, L. M. (2000) The Huntington's disease protein interacts with p53 and CREB-binding protein and represses transcription. *Proc Natl Acad Sci U S A*, 97(12), 6763-8.

Stout, J. C., Jones, R., Labuschagne, I., O'Regan, A. M., Say, M. J., Dumas, E. M., Queller, S., Justo, D., Santos, R. D., Coleman, A., Hart, E. P., Durr, A., Leavitt, B. R., Roos, R. A., Langbehn, D. R., Tabrizi, S. J. & Frost, C. (2012) Evaluation of

longitudinal 12 and 24 month cognitive outcomes in premanifest and early Huntington's disease. *J Neurol Neurosurg Psychiatry*, 83(7), 687-94.

Stout, J. C., Paulsen, J. S., Queller, S., Solomon, A. C., Whitlock, K. B., Campbell, J. C., Carlozzi, N., Duff, K., Beglinger, L. J., Langbehn, D. R., Johnson, S. A., Biglan, K. M. & Aylward, E. H. (2011) Neurocognitive signs in prodromal Huntington disease. *Neuropsychology*, 25(1), 1-14.

Swami, M., Hendricks, A. E., Gillis, T., Massood, T., Mysore, J., Myers, R. H. & Wheeler, V. C. (2009) Somatic expansion of the Huntington's disease CAG repeat in the brain is associated with an earlier age of disease onset. *Hum Mol Genet*, 18(16), 3039-47.

Süssmuth, S. D., Haider, S., Landwehrmeyer, G. B., Farmer, R., Frost, C., Tripepi, G., Andersen, C. A., Di Bacco, M., Lamanna, C., Diodato, E., Massai, L., Diamanti, D., Mori, E., Magnoni, L., Dreyhaupt, J., Schiefele, K., Craufurd, D., Saft, C., Rudzinska, M., Ryglewicz, D., Orth, M., Brzozy, S., Baran, A., Pollio, G., Andre, R., Tabrizi, S. J., Darpo, B., Westerberg, G. & Consortium, P. (2015) An exploratory double-blind, randomized clinical trial with selisistat, a SirT1 inhibitor, in patients with Huntington's disease. *Br J Clin Pharmacol*, 79(3), 465-76.

Tabrizi, S., Leavitt, B., Kordasiewicz, H., Czech, C., Swayze, E., Norris, D., Baumann, T., Gerlach, I., Schobel, S., Smith, A., Lane, R. & Bennett, C. F. Effects of IONIS-HTTRx in Patients with Early Huntington's Disease, Results of the First HTT-Lowering Drug Trial (CT.002). Neurology Apr 2018, 90 (15 Supplement) CT.002.

Tabrizi, S., Leavitt, B., Kordasiewicz, H., Czech, C., Swayze, E., Norris, D., Baumann, T., Gerlach, I., Schobel, S., Smith, A., Lane, R. & Bennett, C. F. (2018) Effects of IONIS-HTTRx in Patients with Early Huntington's Disease, Results of the First HTT-Lowering Drug Trial (CT.002). Neurology Apr 2018, 90 (15 Supplement) CT.002.

Tabrizi, S. J., Langbehn, D. R., Leavitt, B. R., Roos, R. A., Durr, A., Craufurd, D., Kennard, C., Hicks, S. L., Fox, N. C., Scahill, R. I., Borowsky, B., Tobin, A. J., Rosas, H. D., Johnson, H., Reilmann, R., Landwehrmeyer, B., Stout, J. C. & investigators, T.-H. (2009) Biological and clinical manifestations of Huntington's disease in the longitudinal TRACK-HD study: cross-sectional analysis of baseline data. *Lancet Neurol*, 8(9), 791-801.

Tabrizi, S. J., Reilmann, R., Roos, R. A., Durr, A., Leavitt, B., Owen, G., Jones, R., Johnson, H., Craufurd, D., Hicks, S. L., Kennard, C., Landwehrmeyer, B., Stout, J. C., Borowsky, B., Scahill, R. I., Frost, C., Langbehn, D. R. & investigators, T.-H. (2012) Potential endpoints for clinical trials in premanifest and early Huntington's disease in the TRACK-HD study: analysis of 24 month observational data. *Lancet Neurol*, 11(1), 42-53.

Tabrizi, S. J., Scahill, R. I., Durr, A., Roos, R. A., Leavitt, B. R., Jones, R., Landwehrmeyer, G. B., Fox, N. C., Johnson, H., Hicks, S. L., Kennard, C., Craufurd, D., Frost, C., Langbehn, D. R., Reilmann, R., Stout, J. C. & Investigators, T.-H. (2011) Biological and clinical changes in premanifest and early stage Huntington's disease in the TRACK-HD study: the 12-month longitudinal analysis. *Lancet Neurol*, 10(1), 31-42.

Tabrizi, S. J., Scahill, R. I., Owen, G., Durr, A., Leavitt, B. R., Roos, R. A., Borowsky, B., Landwehrmeyer, B., Frost, C., Johnson, H., Craufurd, D., Reilmann, R., Stout, J. C., Langbehn, D. R. & Investigators, t. T.-H. (2013) Predictors of phenotypic progression and disease onset in premanifest and early-stage Huntington's disease in the TRACK-HD study: analysis of 36-month observational data. *Lancet Neurol*.

Tai, Y. F., Pavese, N., Gerhard, A., Tabrizi, S. J., Barker, R. A., Brooks, D. J. & Piccini, P. (2007) Microglial activation in presymptomatic Huntington's disease gene carriers. *Brain*, 130(Pt 7), 1759-66.

Takahashi, K., Tanabe, K., Ohnuki, M., Narita, M., Ichisaka, T., Tomoda, K. & Yamanaka, S. (2007) Induction of pluripotent stem cells from adult human fibroblasts by defined factors. *Cell*, 131(5), 861-72.

Takahashi, K. & Yamanaka, S. (2006) Induction of pluripotent stem cells from mouse embryonic and adult fibroblast cultures by defined factors. *Cell*, 126(4), 663-76.

Tashiro, E., Zako, T., Muto, H., Itoo, Y., Sörgjerd, K., Terada, N., Abe, A., Miyazawa, M., Kitamura, A., Kitaura, H., Kubota, H., Maeda, M., Momoi, T., Iguchi-Ariga, S. M., Kinjo, M. & Ariga, H. (2013) Prefoldin protects neuronal cells from polyglutamine toxicity by preventing aggregation formation. *J Biol Chem*, 288(27), 19958-72.

Taylor, D. M., Moser, R., Régulier, E., Breuillaud, L., Dixon, M., Beesen, A. A., Elliston, L., Silva Santos, M. e. F., Kim, J., Jones, L., Goldstein, D. R., Ferrante, R. J. & Luthi-Carter, R. (2013) MAP kinase phosphatase 1 (MKP-1/DUSP1) is neuroprotective in Huntington's disease via additive effects of JNK and p38 inhibition. *J Neurosci*, 33(6), 2313-25.

The Hd Ipsc Consortium (2012) Induced Pluripotent Stem Cells from Patients with Huntington's Disease Show CAG-Repeat-Expansion-Associated Phenotypes. *Cell Stem Cell*, 11(2), 264-78.

Tong, X., Ao, Y., Faas, G. C., Nwaobi, S. E., Xu, J., Haustein, M. D., Anderson, M. A., Mody, I., Olsen, M. L., Sofroniew, M. V. & Khakh, B. S. (2014) Astrocyte Kir4.1 ion channel deficits contribute to neuronal dysfunction in Huntington's disease model mice. *Nat Neurosci*, 17(5), 694-703.

Trottier, Y., Devys, D., Imbert, G., Saudou, F., An, I., Lutz, Y., Weber, C., Agid, Y., Hirsch, E. C. & Mandel, J. L. (1995) Cellular localization of the Huntington's disease protein and discrimination of the normal and mutated form. *Nat Genet*, 10(1), 104-10.

Trushina, E., Dyer, R. B., Badger, J. D., Ure, D., Eide, L., Tran, D. D., Vrieze, B. T., Legendre-Guillemin, V., McPherson, P. S., Mandavilli, B. S., Van Houten, B., Zeitlin, S., McNiven, M., Aebersold, R., Hayden, M., Parisi, J. E., Seeberg, E., Dragatsis, I., Doyle, K., Bender, A., Chacko, C. & McMurray, C. T. (2004) Mutant huntingtin impairs axonal trafficking in mammalian neurons in vivo and in vitro. *Mol Cell Biol*, 24(18), 8195-209.

Tsvetkov, A. S., Arrasate, M., Barmada, S., Ando, D. M., Sharma, P., Shaby, B. A. & Finkbeiner, S. (2013) Proteostasis of polyglutamine varies among neurons and predicts neurodegeneration. *Nat Chem Biol*, 9(9), 586-92.

van der Burg, J. M., Bjorkqvist, M. & Brundin, P. (2009) Beyond the brain: widespread pathology in Huntington's disease. *Lancet Neurol*, 8(8), 765-74.

van Duijn, E., Kingma, E. M. & van der Mast, R. C. (2007) Psychopathology in verified Huntington's disease gene carriers. *J Neuropsychiatry Clin Neurosci*, 19(4), 441-8.

Vasileva, A. & Jessberger, R. (2005) Precise hit: adeno-associated virus in gene targeting. *Nat Rev Microbiol*, 3(11), 837-47.

Velier, J., Kim, M., Schwarz, C., Kim, T. W., Sapp, E., Chase, K., Aronin, N. & DiFiglia, M. (1998) Wild-type and mutant huntingtins function in vesicle trafficking in the secretory and endocytic pathways. *Exp Neurol*, 152(1), 34-40.

Venkatraman, P., Wetzel, R., Tanaka, M., Nukina, N. & Goldberg, A. L. (2004) Eukaryotic proteasomes cannot digest polyglutamine sequences and release them during degradation of polyglutamine-containing proteins. *Mol Cell*, 14(1), 95-104.

Verny, C., Bachoud-Lévi, A. C., Durr, A., Goizet, C., Azulay, J. P., Simonin, C., Tranchant, C., Calvas, F., Krystkowiak, P., Charles, P., Youssov, K., Scherer, C., Prundean, A., Olivier, A., Reynier, P., Saudou, F., Maison, P., Allain, P., von Studnitz, E., Bonneau, D. & Group, C.-H. S. (2017) A randomized, double-blind, placebo-controlled trial evaluating cysteamine in Huntington's disease. *Mov Disord*, 32(6), 932-936.

Victor, M. B., Richner, M., Hermanstyne, T. O., Ransdell, J. L., Sobieski, C., Deng, P. Y., Klyachko, V. A., Nerbonne, J. M. & Yoo, A. S. (2014) Generation of human striatal neurons by microRNA-dependent direct conversion of fibroblasts. *Neuron*, 84(2), 311-23.

Victor, M. B., Richner, M., Olsen, H. E., Lee, S. W., Monteys, A. M., Ma, C., Huh, C. J., Zhang, B., Davidson, B. L., Yang, X. W. & Yoo, A. S. (2018) Striatal neurons directly converted from Huntington's disease patient fibroblasts recapitulate age-associated disease phenotypes. *Nat Neurosci*, 21(3), 341-352.

Videnovic, A., Leurgans, S., Fan, W., Jaglin, J. & Shannon, K. M. (2009) Daytime somnolence and nocturnal sleep disturbances in Huntington disease. *Parkinsonism Relat Disord*, 15(6), 471-4.

Vijayvargia, R., Epand, R., Leitner, A., Jung, T. Y., Shin, B., Jung, R., Lloret, A., Singh Atwal, R., Lee, H., Lee, J. M., Aebersold, R., Hebert, H., Song, J. J. & Seong, I. S. (2016) Huntingtin's spherical solenoid structure enables polyglutamine tract-dependent modulation of its structure and function. *Elife*, 5, e11184.

von Hörsten, S., Schmitt, I., Nguyen, H. P., Holzmann, C., Schmidt, T., Walther, T., Bader, M., Pabst, R., Kobbe, P., Krotova, J., Stiller, D., Kask, A., Vaarmann, A., Rathke-Hartlieb, S., Schulz, J. B., Grasshoff, U., Bauer, I., Vieira-Saecker, A. M., Paul, M., Jones, L., Lindenberg, K. S., Landwehrmeyer, B., Bauer, A., Li, X. J. & Riess, O. (2003) Transgenic rat model of Huntington's disease. *Hum Mol Genet*, 12(6), 617-24.

Wang, G., Liu, X., Gaertig, M. A., Li, S. & Li, X. J. (2016) Ablation of huntingtin in adult neurons is nondeleterious but its depletion in young mice causes acute pancreatitis. *Proc Natl Acad Sci U S A*, 113(12), 3359-64.

Wang, H. Q., Xu, Y. X., Zhao, X. Y., Zhao, H., Yan, J., Sun, X. B., Guo, J. C. & Zhu, C. Q. (2009) Overexpression of F(0)F(1)-ATP synthase alpha suppresses mutant huntingtin aggregation and toxicity in vitro. *Biochem Biophys Res Commun*, 390(4), 1294-8.

Wang, J., Wang, C. E., Orr, A., Tydlacka, S., Li, S. H. & Li, X. J. (2008) Impaired ubiquitin-proteasome system activity in the synapses of Huntington's disease mice. *J Cell Biol*, 180(6), 1177-89.

Wang, J. Q., Chen, Q., Wang, X., Wang, Q. C., Wang, Y., Cheng, H. P., Guo, C., Sun, Q. & Tang, T. S. (2013) Dysregulation of mitochondrial calcium signaling and superoxide flashes cause mitochondrial genomic DNA damage in Huntington disease. *J Biol Chem*, 288(5), 3070-84.

Wang, N., Gray, M., Lu, X. H., Cantle, J. P., Holley, S. M., Greiner, E., Gu, X., Shirasaki, D., Cepeda, C., Li, Y., Dong, H., Levine, M. S. & Yang, X. W. (2014) Neuronal targets for reducing mutant huntingtin expression to ameliorate disease in a mouse model of Huntington's disease. *Nat Med*, 20(5), 536-41.

Went, L. (1990) Ethical issues policy statement on Huntington's disease molecular genetics predictive test. International Huntington Association. World Federation of Neurology. *J Med Genet*, 27(1), 34-8.

Wetzel, R. & Mishra, R. (2014) Structural Biology: Order, Disorder, and Conformational Flux., in Bates, G., Tabrizi, S. J. & Jones, L. (eds), *Huntington's Disease*, 4th editionOxford University Press.

Wexler, A. (2010) Stigma, history, and Huntington's disease. *Lancet*, 376(9734), 18-9.

Wijeyekoon, R. & Barker, R. A. (2011) The Current Status of Neural Grafting in the Treatment of Huntington's Disease. A Review. *Front Integr Neurosci*, 5, 78.

Wild, E. J., Boggio, R., Langbehn, D., Robertson, N., Haider, S., Miller, J. R., Zetterberg, H., Leavitt, B. R., Kuhn, R., Tabrizi, S. J., Macdonald, D. & Weiss, A. (2015) Quantification of mutant huntingtin protein in cerebrospinal fluid from Huntington's disease patients. *J Clin Invest*, 125(5), 1979-86.

Wild, E. J. & Tabrizi, S. J. (2014) Targets for future clinical trials in Huntington's disease: What's in the pipeline? *Mov Disord*, 29(11), 1434-45.

Woerner, A. C., Frottin, F., Hornburg, D., Feng, L. R., Meissner, F., Patra, M., Tatzelt, J., Mann, M., Winklhofer, K. F., Hartl, F. U. & Hipp, M. S. (2016) Cytoplasmic protein aggregates interfere with nucleocytoplasmic transport of protein and RNA. *Science*, 351(6269), 173-6.

Wong, Y. C. & Holzbaur, E. L. (2014) The regulation of autophagosome dynamics by huntingtin and HAP1 is disrupted by expression of mutant huntingtin, leading to defective cargo degradation. *J Neurosci*, 34(4), 1293-305.

Xia, J., Lee, D. H., Taylor, J., Vandelft, M. & Truant, R. (2003) Huntingtin contains a highly conserved nuclear export signal. *Hum Mol Genet*, 12(12), 1393-403.

Yamamoto, A., Tagawa, Y., Yoshimori, T., Moriyama, Y., Masaki, R. & Tashiro, Y. (1998) Bafilomycin A1 prevents maturation of autophagic vacuoles by inhibiting fusion between autophagosomes and lysosomes in rat hepatoma cell line, H-4-II-E cells. *Cell Struct Funct*, 23(1), 33-42.

Yang, D., Wang, C. E., Zhao, B., Li, W., Ouyang, Z., Liu, Z., Yang, H., Fan, P., O'Neill, A., Gu, W., Yi, H., Li, S., Lai, L. & Li, X. J. (2010) Expression of Huntington's disease protein results in apoptotic neurons in the brains of cloned transgenic pigs. *Hum Mol Genet*, 19(20), 3983-94.

Yang, L., Mali, P., Kim-Kiselak, C. & Church, G. (2014) CRISPR-Cas-mediated targeted genome editing in human cells. *Methods Mol Biol*, 1114, 245-67.

Yang, S. H., Cheng, P. H., Banta, H., Piotrowska-Nitsche, K., Yang, J. J., Cheng, E. C., Snyder, B., Larkin, K., Liu, J., Orkin, J., Fang, Z. H., Smith, Y., Bachevalier, J., Zola, S. M., Li, S. H., Li, X. J. & Chan, A. W. (2008) Towards a transgenic model of Huntington's disease in a non-human primate. *Nature*, 453(7197), 921-4.

Ye, C., Zhang, Y., Wang, W., Wang, J. & Li, H. (2008) Inhibition of neurite outgrowth and promotion of cell death by cytoplasmic soluble mutant huntingtin stably transfected in mouse neuroblastoma cells. *Neurosci Lett*, 442(1), 63-8.

Yu-Taeger, L., Petrasch-Parwez, E., Osmand, A. P., Redensek, A., Metzger, S., Clemens, L. E., Park, L., Howland, D., Calaminus, C., Gu, X., Pichler, B., Yang, X. W., Riess, O. & Nguyen, H. P. (2012) A novel BACHD transgenic rat exhibits characteristic neuropathological features of Huntington disease. *J Neurosci*, 32(44), 15426-38.

Zeitlin, S., Liu, J. P., Chapman, D. L., Papaioannou, V. E. & Efstratiadis, A. (1995) Increased apoptosis and early embryonic lethality in mice nullizygous for the Huntington's disease gene homologue. *Nat Genet*, 11(2), 155-63.

Zhang, N., An, M. C., Montoro, D. & Ellerby, L. M. (2010) Characterization of Human Huntington's Disease Cell Model from Induced Pluripotent Stem Cells. *PLoS Curr*, 2, RRN1193.

Zhang, Y., Leavitt, B. R., van Raamsdonk, J. M., Dragatsis, I., Goldowitz, D., MacDonald, M. E., Hayden, M. R. & Friedlander, R. M. (2006) Huntingtin inhibits caspase-3 activation. *EMBO J*, 25(24), 5896-906.

Zhao, T., Hong, Y., Li, X. J. & Li, S. H. (2016) Subcellular Clearance and Accumulation of Huntington Disease Protein: A Mini-Review. *Front Mol Neurosci*, 9, 27.

Zuccato, C. & Cataneo, E. (2014) Normal function of Huntingtin., in Bates, G. P., Tabrizi, S. J. & Jones, L. (eds), *Huntington's disease.*, 4th. edition. Oxford monographs on medical genetics.Oxford University Press.

Zuccato, C., Ciammola, A., Rigamonti, D., Leavitt, B. R., Goffredo, D., Conti, L., MacDonald, M. E., Friedlander, R. M., Silani, V., Hayden, M. R., Timmusk, T., Sipione, S. & Cattaneo, E. (2001) Loss of huntingtin-mediated BDNF gene transcription in Huntington's disease. *Science*, 293(5529), 493-8.

Zuccato, C., Marullo, M., Conforti, P., MacDonald, M. E., Tartari, M. & Cattaneo, E. (2008) Systematic assessment of BDNF and its receptor levels in human cortices affected by Huntington's disease. *Brain Pathol*, 18(2), 225-38.

Zuccato, C., Tartari, M., Crotti, A., Goffredo, D., Valenza, M., Conti, L., Cataudella, T., Leavitt, B. R., Hayden, M. R., Timmusk, T., Rigamonti, D. & Cattaneo, E. (2003) Huntingtin interacts with REST/NRSF to modulate the transcription of NRSE-controlled neuronal genes. *Nat Genet*, 35(1), 76-83.

Zuccato, C., Valenza, M. & Cattaneo, E. (2010) Molecular mechanisms and potential therapeutical targets in Huntington's disease. *Physiol Rev*, 90(3), 905-81.

Zwilling, D., Huang, S. Y., Sathyasaikumar, K. V., Notarangelo, F. M., Guidetti, P., Wu, H. Q., Lee, J., Truong, J., Andrews-Zwilling, Y., Hsieh, E. W., Louie, J. Y., Wu, T., Scearce-Levie, K., Patrick, C., Adame, A., Giorgini, F., Moussaoui, S., Laue, G., Rassoulpour, A., Flik, G., Huang, Y., Muchowski, J. M., Masliah, E., Schwarcz, R. & Muchowski, P. J. (2011) Kynurenine 3-monooxygenase inhibition in blood ameliorates neurodegeneration. *Cell*, 145(6), 863-74.

Zühlke, C., Riess, O., Bockel, B., Lange, H. & Thies, U. (1993) Mitotic stability and meiotic variability of the (CAG)n repeat in the Huntington disease gene. *Hum Mol Genet*, 2(12), 2063-7.